Department of Geosciences
University of Fribourg (Switzerland)

Changing glacier firn in Central Asia and its impact on glacier mass balance

Thesis

presented to the Faculty of Science and Medicine of the University of Fribourg (Switzerland) in consideration for the award of the academic grade of *Doctor of Philosophy in Geography*

by

Marlene Kronenberg

from
Dagmersellen LU, Switzerland

Thesis Number: 5377
Printed at UniPrint, Fribourg

2022

https://doi.org/10.51363/unifr.sth.2022.005

Accepted by the Faculty of Science and Medicine of the University of Fribourg (Switzerland) upon the recommendation of Prof. Martin Hoelzle (internal expert), Dr. Stanislav Kutuzov (external expert), Prof. Horst Machguth (supervisor), Dr. Francesca Pellicciotti (external expert), and Dr. Ward van Pelt (external expert) as well as the jury president Prof. Christian Hauck.

Fribourg, 11 April 2022

Thesis supervisor	Dean
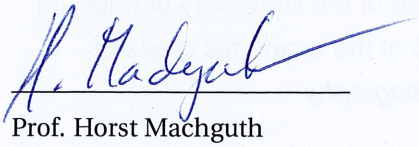	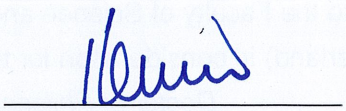
Prof. Horst Machguth	Prof. Gregor Rainer

Abstract

Glaciers in the Central Asian mountain ranges Tien Shan, Pamir and Pamir Alay are important water reservoirs for the dry low lands. These mountain glaciers attracted scientific interest already early. Soviet research programs investigated several sites from the 1960s until the 1990s. The resulting historical data are unique for the region and essential to answer open questions about the glaciers' response to climate change.

Regional-scale remote sensing studies reported balanced or positive mass changes for glaciers in Western High Mountain Asia for the last decades. With glaciers losing mass globally, this is a unique phenomenon. A precipitation increase is discussed to be a potential reason of this mass balance anomaly. However, the lack of *in situ* data hampers strengthening these assumptions and impedes quantifying the uncertainties of studies based on remote sensing data and gridded precipitation products.

The Pamir Alay is located at the edge of the anomalous regions. Soviet researchers collected unique glaciological and meteorological data for Abramov glacier, located in this data-scarce region. Of particular interest are very detailed firn studies that provide information about the past precipitation rates and allow studying accumulation processes. Thanks to the availability of further, exceptionally detailed measurements, it is possible to relate the accumulation processes to the glacier-wide mass balance.

This thesis aims at investigating the historical and present firn conditions of Abramov glacier as well as the changes therein over the past five decades. The firn processes were related to the surface energy and mass balance of Abramov glacier. Thereby, the influence of firn changes on the glacier-wide mass balance was studied. The underlying work involved (i) compiling and processing of historical firn, mass balance and meteorological data; (ii) measuring current firn conditions; and (iii) applying a coupled surface energy balance – multilayer subsurface model to Abramov glacier.

The comparison of historical and current *in situ* data showed that the firn conditions of Abramov glacier have changed little between the 1970s and 2018. The data, however, also suggested a precipitation increase. The results of the coupled firn-mass balance model indicate that the firn properties of the 1970s were the result of specific meteorological

conditions with low precipitation and high incoming solar radiation. These conditions were also reflected in very negative glacier mass balances. Precipitation increased during the following decades and allowed the firn to recover in the upper areas of the accumulation zone. Therefore, the internal accumulation (refreezing of melt water in the firn) increased. It is also shown that internal accumulation substantially contributed to the glacier-wide mass balance of Abramov. For the most recent years, firn conditions become again icier and mass losses increased.

The presented thesis found *in situ* evidence of increased precipitation rates and their positive impact on the mass balance for a glacier located in the data scarce western High Mountain Asia. The work highlights the importance of firn processes for understanding the response of mountain glaciers to climate change. Moreover, it demonstrates the importance of historic (Soviet) research and the suitability of the Russian terminology for analysing firn processes.

Zusammenfassung

Die Gletscher im Zentralasiatischen Pamir-, Pamir Alay- und Tien Shan-Gebirge sind wichtige Wasserspeicher für das tiefer gelegene trockene Vorland. Schon früh haben diese Gletscher wissenschaftliches Interesse geweckt. Sowjetische Forschungsprogramme haben mehrere Standorte von den 1960er bis in die 1990er Jahre intensiv untersucht. Diese historischen Daten sind für die Region einmalig und könnten helfen, offene Fragen bezüglich der dortigen Gletscherveränderungen als Folge des Klimawandels zu beantworten.

Mehrere regionale fernerkundungsbasierte Studien haben gezeigt, dass Gletscher in den westlichen Hochgebirgen Asiens in den letzten Jahrezehnten eine positive oder ausgeglichene Massenbilanz hatten, während weltweit ein Gletscherschwund vorherrscht. Als Ursache für diese Massenbilanzanomalie wird vermutet, dass der Niederschlag angestiegen ist. Um diese Vermutungen zu festigen und um Unsicherheiten von Studien, die auf Fernerkundungsdaten oder meteorologischen Datensätzen basieren, zu klären, fehlt es leider an in-situ Daten.

Der Pamir Alay liegt am Rande der anomalen Gebiete. Sowjetische Forschende haben einmalige glaziologische und meteorlogische Daten für den sich dort befindenden Abramov Gletscher erhoben. Von besonderem Interesse sind die ausführlichen Firnuntersuchungen. Diese Daten vermitteln Hinweise zu den vergangenen Niederschlagsraten und erlauben es, die Akkumulationsprozesse zu untersuchen. Dank der Verfügbarkeit von weiteren, aussergewöhnlich detaillierten Messungen für diesen Gletscher ist es möglich, die Akkumulationsprozesse mit der Gletschermassenbilanz in Zusammenhang zu bringen.

Diese Arbeit hat zum Ziel, die historischen sowohl als auch die gegenwärtigen Firnbedingungen des Abramov Gletschers sowie deren Veränderungen über fünf Dekaden zu untersuchen. Firnprozesse wurden mit der Oberflächen Energie- und Massenbilanz des Gletschers in Zusammenhang gebracht, um den Einfluss der Akkumulations- und Firnveränderungen auf die Gletschermassenbilanz zu verstehen. Dafür wurden die historischen Firn-, Massenbilanz- und meteorologischen Daten aufgearbeitet, neue Firndaten erhoben und ein gekoppeltes Firn-Massenbilanz-Modell angewendet.

Der Vergleich von historischen und aktuellen in-situ Daten hat aufgezeigt, dass sich der

Firn des Abramov Gletschers zwischen den 1970er Jahren und 2018 kaum verändert hat. Die Daten weisen jedoch auf einen Niederschlagsanstieg hin. Die Resultate des gekoppelten Firn-Massenbilanz-Modelles zeigen auf, dass die meteorologischen Bedingungen in den 1970ern unvorteilhaft für den Abramov Gletscher waren. In den folgenden Jahrzehnten nahm der Niederschlag zu und der Firn konnte sich in den höheren Lagen des Akkumulationsgebietes vollständig erholen. Dies führte zu einer erhöhten internen Akkumulation (Wiedergefrieren des Schmelzwassers im Firn), welche einen bedeutenden Anteil an der Gletschermassenbilanz hatte. In den letzten Jahren haben sich die Firnbedingungen und Massenveränderungen wiederum verschlechtert.

Die vorgelegte Arbeit zeigt aufgrund von in-situ Daten, dass der vermutete Niederschlagsanstieg in den westlichen Hochgebirgen Asiens auf den Abramov Gletscher zutrifft und dass dieser Anstieg einen positiven Einfluss auf die Massenbilanzentwicklung des Gletschers hat. Die Ergebnisse dieser Arbeit unterstreichen die Bedeutung von Firnprozessen für das Verständnis der Reaktion von Gebirgsgletschern auf den Klimawandel. Die Arbeit weist ausserdem auf die Relevanz historischer (sowjetischer) Forschung und die Bedeutung der russischen Terminologie für die Analyse von Firnprozessen hin.

Contents

1. Introduction

1.1. Glaciers in Central Asia

Mountain glaciers in the Tien Shan, Pamir and Pamir Alay serve together with other components of the cryosphere (such as seasonal snow and water stored in permafrost) as water towers for the dry low lands of Central Asia (Hoelzle et al., 2019). The glacier fed rivers Amu Darya, Syr Darya and Chu supply more than 90% of the water resources for 22 million people living from irrigated agriculture in downstream Kazakhstan, Turkmenistan and Uzbekistan (Luo et al., 2018). Upstream Kyrgyzstan and Tajikistan store water for energy production during the winter season (Siegfried et al., 2012). Extensive water use has serious environmental consequences causing the desiccation of the Aral Sea with severe impacts also for the local population (Micklin, 2007). The water scarcity and the fact that major rivers extend across national borders has repeatedly led to international disputes over water allocation between Central Asian countries (Bernauer and Siegfried, 2012; Peña-Ramos et al., 2021).

Glacier melt supplies rivers with valuable water resources during the dry summer season. In the Aral Sea basin, the contribution of glacier meltwater to the total runoff peaks in August and was estimated to be 19% (Kaser et al., 2010). Climate change critically affects the glacial contribution to the water cycle (Pellicciotti et al., 2012; Muccione and Cassara, 2019; Yao et al., 2019, 2020). Unsustainably high glacier melting rates produce a temporally high melt season runoff which leads to a reduction of the stored water volume and ultimately causes a reduced glacier meltwater contribution (Huss and Hock, 2018; Nie et al., 2021). In Central Asia, these impacts are expected to be strongly catchment dependent (Saks et al., 2022). Furthermore, global warming related changes in streamflow regimes and the formation and expansion of glacial lakes pose a growing threat to downstream communities (Zheng et al., 2021).

1.2. State of knowledge about glacier changes in Central Asia

The current knowledge about Central Asian's glacier response to climate change is incomplete. Compared to other regions such as the European Alps, *in situ* observations are scarce and discontinuous as important monitoring sites were abandoned after the collapse of the Soviet Union (Unger-Shayesteh et al., 2013; Gärtner-Roer et al., 2019). Before that, starting in the 1960s, Soviet monitoring programs surveyed numerous glaciers in Central Asia. The monitoring was organized using three observation classes: Class 1 contained a few glaciers, which were observed year-round at great detail to investigate basic characteristics and processes, in class 2 main parameters of selected glaciers were periodically observed and class 3 covered larger spatial scales with periodical observations of glacier front positions (Kotlyakov and Severskiy, 2009). Several glaciers in the Tien Shan (e.g. Kara-Batkak, Golubin, Fig. 1.1) were monitored as 'class 2' glaciers (Dyurgerov and Meier, 2005). Two glaciers in Central Asia were subject to thorough and unprecedented 'class 1' observations: Central Tuyusksu located in the Northern Tien Shan and Abramov glacier which is the only monitored site in the Pamir Alay (Fig. 1.1) (Kotlyakov and Severskiy, 2009). Central Tuyuksu is the glacier with the longest continuous mass balance time series in Central Asia (WGMS, 2021). Despite a very dense network of stake measurements, data from the accumulation area is lacking due to accessibility problems (Kapitsa et al., 2020). On Abramov glacier, in addition to more than 45'000 monthly point mass balance observations covering the ablation and accumulation area, repeated firn measurements were performed in deep firn pits (Pertziger, 1996; Suslov and Krenke, 1980). Further measurements on this comparably large glacier include englacial temperature measurements, glacier thickness assessments and meteorological as well as hydrological observations (Kislov et al., 1977; Kuzmichenok et al., 1992; Glazyrin et al., 1993). Similar historical measurements exist for Central Tuyuksu glacier. An overview is given in Nosenko et al. (2016).

Except for Central Tuyuksu and Urumqi Glacier No. 1 (Fig 1.1), all glacier monitoring programs in Central Asia stopped in the 1990s (Hoelzle et al., 2011; Barandun et al., 2020). During the politically unstable time after the collapse of the Soviet Union, also the amount of operating weather stations dropped drastically in the region (Haag et al., 2019). Only parts of the historical data from and research focusing on Central Asia is accessible to international researchers through publications in English language (e.g. Grosvald'd and Kotlyakov, 1969; Pertziger, 1996; Dyurgerov, 2002; Aizen et al., 1995) and international data centres such as the World Glacier Monitoring Service WGMS or the glacier thickness database GlaThiDa (GlaThiDa Consortium, 2020; WGMS, 2021). Soviet glaciological investi-

gations, however, went beyond the data collected by the WGMS or GlaThiDa. Currently, no international data centre collects firn data from mountain glaciers. Such data are thus only available through historical publications and original data possibly stored in local archives to which access is often restricted. Studies about the comprehensive firn investigations on mountain glaciers of the ex-Soviet Union are usually written in Russian (e.g. Dikikh, 1965; Krenke et al., 1970; Golubev et al., 1988) and therefore difficult to access for international researchers. These data access limitations can impede re-examinations at historical measurement sites. Relevant historical data from Central Asian glaciers risk to be buried in oblivion and may therefore not be included into recent studies.

In 2010, thanks to international efforts, several glacier mass balance monitoring programs in Central Asia were re-initiated (Hoelzle et al., 2017). During the last two to three decades, a limited amount of additional *in situ* measurements such as ice core drilling or ice thickness estimations have been performed on a few glaciers. The studies mainly focus on Tien Shan glaciers and include the historical investigation sites Gregoriev ice cap and Inilchek glacier (Fig. 1.1) (Thompson et al., 1993; Kutuzov, 2005; Aizen et al., 2006; Hagg et al., 2013; Takeuchi et al., 2014; Petrakov et al., 2016). In the western Pamir, recent studies performed measurements on Fedchenko glacier (Fig. 1.1) (Lambrecht et al., 2014, 2018). Lambrecht et al. (2020) present recent accumulation measurements and detect strong spatial and temporal variations. However, no historical firn data nor mass balance point observations are available for this site. Overall, an important data gap remains for the late 1990s and 2000s and for only a few glaciers recent *in situ* data is available. *In situ* data is especially rare for glaciers in the Pamir and Pamir Alay.

The few available continuous glaciological data indicate overall negative mass balances. The long term average mass balance for the continuously monitored glacier Central Tuyuksu (Northern Tien Shan) is -0.4 m w.e. a^{-1} for 1957-2017 and -0.5 m w.e. a^{-1} for 1980-2020 for Urumqi No.1 (Eastern Tien Shan) (WGMS, 2021). Gap-filled and extended mass balance time series based on *in situ* data and the application of relatively simple mass balance models also indicate negative mass balances for Bathysh Sook glacier (Kenzhebaev et al., 2017) and Glacier No. 354 (Kronenberg et al., 2016) both located in the Inner Tien Shan (Fig. 1.1) and for Abramov glacier in the Pamir Alay (Barandun et al., 2015).

Complementary data sources such as satellite measurements provide information on glacier changes for periods and areas without *in situ* measurements. Glacier area changes detected on remote sensing imagery indicate an overall reduction of glacier surface with varying retreat rates in the Tien Shan, Pamir and Pamir Alay (e.g. Khromova et al., 2006; Kutuzov and Shahgedanova, 2009; Narama et al., 2010; Kriegel et al., 2013). Satellite mea-

surements of surface elevation are widely employed to analyse glacier elevation changes which are converted to geodetic glacier mass changes by the application of a density conversion factor (Huss, 2013). There are numerous geodetic mass balance estimates for Central Asian glaciers covering varying periods and different spatial extents (e.g. Pieczonka et al., 2013; Pieczonka and Bolch, 2015; Goerlich et al., 2017; Zhang et al., 2016; Bhattacharya et al., 2021). Overall, the mass balance estimates agree relatively well on mass losses for the Tien Shan, whereas larger discrepancies between different assessments are found for the Pamir (incl. Pamir Alay) (Hoelzle et al., 2019). A recent study, which combines geodetic mass changes with snowline observations from satellite data and mass balance modelling for the Tien Shan, Pamir and Pamir Alay for 2000-2018, finds a large spatiotemporal mass balance heterogeneity also for the Tien Shan (Barandun et al., 2021).

Regional mass balance assessments provide methodologically consistent mass balance estimates over wider areas. Several studies investing glacier changes in High Mountain Asia also cover the Central Asian mountain ranges Tien Shan, Pamir and Pamir Alay. Reported regional average geodetic mass changes since 2000 are clearly negative for the Tien Shan and slightly negative for the Pamir and Pamir Alay (Brun et al., 2017; Shean et al., 2020). Positive mass balances in the eastern Pamir indicate that Central Asia is located at the edge of a wider region with positive mass balances, a phenomenon which is named Karakoram anomaly and which is not yet fully understood (Kääb et al., 2015; Forsythe et al., 2017; Farinotti et al., 2020). Miles et al. (2021) find currently balanced conditions for glaciers with large accumulation areas. Topographic factors in combination with recent increases of high altitude precipitation as suggested by several studies (Yao et al., 2012; Wang et al., 2017; De Kok et al., 2020) may thus explain currently stable regional mass balances. Several of theses studies, however, mention important uncertainties which are difficult to quantify due to the lack of *in situ* data from glaciers and weather stations.

1.3. Motivation and objectives of this thesis

Soviet monitoring programs collected exceptional data on glaciers in Central Asia. These data are extraordinary for Central Asia as well as for the entire High Mountain Asia. The investigations on Abramov glacier are the only *in situ* measurements in the Pamir Alay representing a unique long-term mass balance time series measured relatively nearby regions with an anomalous behaviour (Pamir, Kunlun, Karakoram). Furthermore, the historical data include investigations in the accumulation area and firn studies. These data have not yet been taken into account to investigate and understand the assumed

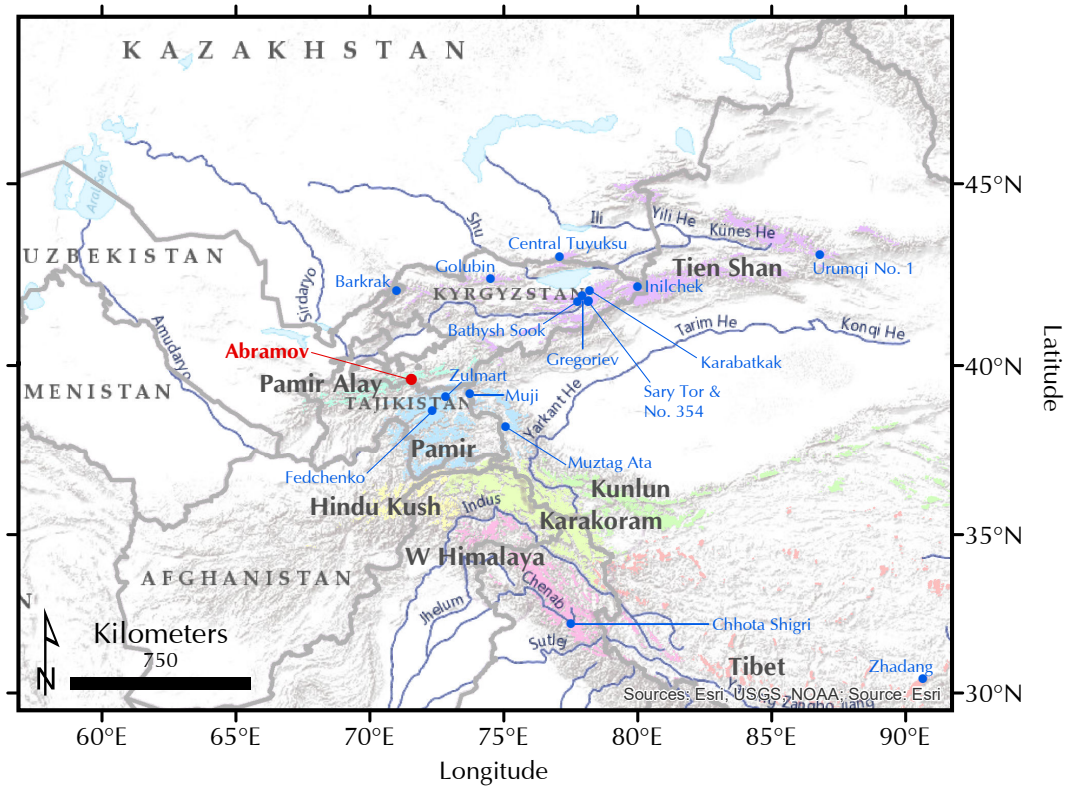

Figure 1.1: Overview map of Central Asia and neighbouring regions. The colour tones visualize the glaciation of different regions (outlines from RGI 6.0, RGI Consortium (2017)). Selected glaciers are indicate with blue dots. The location of Abramov Glacier in the Pamir Alay is shown in red.

accumulation increase that is considered as a cause of the observed mass balance anomaly. In the context of (i) open questions regarding the observed mass balance anomalies in western High Mountain Asia, (ii) the prevailing uncertainties in glacier change estimates for both Central Asia and High Mountain Asia and (iii) the general data gap prevalent in these regions, historical *in situ* measurements are of invaluable importance.

This work makes use of the extraordinary historical data available for Abramov glacier (Section 1.5) to investigate the long-term mass balance evolution in the context of a postulated accumulation increase over western High Mountain Asia.

The aim of this thesis is to analyze the historical and current state of firn; to reconstruct the firn evolution over the past five decades and to relate the firn processes to the surface energy and glacier mass balance of Abramov glacier. Therefore, a combined approach analysing historical data sets, conducting *in situ* measurements and modelling is applied.

A special focus is laid on including historical data that risks to be buried in oblivion as it is not easily accessible to international researchers. This leads to the following main research questions:

1. What are the past and current accumulation rates, firn stratigraphy and density in the accumulation area of Abramov glacier? (state of firn)
2. How did the firn of Abramov glacier evolve over the period from 1968 to 2020? (firn evolution)
3. How are mass exchange processes in the firn and changes therein contributing to the glacier wide mass balance? (impact of firn changes on glacier mass balance)

1.4. Thesis structure

After the introduction (chapter 1), a background into processes and methods relevant for this thesis is given (chapter 2). The main work addressing the above research questions is presented in the form of two research papers: Paper I and Paper II. Complementary figures and tables to both papers presenting additional *in situ* data and model output as well as the supplementary material of Paper II can be found in appendix A-C. In chapter 3, the main results are discussed in the overall research context. This thesis closes with conclusions and perspectives.

Paper I presents an analysis of historical and recent firn characteristics and accumulation rates for a point location on Abramov glacier. The comparison is based on the compilation of historical firn data and own measurements. To allow for a connection of the own data to historical measurements, for which information on the exact location was missing, complementary data including historical photographs, differential GPS and Ground Penetrating Radar (GPR) data had to be used. The comparison of historical and recent firn data, reveal similar firn conditions and indicate an increase of net accumulation rates.

Reference: Kronenberg, M., Machguth, H., Eichler, A., Schwikowski, M., and Hoelzle, M. Comparison of historical and recent accumulation rates on Abramov Glacier, Pamir Alay. Journal of Glaciology, *67(262):253–268, 2021. doi:10.1017/jog.2020.103.*

Paper II provides insights into the distributed long-term evolution of mass balance and firn of Abramov glacier based on modelling. A coupled surface energy balance–multilayer

subsurface model is applied from 1968 to 2020. The model is forced with weather station measurements and corrected reanalysis data for periods without measurements. After calibration, modelled surface mass balance and subsurface characteristics agree well with in independent situ observations. The model results indicate an important contribution of internal accumulation to the glacier-wide mass balance. The results also show that increasing precipitation rates have compensated for increasing air temperatures, preventing an acceleration of mass losss during the modelled 52 years.

Reference: Kronenberg, M., van Pelt, W., Machguth, H., Fiddes, J., Hoelzle, M., and Pertziger, F. Long-term firn and mass balance modelling for Abramov glacier in the data-scarce Pamir Alay. The Cryosphere Discussions (revised and resubmitted manuscript), *2021-380:1–33, 2022.*

Additionally, it shall also be referred to the two co-authored research papers (Denzinger et al., 2021; Mattea et al., 2021) which are thematically related to the context of this thesis. In Denzinger et al. (2021) the geodetic mass balance for Abramov glacier is established for the period 1975-2015. The study thus provides an independent mass balance estimate for Abramov glacier for a period covered by modelling. Mattea et al. (2021) apply the same coupled surface energy balance–multilayer subsurface model as used for Abramov glacier on a cold firn saddle in the Swiss Alps. The study demonstrates that the model is suitable for modelling the warming of cold firn sites, processes which likely also occur on cold firn sites in Central Asia. The abstracts of both papers can be found in the appendix (D). Mattea et al. (2021) is based on one of three different Master theses which were co-supervised as a part of this PhD work. A short overview of the Master projects is given in Appendix E. The appendix furthermore contains an overview of additional firn data measured as a part of this thesis. These data was measured at Gregoriev ice cap, Inner Tien Shan (Appendix F). And finally, the program 'Adventure of Science: Women and glaciers in Central Asia' should be mentioned. The project was founded in the during this PhD work. It aims to stimulate the involvement of local women into scientific activities in Central Asia. Appendix G provides a short description of the project.

1.5. Study site: Abramov glacier

Abramov Glacier (39.50°N, 71.55°N, Fig. 1.2) is located in the Pamir Alay in southern Kyrgyzstan, Central Asia (Fig. 1.1). The glacier drains into the Koksu river, a tributary of Kzsilsu which drains into the Vakhsh watershed, a contributor of Amu Darya. The valley-type glacier is north oriented, spans an elevation range of 3650-5000 m a.s.l. and

has a surface area of 24 km^2 (in 2015). The glacier has temperate firn conditions and cold temperatures were measured in the ablation area (Kislov et al., 1977). For 1968-1998, mean annual air temperature measured at 3837 m a.s.l. was -4.1°C and annual precipitation was 750 mm a^{-1}. Abramov glacier had a predominantly negative mass balance since 1968 (Dyurgerov, 2002; Barandun et al., 2015).

Abramov glacier has a unique history of very detailed measurements. Glaciological investigations started in 1967, when the Central Asian Research Hydrometeorological Institute (SANIGMI, Republic of Uzbekistan) built a research station on a moraine next to the glacier tongue (Hoelzle et al., 2017). The monitoring initiative was started in the framework of the International Hydrological Decade and monthly mass balance observations as well as meteorological and runoff measurements continued for three decades (Pertziger, 1996). Complementary investigations included repeated firn measurements from deep snow pits, englacial temperature measurements and glacier thickness assessments (Suslov and Krenke, 1980; Kuzmichenok et al., 1992). Due to political instabilities after the decay of the Soviet Union, this important glaciological study site was suddenly abandoned in summer 1999. In 2011, thanks to international efforts, mass balance measurements were re-initiated and an automatic weather station was installed (Hoelzle et al., 2017; Schöne et al., 2013).

According to Pertziger (1996), the unique data available for Abramov glacier had resulted in more than 150 scientific publications already in the 1990s. Many of these studies, which were predominantly published in Russian language, are difficult to access for international researchers. Through the 'Abramov Glacier Data Reference Book: Climate, Runoff, Mass Balance' (Pertziger, 1996) important *in situ* data became internationally available. This book presents extracts of the larger database which was set up in 1993 at the SANIGMI (Pertziger, 1996) but does not include data from complementary investigations such as firn measurements.

Comparably few publications, written outside of the former Soviet Union, study Abramov glacier. Even fewer made use of the exceptional historical data. Rather recent publications mention Abramov glacier in the context of energy balance estimates (Oerlemans, 2001), glacier dynamics (Navarro et al., 1999) or they contain, among many other glaciers, estimates of Abramov glacier mass balance (Gardelle et al., 2013; Barandun et al., 2015; Miles et al., 2021). Of the mass balance studies, only Barandun et al. (2015) covers a longer time period and uses historical mass balance data.

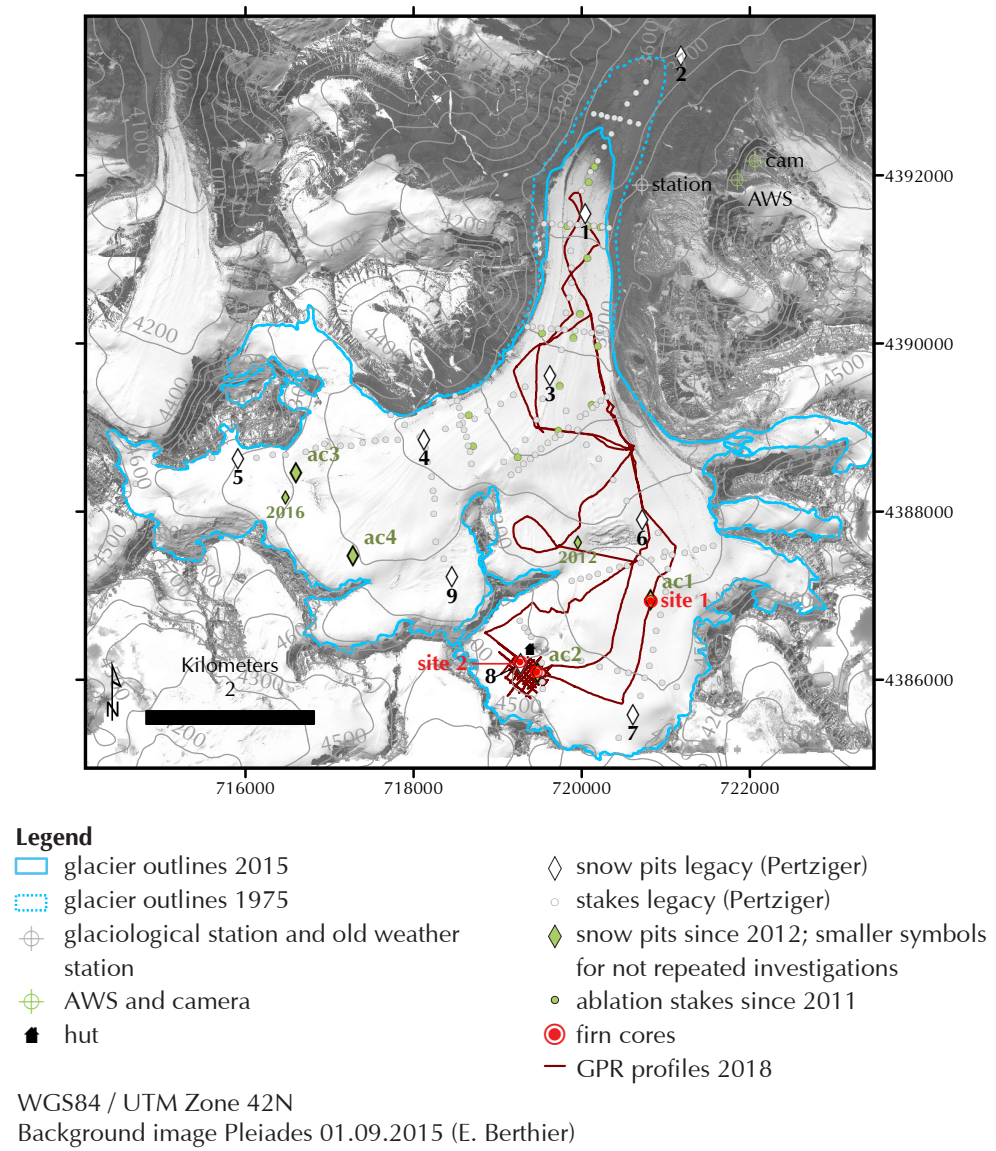

Figure 1.2: Overview map of Abramov glacier. Observation sites of data compiled and measured within this thesis are indicated with symbols and explained in the legend.

2. Processes at the glacier surface

Glaciers are landforms that evolve due to the interaction of different mass and energy exchange processes. This chapter provides the general context and a brief introduction into the main processes important for understanding the thesis. These are processes occurring at the glacier surface. After an introduction into glacier mass balance, more specific background is given on *in situ* measurements and modelling of selected processes relevant for this thesis. Where no references are specified, this chapter is based on the textbooks Cuffey and Paterson (2010) and Singh et al. (2011). For a more comprehensive description of the here outlined theoretical and methodological background, the reader is referred to these textbooks and further references given in the text.

2.1. Glacier mass balance

The total mass of a glacier changes through processes that transfer mass between the glacier and its surroundings (Fig. 2.1). Climatic conditions determine whether and how mass is added or removed at the glacier surface. The mass within a glacier is redistributed through ice flow. The ice flux results from interactions between stresses, thermodynamics, hydrology and mass and energy exchanges at the glacier boundaries. These processes are controlled by the climate, topographic and other site-specific factors such as the albedo. The glacier geometry is the result of all these coupled processes and feedbacks between them. As the climate is changing, glaciers are in a continuous transition to respond to past and current climate conditions. The glacier geometry adapts with a certain delay or response time to a change in the climate forcing. Response times for mountain glaciers generally range from a few decades to a century. Glacier mass changes more directly reflect climate conditions. But, as they vary with altitude, and as the altitude of a glacier surface adjusts with glacier flow, mass changes cannot be completely decoupled from glacier dynamics.

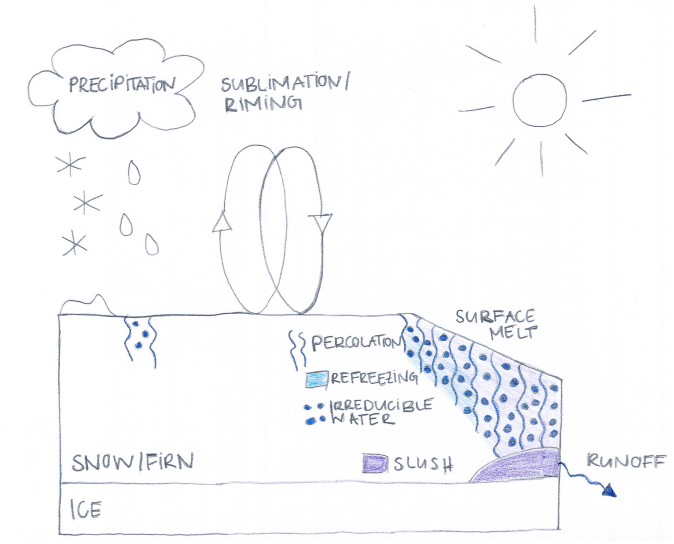

Figure 2.1: Visualization of mass fluxes occurring at the glacier surface. This illustration is inspired by Fig 1.9 in van Pelt (2013).

Mass fluxes adding mass to the glacier are called accumulation processes and the term ablation summarizes mass loss processes. For a land terminating glacier, the sum of accumulation c and ablation a is the mass balance b:

$$b = a + c \tag{2.1}$$

In Eq. 2.1, and all the following equations, unless specified differently, fluxes contributing mass (or elsewhere energy) are positive and negative if they represent mass (energy) sinks.

Ablation and accumulation are not equal throughout the glacier area. For most parts of the glacier one term dominates over the other. Therefore, different zones are distinguished. In the *accumulation area*, which is usually occupying the higher elevated parts of a glacier, accumulation dominates over ablation ($c > a$). In the *ablation area*, ablation is higher than accumulation ($a > c$). The zone where both mass exchange processes are equal during the year ($a = c$) is called *equilibrium line altitude* (ELA).

The mass exchange processes occur either at the glacier surface (surface balance b_{sfc}), the glacier bed (basal balance b_b) or within the glacier (englacial balance b_i). The fluxes are usually described as rates for a glacier column. A general formulation is given by Cogley et al. (2011):

$$\dot{m} = \dot{c}_{sfc} + \dot{a}_{sfc} + \dot{c}_i + \dot{a}_i + \dot{c}_b + \dot{a}_b + (q_{in} + q_{out})/ds \tag{2.2}$$

with the rates of mass change $\dot{m}$, surface accumulation $\dot{c}_{sfc}$ and ablation $\dot{a}_{sfc}$, englacial accumulation $\dot{c}_i$ and ablation $\dot{a}_i$ and the rates of basal accumulation $\dot{c}_b$ and ablation $\dot{a}_b$. q_{in} and q_{out} are the ice flow in and out the column with fixed horizontal dimensions ds. The importance of the different terms varies depending on glacier characteristics and it is common that one or several components of Eq. 2.2 are assumed to be negligible (Cogley et al., 2011). The components of Eq. 2.2 which are relevant for this thesis are further introduced in the following sections (2.2, 2.3, 2.4).

The sum of accumulation and ablation over the entire glacier surface for a given period (normally a season, one or several hydrological years) corresponds to the glacier wide mass balance, which is usually given as an area-averaged (or specific) value (Cogley et al., 2011). As glacier areas change over time, either a constant surface is used to calculate the *conventional mass balance* or the glacier extent of a reference year is used to calculate the *reference mass balance* (Elsberg et al., 2001).

2.2. Surface energy balance and ablation

The surface mass balance usually dominates the mass budget of land terminating glaciers. Surface accumulation processes are introduced in Section 2.3. The main surface ablation process is usually melt followed by sublimation. Wind erosion may play a role locally. Melt and sublimation are driven by the net flux of energy from the atmosphere to the glacier surface. The surface energy balance describes the energy fluxes at the glacier surface given in Eq. 2.3.

$$Q_{melt} = SW_{in}(1-\alpha) + LW_{in} + LW_{out} + Q_{sens} + Q_{lat} + Q_{sub} + Q_{rain}, \tag{2.3}$$

with the total energy available for melting Q_{melt}, the incoming shortwave radiation SW_{in}, the surface albedo α, the incoming and outgoing longwave radiations LW_{in} and LW_{out}, the turbulent sensible and turbulent latent heat fluxes Q_{sens} and Q_{lat}, the heat flux into the subsurface Q_{sub} and the heat flux supplied by liquid precipitation Q_{rain}. The different energy fluxes contributing to the melt energy are visualized in Figure 2.2. The net shortwave radiation SW_{net} depends on the total incoming shortwave radiation and the surface albedo. The sublimation of snow/ice and the evaporation of water at the glacier surface consume latent heat. If riming or condensation occur, latent heat is released. The heat flux provided by liquid precipitation Q_{rain} is usually small. The main sources of energy to the surface energy balance are the sunlight determining the incoming shortwave radiation and the atmospheric heat content acting trough the incoming longwave radiation and the sensible

heat flux. The albedo α of the glacier surface is a critical parameter at it evolves as a response to different processes at the glacier surface which result from the energy balance and the snow accumulation (see section 2.3.2). As a consequence, important melt-accelerating feedbacks can result from changes in the surface albedo.

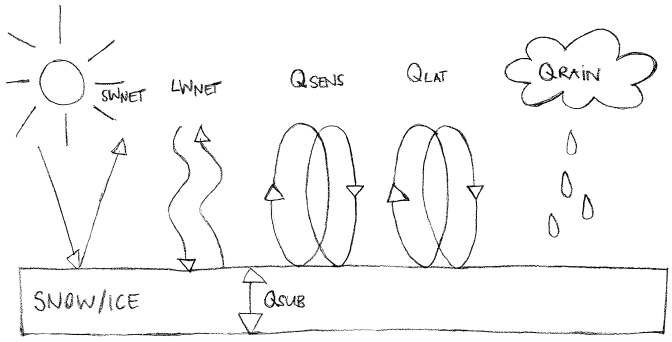

Figure 2.2: Visualization of the energy fluxes which determine the surface energy budget. This illustration is inspired by Fig 1.10 in van Pelt (2013).

2.2.1. Measuring the surface energy balance and ablation

Distributed *in situ* measurements of the surface energy balance components are normally not feasible as such measurements rely on numerous meteorological sensors. Instead, researchers established point-scale energy balances based on local weather station measurements on several glaciers in different climate settings (e.g. Wagnon et al., 1999; Oerlemans and Klok, 2002; Azam et al., 2014b). For glacier-wide assessments, extrapolation techniques are necessary (Hock, 2005). Technological progress created new possibilities for *in situ* data acquisitions in Alpine environments including measurements of all four radiation components (Oerlemans, 2010). Nevertheless, parametrisations remain often necessary to translate weather station measurements into energy fluxes (Hock, 2005; Gabbi et al., 2014). Furthermore, eddy covariance measurements used for quantifying the turbulent heat fluxes are logistically difficult and are therefore rarely available (Cullen et al., 2007; Oerlemans, 2010). Models are thus essential to inter- and extrapolate point measurements, to translate meteorological conditions into glacier mass changes and to quantify the energy balance for longer time periods (Section 2.2.2).

Glaciological ablation measurements have a long tradition and the methods have changed little over time. Ablation measurements consist of repeated height readings of stakes drilled into the glacier ice at multiple point locations on the glacier surface (Ostrem and Brugman,

1993; Kaser et al., 2003). Outside the firn area, height changes are converted into glacier melt (m w.e.) using the density of ice (Cogley et al., 2011). Ablation is usually at least measured at seasonal or annual intervals (Kaser et al., 2003). Observations can either take place at (i) the dates of the glacier mass balance minimum and maximum (*stratigraphic*), at (ii) *fixed* observation dates (usually corresponding to the hydrological year from 1 October to 30 September for the annual balance and to 31 May for the winter balance) or (iii) at *floating* time intervals (Cogley et al., 2011).

Standard ablation measurements using stakes do not allow distinguishing different forms of ablation. Ice ablation is measured only when the stakes are installed into the glacier ice and the surface is snow free for both consecutive observation dates. Otherwise, for example, if the glacier ice is snow covered, the ablation reading may reflect a combination of snow and ice ablation. Ablation observations performed at stakes installed in the firn area either provide firn ablation or combined firn and snow ablation data. In such cases, the estimation of densities to convert height changes into ablation, is an important source of uncertainty (Pertziger, 1996). Furthermore, stake measurements do not allow to distinguish between melt and sublimation. Lysimeters can be used to measure sublimation during field visits (Winkler et al., 2009).

2.2.2. Modelling the surface energy balance and ablation

Glacier melt models with different degrees of complexity have been used in a wide range of applications (e.g. Braun and Aellen, 1990; Braithwaite and Zhang, 1999; Oerlemans, 2001; Hock and Holmgren, 2005; Ragettli and Pellicciotti, 2012). Simple temperature-index (TI) methods calculate glacier melt as a function of air temperature using one or a few calibrated melt parameters (Hock, 2003). Some TI parametrisations are extended and include global radiation (Hock, 1999; Pellicciotti et al., 2005). Such models can be used when the availability of meteorological data is low. They only need air temperature data as model forcing and global radiation is computed from topographical information and assumptions about the atmospheric transmissivity (e.g. assuming clear-sky conditions or average cloudiness) .

More complex models resolve the energy balance (eq. 2.3) quantifying each energy flux separately. Various parametrisations for each of these fluxes have been suggested. Hock (2005) provides a comprehensive overview. The application of energy balance models is often constrained as the high data requirements cannot easily be met. Recently, such models have been forced with the output of regional climate models. A energy balance

model was used for this thesis. A more detailed introduction to energy balance models is given in Paper II.

2.3. Snow accumulation

Surface accumulation processes ($\dot{c}_{sfc}$ in Eq. 2.2) on glaciers include snowfall, avalanche deposition, wind deposition, riming (moisture deposition) and the refreezing of liquid water. Of these, snowfall is the most important process. Topographic effects and topography-wind inter-plays such as snow deposition in the topographic lee lead to variable snow accumulation. Snowfall rates typically increase with elevation until a certain altitude. When temperatures are cold enough, the available humidity is the limiting factor. Wind and avalanches act by redistributing snow and produce heterogenous accumulation patterns.

2.3.1. Measuring snow accumulation

Glaciological *in situ* snow accumulation measurements consist of snow depth measurements in combination with density measurements which are usually performed in snow pits dug to a reference surface (last summer surface) (Mayo et al., 1972). Snow pit studies may be complemented with additional snow depth data from probings or stake readings (Ostrem and Brugman, 1993; Pertziger, 1996). Glaciological accumulation measurements only measure surface accumulation and do not include internal accumulation which happens as refreezing below the last summer horizon (Cogley et al., 2011). Surface accumulation measurements are performed at least at seasonal or annual intervals which correspond to the end of the accumulation season or end of the hydrological year (Kaser et al., 2003). It is usually not feasible to organize field visits to correspond to the stratigraphic minimum or maximum and therefore accumulation measurements are likely measured in a *mixed time-system* (Cogley et al., 2011). Furthermore, the observation date of the reference surface is often unknown unless it was marked the year before.

Recently, new methods have been applied to continuously measure the snow accumulation on glacier surfaces with cosmic ray sensors (Gugerli et al., 2019). Such sensors allow to measure the snow water equivalent and not only the snow height as the more commonly used sonic rangers do. Compared to the glaciological method, the installation of cosmic ray sensors, is however, cost intensive. Furthermore, the necessity of regular entertainment and sufficient energy supply complicate the use of such devices in remote areas.

As glaciological ablation measurements (2.2.1), glaciological accumulation measurements provide information for point locations only. Ground penetrating radar (GPR) is

a complementary geophysical method which can be used to obtain spatially distributed information about the subsurface along measurement profiles (Woodward and Burke, 2007). Two-way travel times (TWT) derived from GPR measurements and the identification of radar reflector horizons in the GPR data can be used to estimate snow depths along measurement transects providing higher spatial resolutions than glaciological point measurements (Machguth et al., 2006; Sold et al., 2013).

2.3.2. Modelling snow accumulation

Sophisticated models have been developed to model seasonal snow accumulation and the subsequent transformation of the snow cover in the context of avalanche forecasting. These models simulate the evolution of the temperature, density and liquid-water profiles in response to weather conditions (Brun et al., 1992). They furthermore describe the snow micro-structure and layering of the snowpack (e.g. Lehning et al., 2002; Vionnet et al., 2012). Typical snow models are one-dimensional and exclude lateral mass or energy transfer between grid points (e.g. Quéno et al., 2020). Detailed snow models have been integrated into complex three-dimensional surface models, which are able to simulate horizontal mass exchange processes like snow drift (Lehning et al., 2006; Vionnet et al., 2012).

A few glacier mass balance studies have used some of the above described snow models (e.g. Dumont et al., 2012; Réveillet et al., 2018). Typical snow models used in glaciology are much simpler. They usually use precipitation and air temperature data to estimate bulk snow accumulation (e.g. Hock, 1999; Huss et al., 2008). Precipitation falling when air temperature is below a certain threshold is considered as accumulation. Often a linear transition from liquid to solid precipitation for a temperature range around the threshold value is applied (e.g. Hock, 1999). As the threshold temperature values depend on various factors, they are usually calibrated or adopted from other studies (Rohrer, 1989). Normally, simplifying approaches are used to include the spatial distribution of accumulation. Models either apply a linear precipitation gradient assuming a linear increase of accumulation with elevation (e.g. Klok and Oerlemans, 2002) or a snow distribution grid, which is constructed from measurements, is used (e.g. Farinotti et al., 2010; Sold et al., 2016). To model snow distribution processes, the simulation of wind fields would be necessary (e.g. Liston and Sturm, 1998; Purves et al., 1998). This is complex for mountain terrain and necessary wind measurements as well as high-resolution snow depth data are usually not available (Dadic et al., 2010).

Statistical approaches to derive snow accumulation distributions might become an alternative to modelling wind fields. Guidicelli et al. (2021) recently presented a statistical

modelling approach to estimate the snow water equivalent in mountainous terrain of the Swiss Alps based on gridded precipitation products, weather station data and topographical data. Due to large biases, the gridded precipitation products needed to be adjusted to *in situ* data prior to the application of the spatial downscaling (cf. Gugerli et al., 2021). The final snow distribution at a high spatial resolution of 25 m agreed well with *in situ* measurements on a selected glacier (Guidicelli et al., 2021).

2.4. Firn

Glacier ice is formed through a densification process which transforms snow to ice. Material at intermediate stages during the densification from snow to ice is called firn. The transformation includes different mechanisms, which vary depending on the prevailing conditions. Along the vertical axis, the conditions change with depth of the firn column and on a wider horizontal scale they vary for different firn facies, which are introduced later in this section.

The transformation from snow to firn to ice is a sintering process. Under pressure, bonds form between the particles and they grow larger. The air space between grains is reduced while the density of the material increases. Firn finally becomes ice when pores close off and the remaining gas is trapped in bubbles inside crystals. The closing of pores happens at a density of roughly 830 kg m^{-3}. The whole transformation is the result of the mutual displacement of particles, shape and size changes and the internal deformation of crystals. After falling, destructive metamorphism occurs and complex snow grains transform into rounded particles. The firn densifies up to 550 kg m^{-3} mainly by settling (particles sliding along each other), which is facilitated by the rounded form of the grains. Already at densities below 550 kg m^{-3} bonds start to form between particles. With increasing density, the overburden pressure raises and re-crystallization and deformation become the dominant processes. The firn temperature profile and the accumulation rate mainly control the transformation from snow to ice. Under colder conditions, the transformation takes longer and higher accumulation rates result in larger firn-ice transition depths but also accelerate the re-crystallization and deformation due to the higher overburden pressure.

The presence of liquid water and conditions at the melting point accelerate the transformation from snow to firn. Melting speeds up the rounding of grains. Liquid water furthermore lubricates grains and allows for a closer packing. Moreover, liquid water filling pore spaces can refreeze and form ice lenses and ice layers. If large amounts of liquid water are present, large amounts of ice can form quickly when the water refreezes. In the

infiltration-congelation zone (see below), the transformation from snow to ice happens within one melt season.

Different classifications of firn zones exist. In the English-speaking literature, the classification by Benson (1996) is most commonly used. However, for this work, the categories developed by Shumskii (1964), which were originally published in Russian (Shumskiii, 1955) and translated into English, are better suited. His classification also includes temperate firn conditions. The latter are defined as conditions with subsurface temperatures at the melting point at the depth of the Zero Annual Amplitude (ZAA). Shumskii's categories are introduced hereafter and visualized in Fig. 2.3. The approximate equivalent zones of Benson (1996) can be found in Table 2.1.

Shumskii (1964) defined the zones as following: in the *recrystallisation* zone, no liquid water occurs and the temperature at depth of the ZAA is similar to the mean annual air temperature (MAAT). Some surface melt occurs in the *recrystallisation-infiltration* zone, liquid water refreezes in the uppermost layers where ice lenses may form, the ZAA firn temperature is above the MAAT. In the *cold infiltration* zone, the whole seasonal snow pack reaches 0°C, some meltwater percolates into deeper layers but there is not enough latent heat to bring lower layers to the melting point. Melt water from the *warm infiltration* zone associated with temperate firn can leave the firn area. Here the cold content is insufficient to refreeze all the available melt water. The *infiltration-congelation* zone is the lowermost part of the accumulation area of cold glaciers just above the ELA. In this zone, water saturated seasonal snow (slush) refreezes to form superimposed ice. Here, the refreezing is limited by the available pore space. Water that cannot find pore space runs off, which limits the release of latent heat. Consequently, temperatures at ZAA remain below zero. On cold glaciers, the *firn line* is the boundary between the *infiltration-congelation* and the *cold infiltration* zone, on temperate glaciers, the firn line is located between the *warm infiltration* zone and the ablation area and thus roughly corresponds to the ELA.

In the Russian-speaking literature Shumskii's classification was later refined (e.g. Krenke, 1982; Kotlyakov, 1984). The later publications use slightly altered names as well as short forms (see Table 2.1) and refer to an additional firn zone which accounts for transient conditions: In the *infiltration* zone, high amounts of melt water occur, but layers of porous firn are still present. The firn layers originate from accumulation of previous years with more favourable conditions or moved downward from other firn zones located at higher elevations of a glacier (Kotlyakov, 1984). The downward transport of firn has been been recently described for Greenland Leone et al. (2020). This study, however, does not refer to the earlier description of the process in the Russian literature.

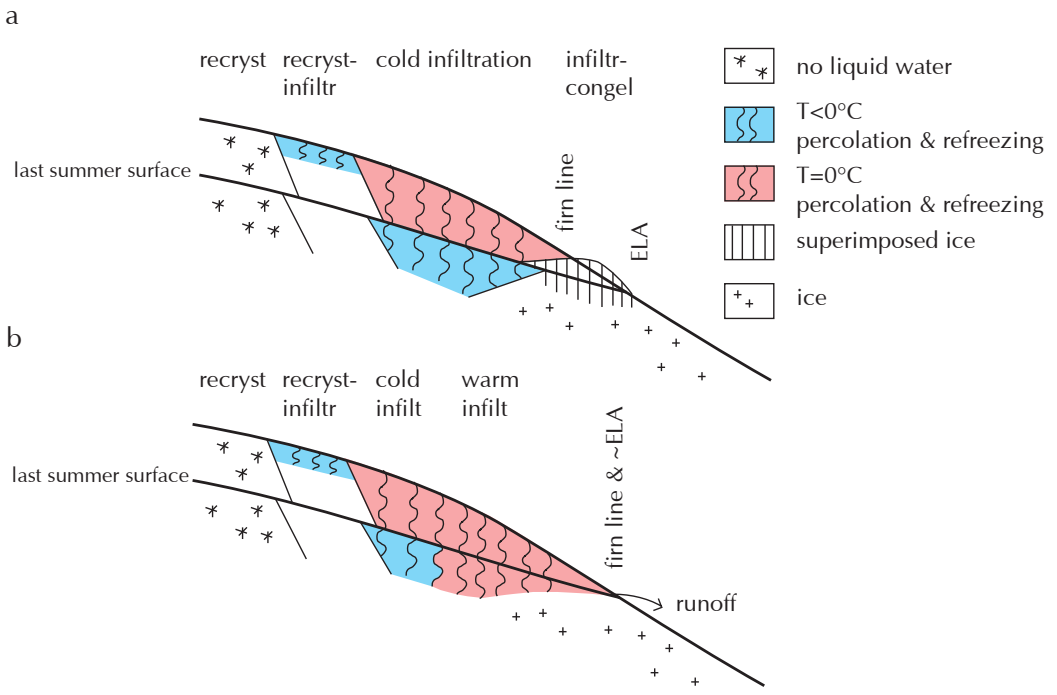

Figure 2.3: Visualisation of the firn zones after Shumskii (1964) for cold (a) and a temperate (b) glacier. The figure was inspired by a figure in Cuffey and Paterson (2010).

Table 2.1: Overview of firn zone classifications by different authors. Kotlyakov (1984) and Krenke (1982) use full names and also provide short names for the different zones which are given in brackets. The roughly corresponding firn facies of the classification by (Benson, 1996) are also listed

Zone name in Shumskii (1964)	**Zone name in Krenke (1982) and Kotlyakov (1984)**	**Facies name by Benson (1996)**
recrystallisation	recrystallisation (snow)	dry snow
recrystallisation-infiltration	recrystallisation-regelation (snow and firn)	percolation
cold infiltration	cold infiltration-recrystallisation (cold firn)	wet snow
warm infiltration	warm infiltration-recrystall. (warm firn)	
-	infiltration (firn-ice)	
infiltration-congelation	infiltration-congelation (superimposed ice)	superimposed ice

Except for the dry *recrystallisation* zone, liquid water is at least temporally present in glacier firn. It originates from liquid precipitation or melt. A small amount is retained in pore spaces by capillary forces (irreducible water) (Trabant and Mayo, 1985) and the rest percolates through the firn following gravity (Marchenko et al., 2017). In temperate firn, melt water can percolate to depth until it reaches impermeable layers where it forms perennial firn aquifers (Shumskii, 1964; Miller et al., 2020). Depending on the availability of cold content and pore space, irreducible and percolating water refreezes within the firn column (Schneider and Jansson, 2004). Refreezing below the last summer surface is internal accumulation (c_i in 2.2) (Cogley et al., 2011). Ice lenses, layers and vertical ice glands or fingers are resulting from refreezing processes within the firn column.

Hard layers may also form due to melt-freeze cycles, which mainly occur during the ablation season. Furthermore, glacier firn (and ice) can contain solid particles such as mineral dust, black carbon or pollen. These particles were transported by the wind and deposited on the glacier surface. As the atmospheric composition changes over time, also the snow and firn pack experiences variations in its chemical composition. The gas composition in a firn layer does not reflect the atmospheric conditions during the snow deposition because air mixing occurs in the porous firn. Furthermore, water soluble chemical species may be relocated if liquid water is present (Eichler et al., 2001).

2.4.1. Measuring firn

Firn characteristics at a point location can be assessed by drilling boreholes. Subsurface properties can then be assessed either by borehole logging or by the analysis of firn cores. Firn has enough cohesion so that intact cores can be retrieved to analyse properties such as stratigraphy, density, porosity, permeability, grain size, and anisotropy. The firn stratigraphy can either be analysed visually or through optical imaging of core sections. Firn properties measured inside boreholes include density, temperature and strain. Whereas the density analysis of discrete core samples has low material requirements, measurement techniques inside boreholes such as neutron probes can be used to measure high-resolution firn density profiles (Hawley et al., 2008). Firn temperature measurements are usually performed at several depths of a borehole. Continuous measurements of borehole temperatures at a high spatial resolution allow to detect refreezing events (Charalampidis et al., 2016), whereas repeated englacial temperature measurements permit to detect warming trends (Hoelzle et al., 2011). As the stratigraphy and density of snow, these firn properties can also be assessed in deep firn pits (e.g. Seligman, 1941; Suslov and Krenke, 1980). Repeated measurements of firn densities from deep pits during subsequent years have been used to quantify internal accumulation (Suslov and Krenke, 1980; Dyurgerov and Mikhalenko, 1995).

The age of firn can be determined by optical layer counting based on the seasonality of deposited materials. Classical methods include the detection and counting of visual dust layers (Hammer et al., 1978). Alternatively, core samples can be chemically analyzed for species which vary seasonally (Eichler et al., 2000). Based on dated firn layers and firn densities, accumulation rates can be reconstructed (Schwikowski et al., 2013). The spatial distribution of accumulation rates can be assessed by combining information from firn cores with GPR measurements (Miège et al., 2013; Sold et al., 2015).

2.4.2. Modelling firn

The firn evolution is modelled for several purposes: the age determination for the depth at which pores close off is necessary for the interpretation of climate records from ice cores. Knowledge about the firn densification is furthermore necessary to quantify the mass balance of glaciers and ice sheets from surface elevation changes. Moreover, firn models are used to estimate the melt water retention capacity of firn (Vandecrux et al., 2020). And last but not least, modelling firn processes is important for quantifying the climatic mass balance (including internal accumulation and liquid water storage) rather than the surface

mass balance (van Pelt et al., 2012). Furthermore, the accurate simulation of the surface energy balance requires a snow model (in order to properly simulate albedo and the subsurface heat flux). Modelled firn processes include densification mechanisms, heat transport and processes related to the presence of liquid water. Historically, firn densification models were developed for Arctic and Antarctic sites. Early models considering subsurface heat conduction and refreezing of liquid water were developed separately. Many recent firn densification models are coupled to heat diffusion models and also simulate the subsurface temperature evolution (Stevens et al., 2020).

Density profiles of dry firn can be modelled using the main driving forces of densification which are overburden pressure (accumulation rate is often used as a proxy) and temperature. Such models use the Arrhenius relation, $f(T) \propto \exp(-Q/RT)$ with the temperature T in Kelvin, the activation energy Q and the gas constant R. Herron and Langway (1980) used empirical data from Antarctica and Greenland to quantify the activation energy Q and to develop an empirical model assuming constant temperature and accumulation rates. Under such steady state conditions (also called 'Sorge's Law', Bader (1954)), the density at a given site and depth does not change over time. Since Herron and Langway (1980), several dry firn models have been developed. Arthern et al. (2010) presented the first model based on measured compaction rates rather than being based on 'Sorge's Law'. An overview of relevant firn compaction models is given by Stevens et al. (2020).

Classical firn densification models do not account for effects of ice flow. Recent efforts include strain related firn layer thinning in climate forced firn densification models (Horlings et al., 2021; Oraschewski and Grinsted, 2021). Models simulating the three dimensional ice flow have previously proven to be suitable to assist the dating of ice cores from the Alpine firn site Colle Gnifetti (e.g. Lüthi and Funk, 2000; Licciulli et al., 2019).

Heat conduction and refreezing were considered by an early mass balance sensitivity study (Greuell and Oerlemans, 1986) and were used to model englacial temperatures on the Greenland ice sheet (Greuell and Konzelmann, 1994). Based on these previous studies, multilayer firn models were developed (Reijmer and Hock, 2008; van Pelt et al., 2012). Multilayer models initially developed for seasonal snow (Brun et al., 1992; Lehning et al., 2002), have also been applied to model firn (Fettweis, 2007; Obleitner and Lehning, 2004).

Vandecrux et al. (2020) compares firn models which account for meltwater retention and percolation. The therein presented models either include meltwater percolation by bucket schemes, by adopting a distribution model to parametrise preferential flow (e.g. Marchenko et al., 2017) or by applying Darcy's law (e.g. D'Amboise et al., 2017).

Paper I

Comparison of historical and recent accumulation rates on Abramov Glacier, Pamir Alay

Kronenberg, M., Machguth, H., Eichler, A., Schwikowski, M., and Hoelzle, M. Comparison of historical and recent accumulation rates on Abramov Glacier, Pamir Alay. *Journal of Glaciology*, 67(262):253–268, 2021. doi:10.1017/jog.2020.103.

Journal of Glaciology

Comparison of historical and recent accumulation rates on Abramov Glacier, Pamir Alay

Marlene Kronenberg[1], Horst Machguth[1], Anja Eichler[2,3], Margit Schwikowski[2,3,4] and Martin Hoelzle[1]

[1]Department of Geosciences, University of Fribourg, Fribourg 1700, Switzerland; [2]Laboratory of Environmental Chemistry, Paul Scherrer Institute, Villigen PSI 5232, Switzerland; [3]Oeschger Centre for Climate Change Research, University of Bern, Bern 3012, Switzerland and [4]Department of Chemistry and Biochemistry, University of Bern, Bern 3012, Switzerland

Article

Cite this article: Kronenberg M, Machguth H, Eichler A, Schwikowski M, Hoelzle M (2021). Comparison of historical and recent accumulation rates on Abramov Glacier, Pamir Alay. *Journal of Glaciology* **67**(262), 253–268. https://doi.org/10.1017/jog.2020.103

Received: 28 April 2020
Revised: 12 November 2020
Accepted: 13 November 2020
First published online: 23 December 2020

Keywords:
Accumulation; ice core; ground-penetrating radar

Author for correspondence:
Marlene Kronenberg,
E-mail: marlene.kronenberg@unifr.ch

Abstract

Glaciers located in western High Mountain Asia (HMA) have shown mass gain or limited mass losses compared to other mountain regions since ~2000. Increases in accumulation may be responsible. Although no contemporary measurements exist to explore this hypothesis, extensive historic measurements including firn density, stratigraphy and accumulation rates at ~4400 m a.s.l. on Abramov Glacier, Pamir Alay, provide valuable indications of accumulation changes. Abramov Glacier is located at the northern margin of western HMA. In this study, we assess unique historical firn data of Abramov Glacier from the 1970s to evaluate past firn conditions in this data sparse region. The current firn state is investigated based on a series of in situ measurements including firn cores and ground-penetrating radar measurements performed in 2018. We compare the legacy data with contemporary firn characteristics. Our results indicate a high year-to-year variability, but generally increasing net accumulation during the last 60 years on Abramov Glacier, with 0.84 ± 0.22 m w.e. for 2011–18 compared to 0.68 ± 0.32 m w.e. for 1965–72 and 0.59 ± 0.22 m w.e. for 1970–97. These results from in situ data provide ground truth for the data-sparse western HMA.

Introduction

The firn cover of mountain glaciers is expected to undergo changes related to global warming. Net accumulation rates derived from firn cores provide information on climatic conditions in the accumulation area of glaciers (Schwikowski and others, 2013) and represent amount of solid precipitation (Sold and others, 2015). Melt conditions at the glacier surface produce meltwater, which percolates through the firn column and may build ice lenses when refreezing within the firn column (Benson, 1996). Changes in firn stratigraphy may therefore reflect varying atmospheric conditions. Furthermore, firn temperatures reflect the short- and mid-term evolution of the energy balance at the glacier surface (Hoelzle and others, 2011). The repeated assessment of firn characteristics thus provides information about climate change, which is especially valuable for data sparse regions such as High Mountain Asia (HMA). Moreover, Mayer and others (2014) showed that in situ measurements from snow pits on a remotely located high elevation site can be related to more general meteorological information.

Processes within the firn are relevant for the overall behaviour of glaciers. Melt in the firn area affects the thermal regime of a glacier and consequently ice viscosity (Phillips and others, 2010; Lüthi and others, 2015) which in turn affects ice dynamics (Ryser and others, 2013). Firn processes influence the glacier mass balance, which is a key parameter in detecting global warming trends. Meltwater retention in firn can either attenuate (Haeberli and Alean, 1985; Suter and others, 2004; Cox and others, 2015) or promote glacier mass loss (Braithwaite and others, 1994; Machguth and others, 2016). A steepening of mass-balance gradients (Dyurgerov and Dwyer, 2001) is likely to be reflected in firn changes. Firn in situ data are an asset to understand the behaviour of mountain glaciers.

Uncertainties in glacier mass-balance estimates are often related to poorly constrained firn processes. For example, Digital Elevation Models (DEMs) used for volume change calculations are prone to errors in the accumulation area (e.g. Kronenberg and others, 2016; Gardelle and others, 2012). This is principally because volume changes are converted into a mass change by the use of a single conversion factor which, in reality, varies with firn extent and density (Huss, 2013).

Several studies have investigated firn on mountain glaciers (e.g. Zagorodnov and Zotikov, 1980; Hoelzle and others, 2011; Zdanowicz and others, 2012; Bezeau and others, 2013; Marchenko and others, 2017; Vincent and others, 2020). However, available firn studies mainly focus on glaciers located in the Arctic and the Alps. In the context of this regional bias, legacy firn investigations performed on two remotely located mountain glaciers in Central Asia in the 1960s and 1970s are of great importance (Dikikh, 1965; Kislov, 1977, 1982). On Gregoriev Ice Cap located in the Inner Tien Shan, firn investigations have been repeated several times and observed changes include an ongoing increase of englacial

cambridge.org/jog

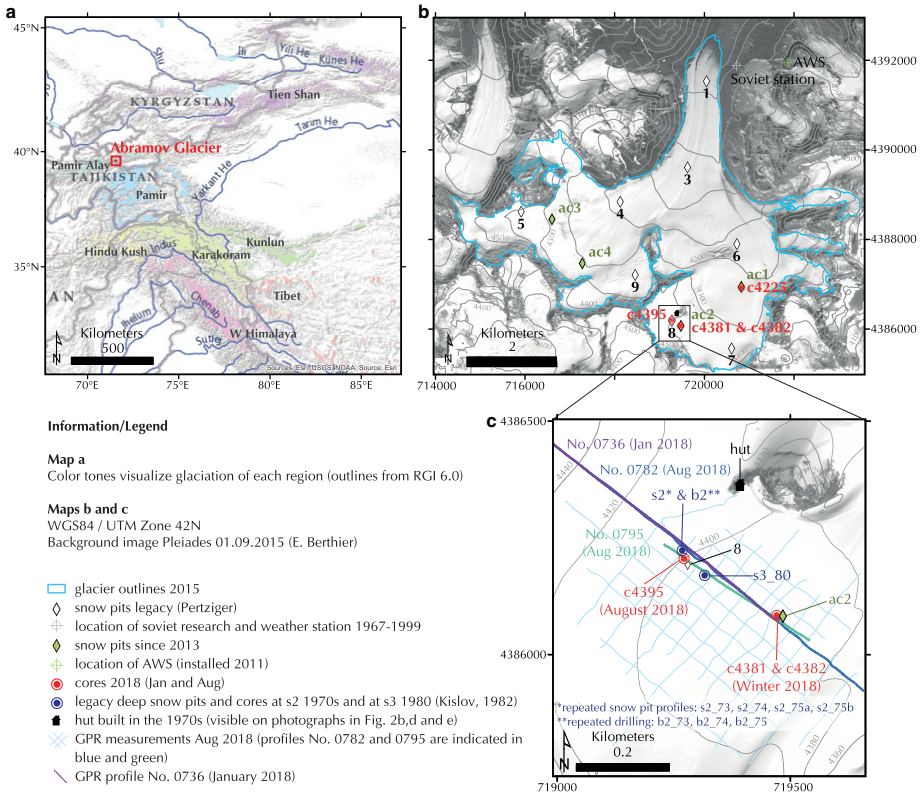

Fig. 1. (a) Overview map showing the location of Abramov Glacier in the Pamir Alay (indicated in red). (b) Map of Abramov Glacier showing the legacy and current observation network. (c) Zoom to main investigation area in the orographic right accumulation area of Abramov Glacier.

temperatures from 1962 to 2003 (Thompson and others, 1997; Kutuzov, 2005). The second firn study site is Abramov Glacier located in the Pamir Alay (Fig. 1). The firn measurements on Abramov Glacier, carried out during the 1970s by Soviet research programmes, have never been repeated.

Central Asian mountain ranges including the Tien Shan, Pamir and Pamir Alay are strongly underrepresented within world-wide glacier monitoring activities (WGMS, 2017). Due to the lack of in situ measurements, glacier mass changes are mainly assessed by remote-sensing studies (e.g. Gardelle and others, 2013; Holzer and others, 2015). In the recent past, close-to-balance region-wide mass budgets were found for the Pamir and Pamir Alay (Brun and others, 2017; Shean and others, 2020). The same conclusion was reached by an investigation of changes of the snowline altitude in the Pamir from 1998 to 2013 (Zhang and Kang, 2017). Other regions of HMA such as the Himalaya have recently undergone accelerations in mass loss (Maurer and others, 2019). The reasons for the mass-balance anomaly in the western HMA are far from being completely understood (Farinotti and others, 2020). An accumulation increase related to an increase of solid precipitation has been suggested as a potential driver for the anomaly (e.g. Yao and others, 2012). However, uncertainties in precipitation trends are high as precipitation gauge measurements are sparse (Unger-Shayesteh and others, 2013) and prone to measurement errors when performed in alpine environments (Rasmussen and others, 2012). Due to the shortage of in situ mass-balance observations for the regions, remotely sensed mass-balance estimates lack validation data. Furthermore, in situ measurements generally centre on the ablation area which may lead to large uncertainties in glaciological mass balances over the accumulation area (Sold and others, 2016). Complementary accumulation and firn investigations may help to address such uncertainties and to improve our understanding of accumulation area processes. Very few recent investigations focus on the accumulation area of glaciers located in the vicinity of the so-called mass-balance anomaly of HMA. Lambrecht and others (2018) assess the elevation change of the upper Fedchenko Glacier, Western Pamir combining in situ and remote-sensing data. The recent accumulation history of the same glacier is reconstructed based on GPR data and the analysis of snow and firn samples in Lambrecht and others (2020). Their results for 2008–2015 indicate relatively stable accumulation conditions compared to the results for 2002–2005 by Aizen and others (2009). Moreover, firn cores were drilled on Inilchek Glacier, Central Tien Shan to investigate atmospheric circulation patterns at the end of the 1990s and beginning of 2000s (Aizen and others, 2004, 2006).

To date, the lack of observations for the western HMA has prevented comprehensive assessment of possible changes in accumulation regimes within the region. Historical firn investigations performed on Abramov Glacier, Pamir Alay (Figs 1b and c) in the 1970s provide a unique dataset of past firn characteristics

and accumulation rates. This dataset, however, has not been evaluated so far. Several studies provide mass-balance estimates for Abramov Glacier: Barandun and others (2015) re-analysed almost five decades of mass-balance data of Abramov Glacier (including data previously published in Pertziger (1996)) and found an overall negative mass balance of -0.44 ± 0.10 m w.e. a^{-1} for the period from 1968 to 2014 with increasing melt rates on the glacier tongue. Their results of -0.51 ± 0.17 m w.e. a^{-1} for 2000–11 disagree with the geodetic mass balance of -0.03 ± 0.14 m w.e. a^{-1} for the same period (Gardelle and others, 2013). Denzinger and others (in press) computed a geodetic mass balance of -0.38 ± 0.12 m w.e. a^{-1} for 1975–2015 and their results indicate that the mass loss of Abramov Glacier has not accelerated recently.

Here, we present a reassessment of the legacy firn data in the context of new measurements. The aims of our study are:

- to determine current accumulation rates, firn stratigraphy and density profiles by drilling new cores at the same location as the measurements made in the 1970s,
- to quantify changes in firn characteristics and accumulation rates at the drill site.

Study site and field data

Abramov Glacier

Abramov Glacier (39.50°N, 71.55° E) is a north oriented valley-type glacier located in the Pamir Alay (north-western Pamir) in Central Asia (Fig. 1). Abramov Glacier is 24 km^2 in surface area and spans an elevation range of 3650–5000 m a.s.l. (in 2015).

Legacy data

Glaciological investigations on Abramov Glacier started during Soviet times in 1967, when the Central Asian Hydrometeorological Institute (SANIGMI) built a research station next to the glacier tongue. Until 1999, SANIGMI operated a meteorological station and maintained a dense network of mass-balance point observations at a monthly time scale. During the 1970s, the investigators conducted a series of complementary measurements including firn studies using deep snow pits and boreholes (Kislov, 1982). Due to political instability, one of the most detailed and comprehensive mass-balance time series in HMA ended abruptly in 1999. In 2011, the mass-balance monitoring on Abramov Glacier was reinitiated and an automatic weather station was installed in vicinity of the glacier (Schöne and others, 2013; Hoelzle and others, 2017).

Monthly mass balance and meteorological data until 1994 are reported in Pertziger (1996). For this study, all measured mass balance and meteorological data until 1999 were provided by F. Pertziger. Mean annual air temperature recorded at the station at 3837 m a.s.l. (Fig. 1b; Soviet station) for the period 1968–1998 was −4.1°C and annual precipitation was 750 mm a^{-1} with maximum precipitation occurring from March to May (Pertziger, 1996). There was a strong vertical precipitation gradient of 1200 mm km^{-1} a^{-1} (Kislov, 1982). The glacier had a temperate accumulation zone (Kislov, 1977; Kislov and others, 1977*a*) and zones of water-saturated firn were observed (Kislov, 1982). The investigators measured water level changes in deep snow pits during the 1974 and 1975 melt seasons (Glazyrin and others, 1977; Kislov, 1982). In a 13 m deep snow pit, located at 4410 m a.s.l., observed water levels relative to the bottom of the pit varied from ~0.4 to 4.5 m. During the main melt season, water levels in the snow pit rose following a delay of 24–48 hours after days with high melt rates. Glazyrin and others (1977) concluded that the water level variability in the deep snow pit was a combined signal of the meltwater availability and the percolation characteristics of the firn surrounding the pit.

The legacy firn data consist of repeated firn density measurements and stratigraphy observations acquired in deep snow pits (the maximum depth of a reported profile from snow pit s2 was 22 m in June 1973) and data from nearby boreholes (drilled with a thermal drill; maximum depth reported was 106 m) (Suslov and Krenke, 1980; Kislov, 1982) (cf. Table 6 in Appendix A). In total, three deep snow pits which were kept open over the investigation years were investigated: s2 and s3 were located next to each other at ~4400 m a.s.l. (in vicinity of snow pit No. 8 shown in Figs 1b and c) and s1 at ~4250 m a.s.l. (in vicinity of snow pit ac1 shown in Fig. 1b). As s3 was abandoned shortly after its establishment (personal communication from F. Pertziger, 2018), only data from s1 and s2 are reported. Furthermore, there were six boreholes, of which three served to monitor englacial temperatures: b0_69 and b0_71 were situated in the ablation area and b1_72 in the vicinity of s1. The other three boreholes (b2_73, b2_74, b2_75) were located in vicinity of s2 (cf. Table 6 in Appendix A).

In this study, we mainly use data from deep snow pit s2 measured between 1973 and 1975. We primarily focus on data acquired in 1973 (b2_73), when the deep snow pit was excavated (as observations from the following years are expected to be affected by lateral effects related to the open pit). Accumulation measurements (mainly from snow pit No. 8 for 1969–99 and ac2 for 2013–18; Figs 1b and c) provide complementary information.

Firn core drilling 2018

To investigate recent firn conditions, we recovered three shallow cores from two sites in winter 2018 (Table 6 in Appendix A). C4225 is located at ac1, c4381 and c4382 are located ~10 m apart at ac2. C4381 was drilled with a FELICS-small (Fast Electromechanical Lightweight Ice Coring System) (Ginot and others, 2002) recovering cores of ~58 mm diameter. c4225 and c4382 were drilled with a KOVACS MarkII coring system recovering cores of ~90 mm diameter. The drill sites were chosen according to the location of recent mass-balance observations performed at ac1 (c4225) and ac2 (c4381 and 4382, Fig. 1b). When re-establishing the mass-balance monitoring network in 2011, the locations of ac1 and ac2 were chosen for annual accumulation measurements on the basis of legacy maps of historical firn investigations at s1 and s2, respectively. However, the analysis of data collected in winter 2018 and the assessment of complementary legacy information revealed that c4381 and c4382 were drilled ~240 m southeast of the original site of the historical firn studies (deep snow pits at s2, cores b2, snow pit No. 8). A fourth core (c4395) was therefore retrieved in August 2018 with a KOVACS MarkII coring system at the location of the historic measurements at s2 (Fig. 1 and Table 6 in Appendix A).

GPR measurements 2018

Spatially distributed subsurface information from the orographic right accumulation area of Abramov Glacier is available from a series of GPR profiles. Several GPR transects were recorded in January 2018 (Walther, 2018). Complementary GPR measurements were performed on 2 August 2018 (Fig. 1c). We used a Malå ProEx system with an 800 MHz shielded antenna to record GPR profiles with a total length of almost 9 km. We simultaneously recorded the position with a GPS receiver (accuracy of ~5 m). The measurements were performed along a ~30 m × ~30 m grid covering the area of the drill sites c4381, c4382 and c4395. The antenna was installed on a plastic sledge

and dragged by foot at a speed of ~2.5 km h^{-1}. With a sampling interval of 0.5 s, this corresponds to a trace spacing of ~0.3 m. The sampling frequency was set to 10.5 GHz and traces were stacked 16-fold.

Methods

We first describe the homogenisation of legacy data, then we outline the firn core analysis and dating of cores drilled in 2018. One core (c4382) was dated based on chemical analysis while the other cores were only analysed in the field. The third subsection describes our GPR processing approach. Subsequently we explain how we interpret the GPR data and in the context of 2018 firn cores to relate the different datasets. Finally, we explain how we use accumulation rates and other parameters to describe legacy and 2018 firn profiles.

Homogenisation of legacy data

The preparation of historical data involved (i) the determination of the location of historical investigations and (ii) the compilation of firn data into common formats to match recent observations.

Data from the legacy investigations on Abramov Glacier are published and archived with coordinates in a local coordinate system. For some data points, only elevation information is reported and approximate locations are available from schematic maps. Local coordinates are available for each snow pit shown in Figure 1b and 165 ablation stakes as well as for a series of benchmark locations, where tripods were permanently installed (personal communications from F. Pertziger, 2018 and A. Merkushkin, 2014). We used a Topcon differential GPS (DGPS) to measure the coordinates of several points located on peaks and crests surrounding the glacier. We selected three points, located on stable terrain, clearly assignable to benchmarks described by past investigators and distributed around the glacier, to perform a coordinate transformation using the Spatial Adjustment Toolbar (affine projection) in ArcGIS.

In contrast to the mass-balance monitoring points, no coordinates were reported for the firn investigation sites of Kislov (1982). Only elevation information is available. The corresponding symbols on legacy published maps provide only approximate (±500 m) locations of deep snow pits and boreholes. The deep snow pit s1 (cf. Table 6 in Appendix A) was located at an elevation of 4250 m a.s.l. next to the stake profiles connecting two legacy snow pits, approximately corresponding to ac1/c4225 (Fig. 1). The elevation of s2 (4410 m a.s.l., Table 6 in Appendix A) corresponds to the elevation reported for snow pit No. 8 (cf. Fig. 1b). According to F. Pertziger (personal communication, 2018), s2 was located in immediate vicinity of pit No. 8 and boreholes b2_73, b2_74 and b2_75 were drilled not more than 50 m away from pit No. 8. Kislov (1982) stated that the distance between the pit face of s2 and b2_73, b2_74 and b2_75 was 5, 8 and 14 m. Historical photographs provided by Y. Tarasov and A. Yakovlev allowed us to determine the location of the legacy measurement site of s2/pit No. 8. We used two pictures. One picture was taken between 1973 and 1975 and shows the firn drilling at ~4400 m a.s.l. (Fig. 2a). The second photograph shows snow pit No. 8 and was taken in the 1980s (Fig. 2b). In August 2018, these photographs allowed us to determine the locations where the historical images were photographed. At these sites we took new images with a 50 mm lens on a full frame (24 by 36 mm sensor) digital camera. This camera setup was chosen as ~50 mm focal length on 35 mm film is the most likely way the historical images were recorded. The new pictures are shown in Figures 2c and d and overlaid on the legacy pictures in Figures 2e and f. The skylines of legacy and new pictures match well (Figs 2e and f). The minor discrepancies are related to the lowering of the glacier surface of ~5 m as observable on Figures 2b, d and f. The location of the historical photographs could thus be reconstructed and we estimate the legacy drill/deep snow pit location to be within <50 m of the reconstructed photographer location.

We digitised legacy firn data from figures showing the visible stratigraphy, density, temperature and dust concentration profiles of deep pits and cores. In Kislov (1982), a series of terms were used to describe the firn stratigraphy, which we summarise into three classes. When using the class *snow* we refer to Kislov's 'seasonal snow', the class *firn* summarises 'medium-grained firn', 'coarse firn', 'firn' and 'contaminated firn', as well as 'firn with ice inclusions' and 'icy firn' (for both an ice content of 50% is plotted); and *ice* stands for 'ice layer with variable thickness', 'nodule/ice lens' and 'ice'. We only refer this simplified stratigraphy for further analysis as it is mainly based on the distinction between ice and firn, which is relatively objective.

Firn core analysis and dating

Cores c4381, c4225 and c4395 were analysed on site directly after drilling. We inspected the core stratigraphy visually and distinguished the following classes: *snow, firn, firn with ice* (amount of ice in %) and *ice*. We furthermore identified dust and visible cryoconite and took note of complementary information such as water saturated core segments. To determine the density profile, we used a steel saw to cut cores into segments of 20 cm length. We weighed the segments with a digital scale, measured the length and diameter of each sample and estimated the percentage of segment volume preserved (to account for defects caused by core catchers and/or uneven breaks).

Core c4382, excluding the uppermost 0.7 m (fresh snow), was stored in polyethylene bags in 0.4–0.7 m segments and shipped to Switzerland for chemical analysis. In a −20°C laboratory, the core segments were inspected visually and the stratigraphy was described using the same classes as for the cores analysed in the field. A picture was taken of each segment with a Nikon Coolpix 500V1.1 camera. Segment length, diameter and weight were recorded to calculate the segment density before removing outer core parts, potentially contaminated by the drilling and handling. Inner decontaminated parts were cut into samples with dimensions of ~80 mm × 18 mm × 18 mm using a modified band saw with stainless-steel blades, Teflon-covered tabletops and saw guides. For each of these inner samples, dimensions and weight were measured to calculate the sample density. Differences between densities determined for the whole core segments and the inner samples lie within ±10%, averages of both measurements were used for further calculations. Prior to analyses, samples were melted in individual pre-cleaned 50 ml plastic tubes under inert gas (N_2). We measured the concentration of major soluble cations and anions including ammonium (NH_4^+) by ion chromatography (Metrohm 850 Professional IC combined with an 872 Extension Module and an 858 Professional Sample Processor autosampler). The water stable isotopes δD and $\delta^{18}O$ were determined with a wavelength-scanned cavity ring down spectrometer (Picarro WS-CRDS, L2130-i Analyzer). Additionally, we measured black carbon (BC) concentrations with a single-particle soot photometer (SP2, Droplet Measurement Technologies).

Annual layers of c4382 are determined using the seasonality of the analysed species: NH_4^+, $\delta^{18}O$ and BC (all of them peaking in summer (Dansgaard, 1964; Eichler and others, 2000)) and visible dust layers. For each year, we identified one sample to obtain the depth of the annual horizon. The depth ranges between adjacent samples with increased chemical signals and/or the

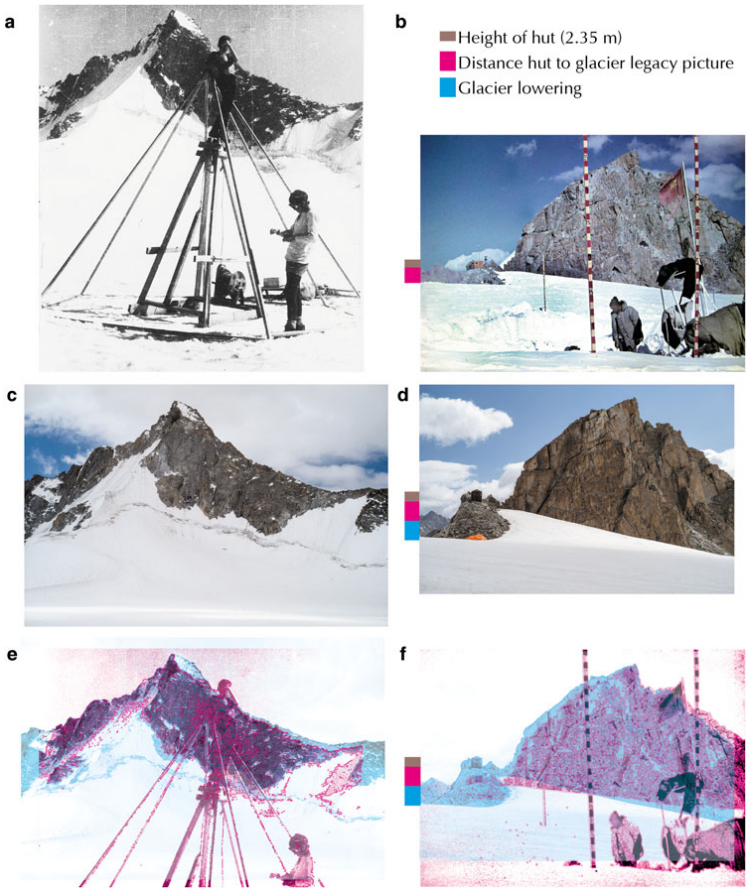

Fig. 2. Historical photographs of past investigations on Abramov Glacier. (a) Picture taken between 1973 and 1975, showing the core drilling at ~4400 m with a thermal drill (unknown photographer, picture provided by Y. Tarasov). (b) Picture from the 1980s showing regular mass-balance measurements at snow pit No. 8 (picture taken by Y. Tarasov and provided by the Centre of Hydrometeorological Service at Cabinet of Minister's of Republic of Uzbekistan (UZHYDROMET). In (c) and (d), pictures from the same locations taken in August 2018 are shown. In (e) and (f), the pictures taken in August 2018 (blue shading) are overlaid by the historical pictures (pink). A lowering of the glacier surface is visible when comparing pictures (b), (d) and (f) (indicated with blue bar to the left of the pictures).

occurrence of dust layers are interpreted as the uncertainty of the horizon depth $\sigma_{horizon}$.

Processing of GPR data

Several studies have used GPR measurements to quantify annual accumulation on temperate glaciers (e.g. Machguth and others, 2006; Sold and others, 2015). It is assumed that near the surface, each echo is produced by a single reflector (contrast in dielectric properties) and that these reflectors are ice lenses or other sharp density contrasts in the snowpack (Kohler and others, 1997). Such density contrasts usually result from ice layers and crusts, which form at the snow surface during summer months. The high net accumulation rates in the investigated area are expected to prevent closely spaced reflectors and therefore, the risk of interference between closely spaced echoes is assumed to be minimal and the identification of isochronous horizons possible (Miège and others, 2013).

To improve the visibility of reflectors and reduce noise we processed our GPR data following Sold and others (2013). In addition, a static correction was added to correct for the time delay of the first signal from the snow surface. We used the processing software ReflexW (Sandmeier Scientific Software). First, data are spatially interpolated to correct for varying walking speed. A linear interpolation is used to obtain traces with a regular distance of 0.5 m. Second, a frequency bandpass 500–1200 MHz is applied to filter low-frequency noise and high-frequency signal offset and bending. Third, a background removal subtracting the average from all traces in the profile reduces effects of signal ringing and the airwave. Fourth, the profile is corrected statically and fifth, we use a gain function (linear and exponential) to counteract the signal attenuation with depth.

The applied processing steps allow for the identification of a series of internal reflection horizons (IRHs) with maximum two-way travel times (TWT) of 100–165 ns, depending on the site. We identified up to seven IRHs, which are marked manually within ReflexW (cf. Fig. 3). As the IRH are continuous and clearly distinguishable, they are considered as annual layers. To extract annual accumulation layers, it is necessary that between the upper- and lowermost detected IRHs all other IRHs of summer surfaces are present and can be distinguished (Sold and others, 2015). Only considering the profile sections in which all seven IRHs are visible, the dataset is reduced to 1.9 km of GPR data. When looking at the four uppermost IRHs, 7.1 km of GPR data remain. When focussing on the uppermost reflector, which is interpreted as summer 2017, 0.5 km of GPR data need to be excluded because of some ambiguity in signal interpretation and 8.4 km are retained. The resulting dataset provides spatially distributed information about the subsurface across the study area for one to seven horizons.

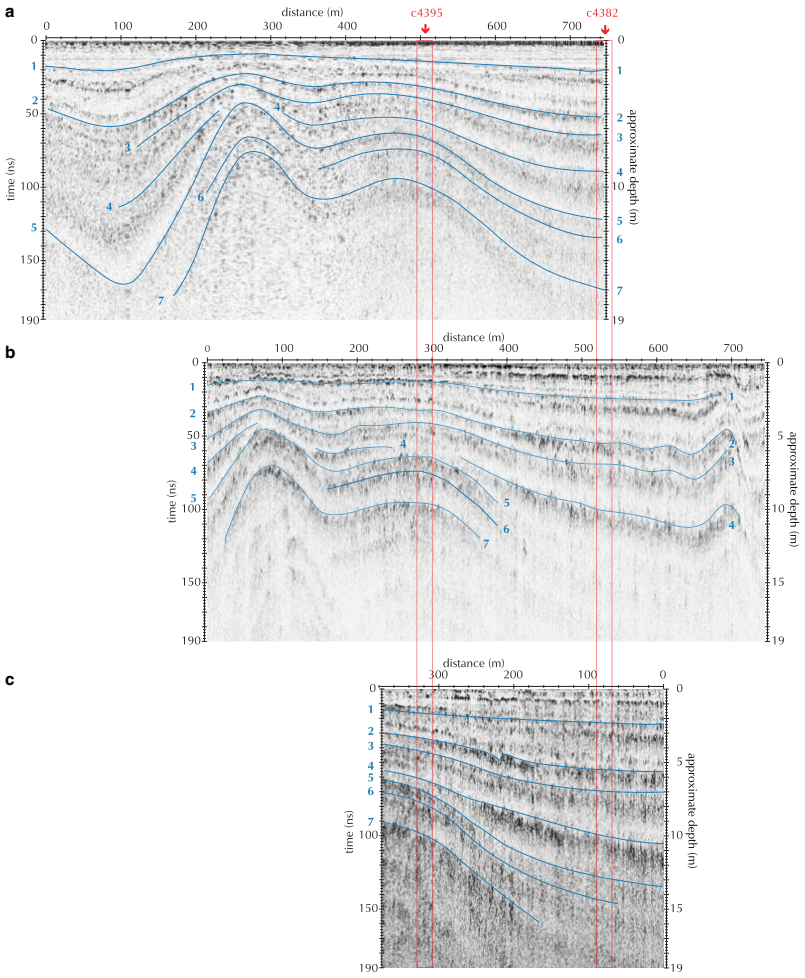

Fig. 3. Processed GPR transects No. 0736 (January 2018, a), No. 0782 (August 2018, b) and No. 0795 (August 2018, c) showing IRHs within the firn in the orographic right accumulation area of Abramov Glacier. The profiles are oriented from north-west to south-east (cf. Fig. 1c). Numbered blue lines highlight the identified IRHs 1–7. The firn coring sites are indicated. The TWT time was converted into approximate depths using an average radar wave velocity of 0.2 m ns^{-1}.

To evaluate the layer picking accuracy σ_{GPR}, the TWT at intersection points of radar transects are analysed. The average misfit of TWT picks averaged across all depths is 1 ns with lowest absolute misfits for the uppermost horizons. This corresponds to relative misfits between 0.2 and 3.2% for the different layers.

Interpretation of GPR data and in the context of 2018 firn cores

The GPR data are used to relate information from the dated core c4382 to the undated core c4395. For the interpretation of the GPR data measured in January and August 2018, we use complementary information from snow pit and core measurements including densities and firn stratigraphy. The measured density profiles ρ from cores c4381, c4382 and c4395 are used to obtain depth estimates from the radar data which are measured in the time domain. Therefore, we estimate the relative permittivity according to Frolov and Macheret (1999):

$$\varepsilon'_{\mathrm{d}} = (1 + 0.857 \times \rho)^2 \quad (1)$$

and then obtain the mean radar wave velocity u as follows:

$$u = c \times (\varepsilon'_{\mathrm{d}})^{-0.5}. \quad (2)$$

The radar wave velocities obtained for the different horizons based on averaged annual layer densities (ranging from $u_1 = 0.21$ m ns^{-1} to $u_7 = 0.19$ m ns^{-1}) for core c4382 were used to convert the TWT into depth at the drilling locations. An average radar wave velocity of $\overline{u} = 0.2$ m ns^{-1} was used to convert TWTs into approximate depths for visualisation in figures and a first interpretation. Subsequently, updated radar wave velocities for each IRH were used to definitely assign IRHs to the visible stratigraphy of c4382.

Based on the obtained depth estimates, we linked GPR transect No. 0736, recorded in January 2018 (Walther, 2018) to c4382

drilled during the same field campaign. Next, reflectors detected in the GPR data from August 2018 were allocated to reflectors in profile No. 0736 along the same transect (No. 0782, Figs 3 and 1c). The nearby located GPR transect No. 0795, which was measured in August 2018 and directly connects both drilling sites, was visually matched with the stratigraphy of c4395. This information along with a visual matching of the stratigraphies of both cores (c4382 and c4395) was used to transfer the layer dating to core c4395. In addition, we estimated the dry firn velocity for densities measured at c4395 to range between 0.21 and 0.20 m ns^{-1}.

Accumulation rate calculation

Net annual accumulation rates and related uncertainties were calculated for (i) legacy firn measurements at deep snow pit s2 from the 1970s, (ii) long-term glaciological measurements at snow pit No. 8 for 1969–99 and for (iii) firn cores c4381, c4382 and c4395 drilled in 2018.

Accumulation rates were calculated based on depths of annual horizons d_{horizon} and densities ρ. The uncertainties of the accumulation rates σ_{acc} are related to uncertainties in the reported/measured densities σ_ρ and horizon depths $\sigma_{horizon}$. The uncertainties σ_ρ and $\sigma_{horizon}$ were assumed to be independent and combined following Eqn (3) to obtain the accumulation rate uncertainty σ_{acc}. For averaged accumulation rates over several years, σ_{acc} was combined with the spread (standard error) of the annual accumulation rates:

$$\sigma_{\text{acc}} = \sqrt{d_{\text{horizon}}^2 \times \sigma_\rho^2 + \rho^2 \times \sigma_{\text{horizon}}^2} \tag{3}$$

For (i) the legacy firn measurements at deep snow pit s2, depth and density information were extracted from digitised figures. We assumed σ_ρ to be within 10% of values extracted from figures. The depth range between density and facies changes above and below annual layers assignments in digitised figures was interpreted as $\sigma_{horizon}$.

Data from snow pit No. 8 (ii), measured at the end of the ablation season in September, were used for assessing the long-term evolution of net accumulation from 1968–98. For 13 of these 31 years, only accumulation measurements performed at the end of the accumulation season in May are available. These values could not be directly compared to annual accumulation measured in cores or deep pits, which reflect net accumulation roughly over a hydrological year (autumn of year n to autumn of year $n+1$). We used a multiple linear regression with two predictors to estimate end of ablation season mass balance for all years. Predictor 1 was the net accumulation in w.e. measured in May of the corresponding year and predictor 2 was the positive degree day sum from June, July and August calculated from daily average temperatures measured at 3837 m a.s.l. which we extrapolated to 4410 m a.s.l. using the reported gradient of −5°C km^{-1} (Kislov, 1982). The multiple linear regression based on 18 observations yielded an R^2 of 0.83. The root mean square error between measured and extrapolated net accumulation for September is interpreted as the extrapolation uncertainty (σ_{extr} = 0.18 m w.e.). To estimate the uncertainties of measured net accumulation rates Eqn (3) is used. We adopted the values reported by Thibert and others (2008) to estimate σ_ρ and $\sigma_{horizon}$. σ_ρ was set to 5% of the measured density and $\sigma_{horizon}$ = 0.35 m. For the filled time series, σ_{extr} was added following the rules of Gaussian error propagation. For averaged accumulation rates over several years, we furthermore added the standard error of the annual accumulation rates to the error budget.

Annual net accumulation rates for cores drilled in 2018 (iii) were calculated based on determined layer depths and measured densities. For c4382, which was dated based on chemical measurements, the average density calculated from measured segment and sample densities was used (see section 'Firn core analysis and dating' for a description of these measurements). We determined $\sigma_{horizon}$ as described above. To estimate σ_ρ, we combined the uncertainties of the core segment density measurement (related to the variations in segment length (0.5 cm) and diameter (0.1 cm) and to the accuracy of the scale of 0.2 g) and the uncertainties of the sample density measurement (related to the accuracy of the scale of 0.2 g and measured sample dimensions of 0.05, 0.1 and 0.1 cm). A further source of uncertainty is related to the potential loss of core material when transporting the core to the lab. We found that the difference of the total length of the lab analysed c4382 and the estimated borehole depth was < 5% and therefore do not account for this in our uncertainty estimates.

For c4381 and c4395 accumulation rates were determined based on density measurements in the field and the transferred layer dating as described above for c4395. Uncertainties of the density measurements (σ_ρ) performed in the field (as for cores c4225, c4381 and c4395) are related to the accuracy of the scale (0.3 g), variations in core length (0.5 cm) and diameter (0.1 cm). Short-term changes of the segment weight due to the loss of water in the case of saturated segments (only core c4395 was affected) were not taken into account. It was not possible to measure the loss of water when retrieving the core of the borehole, and dripping from the wet cores was minimal. For both cores c4382 and c4395, the depth range between ice and dust layers above and below the identified summer horizon was interpreted as $\sigma_{horizon}$. For c4225 we did not calculate accumulation rates as we were not able to transfer the dating to this core.

Our uncertainty estimate does not account for general misinterpretations of the stratigraphy; instead, we use independent information from annual accumulation measurements to validate our interpretation. Furthermore, to reduce the impact of classification biases due to a subjective interpretation, the same observer logged the visible stratigraphy in the field and in the lab.

Firn profile metrics

In addition to net accumulation rates, we determined a series of further parameters namely (i) the simplified ice fraction, (ii) the average firn fraction density and (iii) the average thickness of annual net accumulation layers.

(i) The simplified ice fraction F_i is calculated to compare whether the ice content changed over time. We calculate the F_{i} of the different firn profiles following Koerner (1977) and Fisher and others (2012):

$$F_{\text{i}} = \frac{\sum T_{\text{i}}}{d} \times 100 \tag{4}$$

where F_{i} is a percentage calculated from the sum of the thickness of ice layers T_{i} divided by the total profile depth d. For the ice fraction F_{i}, only continuous ice lenses (i.e. continuous over the full width of the core) and ice layers (i.e. *ice*) are considered (firn layers with variable ice content i.e. *firn with ice* are ignored).

(ii) The average firn fraction density is the average density of the entire profile excluding the sections classified as *ice*.

(iii) The average thickness of annual net accumulation layers is independent from density measurements. This parameter therefore enables rough comparison of recent firn profiles to historical profiles for which density measurements are not available. For recent profiles, the thickness of dated annual net accumulation layers is averaged. For legacy profiles, the thickness of published annual net accumulation layers is averaged. We combined $\sigma_{horizon}$ and the standard error of the annual net accumulation thickness to estimate corresponding uncertainties.

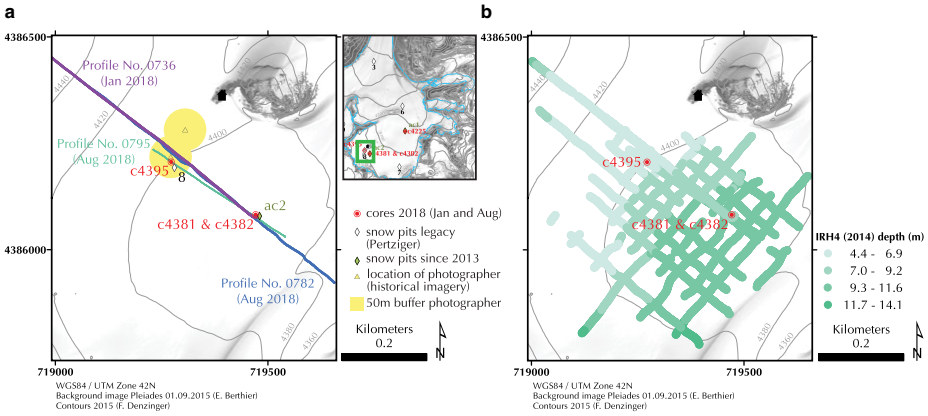

Fig. 4. (a) Map of the main study site located in the orographic right accumulation area of Abramov Glacier (see green box on the map in the upper right corner). The coordinates of recent firn profiles are indicated in red and the locations of legacy investigations based on coordinate transformation and photographer location are shown. The GPR transects shown in Figure 3 are also indicated. Map (b) shows the same area as shown in (a) and gives an overview of the accumulation heterogeneity in the investigation zone. Depth of IRH4 of the analysed GPR transects of the measurements performed in August 2018 are shown. The drill sites of recent cores are indicated with red circles.

Results

Location of historical firn measurements

According to the information available to us in January 2018, we believed that we were drilling c4381 and c4382 at the study site of the historical firn investigations performed in the 1970s. The subsequent analysis of GPR data revealed a subsurface heterogeneity in the orographic right accumulation area of Abramov Glacier. We therefore gathered additional data as described above. Based on these data the assessment of the location of the historical firn investigations was revised and an additional core (c4395) was drilled in August 2018.

The location of the historical firn investigation site is shown in Figure 4a. The map shows the very close vicinity of the legacy snow pit No. 8 (converted legacy coordinates) and the location of the photographer taking the drilling picture from the 1970s (picture displayed in Fig. 2a). The second historical photograph from the 1980s showing snow pit No. 8 (Fig. 2b) is ~70 m northwest from the converted coordinates of snow pit No. 8. The site identified by the coordinate conversion and confirmed by the picture of the historical drilling in the 1970s was selected for the drilling of c4395. By chance, this site almost falls onto our previously recorded GPR profile No. 0736 (Fig. 4a).

Net accumulation rates determined in a recent core

The visible stratigraphy of c4382 is characterised by melt features including ice lenses and dust layers (Fig. 5a). The density profile shows strong fluctuations, but generally increases with depth. Highest densities occur coincident with lenses of bubble-poor ice. Dust layers are sometimes, but not always, accompanied by ice lenses. Moreover, dust layers generally coincide with peaks of one or several of the following analysed species: BC, NH_4^+ and $\delta^{18}O$ (Fig. 5b). These peaks are interpreted as annual summer horizons. The respective depths are listed in Table 1 and the uncertainty range of each horizon is indicated with grey shading in Figure 5. Summers 2017, 2016 and 2015 correspond to clear peaks of BC, NH_4^+ and $\delta^{18}O$ and a visible dust layer occurs at each corresponding depth. For summers 2014 and 2013, the BC and NH_4^+ signals are high and peaks coincide with dust layers, whereas the $\delta^{18}O$ signal is strongly smoothed. Summers 2012 and 2011 can be linked to peaks in BC and $\delta^{18}O$. Ice lenses coincide with or occur slightly below dust layers for summers 2017, 2016, 2015, 2014 and 2011. No ice was identified close to the summer surface 2013 and densities are relatively low. Summer 2012 is marked with thin ice lenses. Three additional thick ice lenses are visible in the lower part of the core: a dust-ice layer was formed below the dust horizon of summer 2013 at a depth of 11.7 m, a thick ice lens was formed below the summer surface 2012 at a depth of 13.7 m and another below the summer surface 2011 at a depth of 16.0 m (indicated by black arrows in Fig. 5).

Based on the dated horizons, we determined net accumulation rates for each mass-balance year from 2011/12 to 2016/17 (Table 1). The average net accumulation rate for 2011/12–2016/17 was 1.45 ± 0.34 m w.e. Minimum net accumulation of 1.09 ± 0.12 m w.e. occurred in 2015/16 and accumulation was largest in 2011/12 with 2.03 ± 0.18 m w.e.

Spatial distribution of accumulation

The spatial distribution of accumulation can be derived from GPR data. The information available for c4382 provides local reference information. The detected IRHs are linked to the visible stratigraphy of this core (Table 2). For the four most recent summer surfaces (2014–17), IRHs can be identified and followed throughout the investigated area. In the GPR data from summer 2018, three subjacent IRHs are visible only in the north-western part of the investigated area, where they are located at shallower depths. IRH5, IRH6 and IRH7 are linked to the dated core c4382 using GPR profile No. 0736 acquired in January 2018 (Walther, 2018). In transect No. 0736, IRH5–IRH7 are also visible at lower depths around c4382 (Fig. 3a). IRH5 is attributed to the ice lens below the dust layer of summer 2013 (at 11.7 m in c4382). IRH6 is matched with the ice lens of summer 2012 at 12.5 m depth in c4382. IRH7 matches with the ice lens located just below the dust layer of summer 2011 at a depth of 16 m (Fig. 5). Depth discrepancies between the values given in Table 2 and visible from Figure 3 are due to the constant radar wave velocity used for plotting the figure.

Although the core analysis provides accurate knowledge of accumulation rates at point scale, the GPR measurements indicate that accumulation in the investigated area of Abramov Glacier varies strongly in space. Layer thickness generally increases

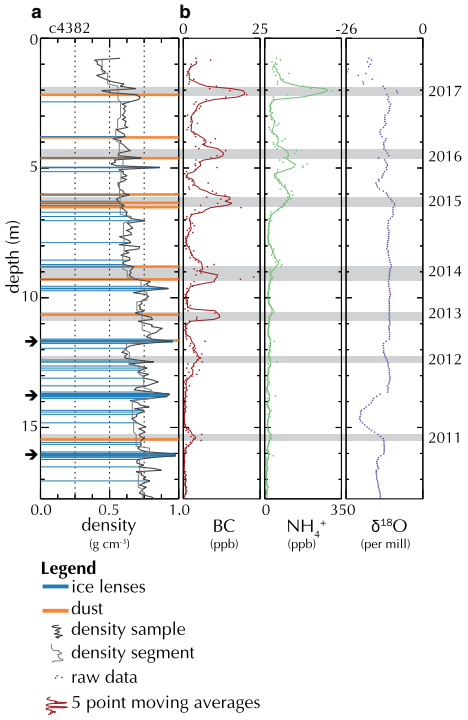

Fig. 5. Firn characteristics and chemical records of c4382 drilled at 4381 m a.s.l. on Abramov Glacier in February 2018. Plot (a) shows the firn stratigraphy (ice lenses in blue; visible dust layers in orange) and density profile (density from core segments in grey and sample densities in black). Measured BC, ammonium (NH_4^+) and $\delta^{18}O$ records are plotted as lines (five point moving averages for BC and NH_4^+, raw data for $\delta^{18}O$) under (b). The uncertainty range of identified summer horizons is shaded grey and labelled with their respective year. Arrows indicate additional ice lenses between summer surfaces. The uppermost 0.7 m of the core were not analysed.

Table 1. Depths of annual horizons and net accumulation rates c_{net} obtained from the dated core c4382

Horizon	Depth m	Mass-balance year	c_{net} m w.e.
2017	2.1	2017/18	n.a.
2016	4.4	2016/17	1.37 ± 0.14
2015	6.3	2015/16	1.09 ± 0.12
2014	9.1	2014/15	1.71 ± 0.19
2013	10.7	2013/14	1.19 ± 0.17
2012	12.5	2012/13	1.31 ± 0.13
2011	15.3	2011/12	2.03 ± 0.18
Average		2011/12–2016/17	1.45 ± 0.34

from the north-east towards the south-west of the studied zone (Fig. 4b). In the north-western part, where layers are shallower, three more layers (IRH5–IRH7) can be identified and allow the accumulation distribution to be tracked back to 2011 (IRH7 in Table 2). Total thickness of the accumulation of seven years (2011/12–2017/18) varies from ~7 m to more than ~16 m.

Linking accumulation rates between two drill sites

Of the cores drilled in 2018, only c4382 was shipped to Switzerland and dated based on analysed chemical species. Core

Table 2. Overview of picked IRHs in the GPR profiles acquired in August 2018. IRH1 to 7 are linked to the visible stratigraphy of core c4382 (Fig. 5). Depth refers to the horizon depth at core c4382. For IRH5, IRH6 and IRH7 a complementary GPR profile (No. 0736) measured in January 2018 was used to compare IRHs with c4382. Length refers to the total length of GPR transects where the corresponding horizon and the ones above were identified

IRH	Summer	Depth m	Length km	Comment
1	2017	2.1	8.4	
2	2016[a]	5.0	8.0	
3	2015	6.3	7.8	
4	2014[b]	8.8	7.1	
5	2013[c]	11.7	2.8	Profile No. 0736
6	2012	12.5	2.0	Profile No. 0736
7	2011[d]	16.0	1.9	Profile No. 0736

[a]Ice lens below 2016 dust horizon.
[b]Upper edge 2014 dust horizon.
[c]Ice lens below 2013 dust horizon.
[d]Ice lens below 2011 dust horizon.

c4382 was used to cross-date the later drilled c4395. Core c4395 drilled ~240 m northwest of c4382 is characterised by a higher ice content and higher densities than c4382 (Table 3 and Fig. 6). Furthermore, when drilling c4395 in August 2018, we retrieved firn segments with visible liquid water at depths of 8.5–10 m and between 12.1 and 18.4 m, corresponding to 40% of the profile length. Between the two sections with visible liquid water content, drilled firn segments appeared dry. Core c4382 and all other cores drilled in winter 2018 appeared dry.

Comparing the visible stratigraphy of both cores, the layers in c4395 seem to be compressed indicating reduced net accumulation rates compared to the site of c4382. This is confirmed by spatial distribution of IRHs shown in Figures 3 and 4b. Core c4395 lies in a zone with shallow depths of reflectors where also the lowermost two IRHs were visible in the GPR profiles acquired in summer 2018. In c4395, the summer horizon 2011 corresponds to a depth of 9.5 m. Annual net accumulation rates 2011/12–17/18, calculated based on the transferred layer dating and locally measured densities, are 0.84 ± 0.22 m w.e. a^{-1} at c4395. Annual accumulation rates are listed in Table 4.

We furthermore evaluate the GPR picks of IRH7 within 50 m of c4395 and find an average depth of 9.9 m and a standard deviation of 0.7 m ($u = 0.19$ m ns^{-1} locally calibrated at c4395, see Appendix C) which is somewhat larger than the depth of IRH7 at c4395. The respective minimum and maximum depths of IRH7 within this radius were 8.7 m and 11.6 m ($u = 0.19$ m ns^{-1}). We use these depths and the average density of c4395 for 2011/12–17/18 (620 kg m^{-3}) to calculate minimum and maximum annual net accumulation rates for 2011/12–17/18 within the 50 m radius and obtain 0.77 and 1.0 m w.e. a^{-1}.

Comparison of recent and legacy firn profiles

In the following, we analyse core c4395 drilled in summer 2018 together with repeated firn observations from the same location from the 1970s. First, we compare the visible stratigraphy, core metrics and accumulation rates of c4395 with measurements at s2_73 from 1973. Then, the comparison is extended to legacy measurements from following years at the same location (s2_74 and s2_75b).

Figure 7 shows the stratigraphy and density profiles of c4395 compared to the legacy firn profiles measured at the same site in 1973 (s2_73). Both profiles are water-saturated in the lower part. Whereas s2_73 is characterised by more ice lenses, c4395 has a higher abundance of firn with variable ice contents. In both profiles, the density increases with depth. Overall densities

Table 3. Summary of analysed core characteristics for the entire core or respective segments as specified under *period* (dating is not always available for the entire profile length). *Depth* refers to the depth of the entire core, respectively to the depth range of the section considered (depth from surface at the corresponding investigation date). *Overall density* is the average density over the respective profile with the corresponding uncertainty (σ_ρ) and *ice fraction* is the relative ice content considering the core sections classified as *ice*. *Firn fraction density* refers to the density excluding segments classified as *ice*. *Accumulation thickness* refers to the average thickness of annual net accumulation layers with its uncertainty $\sigma_{horizon}$ and *accumulation rate* to the annual averaged net accumulation rates for the investigated periods and their corresponding uncertainties (σ_{acc}). Legacy measurements at s2 are listed first, the second part of the table contains data for the same location measured in 2018.

ID	Period	Depth m	Overall density kg m^{-3}	Ice fraction %	Firn fraction density kg m^{-3}	Accumulation thickness m a^{-1}	Accumulation rate m w.e. a^{-1}
s2_73	Entire profile	20.5	665 ± 66	38	565	n.a.	n.a.
		0–18.4	650 ± 65	30	565	n.a.	n.a.
	1965/66–1971/72	4.6–12	648 ± 65	25	580	1.06 ± 0.41	0.68 ± 0.32
s2_74	Entire profile	10	618 ± 62	21	553	n.a.	n.a.
	1965/66–1972/73	2.6–10	678 ± 68	28	605	0.92 ± 0.34	0.63 ± 0.30
	1965/66–1971/72	2.8–10	678 ± 68	28	606	1.03 ± 0.35	0.70 ± 0.31
s2_75b	Entire profile	7.7	704 ± 70	50	593	n.a.	n.a.
	1965/66–1974/75	0.2–7.7	710 ± 71	51	601	0.75 ± 0.33	0.51 ± 0.29
	1965/66–1971/72	0.5–7.7	714 ± 71	51	611	1.03 ± 0.38	0.73 ± 0.34
b2_73	Entire profile	50.7	n.a.	80	n.a.	1.01 ± 0.15	n.a.
c4395	Entire core	18.4	724 ± 45	21	692	n.a.	n.a.
	2011/12–2017/18	0–9.5	620 ± 37	18	595	1.36 ± 0.24	0.84 ± 0.22
	2011/12–2016/17	1.8–9.5	653 ± 39	15	625	1.28 ± 0.26	0.83 ± 0.23
c4381	Entire core	17.0	586 ± 46	7	571	n.a.	n.a.
	2011/12–2016/17	2.1–15.5	612 ± 47	6	605	2.24 ± 0.09	1.37 ± 0.30
c4225	Entire core	12.1	640 ± 42	30	559	n.a.	n.a.
c4382	Entire core	17.7	642 ± 57	7	634	n.a.	n.a.
	2011/12–2016/17	2.1–15.3	661 ± 58	7	654	2.19 ± 0.04	1.45 ± 0.34

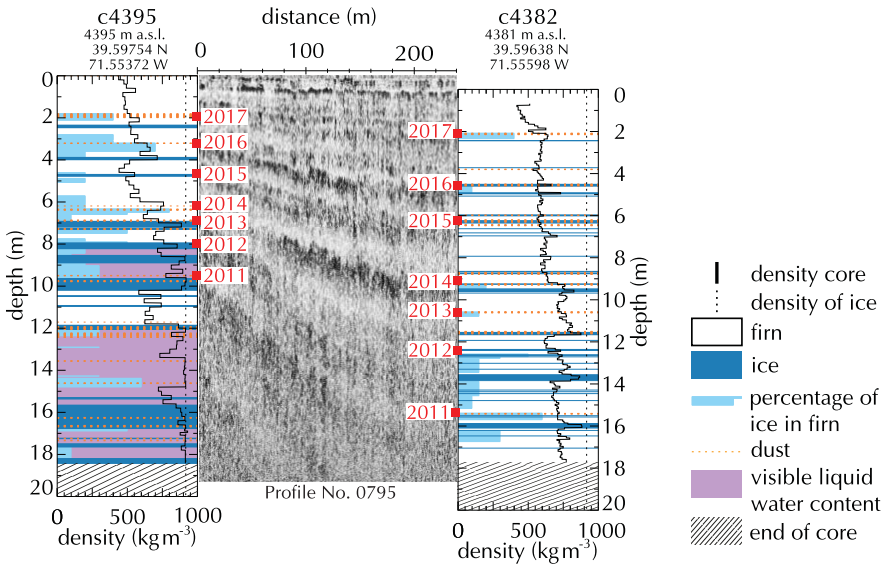

Fig. 6. Connection of information from two recent firn profiles on Abramov Glacier. The firn stratigraphy observed in the dated c4382 (drilled in February 2018, left profile) is linked to the stratigraphy of c4395 (drilled in August 2018, right profile) using a connecting GPR transect (No. 0795) from August 2018

as well as firn fraction densities (excluding layers classified as *ice*) down to a depth of 18 m are higher for profile c4395, whereas the calculated ice fraction is lower for the recent profile (Table 3). Net accumulation rates at s2_73 were 0.68 ± 0.32 m w.e. a^{-1} for 1965/66-–1971/72, whereas a net accumulation of 0.84 ± 0.22 m w.e. a^{-1} is found for 2011/12–2017/18 at c4395.

Measurements at s2 were repeated in the two following years. The measurements from 1974 and 1975 are summarised in Table 3. For comparison, the different values are given for core sections without seasonal snow (1965/66–1971/72 for legacy profiles s2_73, s2_74 and s2_75b and 2011/12–2016/17 for c4395). For s2_73 and the period 1965/66–1971/72, overall density is 648 ± 65 kg m^{-3} which is similar to 653 ± 39 kg m^{-3} for c4395 (2011/12–2016/17). For the corresponding core sections (without fresh snow), the ice fraction remains higher and the firn fraction density lower for s2_73 compared to c4395. The firn fraction

Table 4. Depths of annual horizons and net accumulation rates c_{net} obtained from core c4395

Horizon	Depth m	Mass-balance year	c_{net} m w.e.
2017	1.8	2017/18	0.89 ± 0.21
2016	3.2	2016/17	0.76 ± 0.34
2015	4.6	2015/16	0.80 ± 0.40
2014	6.2	2014/15	0.90 ± 0.30
2013	6.9	2013/14	0.49 ± 0.30
2012	8.0	2012/13	0.78 ± 0.45
2011	9.5	2011/12	1.27 ± 0.54
Average		2011/12–2016/17	0.83 ± 0.23
Average		2011/12–2017/18	0.84 ± 0.22

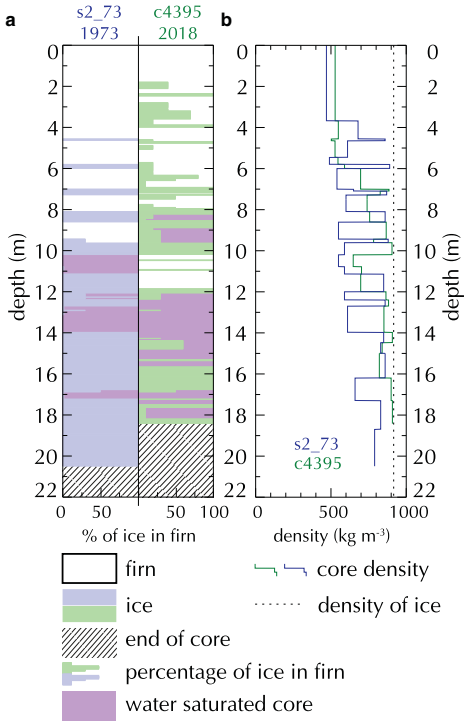

Fig. 7. Comparison of 1973 to 2018 firn stratigraphy. Legacy firn characteristics measured on Abramov Glacier at s2_73 in June 1973 (digitised from Kislov (1982)) (blue) and current firn characteristics measured at c4395 drilled in August 2018 (green). The depth axes refer to the depth from surface at the corresponding investigation date. (a) Visible stratigraphy of both profiles including ice lenses, and firn with variable ice content (percentage of ice in firn) and visible liquid water content. (b) Measured densities for homogenised depth sections for both profiles.

densities and overall densities as well as the ice fraction increase from 1973 to 1975. Overall densities are somewhat higher for legacy profiles s2_74 and s2_75b than for c4395 and firn fraction densities are approaching values of firn fraction densities observed for c4395. Comparably high ice contents were reported for s2_74 and especially for s2_75b (1965/66–1971/72).

Long-term changes of net accumulation rates

Average net accumulation rates determined from the 1970s for legacy profiles s2_73, s2_74 and s2_75b are lower than values determined for recent years at c4395, but the differences lie within the estimated uncertainties. In Figure 8 and Table 5 the annual net accumulation rates determined for s2_73 and c4395 are compared to averaged net accumulation rates measured at snow pit No. 8. Accumulation was not measured between 1998 and 2011. Net accumulation rates measured at snow pit No. 8 show an increase over time and highest values were measured for 2011/12–2017/18. We found a significant increasing trend ($p = 0.006$). Including the net accumulation rates measured at s2_73, which were higher than early measurements at snow pit No. 8, the increase remains significant ($p = 0.04$).

Discussion

Spatial and temporal representativeness of measurements and implications

Repeated melt and refreezing took place at the drilling site (e.g. ice lenses in Fig. 5). These processes can also cause relocation of chemical species. Typically, NH_4^+ and $\delta^{18}O$ are less affected by meltwater re-distribution in firn compared to other chemical species (see e.g. Eichler and others, 2001; Trachsel and others, 2019). Preserved seasonality for BC has been shown in a temperate glacier (Pavlova and others, 2015). Thus, accumulation rates could be determined for c4382 based on NH_4^+, $\delta^{18}O$ and BC seasonality as well as on visible dust layers. The comparison of the net accumulation rates determined for c4382 to annual snow pit measurements at ac2 is shown and discussed in Appendix B.

The localisation of the historical investigation site is fundamental to our comparisons. Thanks to the use of two independent inputs consisting of (i) transformed legacy coordinates and (ii) a picture showing the drilling of b2 in the 1970s (Figs 2b, d and f), uncertainties related to the location could be reduced. Core c4395 was drilled within a distance of maximum 50 m from the legacy investigations at s2. GPR profiles around c4395 show that layer depths do not vary substantially within this distance as also visible from IRH4 in Figure 4b. The assessment of IRH7 within the 50 m radius shows that (i) the average depth of IRH7 is deeper than directly at c4395 and (ii) annual net accumulation rates remain somewhat above legacy values even if the most shallow layer picks of IRH7 are used for calculation. Furthermore, comparison of firn characteristics from different profiles acquired within ~10 m distance (c4381 and c4382, not shown) reveals that the stratigraphies are representative at a local scale. Despite the investigation of manifold data, there are uncertainties related to the spatial representativeness of our comparison. The found increase of net accumulation, however, is in line with the glacier-wide mass-balance estimates by Barandun and others (2015). They showed that since the 1970s net mass balance has become more positive in the accumulation area, whereas melt rates have increased in the ablation area.

The visible firn stratigraphy is not only affected by the observer but by the classification system in general. Whereas a single observer and a consistent system were used for current firn conditions, legacy data was collected in a separate setup. An important difference is the sample size considered for the stratigraphic interpretation. We analysed cores of a few centimetres in diameters while in the 1970s the stratigraphy was described for an ~1 m wide wall of a deep snow pit. Some of the observed differences between s2_73 and c4395 (more ice lenses/less firn with variable ice content in the past) may to some extent be related to different classification systems.

Net accumulation rates derived from firn cores and deep snow pits represent the climatic mass balance including internal accumulation from refreezing below the last summer horizon for the uppermost years and partially account for refreezing for subjacent annual horizons. However, net accumulation rates derived from

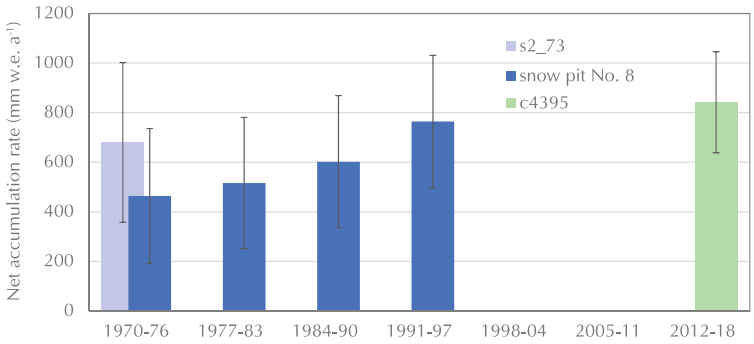

Fig. 8. Long-term net accumulation rates measured in the orographic right accumulation area Abramov Glacier at ~4400 m a.s.l. Annual net accumulation rates are averaged over seven mass-balance years. Averaged annual net accumulation for 1965/66–1971/72 determined from firn profile s2_73 (Kislov, 1982) (light blue). Annual net accumulation measured at snow pit No. 8 in September (provided by F. Pertziger and partly published in Pertziger (1996)) (blue). Averaged annual net accumulation for 2011/12–2017/18 determined from c4395 (green). Error bars refer to calculated uncertainties. Periods refer to time ranges of seven mass-balance years ('1970–76' refers to the period from 1969/70 to 1975/76).

Table 5. Net accumulation rates obtained from snow pit No. 8 averaged over seven mass-balance years compared to net accumulation rates from s2_73 and c4395

Period	Accumulation m w.e.	Measurement site
1965/66–71/72	0.68 ± 0.32	s2_73
1969/70–75/76	0.46 ± 0.27	Snow pit No. 8
1976/77–82/83	0.52 ± 0.27	Snow pit No. 8
1983/84–89/90	0.60 ± 0.27	Snow pit No. 8
1990/91–96/97	0.76 ± 0.27	Snow pit No. 8
1969/70–96/97	0.59 ± 0.22	Snow pit No. 8
2011/12–17/18	0.84 ± 0.22	c4395

snow pit No. 8 (and also ac2) only account for the surface mass balance. Figure 8 thus shows slightly overestimated accumulation rates for the periods 1965/66–1971/72 and 2011/12-2017/18. However, this overestimation is relatively small as only refreezing of the uppermost year of each firn profile is fully accounted for. According to Suslov and Krenke (1980), 90–93% of refreezing takes place in the uppermost 6 m of the firn column (excluding the seasonal snow pack). This means that the accumulation rates estimated for c4395 (2011/12–2017/18 down to a depth of 9.5 m) only include the entire internal accumulation for 2017/18 and reduced shares for the subjacent horizons. Therefore, the contribution of internal accumulation to net accumulation rates determined in firn profiles remains negligible for the comparison presented in Figure 8.

Data from the repeated historical investigations including overall density, firn fraction density and ice fraction at deep pit s2 (s2_73, s2_74, s3_75b in Table 3) highlight that the firn profiles at ~4400 m a.s.l. are affected by annual melt conditions. For s2_75b measured in October 1975, after a summer of extraordinary melt, overall density, firn fraction density and ice fraction are higher than for profiles s2_73 and s_74 (measured in June). Also the recent data indicate a year-to-year variation with net accumulation rates varying between 1.27 ± 0.54 and 0.49 ± 0.3 m w.e. with most positive net accumulation observed for 2011/12 (Table 4). Despite these year-to-year variations, the recent investigations are assumed to be representative for present conditions. Since the re-initialisation of mass-balance measurements on Abramov Glacier in 2011, positive net mass balances have been observed at ~4400 m a.s.l. Even if surface melt continued after the drilling of c4395 in August 2018, further refreezing and a corresponding increase in ice fraction and firn density is hampered by the fact that subsurface temperatures were already at the melting point in August 2018. The substantial data gap after the cessation of the Soviet monitoring activities reduces the temporal representativeness of the presented net accumulation time series. Based on the available data it is not possible to determine whether accumulation conditions at the investigation site have been stable since the 1990s, when net accumulation rates were similar to today's values.

Discussion of firn observations and underlying processes

There has not been a substantial change of the firn cover at ~4400 m a.s.l. on Abramov Glacier. The densities observed in 2018 remain similar to legacy values, the visible stratigraphy of c4395 and s2_73 look comparable and liquid water was observed in both firn columns. Today's ice fraction, however, is lower than the values observed in the 1970s. Furthermore, we find an increase of net accumulation rates. The decrease in ice fraction may be related to the increase of snow and firn volume with today thicker seasonal snow packs insulating the subsurface from the winter cold, thereby reducing the cold content available to refreeze meltwater. Today, melt conditions are abundant at ~4400 m a.s.l. as evident from melt features within firn cores and the persistence of firn with visible liquid water content. As described above, it is also possible that apparent differences in ice fraction may be caused to some extent by differences in classification systems and related uncertainties.

The presence of liquid water within the firn column during the melt season indicates that surface melt and subsurface water storage are lasting processes in the accumulation area of Abramov Glacier. In core c4395, we observed liquid water above and below firn segments which appeared dry (Figs 6 and 7). An ice layer at 10 m depth seemed to prevent further downward percolation of water. It is possible that the water trapped below the ice layer was transported there by lateral percolation. The reduced visibility of GPR signals at depths below ~10 m in profiles measured during summer 2018 compared to profile No. 0736 from January 2018 is possibly linked to seasonal fluctuations in firn water content (Fig. 3). Appendix B contains further discussion of the impact of firn water content upon GPR measurements. Investigations in the 1970s showed that the subsurface water table fluctuates in response to surface melt, but it was also observed that liquid water occurred below ice layers (Glazyrin

and others, 1977; Kislov, 1982). Based on this observation, Kislov (1982) interpreted that subsurface water was also present during winter. Furthermore, both studies explained the presence of water below ice lenses with water transport through crevasses, locally thinner ice lenses and horizontal flow.

Although the differences of net accumulation rates at c4395 compared to s2_73 lie within calculated uncertainties, a recent increase of net accumulation rates at ~4400 m a.s.l. is significant when data measured at snow pit No. 8 from 1969 1997 are considered (Fig. 8 and Table 5). We also note that the long-term average thickness of annual net accumulation layers 1923–73 derived by dust layer counting for b2_73 was ~1 m a^{-1} (Kislov and Nozdrukhin, 1975). Current average thickness of annual net accumulation is 1.3 times higher than this long-term value (Table 3). This even indicates that current amounts of precipitation are above long-term averages of the 20th century. According to snow pit No. 8 (Fig. 8 and Table 5), accumulation rates were lowest in the 1970s and 1980s when the glacier wide mass balance was also very negative (Barandun and others, 2015).

According to regional trends from the gridded data product Climatic Research Unit TS 4.01 for 1950–2016, air temperatures in Central Asia continued to increase after the 1970s and 1980s (Haag and others, 2019). In the context of increasing air temperatures, a recent increase of melt rates in the accumulation area of Abramov Glacier is likely. The observed net accumulation increase might thus only partly reflect a recent increase of solid precipitation. Recently increased melt rates and increased precipitation rates may compensate each other at ~4400 m a.s.l. on Abramov Glacier. Meanwhile, ablation has increased in the ablation area (Barandun and others, 2015). Following Dyurgerov and Dwyer (2001), this concurrent increase of net accumulation in the accumulation area and melt in the ablation area could lead to a steepening of the mass-balance gradient compared to the 1970s.

Given the trend towards increased net accumulation rates at ~4400 m a.s.l., the slight surface lowering since the 1980s detected based on legacy pictures is not self-explanatory. The observed lowering agrees with the geodetic elevation changes (1975–2015) for this part of the glacier determined by Denzinger and others (in press). The very moderate surface lowering in the accumulation area contrasts sharply with the observed surface lowering of up to 151.3 ± 5.5 m on the glacier tongue (Denzinger and others, in press). The slight surface lowering in the accumulation area may be related to glacier dynamics and/or may have happened in the 1980s or during the period without available observations.

Regional context

Our results of increased net accumulation rates for Abramov Glacier, based on in situ data, provide complementary information to local and regional studies based on remote-sensing data and modelling approaches. Whereas the glaciological mass balance of Abramov Glacier has been predominantly negative over the last years, no acceleration of mass loss has been detected (Denzinger and others, in press). No acceleration of mass loss was identified by modelling studies covering the 1999–2011 period without in situ measurements (Barandun and others, 2015, 2018). This is in contrast to the findings for the Himalaya by Maurer and others (2019) who found a doubling of the average mass loss from 2000–2016 compared to 1975–2000. The increased net accumulation rates on Abramov Glacier suggest that in the accumulation area the mass loss effects of atmospheric warming are potentially compensated by recent increases in solid precipitation. Abramov Glacier is located close to the Kunlun Shan and East Pamir regions for which Shean and others (2020) identified a positive mass change during 2000–18. An increase in solid precipitation may be the reason for this so-called mass-balance anomaly (Yao and others, 2012; de Kok and others, 2018). Our results suggest that the accumulation area of Abramov Glacier is affected by this precipitation increase. Furthermore, Haag and others (2019) show that Abramov Glacier is located on the edge of a region with positive precipitation trends for 1950–2016. The effect of a precipitation increase, however, cannot fully compensate for the increase of available melt energy at the low(er) elevation Abramov Glacier. Despite the presumed precipitation increase, the glacier-wide mass balance of Abramov Glacier is negative and ablation rates on the glacier tongue have increased over the last few decades (Barandun and others, 2015, 2018). Overall, our results in the context of glacier-wide mass balances of Abramov Glacier (Barandun and others, 2015, 2018) are in accordance with the regional mass change distribution found by Brun and others (2017), who argue that the Pamir is a region of transition from positive to negative mass balances and located between regions with mass gains and losses. They found relatively low mass losses for the Pamir and Pamir Alay and state that the positive mass anomaly centres upon the Western Kunlun Shan, where glaciers are located at high elevations. Abramov Glacier, which is located at lower elevations, has a negative glacier-wide mass balance, but the net accumulation increase at ~4400 m a.s.l. indicates that the glacier is still affected by a recent precipitation increase. Conversely, Lambrecht and others (2018) investigated the relatively nearby Fedchenko glacier (Western Pamir) and found an overall large glacier thickness decrease both at high elevations and in recent years. Given these differences, it is thus valuable to have in situ information from several sites to better understand patterns identified by remote-sensing and modelling studies.

Conclusions and outlook

We presented a comparison of unique in situ historical firn data from the 1970s to a current firn profile for Abramov Glacier located in a data sparse region. Our results indicate that the firn column at ~4400 m a.s.l. on Abramov Glacier has not seen substantial changes since the 1970s although the net accumulation rates have increased recently (0.84 ± 0.22 m w.e. for 2011–18 compared to 0.68 ± 0.32 m w.e. for 1965–72 and 0.59 ± 0.22 m w.e. for 1970–97). Recent net accumulation rates are characterised by high year-to-year variations. As there is no data available for more than one decade prior to the most positive of the recent mass-balance years (2011/12), we were not able to assess the exact timing of the accumulation increase.

Our results reveal a series of questions which go beyond the scope of this study. The application of a coupled subsurface and energy balance model could contribute to a better understanding of the firn evolution of Abramov Glacier and its effect on the glacier mass balance. Such an approach has the potential to (i) quantify refreezing processes within the firn column, (ii) assess compensating effects related to changes in precipitation amounts and the availability of melt energy and (iii) investigate the period from 1999 and 2011 for which no data are available. To understand the potential changes of the atmospheric drivers of glacier evolution in general and to run such a model, it is necessary to assess meteorological data. As data from weather stations are sparse for this region, use of reanalysis data is a prerequisite. Efforts to downscale regional climate data over the western edge of HMA will contribute valuable input data to increase our process understanding of glacier changes in this data sparse region.

Acknowledgments. We thank Anastasia Cheremnykh, Mukhammed Esenaman Uluu, Daniel Farinotti, Adrien Gilbert, Sven Girod, Matthias Huss, Ruslan Kenzhebaev, Mario Kummert, Anna-Lena Kopp, Ivan

Lavrentiev, Andreas Linsbauer, Philipp Schuppli, Silas Walther, Firdavz Vosidov and Jonas Wicky for their efforts in the field and to Theo Jenk, Bolot Moldobekov, Azamat Ozmonov and Ryskul Usubaliev for their support with logistics. A special thanks goes to Martina Barandun and Tomas Saks for their invaluable support in coordinating diverse field activities. We thank Sabina Brütsch for the lab analysis and Leo Sold for his help with data plotting. We greatly acknowledge the valuable comments and information on legacy investigation that we received from Felix Pertziger, Alex Merkushkin, Yuri Tarasov and François Valla and Andrey Yakovlev. We thank Andrew Tedstone for edits that increased the clarity of this paper. We sincerely thank the scientific editor Dr. Carleen Reijmer, the Associate Chief Editor Dr. Hester Jiskoot and the two anonymous reviewers whose thorough comments helped us to improve this manuscript. This study was financed by the Swiss National Science Foundation (SNSF), grant 200021_169453 and the Project CICADA (Cryospheric Climate Services for improved Adaptation, contract no. 81049674 between the Swiss Agency for Development and Cooperation and the University of Fribourg).

References

Aizen VB and 5 others (2004) Association between atmospheric circulation patterns and firn-ice core records from the Inilchek glacierized area, central Tien Shan, Asia. *Journal of Geophysical Research* **109**(D08304), 1–18. doi: 10.1029/2003JD003894.

Aizen VB and 5 others (2006) Climatic and atmospheric circulation pattern variability from ice-core isotope/geochemistry records (Altai, Tien Shan and Tibet). *Annals of Glaciology* **43**, 49–60. doi: 10.3189/172756406781812078.

Aizen VB and 9 others (2009) Stable-isotope and trace element time series from Fedchenko glacier (Pamirs) snow/firn cores. *Journal of Glaciology* **55**(190), 275–291. doi: 10.3189/002214309788608787.

Anokhin YA and 5 others (1978) The glacier as a study object for the dynamic of atmospheric pollution [in Russian]. *Materialy Glatsiologicheskih Issledovanii (Data of glaciological studies)* **34**, 192–197.

Barandun M and 10 others (2015) Re-analysis of seasonal mass balance at Abramov glacier 1968–2014. *Journal of Glaciology* **61**(230), 1103–1117. doi: 10.3189/2015JoG14J239.

Barandun M and 7 others (2018) Multi-decadal mass balance series of three Kyrgyz glaciers inferred from modelling constrained with repeated snow line observations. *The Cryosphere* **12**, 1899–1919.

Benson CS (1996) *Stratigraphic Studies in the Snow and Firn of the Greenland Ice Sheet*. (Research Report 70). U.S. Army Snow, Ice and Permafrost Research Establishment.

Bezeau P, Sharp M, Burgess D and Gascon G (2013) Firn profile changes in response to extreme 21st-century melting at Devon Ice Cap, Nunavut, Canada. *Journal of Glaciology* **59**(217), 981–991. doi: 10.3189/2013JoG12J208.

Bradford JH, Harper JT and Brown J (2009) Complex dielectric permittivity measurements from ground-penetrating radar data to estimate snow liquid water content in the pendular regime. *Water Resources Research* **45**(8), 1–12. doi: 10.1029/2008WR007341.

Braithwaite RJ, Laternser M and Pfeffer WT (1994) Variations of near-surface firn density in the lower accumulation area of the Greenland ice sheet, Pakitsoq, West Greenland. *Journal of Glaciology* **40**(136), 477–485. doi: 10.1088/0022-3727/48/32/325305.

Brun F, Berthier E, Wagnon P, Kääb A and Treichler D (2017) A spatially resolved estimate of High Mountain Asia glacier mass balances from 2000 to 2016. *Nature Geoscience* **10**, 668–674. doi: 10.1038/ngeo2999.

Cogley JG and 10 others (2011) Glossary of Glacier Mass Balance. *IHP-VII Technical Documents in Hydrology, IACS Contribution No. 2*, **86**, 114.

Cox C, Humphrey N and Harper J (2015) Quantifying meltwater refreezing along a transect of sites on the Greenland Icesheet. *The Cryosphere* **9**, 691–701. doi: 10.5194/tc-9-691-2015.

Dansgaard W (1964) Stable isotopes in precipitation. *Tellus* **16**(4), 436–468.

de Kok RJ, Tuinenburg OA, Bonekamp PN and Immerzeel WW (2018) Irrigation as a potential driver for anomalous glacier behavior in high mountain Asia. *Geophysical Research Letters* **45**(4), 2047–2054. doi: 10.1002/2017GL076158.

Denzinger F and 7 others (in press) Geodetic mass balance of Abramov Glacier from 1975 to 2015. *Journal of Glaciology*. doi: 10.1017/jog.2020.108

Dikikh AN (1965) Temperature regime of flat-top glaciers (using Grigoriev as an example) [in Russian]. *Glyatsiol. Issledovaniya na Tyan-Shane, Frunze* **11**, 32–35.

Dyurgerov M and Dwyer J (2001) The steepening of glacier mass balance gradients with northern hemisphere warming. *Zeitschrift für Gletscherkunde und Glazialgeologie* **36**(2000), 107–118.

Eichler A and 7 others (2000) Glaciochemical dating of an ice core from upper Grenzgletscher (4200 m a.s.l.). *Journal of Glaciology* **46**(154), 507–515.

Eichler A, Schwikowski M and Gäggeler HW (2001) Meltwater-induced relocation of chemical species in Alpine firn. *Tellus, Series B: Chemical and Physical Meteorology* **53**(2), 192–203. doi: 10.1034/j.1600-0889.2001.d01-15.x.

Farinotti D, Immerzeel WW, de Kok RJ, Quincey DJ and Dehecq A (2020) Manifestations and mechanisms of the Karakoram glacier anomaly. *Nature Geoscience* **13**, 8–16. doi: 10.1038/s41561-019-0513-5.

Fisher D and 6 others (2012) Recent melt rates of Canadian Arctic ice caps are the highest in four millennia. *Global and Planetary Change* **84-85**, 3–7. doi: 10.1016/j.gloplacha.2011.06.005.

Frolov AD and Macheret YY (1999) On dielectric properties of dry and wet snow. *Hydrological Processes* **13**, 1755–1760.

Gardelle J, Berthier E and Arnaud Y (2012) Impact of resolution and radar penetration on glacier elevation changes computed from DEM differencing. *Journal of Glaciology* **58**(208), 419–422. doi: 10.3189/2012JoG11J175.

Gardelle J, Berthier E, Arnaud Y and Kääb A (2013) Region-wide glacier mass balances over the Pamir–Karakoram–Himalaya during 1999–2011. *The Cryosphere* **7**, 1263–1286. doi: 10.5194/tc-7-1263-2013.

Ginot P, Stampfli F, Stampfli D, Schwikowski M and Gäggeler H (2002) FELICS, a new ice core drilling system for high-altitude glaciers. *Memoirs of National Institute of Polar Research* **56** (Special Issue), 38–48.

Glazyrin GE, Glazyrina EL, Kislov BV and Pertzinger FI (1977) Water level regime in deep firn pits on Abramov glacier [in Russian]. *Trudy SARNIGMI* **45**(126), 54–61.

Haag I, Jones PD and Samimi C (2019) Central Asia's changing climate: how temperature and precipitation have changed across time, space, and altitude. *Climate* **7**(123), 1–19. doi: 10.3390/cli7100123.

Haeberli W and Alean J (1985) Temperature and accumulation of high altitude firn in the Alps. *Annals of Glaciology* **6**, 161–163.

Hoelzle M and 20 others (2017) Re-establishing a monitoring programme for glaciers in Kyrgyzstan and Uzbekistan, Central Asia. *Geoscientific Instrumentation, Methods and Data Systems* **6**(2), 397–418. doi: 10.5194/gi-6-397-2017.

Hoelzle M, Darms G, Lüthi MP and Suter S (2011) Evidence of accelerated englacial warming in the Monte Rosa area, Switzerland/Italy. *The Cryosphere* **5**, 231–243. doi: 10.5194/tc-5-231-2011.

Holzer N and 5 others (2015) Four decades of glacier variations at Muztagh Ata (eastern Pamir): a multi-sensor study including Hexagon KH-9 and Pléiades data. *The Cryosphere* **9**, 2071–2088. doi: 10.5194/tc-9-2071-2015.

Huss M (2013) Density assumptions for converting geodetic glacier volume change to mass change. *The Cryosphere* **7**, 877–887. doi: 10.5194/tc-7-877-2013.

Kislov BV (1977) About the question of determining the internal accumulation of temperate glaciers [in Russian]. *Trudy SARNIGMI* **45**(126), 62–72.

Kislov BV (1982) *Formation and regime of the firn-ice stratum of a mountain glacier [in Russian]* (Ph.D. thesis). SARNIGMI Tashkent.

Kislov BV and Nozdrukhin VK (1975) Natural impurities in the firn-ice layer of Abramov glacier [in Russian]. *Trudy SARNIGMI* **27**(108), 86–94.

Kislov BV, Nozdrukhin VK and Pertzinger FI (1977*a*) Temperature regime of the active layer of Abramov Glacier [in Russian]. *Materialy Glatsiologicheskih Issledovanii (Data of glaciological studies)* **30**, 199–204.

Kislov BV, Nozdrukhin VK and Suslov VF (1977*b*) *Changes in Pamiro-Alai Glacier Contamination during the Last 100 Years According to Data from Deep Wells*, vol. **118**. Grenoble, France: IAHS-AISH Publication, pp. 415–416.

Koerner RM (1977) Devon Island ice cap: core stratigraphy and paleoclimate. *Science* **196**(4285), 15–18. doi: 10.1126/science.196.4285.15.

Kohler J, Moore J, Kennett M, Engeset R and Elvehøy H (1997) Using ground-penetrating radar to image previous years' summer surfaces for mass-balance measurements. *Annals of Glaciology* **24**, 355–360.

Kronenberg M and 9 others (2016) Mass-balance reconstruction for Glacier No. 354, Tien Shan, from 2003 to 2014. *Annals of Glaciology* **57**(71), 92–102. doi: 10.3189/2016AoG71A032.

Kutuzov S (2005) *Glacier Changes in the Inner Tien-Shan Mountains since the end of the 19th century [in Russian]*. (Ph.D. thesis). Moscow State (Lomonosov) University.

Lambrecht A, Mayer C, Bohleber P and Aizen V (2020) High altitude accumulation and preserved climate information in the western Pamir,

observations from the Fedchenko Glacier accumulation basin. *Journal of Glaciology* **66**(256), 219–230. doi: 10.1017/jog.2019.97.

Lambrecht A, Mayer C, Wendt A, Floricioiu D and Völksen C (2018) Elevation change of Fedchenko Glacier, Pamir Mountains, from GNSS field measurements and TanDEM-X elevation models, with a focus on the upper glacier. *Journal of Glaciology* **64**(246), 637–648. doi: 10.1017/jog.2018.52.

Lüthi MP and 7 others (2015) Heat sources within the Greenland Ice Sheet: dissipation, temperate paleo-firn and cryo-hydrologic warming. *The Cryosphere* **9**, 245–253. doi: 10.5194/tc-9-245-2015.

Macheret YY, Moskalevsky MY and Vasilenko EV (1993) Velocity of radio waves in glaciers as an indicator of their hydrothermal state, structure and regime. *Journal of Glaciology* **39**(132), 373–384. doi: 10.1017/S0022143000016038.

Machguth H and 9 others (2016) Greenland meltwater storage in firn limited by near-surface ice formation. *Nature Climate Change* **6**, 390–393. doi: 10.1038/nclimate2899.

Machguth H, Eisen O, Paul F and Hoelzle M (2006) Strong spatial variability of snow accumulation observed with helicopter-borne GPR on two adjacent Alpine glaciers. *Geophysical Research Letters* **33**(L13503), 1–5. doi: 10.1029/2006GL026576.

Marchenko S and 7 others (2017) A plot-scale study of firn stratigraphy at Lomonosovfonna, Svalbard, using ice cores, borehole video and GPR surveys in 2012–14. *Journal of Glaciology* **63**(237), 67–78. doi: 10.1017/jog.2016.118.

Maurer JM, Schaefer JM, Rupper S and Corley A (2019) Acceleration of ice loss across the Himalayas over the past 40 years. *Science Advances* **5**(6), eaav7266. doi: 10.1126/sciadv.aav7266.

Mayer C and 6 others (2014) Accumulation studies at a high elevation glacier site in Central Karakoram. *Advances in Meteorology* **2014**(215162), 1–12. doi: 10.1155/2014/215162.

Miège C and 6 others (2013) Southeast Greenland high accumulation rates derived from firn cores and ground-penetrating radar. *Journal of Glaciology* **54**(63), 322–332. doi: 10.3189/2013AoG63A358.

Pavlova PA and 5 others (2015) Polychlorinated Biphenyls in a temperate Alpine Glacier: 1. Effect of percolating meltwater on their distribution in Glacier Ice. *Environmental Science and Technology* **49**(24), 14085–14091. doi: 10.1021/acs.est.5b03303.

Pertziger F (1996) *Abramov Glacier Data Reference Book: Climate, Runoff, Mass Balance*. Tashkent: Central Asian Hydrometeorlogical Institute.

Phillips T, Rajaram H and Steffen K (2010) Cryo-hydrologic warming: a potential mechanism for rapid thermal response of ice sheets. *Geophysical Research Letters* **37**(20), L20503. doi: 10.1029/2010GL044397.

Rasmussen R and 14 others (2012) How well are we measuring snow: the NOAA/FAA/NCAR winter precipitation test bed. *Bulletin of the American Meteorological Society* **93**(6), 811–829. doi: 10.1175/BAMS-D-11-00052.1.

Ryser C and 5 others (2013) Cold ice in the ablation zone: its relation to glacier hydrology and ice water content. *Journal of Geophysical Research* **118**, 693–705. doi: 10.1029/2012JF002526.

Schöne T and 8 others (2013) A new permanent multi-parameter monitoring network in Central Asian high mountains – from measurements to data bases. *Geoscientific Instrumentation, Methods and Data Systems* **2**, 97–111. doi: 10.5194/gi-2-97-2013.

Schwikowski M, Schläppi M, Santibanez P, Rivera A and Sasassa G (2013) The Cryosphere Net accumulation rates derived from ice core stable isotope records of Pío XI glacier, Southern Patagonia Icefield. *The Cryosphere* **7**, 1635–1644. doi: 10.5194/tc-7-1635-2013.

Shean DE and 5 others (2020) A systematic, regional assessment of high mountain Asia Glacier mass balance. *Frontiers in Earth Science* **7**(363), 1–19. doi: 10.3389/feart.2019.00363.

Sold L and 5 others (2013) Methodological approaches to infer end-of-winter snow distribution on alpine glaciers. *Journal of Glaciology* **59**(218), 1047–1059. doi: 10.3189/2013JoG13J015.

Sold L and 8 others (2016) Mass balance re-analysis of Findelengletscher, Switzerland; benefits of extensive snow accumulation measurements. *Frontiers in Earth Science* **4**, 18, 1–16. doi: 10.3389/feart.2016.00018.

Sold L, Huss M, Eichler A, Schwikowski M and Hoelzle M (2015) Unlocking annual firn layer water equivalents from ground-penetrating radar data on an Alpine glacier. *The Cryosphere* **9**, 1075–1087. doi: 10.5194/tc-9-1075-2015.

Suslov VF and Krenke AN (1980) *Abaramov Glacier (Alay Range) [in Russian]*. St. Petersburg: Gidrometeoizdat.

Suter S, Hoelzle M and Ohmura A (2004) Energy balance at a cold alpine firn saddle, Seserjoch, Monte Rosa. *International Journal of Climatology* **24**, 1423–1442. doi: 10.1002/joc.1079.

Thibert E, Blanc R, Vincent C and Eckert N (2008) Glaciological and volumetric mass balance measurements: error analysis over 51 years for the Sarennes glacier, French Alps. *Journal of Glaciology* **54**(186), 522–532.

Thompson LG and 8 others (1997) Ice core records of recent climatic variability: Gregoriev and It-Tish ice caps, in central Tien Shan, Central Asia. *Materialy Glatsiologicheskih Issledovanii (Data of Glaciological Studies)* **81**, 100–109.

Trachsel JC and 6 others (2019) Microscale rearrangement of ammonium induced by snow metamorphism. *Frontiers in Earth Science* **7**, 194, 1–19. doi: 10.3389/feart.2019.00194.

Unger-Shayesteh K and 6 others (2013) What do we know about past changes in the water cycle of Central Asian headwaters? A review. *Global and Planetary Change* **110**, 4–25. doi: 10.1016/j.gloplacha.2013.02.004.

Vincent C and 9 others (2020) Strong changes in englacial temperatures despite insignificant changes in ice thickness at Dôme du Goûter glacier (Mont Blanc area). *The Cryosphere* **14**, 925–934. doi: 10.5194/tc-14-925-2020.

Walther S (2018) *Accumulation Distribution on Abramov Glacier from GPR Measurements* (M.Sc. thesis). University of Fribourg.

WGMS (2017) *Global Glacier Change Bulletin No. 2 (2014–2015) ICSU(WDS)/IUGG(IACS)/UNEP/UNESCO/WMO*. Zurich, Switzerland: World Glacier Monitoring Service (WGMS). doi: 10.5904/wgms-fog-2017-10.

Yao T and 14 others (2012) Different glacier status with atmospheric circulations in Tibetan Plateau and surroundings. *Nature Climate Change* **2**(9), 663–667. doi: 10.1038/nclimate1580.

Zagorodnov VS and Zotikov IA (1980) Core drilling at Spitsbergen [in Russian]. *Materialy Glatsiologicheskih Issledovanii (Data of glaciological studies)* **40**, 157–163.

Zdanowicz C and 6 others (2012) Summer melt rates on Penny Ice Cap, Baffin Island: past and recent trends and implications for regional climate. *Journal of Geophysical Research* **117**, F02006. doi: 10.1029/2011JF002248.

Zhang Q and Kang S (2017) Glacier snowline altitude variations in the Pamirs, Tajikistan, 1998–2013: Insights from remote sensing images. *Remote Sensing Letters* **8**(12), 1220–1229. doi: 10.1080/2150704X.2017.1375611.

Appendix A: Overview of available deep snow pit and core data

An overview of firn data from deep snow pits and cores is given in Table 6.

Table 6. Overview of available deep snow pit and core data. The table contains historical data from the 1970s. Type specifies whether the reported data were measured in a deep pit or from a bore hole/core drilled with an electrothermal drill. Own data including firn cores drilled in 2018 are listed in the second part of the table. Either a FELICS or a KOVACS Mark II corer were used (specified under type). The column data specifies which data are reported. 'strat' refers to visible stratigraphy, 'dens' to density, 'temp' to temperature, 'dust' to dust concentration

Profile	ID	Type	Date	Elevation m a.s.l.	Depth m	Data	Comment	Reference
s1_73	s4250_197310	Deep pit	10.1973	4250	16	strat, dens		Figure 24[(1)], Figure 2.3[(2)]
s1_74	s4250_197410	Deep pit	10.1974	4250	16	strat		Figure 24[(1)], Figure 2.3[(2)]
s1_75	s4250_197506	Deep pit	06.1975	4250	16	strat, dens		Figure 24[(1)], Figure 2.3[(2)]
s2_73	s4410_197306	Deep pit	06.1973	4410	20.5	strat, dens		Figure 2.1[(2)]
s2_74	s4410_197406	Deep pit	06.1974	4410	10.0	strat, dens		Figure 23[(1)], Figure 2.2[(2)]
s2_75a	s4410_197506	Deep pit	06.1975	4410	10.9	strat		Figure 23[(1)], Figure 2.2[(2)]
s2_75b	s4410_197510	Deep pit	10.1975	4410	7.7	strat, dens, temp		Figure 23[(1)], Figure 2.2[(2)]
s3_80	s4400_1980	Deep pit	1980	~4400	17	n.a.		p. 18[(2)]
b0_69	b3830_196910	borehole	10.1969	3830	27	temp 1969–70	Ablation area	Figure 2.3[(2),(4)]
b0_71	b4070_197111	borehole	11.1971	4070	24	temp 1971–72	Ablation area	Figure 2.3[(2),(4)]
b1_72	4250_197205	borehole	05.1972	4250	15	temp 1972–73	Near s1	Figure 2.3[(2),(4)]
b2_73	b4400_197309	Core	09.1973	~4400	50.7	strat, dust	5 m from s2	p. 18[(2),(4),(5)]
b2_74	b4400_1974	Core	1974	~4400	106	n.a.	8 m from s2	p. 99[(1)], p. 18, 154[(2),(5)], [(6)]
b2_75	b4400_1975	Core	1975	~4400	80	n.a.	14 m from s2	p. 18[(2),(5)]
8	sp8_1969–99	Snow pit	1969–99	4410	~0–6	strat, dens	Monthly acc	Pertziger (1996)[(7)]
c4381	c4381_201801	FELICS	22.01.2018	4381	17.0	strat, dens		Own data
c4225	c4225_201801	KOVACS	24.01.2018	4225	12.1	strat, dens		Own data
c4382	c4382_201802	KOVACS	01.02.2018	4381	17.7	strat, dens, temp	Core analysed[a]	Own data
c4395	c4395_201808	KOVACS	02.08.2018	4395	18.4	strat, dens		Own data
ac_2	ac2_2013–18	Snow pit	2013–18	4380	~2–4	strat, dens	Annual acc	Own data

(1) Suslov and Krenke (1980), (2) Kislov (1982), (3) Kislov and others (1977*a*); (4) Kislov and Nozdrukhin (1975); (5) Anokhin and others (1978); (6) Kislov and others (1977*b*); (7) annual data published in Pertziger (1996), monthly data provided by F. Pertziger.
[a]Anions/cations, BC, water stable isotopes.

Appendix B: Comparison of net accumulation rates to annual measurements

We compared net accumulation rates determined for c4382 to independent annual accumulation measurements performed at ac2. Obtained annual layer thickness in m w.e. agree relatively well with the measurements carried out at the same site for the years 2013–2015 (see Table 7). Measurements at ac2 were performed in a combined time system (Cogley and others, 2011), in which the mass balance is determined based on the detection of a stratigraphic minimum on a floating observation date (corresponding dates given in Table 7). This especially affects the measurements of the years 2016 and 2017, when annual accumulation measurements were performed relatively early in the ablation season at the beginning of August. Annual layer thicknesses obtained from the core indicate that there was a mass loss of about 80 mm w.e. between the investigation date and the end of the ablation season for both years. This agrees well with a model-based temporal homogenisation of the annual layer thickness measurements following Barandun and others (2015). These differences between net accumulation rates determined at the firn profile and with annual snow pit measurements thus indicate the implications of varying observation periods for glaciological mass balance time series. Equally, mass balance measurements provide valuable complementary information to reduce uncertainties in layer dating for melt-affected cores.

Table 7. Net accumulation rates c_{net} obtained from core c4382 compared to annual net accumulation data from ac2, measured in a combined time system. The floating observation dates of measurements at ac2 are indicated

mb year	c4382 c_{net} m w.e.	ac2 c_{net} m w.e.	Date
2017/18	n.a.	1.59 ± 0.21	20180801
2016/17	1.37 ± 0.14	2.07 ± 0.22	20170802
2015/16	1.09 ± 0.12	1.81 ± 0.19	20160801
2014/15	1.71 ± 0.19	1.45 ± 0.22	20150825
2013/14	1.19 ± 0.17	0.87 ± 0.20	20140818
2012/13	1.31 ± 0.13	1.19 ± 0.18	20130817
2011/12	2.03 ± 0.18	n.a.	n.a.

Appendix C: Discussion of firn with visible liquid water content with regards to GPR data

The occurrence of water-saturated firn on the one hand hampers the propagation of the GPR signal, allowing for an estimate of the spatial extent of the presence of liquid water within the firn. On the other hand, variable firn water content affects the radar wave velocity Bradford and others (2009), complicating the TWT to depth conversion. The liquid water content in the accumulation area of Abramov Glacier, is however limited. No water table is visible in any of the GPR data from Abramov Glacier, whereas Lambrecht and others (2020) observed such meltwater tables on even higher locations on Fedchenko glacier. On Abramov Glacier, meltwater seems to run off through crevasses which are abundant in the area. We were not able to measure the firn water content in the field and therefore used a dry firn assumption to estimate radar wave velocity despite the observed liquid water in c4395. The velocity of $\overline{u} = 0.2\ \mathrm{m\ ns^{-1}}$ appears to be a valid estimate as Macheret and others (1993) reported $0.18\ \mathrm{m\ ns^{-1}}$ for the same site. We expect the velocities for the GPR profiles measured in 2018 (especially for profile no. 0736 measured in winter) to be higher than the published value for several reasons: (i) The value reported by Macheret and others (1993) was determined from radar measurements performed during summer when liquid water content is expected to be higher than during winter. (ii) The radar wave velocity was determined for a reflector depth of 32.5 m whereas the horizons of interest in our case are located at shallower depths (max. ~16 m). Average velocities are expected to be lower at greater depths. Macheret and others (1993) mention an overall firn density of $734\ \mathrm{kg\ m^{-3}}$ whereas the densities to the depths of ~9.5 m at c4395 and ~15.5 m at c4381/c4382 were lower (cf. Table 3). To further evaluate the dry firn assumption, we recalculated velocities after relating TWTs to layer depths in cores. This analysis was done for winter GPR profile no. 0736 and c4382 as well as for summer GPR profile no. 0795 and c4395. Resulting velocities at depth (IRH7) were $\sim 0.01\ \mathrm{m\ ns^{-1}}$ lower than the estimates using the dry firn assumption for the respective depth for summer and winter. The overall obtained minimum velocity was $u = 0.19\ \mathrm{m\ ns^{-1}}$.

Paper II

Long-term firn and mass balance modelling for Abramov glacier in the data-scarce Pamir Alay

Kronenberg, M., van Pelt, W., Machguth, H., Fiddes, J., Hoelzle, M., and Pertziger, F. Long-term firn and mass balance modelling for Abramov glacier in the data-scarce Pamir Alay. *The Cryosphere Discussions (revised and resubmitted manuscript)*, 2021-380:1–33, 2022

Long-term firn and mass balance modelling for Abramov glacier in the data-scarce Pamir Alay

Marlene Kronenberg[1], Ward van Pelt[2], Horst Machguth[1], Joel Fiddes[3], Martin Hoelzle[1], and Felix Pertziger[4]

[1]Department of Geosciences, University of Fribourg, Fribourg, Switzerland
[2]Department of Earth Sciences, Uppsala University, Uppsala, Sweden
[3]WSL Institute for Snow and Avalanche Research SLF, Davos, Switzerland
[4]GIS consultant, Auckland, New Zealand

Correspondence: Marlene Kronenberg (marlene.kronenberg@unifr.ch)

Abstract. Several studies identified heterogeneous glacier mass changes in western High Mountain Asia over the last decades. Causes for these mass change patterns are still not fully understood. Modelling the physical interactions between glacier surface and atmosphere over several decades can provide insight into relevant processes. Such model applications, however, have data needs which are usually not met in these data scarce regions. Exceptionally detailed glaciological and meteorological data exist for the Abramov glacier in the Pamir Alay range. In this study, we use weather station measurements in combination with downscaled reanalysis data to force a coupled surface energy balance–multilayer subsurface model for Abramov glacier for 52 years. Available *in situ* data are used for model calibration and validation. We find an overall negative mass balance of -0.27 m w.e. a^{-1} for 1968/1969-2019/2020 and a loss of firn pore space causing a reduction of internal accumulation. Despite increasing air temperatures, we do not find an acceleration of glacier-wide mass loss over time. Such an acceleration is compensated by increasing precipitation rates (+0.0022 m w.e. a^{-1}, significant at a 90% confidence level). Our results indicate a significant correlation between annual mass balance and precipitation (R^2=0.72).

1 Introduction

Spatially heterogeneous mass changes of glaciers in High Mountain Asia (HMA) during the last decade have been detected by several regional studies (e.g. Kääb et al., 2012; Brun et al., 2017; Shean et al., 2020; Jakob et al., 2021). Topographical effects in combination with precipitation increases are suggested as reasons for balanced or positive mass changes for numerous glaciers in the Karakoram, Kunlun Shan, Pamir, Pamir Alay, and Tibetan Plateau subregions (Miles et al., 2021). Whereas reliable precipitation data from *in situ* measurements are very scarce for the region (Pohl et al., 2015), the analysis of the gridded Global Precipitation Climatology Project over thirty years has indicated a precipitation increase in the Western part of HMA due to large-scale atmospheric circulation patterns (strengthening westerlies) (Yao et al., 2012). Based on regional climate model data, glacier modelling and moisture tracking, De Kok et al. (2020) conclude that changes in irrigation patterns and climate are responsible for the identified mass balance patterns in HMA.

Including *in situ* data and investigating processes at a local scale over several decades can be helpful in better understanding the influence of atmospheric conditions on glacier mass changes (Mölg et al., 2012; Zhu et al., 2020). Mass balance models of varying complexity have been applied to investigate the mass balance response of mountain glaciers to climate (e.g. Klok and Oerlemans, 2002; Pellicciotti et al., 2009; Sicart et al., 2011). Models solving the energy balance at the glacier surface are more physically based and therefore considered more suitable for longer time periods with unknown climates than temperature-index parametrisations calibrated for stationery conditions (Hock, 2005). Energy balance models are, however, only applicable if sufficient data are available to generate a complete climate forcing and to calibrate uncertain model parameters. Important processes in the accumulation zone, which reduces mass loss due to refreezing and water storage, are not included into surface energy balance models. Several studies have applied energy balance models coupled to multi-layer snow models to simulate refreezing processes within the snow and firn as well as heat conduction which are relevant for the glacier mass and energy balance (e.g. Reijmer and Hock, 2008; Huintjes et al., 2015b). Simulating the physical connection between the atmosphere and the glacier provides insights into the climatic control of glacier mass gain or loss (Mölg and Hardy, 2004).

A few studies have applied energy balance models for glaciers in HMA: Kayastha et al. (1999) applied a point-scale energy balance model to Glacier AXOIO in the Nepalese Himalaya. Azam et al. (2014) modelled the point energy balance of Chhota Shigri Glacier glacier in the Western Himalaya. Several studies focus on glaciers and ice caps located on the Tibetan Plateau (Mölg et al., 2012; Zhang et al., 2013; Huintjes et al., 2015b, a, 2016). Zhu et al. (2020) applied a surface energy balance model to Muji Glacier, located in the north-eastern Pamir. Except for Huintjes et al. (2016), who used a coupled snowpack and ice surface energy and mass balance model (COSIMA) to reconstruct the climate on the Tibetan Plateau during the little ice age, only relative short periods up to one decade have been investigated. The availability of historical data for the Abramov glacier located in the Pamir Alay provides a unique opportunity for detailed modelling over longer periods than covered by those previous studies.

Abramov glacier is located in the western part of HMA nearby to the data scarce regions for which positive or balanced mass changes have been identified (Fig. 1). Barandun et al. (2015) previously calculated the long term mass balance of Abramov glacier by applying a simplified energy balance model (Oerlemans, 2001) and calibrating it to *in situ* measurements. Denzinger et al. (2021) computed the geodetic mass balance based on aerial imagery from 1975 and satellite stereo pairs from 2015. Both studies found an overall negative mass balance of -0.44 ± 0.10 m w.e. a^{-1} for 1968-2014 and of -0.38 ± 0.12 m w.e. a^{-1} for 1975-2015. According to Barandun et al. (2021), Abramov glacier has a similar mass balance to other glaciers in the Pamir Alay. Recent firn investigations at a point site at $\sim$4400 m a.s.l. on Abramov glacier (site 2 in Fig. 1b) suggest that the glacier experienced a precipitation increase compared to the 1970s and that firn conditions remained similar since then (Kronenberg et al., 2021a). These field data, however, only provide information about net accumulation rates and furthermore have a limited temporal and spatial resolution. Modelling the continuous firn and mass balance evolution of Abramov glacier with a process-based model will allow to put the observations into context and give insights into underlying processes. Such a model application of for western HMA unprecedented detail is possible thanks to detailed glaciological and meteorological measurements available for the temperate, valley-type Abramov glacier (Kislov, 1982; Pertziger, 1996; Schöne et al., 2013; Hoelzle et al., 2017).

Here, we apply a coupled surface energy balance – multilayer subsurface model (van Pelt et al., 2012, 2019) to simulate the firn and mass balance evolution from 1968 to 2020. Our objective is to better understand the underlying processes of observed mass balances for this glacier in response to climatic conditions which may likely be relevant also for other sites in the region. In our analysis, we put a main focus on the accumulation area aiming on a process-based temporally resolved quantification of accumulation processes within the firn as well as their contribution to the glacier-wide mass balance.

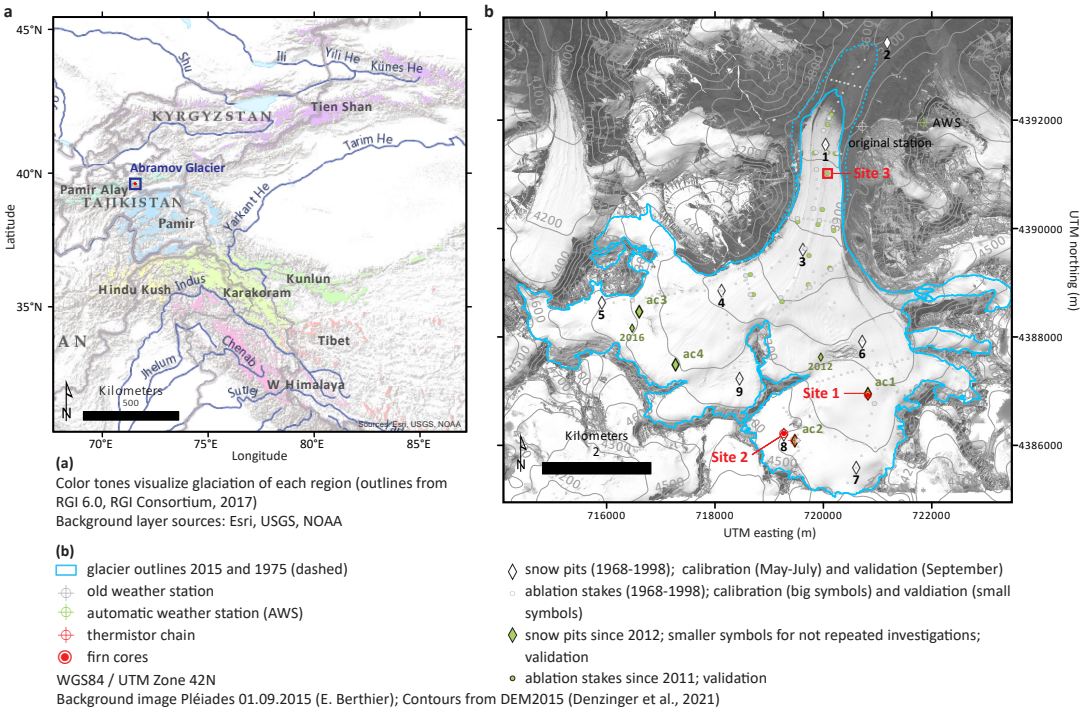

(a)
Color tones visualize glaciation of each region (outlines from RGI 6.0, RGI Consortium, 2017)
Background layer sources: Esri, USGS, NOAA

(b)
- glacier outlines 2015 and 1975 (dashed)
- old weather station
- automatic weather station (AWS)
- thermistor chain
- firn cores
- snow pits (1968-1998); calibration (May-July) and validation (September)
- ablation stakes (1968-1998); calibration (big symbols) and valdiation (small symbols)
- snow pits since 2012; smaller symbols for not repeated investigations; validation
- ablation stakes since 2011; validation

WGS84 / UTM Zone 42N
Background image Pléiades 01.09.2015 (E. Berthier); Contours from DEM2015 (Denzinger et al., 2021)

Figure 1. (a) Overview map showing the location of Abramov Glacier in the Pamir Alay (indicated in blue). (b) Map of Abramov Glacier and surroundings showing the location of weather stations and the mass balance observation network. (Own maps; layer sources are indicated in the legend)

2 Methods

2.1 Study site

Abramov glacier (39.50°N, 71.55°E) is located in the Pamir Alay (north-western Pamir) in Kyrgyzstan (Fig. 1). The north facing valley-type glacier spans an elevation range from 3650-5000 m a.s.l. and covers an area of 24 km^2 (in 2015). In 1972/73 the glacier advanced suddenly (e.g Glazyrin et al., 1993). Since then, the glacier retreated by about 1 km (Barandun et al., 2015). The mean annual air temperature (1968-1998) measured at 3837 m a.s.l. next to the glacier tongue (Fig. 1b, original station) was -4.1°C and annual precipitation sums for the same period are 750 mm a^{-1}. Abramov glacier has temperate firn conditions (Kislov, 1977) and cold subsurface conditions were measured in the ablation area throughout the year (Kislov et al., 1977). Liquid water was observed at depths of about 8.5 to 13 m around 4400 m a.s.l. (Glazyrin et al., 1977; Kislov, 1982). The glacier's detailed and comprehensive mass-balance time series ended abruptly in 1999, but where were re-initiated in 2011 and an automatic weather station (AWS) was installed in 2011 (Schöne et al., 2013; Hoelzle et al., 2017; Zech et al., 2021).

2.2 Model description

We simulate the mass balance evolution of Abramov glacier using a coupled surface energy balance–multilayer subsurface model (EBFM) by van Pelt et al. (2012). The surface energy balance model was developed following Klok and Oerlemans (2002) and the subsurface model based on SOMARS by Greuell and Konzelmann (1994). The original model was first employed to simulate the mass balance of Nordenskiöldbreen located on Svalbard. A parameterized water percolation routine was introduced by Marchenko et al. (2017) and the albedo decay scheme was updated based on the work by Bougamont et al. (2005). The model has participated in the firn meltwater Retention Model Intercomparison Project (RetMIP) as "UppsalaUniDeepPerc" (Vandecrux et al., 2020) and it has been applied to several other glaciers located in the Arctic and the Alps (e.g. van Pelt and Kohler, 2015; van Pelt et al., 2021; Mattea et al., 2021). Here, we use the model version described by van Pelt et al. (2019) and we include an updated parametrisation for seasonal snow densification after van Kampenhout et al. (2017). As the model has been previously described in detail, only a short model overview is given in the following. For full details the reader is referred to van Pelt et al. (2019) and preceding studies.

2.2.1 Surface energy balance model

The surface energy balance model is forced by meteorological input data and calculates the energy fluxes which contribute to the surface energy budget (fluxes towards the surface are defined as positive):

$$Q_{melt} = SW_{net} + LW_{net} + Q_{sens} + Q_{lat} + Q_{sub}, \tag{1}$$

with the total energy available for melting Q_{melt}, the net shortwave radiation SW_{net}, the net longwave radiation LW_{net}, the turbulent sensible and latent heat fluxes Q_{sens} and Q_{lat} and the heat flux into the subsurface Q_{sub}. The model iteratively solves Eq. 1 to find the surface temperature, which is the only unknown and cannot be larger than 0°C.

Surface ablation either occurs in form of melt or as sublimation when the latent heat flux is negative. Surface accumulation occurs either in form of solid precipitation, which is calculated based on air temperature and precipitation forcing using a linear transition from rain to snow around a threshold temperature ($T_{sr}\pm1$ K), or in form of riming. In case of a snow or firn surface, liquid water originating from surface melt, rain or condensation is added to the subsurface (section 2.2.2) and in case of an ice surface leaves the system as runoff. For the entire modelling period, the incoming shortwave radiation SW_{in} is simulated as described in Klok and Oerlemans (2002) and van Pelt et al. (2012) and accounts for grid aspect and shading by surrounding terrain. The attenuation by clouds (τ_{cl}) is calculated using Eq. 6 with parameters determined for Nordenskiöldbreen, Svalbard, by van Pelt et al. (2012). We also tested the parameter values determined by Greuell et al. (1997) for an Alpine glacier. Using the values determined for Svalbard, however, yielded a better agreement between modelled SW_{in} and AWS measurements. The outgoing shortwave radiation SW_{out} depends on the surface albedo. In case snow is present, the albedo α_{snow} is a function of the snow temperature, wetness and age, as described in van Pelt et al. (2019). In absence of snow the ice albedo α_{ice} applies. The computation of the longwave radiation follows the Stefan-Boltzmann law. The sky emissivity depends on cloud cover, air temperature and humidity following relations in Konzelmann et al. (1994) and Greuell and Konzelmann (1994).

The turbulent sensible and latent heat fluxes Q_{sens} and Q_{lat} are calculated for large-scale atmospheric conditions following Oerlemans and Grisogono (2002). The equations are available in Klok and Oerlemans (2002). The subsurface heat flux Q_{sub} is calculated based on the modelled temperature and conductivity. To obtain Q_{sub}, a linear gradient through the two uppermost layers is applied (section 2.2.2). The heat supplied by liquid precipitation is neglected.

2.2.2 Subsurface model

The subsurface model computes the temporal evolution of subsurface temperature, density and liquid water content for discrete layers. The temperature depends on heat conduction (vertical diffusive heat flux) and refreezing of percolating melt, rain water and condensed moisture (van Pelt et al., 2012). The expressions for heat capacity and effective conductivity are adopted from Sturm et al. (1997) and Yen (1981). Heat (and mass) advection is accounted for by describing vertical layer movement on a Lagrangian grid. The penetration of shortwave radiation into the subsurface and therefore also subsurface melting are neglected. We use an updated subsurface densification routine compared to previous EBFM applications. For layer densities above ρ_{firn} = 500 kg m^{-3}, the parametrisation described in van Pelt et al. (2012), which is based on the gravitational densification by Arthern et al. (2010) and modified after Ligtenberg et al. (2011), is applied. For layers with a density below ρ_{firn} = 500 kg m^{-3} a newly introduced fresh snow densification parametrisation following van Kampenhout et al. (2017) is used. Seasonal snow densifies due to destructive metamorphism and compaction by overburden pressure. Van Kampenhout et al. (2017) furthermore include a snow densification due to drifting snow for densities below 350 kg m^{-3}. Snow drift is not included here, as we are not focusing on dynamics of fresh snow. In order to increase numerical efficiency, the fresh snow ρ_{fresh} density is set to 350 kg m^{-3}. The densification due to destructive snow metamorphism is depth independent but varies according to the layer temperature T:

$$\frac{\partial \rho}{\partial t} = c_{dm3} c_{dm2} c_{dm1} exp(-c_{dm4}(T_0 - T)), \tag{2}$$

with the constants c_{dm3} = 2.777×10^{-6} s^{-1}, c_{dm4} = 0.04 K^{-1}, c_{dm2} = 1 (c_{dm2} = 2) in case of absence (presence) of liquid water and a tapering constant c_{dm1} = 1 in the range of ρ = $\in$ [0,ρ_{max}] and exponentially decreasing above ρ_{max}. The densification due to overburden pressure P (kg m^{-3}) depends on a viscosity coefficient η (kg s^{-1} m^{-3})

$$\frac{\partial \rho}{\partial t} = \frac{P}{\eta}, \tag{3}$$

The viscosity coefficient η is calculated following van Kampenhout et al. (2017) who slightly simplified the expression of Vionnet et al. (2012):

$$\eta = f_1 \times 4 \times \eta_0 \frac{\rho}{c_\eta} \exp(a_\eta(T_0 - T) + b_\eta \rho), \tag{4}$$

with a correction factor accounting for the liquid water content f_1, η_0 = 7.62237 × 10^6 kg s^{-1} m^{-3}, a_η = 0.1 K^{-1}, b_η = 0.023 m^3 kg^{-1} and c_η = 358 kg m^{-3}.

The subsurface water within the firn column originates from percolating melt water, rain or condensed moisture. Preferential percolation is parametrised as described by Marchenko et al. (2017). Liquid water is instantly distributed along the depth axis following a normal distribution until a maximum depth z_{lim} unless it reaches an impermeable ice layer before. Refreezing of percolating water raises subsurface temperatures and densities until the melting point or the density of ice is reached. A small amount of liquid water is stored as irreducible water held by capillary forces and the remaining water percolates further downwards until an impermeable ice layer is reached where it forms a slush layer. The maximum irreducible water content is calculated from the porosity (ratio between pore space and the total volume of the snow/firn layer) following Schneider and Jansson (2004). Below z_{lim}, percolation occurs non-preferentially following a bucket-scheme. Water moves to the next underlying layer if the refreezing capacity is eliminated (layer density or temperature reach density of ice or melting temperature) and the maximum irreducible water content is reached. Surface runoff happens instantaneously and occurs when bare ice is at the surface.

2.3 Model set up

The surface energy balance and subsurface profiles are updated with a temporal resolution of three hours. We use a grid of 107×107 grid points with a horizontal resolution of 100 m, only 2654 of these grid points are assigned to the glacier using glacier outlines from 1975. We use a digital elevation model from 1968 to define the initial elevation of each grid point and update the elevation for each three-hour time step based on a linearly downscaled annual height change grid. The topographical data was provided by Barandun et al. (2015); Denzinger et al. (2021); Stainbank (2018). Please refer to the supplementary material (section S1.1) for further information on topographical data.

For each three-hour time step, we derive topographical parameters used for the computation of incoming solar radiation as described in van Pelt et al. (2012). While modelling, the glacier surface is assumed to be constant and glacier grid points are classified as glacier throughout the modelling period. Distributed characteristics are thus computed for a fixed reference glacier surface and spatial varying elevation in time. We later account for a reduction of glacier surface when analysing the model output as described in section 2.8.

The subsurface modelling domain consists of 100 vertical layers extending down to a depth of about 35 m below the surface in the accumulation area. The initial layer thickness at the surface is 0.1 m and at layer numbers 15, 25 and 35 (corresponding to initial depths of 1.5, 3.5 and 7.5 m). Layer thickness reduces with time due to gravitational densification of snow and firn. The subsurface layers move along the depth axes to respond to mass gain or loss at the surface. Due to accumulation, the thickness of the uppermost layer can increase until the thickness of 0.1 m is reached, additional accumulation leads to the creation of a new layer and the removal of the lowermost layer of the modelling domain. In the EBFM, horizontal mass and energy fluxes are neglected and mass and energy exchange between grid cells is only possible along the vertical depth axes.

2.4 Model forcing

The EBFM is forced by meteorological data with a three-hourly resolution. The necessary input consists of the following variables: Air temperature, precipitation, air pressure, relative humidity, precipitation, wind speed and cloud cover fraction. Long-term weather station measurements are available for 1968 to 1998 (Fig. 1b, original station), we extend the time-series until 2020 using downscaled ERA5 reanalysis data which is continuously available from 1979 to present (Hersbach et al., 2020).

2.4.1 Original weather station data

The original Abramov glacier weather station was located on a moraine next to the glacier tongue at 3837 m a.s.l. and was operational from October 1967 until summer 1999. The meteorological data are published in Pertziger (1996) who also compiled the data in digital format (daily resolution). Here, we use data from January 1968 until December 1998 for the following parameters: daily average air pressure, wind speed, relative humidity and temperature, as well as daily precipitation sum, daily minimum air temperature and cloud cover and daily maximum temperature and cloud cover. More details about the station data can be found in the supplementary material (Table S1).

Based on these data, we created three-hourly value for each variable. We use a scaled sine function to calculate three-hourly air temperatures. The scaling factor is determined for each day based on measured minimum and maximum temperatures and daily averages of the three-hourly time series correspond to reported average air temperature measurements. For air pressure and relative humidity the mean value is applied throughout the daily cycle. Daily precipitation sums are divided by eight to obtain three-hourly data. During the melt season, convection is a main driver of cloudiness and cloud formation mainly takes place along the mountain ridges (Suslov and Krenke, 1980). We therefore assume cloud cover to be lower in the morning hours and lower for large areas of lower parts of the glacier than observed averages. Consequently, we assign observed daily minimum cloud cover to the first four timesteps and daily average cloud cover for the rest of the day.

2.4.2 TopoSCALE ERA5 data

Long-term weather station measurements are available for 1968 to 1998 (Fig. 1b, original station), we extend the time-series until 2020 using downscaled ERA5 reanalysis available from ECMWF (Hersbach et al., 2020). We use hourly output from

ERA5 for 1980-2020. Data from the original Abramov weather station as well as data from the AWS are completely independent from the ERA5 data set, as the stations are not used during the assimilation procedure (Personal communication from H. Hersbach, ECMWF 2021). We interpolate ERA5 data from the nine grid points located nearest to Abramov glacier (Fig. S1). Air temperature, air pressure, relative humidity, precipitation, global and clear sky radiation are downscaled using TopoSCALE (Fiddes and Gruber, 2014) which performs a 3D interpolation of atmospheric fields available on pressure levels (to account for time-varying lapse rates) and a topographic correction of radiative fluxes. The latter includes a cosine correction of incident direct short-wave radiation on a slope, an adjustment of diffuse short-wave and long-wave radiation by the sky view factor, and an elevation correction of both long-wave and direct short-wave radiation. It has been extensively tested in various geographical regions and applications, e.g. permafrost in the European Alps (Fiddes et al., 2015), permafrost in the North Atlantic region (Westermann et al., 2015), Northern Hemisphere permafrost (Obu et al., 2019), Antarctic permafrost (Obu et al., 2020), Arctic snow cover (Aalstad et al., 2018), Arctic climate change (Schuler and rn Ims Østby, 2020), and Alpine snow cover (Fiddes et al., 2019). This approach enables us to provide a climate length pseudo-observation time series globally while accounting for the main topographic effects on atmospheric forcing.

2.4.3 Cloud fraction calculated from TopoSCALE ERA5 data

Cloud cover fraction is not directly available from ERA5 but a required input for the model. We therefore, calculate the TopoSCALE cloud fraction from the TopoSCALE global I and the clear-sky radiation I_{cs}. In a first step, the cloud transmissivity τ_{cl} is calculated following Klok and Oerlemans (2002):

$$\tau_{cl} = I/I_{cs} \tag{5}$$

We use the three-hourly average values of I and I_{cs} to calculate τ_{cl} for each time step for which I and I_{cl} are both above 0. We use the the expression by Greuell et al. (1997):

$$\tau_{cl} = 1.00 - c1 \times n - c2 \times n^2 \tag{6}$$

to calculate the cloud cover n from the cloud transmissivity τ_{cl}. The parameters $c1$=0.128 and $c2$=0.346 are adopted from van Pelt et al. (2012). Night time cloud cover n values are linearly interpolated from neighboring, non-missing values.

2.4.4 Bias correction of TopoSCALE ERA5 data and creation of a continuous data set

ERA5 is a global reanalysis product and its quality is dependent on density of assimilated observations, which varies globally. Central Asia in general and mountainous regions of the Pamir specifically, are data poor and therefore the reanalysis is less well constrained as compared to data rich regions such as Europe, for example. Therefore, even after downscaling (accounting for resolution differences between the model grid and point of interest) we can expect there to be residual biases, which we address with the following procedure. We aggregate TopoSCALE data to monthly averages to compare them to data from the original

weather station. Biases are calculated for monthly air temperature, pressure and wind speed for the period 1980-1998 and then used to correct TopoSCALE air temperature, pressure and wind speed for 1980-2020. Monthly average ratios between monthly aggregated station measurements and TopoSCALE data are calculated for precipitation (sums) and cloud fraction (averages) and relative humidity (averages) for the period 1980-1998 and used to correct the TopoSCALE time series for 1980-2020. The resulting cloud fraction time series for summer months (July to September) shows a reduced amplitude compared to the station time series for 1968-98. We use the precipitation time series to correct for this by setting the cloud cover to 0 for days without precipitation and to 1 if precipitation is higher than a monthly threshold value (cf. supplement section S1.4). Monthly averages of the final cloud fraction time series correspond to monthly averages prior to this correction. We combine the three-hourly observed data from 1968 to 1998 with the bias corrected TopoSCALE ERA5 data for the years 1999-2020 to obtain a final data set for 1968-2020. An alternative data set is created using historical measurements for the period 1968-1979 and TopoSCALE ERA5 data for the years 1980-2020 (Fig. 2). The both data sets thus differ for the period 1980-1998. The forcing data sets are visualized in Figs. S2 and S3 and the trends of original forcing are given in Table 4.

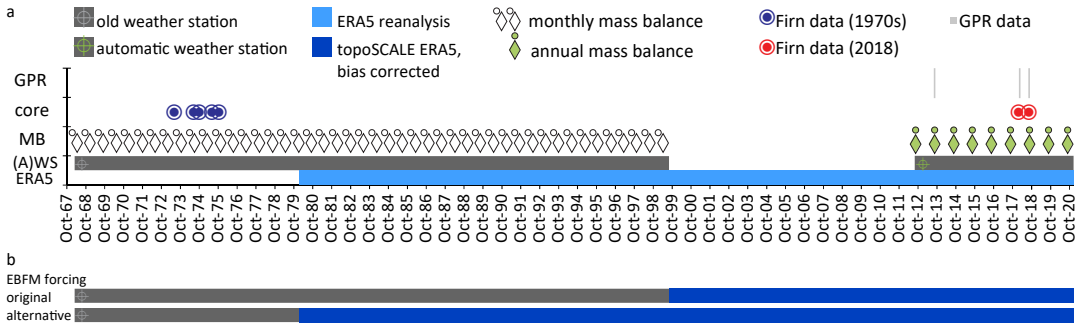

Figure 2. Temporal overview of data available for this study. The availability of different *in situ* and gridded datasets (ERA5 reanalysis) is shown in a. Panel b summarizes which data are used for forcing the model. We mainly show results using the original forcing. A sensitivity model run was performed using the alternative forcing (applying the same parameters as in the original run). Results are shown in the supplementary material

2.5 Calibration and validation data

The EBFM calibration and validation is mainly based on glaciological *in situ* measurements which are available for two periods: Historical data cover three decades at the beginning of the simulation period (1968-1998) and *in situ* are again available for the most recent eight years (2012-2020, (Fig. 2a). We split the historical data into calibration and validation data and use the recent glaciological data for validation only. Additionally, we use data from an AWS installed in 2012 to constrain parameters of the energy balance formulation (see supplementary material section S1.5 for more information).

2.5.1 Monthly point mass balance data 1967-1998

For Abramov glacier, very detailed mass balance measurements are available for the period from 1967-1998 (Fig. 2). The data set consists of mass balance point observations at a monthly resolution performed at eight snow pit and 165 stake locations totalling in 42961 stake and 2179 snow pit measurements. More details about this exceptional data set are given in the supplementary material (section S1.3). We use a subset of these data to calibrate several parameters of the EBFM as described in section 2.6. The calibration data set consists of snow pit measurements from March, June and July and September and measurements from 19 selected stakes locations performed at the end of the hydrological year in September (annual mass balance measurements). The stakes were selected to correspond to the location of current mass balance point observations (see section 2.5.2). Up to 146 independent annual stake measurements per mass balance year are used to validate the modelled surface mass balance for the years 1968/69-1997/1998. The spatial distribution of the calibration and validation data sets are shown in Fig. 1b.

2.5.2 Annual point mass balance data 2011-2020

For recent years, the modelled surface mass balances are validated against annual mass balance measurements which are available from up to 20 points since 2011/2012 (Barandun et al., 2015; Hoelzle et al., 2017). The new monitoring network consists of 16 stakes in the ablation area and up to four snow pits in the accumulation area (Fig. 1). Whereas the stake locations were roughly kept constant over time, the locations of the snow pits varied during the first years. Field visits took place once a year during July/August and exact observation dates are available. Only ablation stake readings from snow free locations are considered and the density of ice ($900\,\mathrm{kg\,m^{-3}}$) is used to calculate floating-date mass balances between the two observation dates. Due to the stratigraphic nature of snow pit observations, the beginning of the accumulation season is not known and we assume the last summer surface to have formed at the beginning of the hydrological year. Point accumulation values are thus calculated for the period from the 1 October until the observation date using the snow density and depth measurement of each snow pit.

2.5.3 Firn profile data

Density profiles dating back to the 1970s are available from deep firn pits that were located in the eastern branch of the accumulation area at $\sim$4400 m a.s.l. and $\sim$4250 m a.s.l. (Kislov, 1982). In 2018, firn cores were drilled at similar and nearby locations (Fig. 2a). We refer to Kronenberg et al. (2021a) for a detailed description of legacy and recent firn profiles. In addition to density measurements, continuous subsurface temperature measurements from four thermistors located in a borehole at $\sim$4380 m a.s.l. are available from February 2018 until April 2020. Based on historical firn densities, one subsurface parameter was optimised (section 2.6). The rest of the subsurface data are used for validation only.

2.6 Parameter selection and calibration

In order to reflect the local conditions of Abramov glacier we adjusted several model parameters based on data available from *in situ* measurements and other studies from HMA. We selected the calibration parameters based on their relevance for our site and the existence of data. The order of calibration is chosen considering the dependence of parameters on calibration of other parameters. First lapse rates to extrapolate the meteorological forcing over the glacier area are determined, then the incoming radiation parameters are estimated (see supplement S1.5 for details). Thereafter, we optimise accumulation parameters and finally parameters affecting summer melt. Model parameters different from values used by van Pelt et al. (2019) are summarized in Table 2, the last column indicates whether a parameter was optimised (y/n).

We use *in situ* mass balance measurements from eight snow pits located on the glacier and data from a selection of 19 ablation stakes for the period 1969-1998 (Table 1) for calibration. With these data we manually optimise a set of accumulation and ablation parameters. Final parameters are determined by minimizing bias between modelled surface mass balances for grid cells corresponding to point locations with *in situ* measurements. We use precipitation correction factors in order to debias the precipitation forcing. The correction mainly compensates for undercatch, but also accounts for all other biases present in the precipitation forcing. We consider March accumulation measurements to be least affected by melt and use them to calibrate the precipitation bias correction factor $Prec_{c-w}$ applied for October-June. During summer months, the precipitation undercatch is assumed to be reduced compared to autumn, winter and spring and we adopt a value of $Prec_{c-s}$=1.15 determined for Alpine locations in Switzerland from Sevruk (1985). The bias between modelled and measured June and July snow pit measurements is reduced by a two-parameter exploration for α_{fresh} and t^*_{wet}. And finally, α_{ice} is optimised using September surface mass balance measurements (snow pits and ablation stakes).

Parameters in the subsurface model are default values except for the critical density of destructive metamorphism ρ_{max} which is optimised to obtain a better fit between modelled and measured subsurface densities at ∼4410 m a.s.l.

The comparison of optimized model simulations to surface mass balance observations used for model calibration shows a stronger Root Mean Square Error (RMSE) for the annual mass balance, and despite some bias in the linear fit, the datasets generally approach the 1:1 linear fit line (Fig. S4).

Table 1. Number of point measurements used for calibration of surface energy balance parameters (cf. Table 2). Accumulation measurements were performed at eight sites on the glacier surface and all available measurements are used for the selected months. We use 19 out of 165 ablation stakes for calibration. Stakes are selected to correspond to current observation sites

type	period	use	number of data points
March snow pit measurements	1969-1998	calibration $Prec_{c-w}$	225
June snow pit measurements	1969-1998	calibration α_{fresh}, t^*_{wet}	203
July snow pit measurements	1969-1998	calibration α_{fresh}, t^*_{wet}	141
annual mass balance measurements	1969-1998	calibration α_{ice}	532

Table 2. List of EBFM parameter choices with references. For parameters optimised by EBFM simulations for Abramov glacier (opt), the initial value is given in brackets.

	parameter	unit	value (initial)	reference	opt
dT/dz	temperature lapse rate	K m^{-1}	-0.005	Kislov (1982)	n
$dPrec/dz$	precipitation lapse rate (factor)	m^{-1}	0.0013	calculated from in situ data	n
$dPres$	Pressure decay parameter	-	-1.45*10^{-4}	calculated from in situ data	n
dRH/dz	relative humidity gradient	% m^{-1}	0.01	Huintjes et al. (2016)	n
γ	potential temperature lapse rate	K m^{-1}	0.0055	from in situ and pseudostation data	n
$Prec_{c-w}$	precipitation bias correction winter (factor)	-	1.85 (2)	-	y
$Prec_{c-s}$	precipitation bias correction summer (factor)	-	1.15	Sevruk (1985)	n
α_{ice}	ice albedo	-	0.23 (0.3)	Mölg et al. (2012)	y
α_{fresh}	fresh snow albedo	-	0.81 (0.85)	Mölg et al. (2012)	y
t^*_{wet}	albedo decay time scale wet snow	days	7 (15)	van Pelt et al. (2019)	y
P_{th}	snowfall threshold to reset to α_{fresh}	m w.e. s^{-1}	3.5d-8	Zhu et al. (2020)	n
C_b	background turbulent exchange coefficient	-	0.0037	Klok and Oerlemans (2002)	n
$c1$	cloud transmissivity parameter	-	0.128	van Pelt et al. (2012)	n
$c2$	cloud transmissivity parameter	-	0.346	van Pelt et al. (2012)	n
k_{aer}	aerosol transmission constant	-	0.982	Klok and Oerlemans (2002)	n
b	clear sky emissivity parameter	-	0.433	calculated from in situ data	n
ϵ_{cl}	overcast emissivity	-	0.960	default value	n
λ	optical thickness empirical constant	-	3.00	Smith (1966)	n
z_{lim}	preferential percolation depth	m	6.0	default value	n
ρ_{max}	critical density destructive metamorphism	kg m^{-3}	300 (200)	-	y
ρ_{fresh}	fresh snow density	kg m^{-3}	350	Klok and Oerlemans (2002)	n

2.7 Model initialisation, performed simulations and sensitivity experiments

To initialize subsurface conditions the model is run twice over the period 1968-98 using the three-hourly weather station data to force the model. The first iteration is started with identical subsurface conditions throughout the glacier with a vertical grid consisting of temperate ice (273.15 K). The second initialisation run is started from the final stage of a first run.

We perform several model runs for selected grid points corresponding to the locations of selected ablation stakes and snow pits indicated in Fig. 1 to adjust model parameters (section 2.6) using the final combined three-hourly forcing consisting of station (1968-1998) and bias corrected TopoSCALE ERA5 data (1999-2020). Thereafter, we perform a final distributed model run for the period from 1 January 1968 until 31 December 2020 using the same forcing.

To assess the model sensitivity towards parameter choices, we performed several model runs for three selected grid points (sites 1, 2 and 3, Fig. 1b) testing single parameter perturbations following Klok and Oerlemans (2002). Additional sensitivity runs are performed using different cloud cover forcings. To assess the overall sensitivity to the model forcing, we carried out an alternative distributed run using the alternative data set with a shorter period of station measurements (1968-1979, Fig. 2). Detailed results of these sensitivity experiments are presented in the supplementary material (Figs. S7-S15).

2.8 Analysis of model output and mass balance calculation

We calculate the climatic mass balance as the sum of the surface and the internal mass balance for hydrological years (1 October-30 September) (Cogley et al., 2011). The surface mass balance is the result of accumulation (+) and ablation (-) at the surface including precipitation (+), moisture exchange (+/-), mass loss through runoff (-). The internal mass balance accounts for re-freezing and storage of liquid water below the previous summer surface.

While the model grid elevation is updated for each time step, the modelling extent is kept constant using the glacier mask from 1975 for the entire simulation period. After modelling, the glacier wide mass balance and other results are calculated for decade-wise updated glacier extents. Until the end of the hydrological year 1978, the entire model output is analysed corresponding to the glacier area of 1975. For the next ten hydrological years, a glacier mask corresponding to the glacier area from 1986 is used and output outside this domain is not considered. Masks based on outlines from 1998, 2005 and 2015 are used for 1988/1989-1997/1998, 1998/1999-2007/2008 and 2008/2009-2019/2020.

The equilibrium line altitude ELA is calculated as the mean elevation of grid points with a mass balance equal to 0 m w.e. at the end of a the hydrological year. Grid points with a negative mass balance value at the end of the hydrological year are used to calculate ablation gradients, which is the linear relation between elevation and modelled ablation.

For comparison to in situ point measurements, the modelled surface mass balance of the grid point nearest to the stake/snow pit location is used. The daily model output is aggregated at the end of the month of interest with respect to the beginning of the hydrological year (1 October) to compare to accumulation observations. For comparison to ablation observations, data is accumulated until the reported observation date (section 2.5.1). For *in situ* observations since 2011, the stake installation dates are earlier in the melt season and model output is extracted for exact periods between stake installation and stake reading (section 2.5.2).

3 Results

3.1 Long term mass balance

The distributed mean annual climatic mass balance for 1968/1969-2019/2020 is shown in Fig. 3. The mass balance of Abramov glacier is predominantly negative for the years from 1968/1969 to 2019/2020, with a mean value of -0.27 m w.e. a^{-1}, and shows no significant trend in annual mass balances (+0.0002 m w.e. a^{-1}, p-value=0.979 and Fig. 4c). The most negative modelled mass balances occur at the start of the period, while the two decades between 1978 and 1998 are characterised by an almost

balanced mass budget, thereafter becoming more negative again (Fig. 4a,c and Table 3). The modelled elevation distribution of mass balance shows that accumulation is lowest during the first decade (1968/1969-1977/1978) and highest during the last modelled decade (2008/2009-2017/2018), and ablation is largest during the first decade, followed by the second last decade (1998/1999-2007/2008) (Fig. 5b).

The RMSE between simulated surface mass balances and independent point measurements not used for calibration is similar for the recent and historical investigation periods ($\sim$0.7), whereas the mean bias lower for the period of historical measurements (+0.05) than for recent years (+0.28) (Fig. 6a and b). Differences in the mean bias are partly related to the spatial distribution of the validation data. As visible from 6a,b and 4b), both, accumulation and ablation were underestimated whereas more accumulation measurements are available for the historical period (1b).

Table 3. Mean glacier-wide climatic mass balance, internal accumulation Equilibrium Line Altitude ELA and ablation gradients for each decade and different periods used for comparison with other studies. The periods are hydrological years (e.g. 1968/1969-1977/1978 refers to 1 October 1968 - 30 September 1978) unless precise dates are specified. The mean glacier surface used for the mass balance calculation is also indicated

period	climatic mass balance	internal accumulation	ELA	ablation gradient	mean glacier surface
	m w.e. a^{-1}	m w.e. a^{-1}	m a.s.l.	m w.e. m^{-1}	km^2
1968/1969-1977/1978	-0.63	0.11	4250	0.0077	26.54
1978/1979-1987/1988	-0.04	0.1	4170	0.0078	25.78
1988/1989-1997/1998	-0.08	0.13	4180	0.0083	25.24
1998/1999-2007/2008	-0.33	0.12	4220	0.0076	25.16
2008/2009-2017/2018	-0.23	0.1	4222	0.0066	25.06
1968/1969-1997/1998	-0.25	0.12	4200	0.008	25.85
1968/1969-2013/2014	-0.26	0.12	4207	0.0077	25.6
1971/1972-1993/1994	-0.26	0.11	4200	0.0079	25.87
1975/1976-2014/2015	-0.26	0.11	4208	0.0076	25.42
15 Jul 1975-1 Sep 2015	-0.30	0.11	4208	0.0076	25.42
1998/1999-2019/2020	-0.31	0.11	4225	0.007	25.11
2011/2012-2019/2020	-0.38	0.08	4248	0.0065	25.06
1968/1969-2019/2020	-0.27	0.11	4211	0.0076	25.54

3.2 Internal accumulation

The average glacier-wide modelled internal accumulation is 0.11 m w.e. a^{-1}. Internal accumulation occurs in large parts of the accumulation area and is more pronounced in the orographic right of the accumulation area (Fig. 7) and varies over time. Highest internal accumulation rates are modelled for the years 1968/1969-1977/1978 between 4400 and 4500 m a.s.l (Fig. 5c). The decades 1988/1989-1997/1998 and 1998/1999-2007/2008 are characterised by higher internal accumulation rates at lower

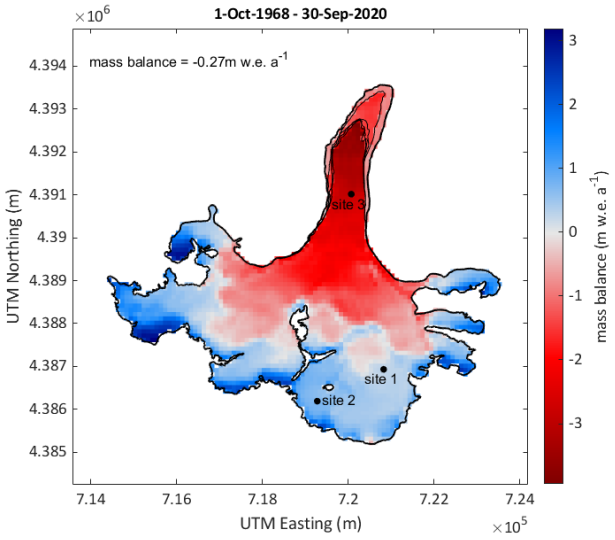

Figure 3. Modelled mean annual distributed mass balance for updated glacier extents for the period from 1 October 1968 to 30 September 2020. Note, that the mean annual mass balance for the entire period and updated glacier surfaces is shown. Values are thus reduced on the glacier tongue, where the glacier area reduced over time. The different glacier outlines are shown with black lines. Furthermore, the location of three selected points is indicated.

elevations around 4250 m a.s.l. (Fig. 5b) where the glacier covers large areas (Fig. 5c). Lowest internal accumulation rates are modelled for the second and the last decade (Table 3).

3.3 Firn evolution

Modelled subsurface densities are higher at site 1, ∼4250 m a.s.l. (Fig. 8a-c) than at site 2, ∼4400 m a.s.l. (Fig. 9a-c) and increase over time at both sites. At site 1, a significant increasing trend of subsurface densities for the depth range of 0-10 m is found for 1968/1969-2019/2020 (+1.14 kg m^{-3} a^{-1}, p-value = 0.014), whereas the trend is significant at site 2 when the first two decades are excluded (+1.53 kg m^{-3} a^{-1}, p-value = 0.005 for 1988/1989-2019/2020). At the lower site (∼4250 m a.s.l., Fig. 8a-c) densities at depth reach the density of ice. Modelled firn densities correspond well with measurements shown for four different dates in Fig. 10. The mean biases between modelled and measured densities for the depth covered by measurements are -18.9 kg m^{-3} for June 1973, +52.6 kg m^{-3} for June 1974, +20.4 kg m^{-3} for June 1975 and -23.8 kg m^{-3} for August 2018.

For early years, the modelled subsurface temperatures indicate temperate firn conditions and propagation of winter cooling down to depths of about 10 m in the accumulation area at site 1 (∼4250 m a.s.l., Fig. 8d). In later years, the cold content

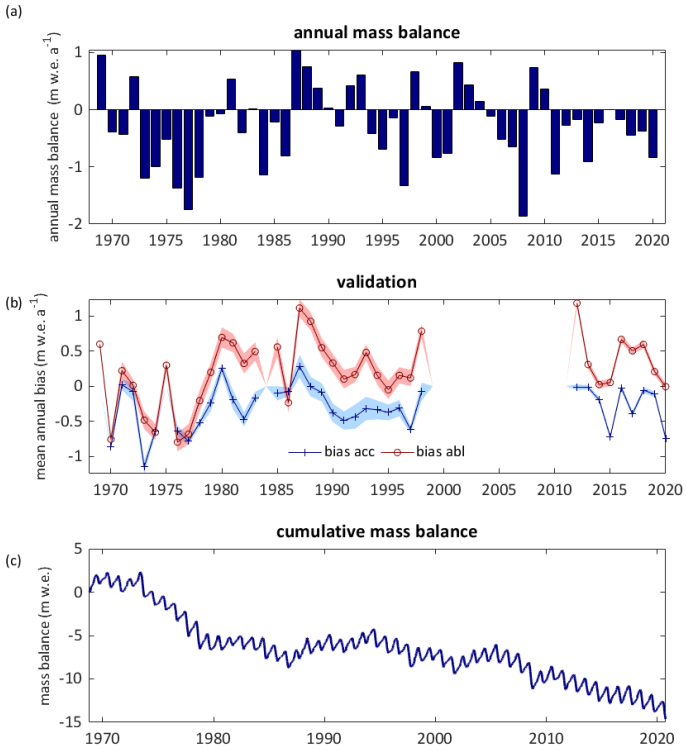

Figure 4. Temporal evolution of modelled climatic mass balance. (a) Modelled mean annual mass balance for updated glacier extents. (b) Mean annual bias between measured and modelled surface accumulation in blue and ablation in red. The shaded area refers to the measurement uncertainty calculated following Thibert et al. (2008). (c) Modelled cumulative mass balance for updated glacier extents.

propagates to greater depths and overall cold subsurface conditions are modelled for most recent years (Fig. 8e-f). For the depth range of 0-10 m, the subsurface cooling trend is -0.036 K a^{-1} (p-value < 0.001 for 1968/1969-2019/2020).

In contrast to the results at site 1, the modelled firn temperatures for site 2 (∼4400 m a.s.l.) indicate continuously temperate firn conditions and propagation of winter cooling down to depths of about 10 m (Fig. 9d-f). Also here, a slight cooling trend was found (-0.0041 K a^{-1} p-value=0.043 for 1968/1969-2019/2020).

In Fig. 11, modelled firn temperatures at S2 are compared to thermistor measurements from spring 2018. Measured as well as modelled temperatures remain temperate at depths greater than about 10 m. In March (Fig. 11 a,b), modelled temperatures

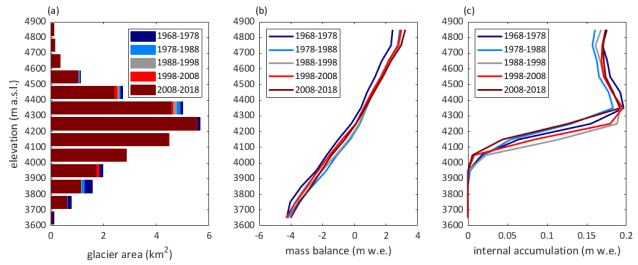

Figure 5. Modelled mass balance and internal accumulation versus elevation. The elevation distribution of the glacier area for different glacier extents are shown in panel panel (a). In panel (b) the climatic mass balance is plotted versus the elevation for the modelled decades. In panel (c) the internal accumulation is plotted versus elevation. The periods are hydrological years (e.g. 1968-1978 refers to 1 October 1968 - 30 September 1978).

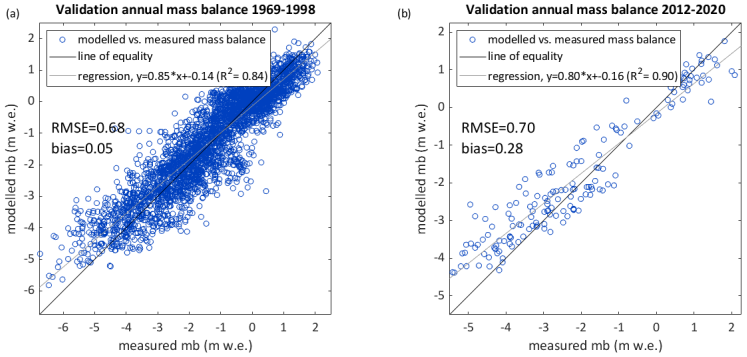

Figure 6. Model validation: Measured versus modelled annual surface mass balance for an independent set of point measurements from 1968/1969-1997/1998 (3292 point measurements) (a) and from 2011/2012-2019/2020 (164 point measurements) (b).

near the surface correspond well with observations. At a depth of about 7 m, the modelled temperatures are a bit higher. In April (shown in Fig. 11c), modelled firn temperatures are warmer than measurements also for the uppermost thermistor location. At a depth of about 7 minimum subsurface temperatures are recorded for 6 June 2018. On this date, modelled firn temperatures are temperate except for a small zone around 7 m depth (Fig. 11d).

3.4 Temporal variation of climate variables, mass and energy fluxes

Significant increasing trends for model forcing air temperature (mean over hydrological years) and mean summer air temperatures are found for 1968/1969-2019/2020 (Table 4). Trends are also significant for air pressure (increase), relative humidity (decrease), cloud cover fraction (decrease) and precipitation sums (increase) (Table 4). Highest amounts of precipitation were

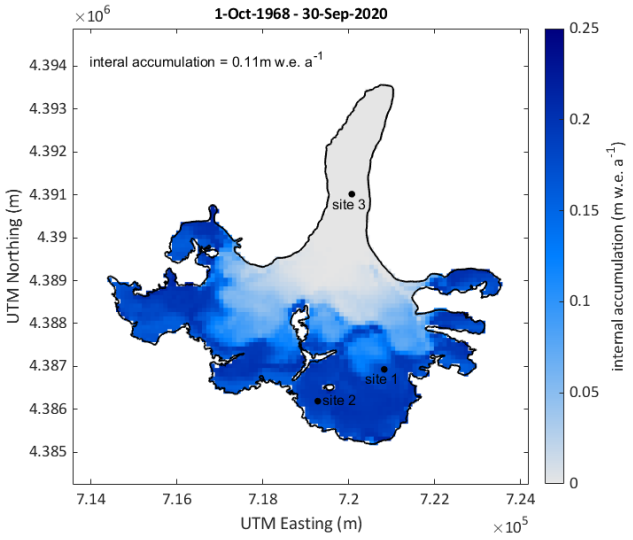

Figure 7. Map of mean annual internal accumulation for the mass balance years 1968/1969-2019/2020. The location of three selected points is indicated.

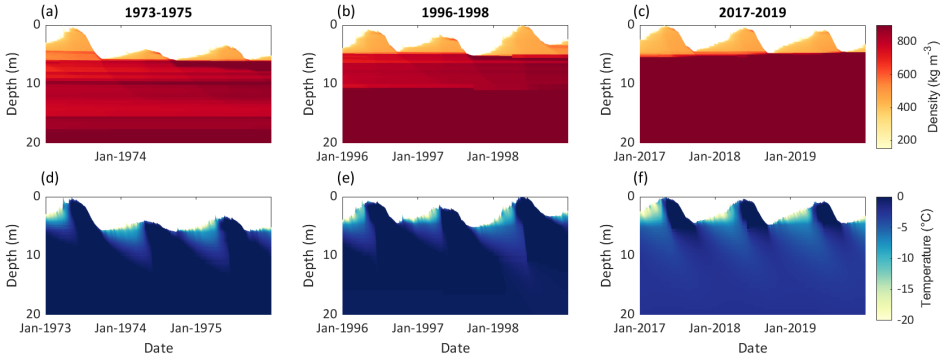

Figure 8. Modelled subsurface conditions at site 1 (∼4250 m a.sl.) for three selected periods: 1973-1975 (panels a and d), 1996-1998 (b,e) and 2017-2019 (c,f). Panels a, b and c show the subsurface density and panels e, d and f the subsurface temperature. The location of the site is indicated in Fig.1 b

recorded from 1978/1979 to 1997/1998 and from 2008/2009 to 2017/2018 (Table S2). Whereas the earlier two decades are characterised by almost balanced mass changes, more negative values were simulated for the most recent decade, when the

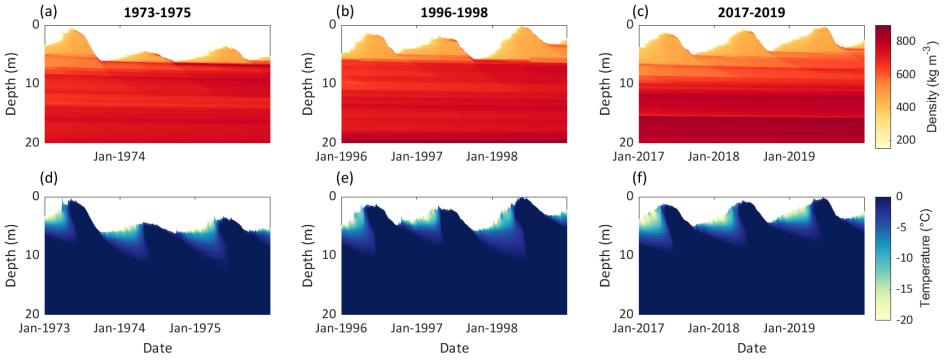

Figure 9. Modelled subsurface conditions at site 2 (∼4400 m a.sl.) for three selected periods: 1973-1975 (panels a and d), 1996-1998 (b,e) and 2017-2019 (c,f). Panels a, b and c show the subsurface density and panels e, d and f the subsurface temperature. The location of the site is indicated in Fig.1b

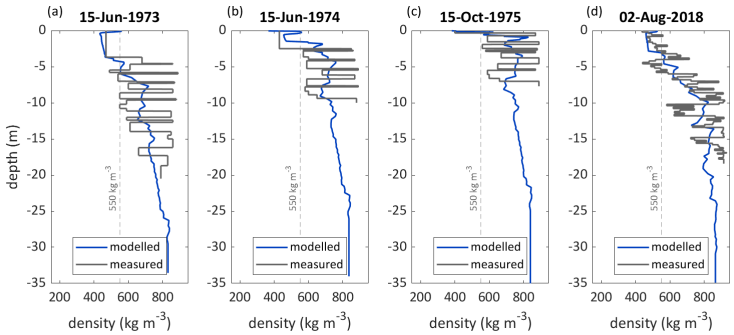

Figure 10. Modelled and measured subsurface densities for site 2 (∼4400 m a.sl.). Measured subsurface densities from the 1970s are digitised from figures 2.1 and 2.2 in Kislov (1982) (a-c) and own measurements are shown for 2018 (d). The location of the site is indicated in Fig.1b.

internal accumulation was strongly reduced compared to earlier years (Table 3). Low internal accumulation was also simulated for the second and most balanced decade (1978/1979 to 1987/1988) (Table 3). Both decades of low internal accumulation follow years with exceptionally high amounts of available melt energy and comparably low precipitation rates (especially from (1968/1969 to 1977/1978) (Tables 3, S2; Figs. 12 and S5). Overall, the preceding conditions led to a reduction of the area where internal accumulation could take place (only higher elevation bands in Fig. 5c, see also video supplement). Following 1978/1979-1987/1988, when precipitation was high, the area where internal accumulation takes place in larger areas (Fig. 5c and video supplement). In most recent years which follow another decade characterised by negative mass balances the area

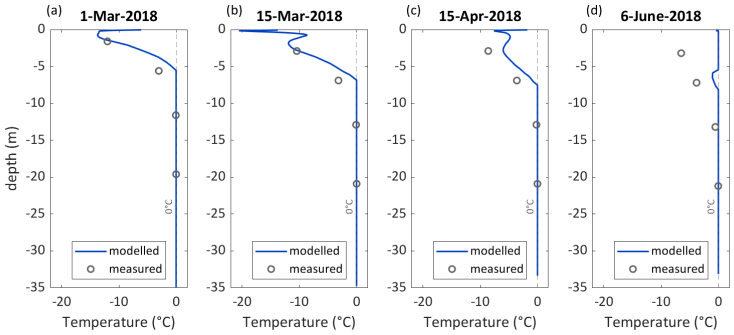

Figure 11. Modelled and measured subsurface temperature for a station located nearby site 2 (∼4400 m a.sl.). The location of the site is indicated in Fig.1b.

and amount of internal accumulation are strongly reduced (Table 3, Fig. 5). In general, the simulated annual mass balances are more strongly correlated with annual precipitation (R^2=0.72) than to the summer air temperatures (R^2=0.29) Fig. S6).

Examining the modelled energy fluxes for different sampled locations (lower accumulation area site1, accumulation area site 2 and ablation area site3, Fig. 1b) highlights, that most heat fluxes are characterised by an increasing trend (Table 4), whereas high incoming shortwave radiation occurred during the first decade characterised by the most pronounced mass loss (Figs. 12 and S5). In 2008/2009-2017/2018, when melt rates were highest for the points in the accumulation area, sensible heat flux and incoming long-wave radiation were high (Figs. 12, S5 and Table S2).

4 Discussion

4.1 Long-term mass balance and firn evolution

The modelled long-term mean mass balance for Abramov glacier indicates an overall mass loss of -0.27 m w.e. a-1 for the period 1968/1969-2019/2020 which is in agreement with the findings of other recent studies. Barandun et al. (2015) and Denzinger et al. (2021) found somewhat more negative mass balances. Barandun et al. (2015) estimate the mass balance for 1967/1968-2013/2014 as -0.44 ± 0.10 m w.e. a^{-1}. Their estimate is based on the application of a calibrated surface mass balance model and a simple approximation of internal accumulation as well as basal ablation which together contribute $+0.07$ m w.e. a^{-1}. In Fig. 13 annual mass balances of different studies are compared to our results: Previous analysis of annual mass balance data for 1971-1994 provided different estimates, but yielded all more negative mass changes than our study (Barandun et al. (2015): -0.39 m w.e. a^{-1}, Dyurgerov (2002): -0.50 m w.e. a^{-1}, and Pertziger (1996): -0.61 m w.e. a^{-1}) than the EBFM (-0.26 m w.e. a^{-1}). Denzinger et al. (2021) calculate the geodetic mass balance as -0.38 ± 0.12 m w.e. a^{-1} for 15 July 1975 until 1 September 2015. Our result for the same time period (-0.30 m w.e. a^{-1}) is within their calculated uncertainties.

Table 4. Trends and p-values for climate variables and energy balance components for the period from the 1 October 1968 until the 30 September 2020 (hydrological years) are listed for a grid point in the ablation area at ∼3850 m a.s.l. Values in brackets refer to site 2 located in the accumulation area at ∼4400 m a.s.l. y/n stand for significant or not significant at a 90% confidence level. The point location of both grid points are indicated in Fig.1. The trends for glacier-wide mass balance, glacier wide internal accumulation and original climate forcing (for the elevation of the weather station at 3837 m a.s.l.; 1 October 1968 - 30 September 2020) are also given

variable	trend	unit	p-value	significant
mean annual air temperature	+0.0295 (+0.0236)	$K\,a^{-1}$	<0.001 (<0.001)	y (y)
mean summer (JJAS) air temperature	+0.0208 (+0.0149)	$K\,a^{-1}$	0.003 (0.003)	y (y)
annual precipitation sum	+0.0018 (+0.0068)	$m\,w.e.\,a^{-1}$	0.421 (0.076)	n (y)
mean annual incoming shortwave radiation	-0.4297 (-0.2815)	$W\,m^{-2}\,a^{-1}$	<0.001 (<0.001)	y (y)
mean annual outgoing shortwave radiation	-0.3989 (-0.2362)	$W\,m^{-2}\,a^{-1}$	<0.001 (<0.001)	y (y)
mean annual incoming longwave radiation	+0.0702 (+0.0432)	$W\,m^{-2}\,a^{-1}$	0.074 (0.251)	y (n)
mean annual outgoing longwave radiation	+0.0507 (+0.0388)	$W\,m^{-2}\,a^{-1}$	0.005 (0.029)	y (y)
mean annual sensible heat flux	+0.0550 (+0.0417)	$W\,m^{-2}\,a^{-1}$	0.001 (0.003)	y (y)
mean annual latent heat flux	+0.0515 (+0.0473)	$W\,m^{-2}\,a^{-1}$	<0.001 (<0.001)	y (y)
mean annual heat flux from the subsurface	-0.0202 (-0.0153)	$W\,m^{-2}\,a^{-1}$	<0.001 (0.001)	y (y)
mean annual glacier wide mass balance	+0.0002	$m\,w.e.\,a^{-1}$	0.979	n
mean annual internal accumulation	-0.0003	$m\,w.e.\,a^{-1}$	0.159	n
mean annual air temperature 3837 m a.s.l.	+0.0222	$K\,a^{-1}$	<0.001	y
mean summer (JJAS) air temperature 3837 m a.s.l.	+0.0136	$K\,a^{-1}$	0.047	y
annual precipitation sum 3837 m a.s.l.	+0.0022	$m\,w.e.\,a^{-1}$	0.074	y
mean annual cloud cover fraction 3837 m a.s.l.	-0.0012	-	0.002	y
mean annual relative humidity 3837 m a.s.l.	-0.1240	$\%\,a^{-1}$	0.002	y
mean annual air pressure 3837 m a.s.l.	+1.6274	$Pa\,a^{-1}$	0.008	y

We do not find a significant trend in the evolution of annual mass balances (+0.0002 m w.e. a^{-1}, p-value = 0.979), nor in the reduction of mean annual internal accumulation (-0.0003 m w.e. a^{-1}, p-value = 0.159) for the period 1968/1969-2019/2020 despite significant trends within all variables used as model forcing (Table 4). Comparing annual mass balances with annual precipitation sums and summer air temperatures shows that annual mass balances are more strongly correlated to precipitation sums than to summer air temperatures (Fig. S6). The effect of the substantial warming (+0.0222 K a^{-1}, p-value < 0.001) thus seems to be attenuated by increasing precipitation (+0.0022 m w.e. a^{-1}, p-value = 0.074). The increase of net accumulation in the accumulation area (Fig. 5b) may thus be attributed to an increase of solid precipitation (Tables S2 and 4). Barandun et al. (2015) also find an increase of accumulation based on their modelling results as does the field study of Kronenberg et al. (2021a), who identified a net accumulation increase for a point location at ∼4400 m a.s.l. We can speculate that Abramov glacier might be affected by the same changes in precipitation patterns that could be partly responsible for the mass balance anomaly in western HMA (e.g. Miles et al., 2021). Barandun et al. (2015) furthermore describe a tendency towards more

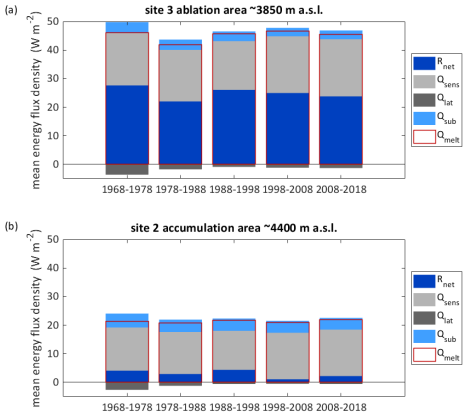

Figure 12. Mean modelled energy fluxes per decade for a grid point located in the ablation area at ∼3850 m a.s.l. (a) and in the accumulation area at at ∼4400 m a.s.l. (b). The point locations are indicated in Fig.1. R_{net} is the net radiation, Q_{sens} the sensible and Q_{lat} the latent heat flux, Q_{lat} the heat flux from/into the subsurface and Q_{melt} the total energy available for melt. The periods are hydrological years (e.g. 1968-1978 refers to 1 October 1968 - 30 September 1978).

ablation during recent decades. We find high ablation rates for the first decade and for 1998/1999-2007/2008 (Fig. 5b). In contrast to previous studies (e.g. Dyurgerov and Dwyer, 2001), we do not find a steepening of ablation gradients. The ablation gradient is higher for 1968/1969-1997/1998 (0.0080 m w.e. m^{-1}) than for 1998/1999-2019/2020 (0.0070 m w.e. m^{-1}). Miles et al. (2021) calculate an ablation gradient of 0.0084 m w.e. m^{-1} for 2012-2016. Whereas their ablation gradient is higher, their ELA of 4163 m a.s.l. is located lower than the here modelled ELA (Table 3).

We find a relevant contribution of refreezing below the last summer horizon to the overall mass balance, and this contribution evolves over time (Fig. 5c and Table 3). In the lower accumulation area up to ∼4300 m a.s.l., internal accumulation strongly increases with elevation and lowest values are modelled for the last decade (Fig. 5c). At site 1, within this zone, the subsurface density reaches the density of ice (Fig. 8a-c), which will hinder subsequent internal accumulation. An increase of subsurface densities also occurs higher up in the accumulation zone at site 2 around ∼4400 m a.s.l. as shown in Fig. 9a-c. The lowest internal accumulation rates are found for the second (1978/1979-1987/1988) and the last (2008/2009-2017/2018) modelled decade. Both of these periods follow decades with clearly negative mass balances and high refreezing rates (Table 3). This is confirmed by *in situ* measurements from several years during the first decade which indicate negative annual mass balances at several or all point observation sites in the accumulation area (Kislov, 1982; Pertziger, 1996). The model results suggest, that thanks to high accumulation and limited ablation, the firn could recover during the following years allowing for higher internal accumulation rates thereafter. Results from the most recent decade and years, however, indicate that the necessary pore space

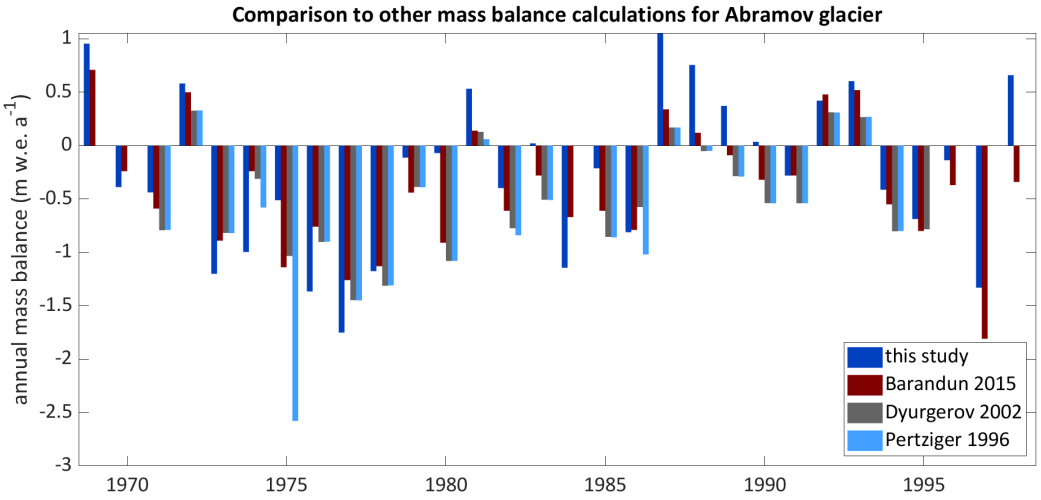

Figure 13. Comparison of annual mass balance results to previously published values for Abramov glacier based on *in situ* data (Pertziger, 1996; Dyurgerov, 2002) and based on modelling asssimilating *in situ* data (Barandun et al., 2015)

.

for refreezing is again reducing. Whereas the subsurface density at ∼4250 m a.s.l. decreases throughout the modelling period, a significant decrease is found for ∼4400 m a.s.l. after 1987/1988 only.

Abramov glacier is thus losing its capacity to buffer mass loss through refreezing. The loss of pore space occurs despite high amounts of solid precipitation (Table S2) responsible for the increased accumulation compared to the first decade (Fig. 5b) and affects large areas of the accumulation zone (Fig. 5a). For the upper elevation bands, modelled internal accumulation remains high for recent decades. Based on the observations from the lower firn sites, with further warming, these uppermost zones are, however, expected to also lose pore space. The changes are also reflected in a decrease of subsurface temperatures. The reduction and later absence of latent heat release through refreezing leads to cold firn properties at ∼4250 m a.s.l. for recent years (Fig. 8d-f). The slight cooling trend for ∼4400 m a.s.l. (Fig. 9d-f), together with the recent increase of subsurface densities, highlight that firn zone changes start to occur also at higher elevations.

Firn changes and effects on internal accumulation as identified for Abramov glacier likely also occur elsewhere in HMA. The impacts may be delayed for glaciers with higher located elevation areas, where firn conditions may still be cold and refreezing limited. The recent propagation of changes to higher elevation ranges indicates that also higher located glaciers may experience firn regime changes in future ultimately leading to a reduction of their firn area.

Mass balance observations often neglect internal accumulation or account for the process only in a simplified manner. This applies for mass balance calculation based on glaciological data but also for geodetic mass change estimates. The latter usually

use constant density conversion factors to convert elevation to mass changes. Our results indicate that internal accumulation can play an important role for glaciers with temperate accumulation areas. Whereas mass change calculations neglecting the internal accumulation may be overestimating the mass loss for periods with available pore space, this error will likely be reduced as glaciers lose pore space.

Evidence from *in situ* measurements of pore space amount and change in glaciers of HMA is very scarce. Lambrecht et al. (2020) expect a strong elevation gradient of melt water refreezing on Fedschenko Glacier, western Pamir. The chemical signature of annual accumulation layers is currently only preserved at elevations above 5200 m a.s.l., but evidence of summer melt was found at elevations of more than 5300 m a.s.l. Based on a sensitivity experiments with a region-wide application of a simple model, Wang et al. (2019) concluded that under warmer conditions, refreezing will increase for continental glaciers and decrease for glaciers located in more humid and warmer environments. In their study, Abramov glacier is located in a region for which they find an increase of refreezing. Our results indicate a decrease of internal accumulation related to the retreat of the firn line. A retreat of the firn line is likely also occurring elsewhere, however, the underlying processes are often not sufficiently included into simple, regional approaches.

4.2 Uncertainties, model sensitivities and validation

EBFM reproduces the observations satisfactorily, as shown by the comparison of modelled and measured surface mass balances (Fig. 6) and the comparison of subsurface properties (Figs. 10, 11). These comparisons of modelled and measured data provide an overall estimate of the combined modelling and observational uncertainty. The sources of the modelling uncertainty are diverse and sometimes not readily quantifiable, we here discuss the general sources and likely implications based on the performed sensitivity experiments and general considerations, rather than producing a formal uncertainty assessment for the model output.

Several uncertainties are related to the model setup. The spatial vertical and horizontal as well as temporal resolutions are too coarse to resolve all the observed variations and to reproduce all relevant processes. Consequences of the horizontal resolutions are for example that several point observations shown in Figs. S4 and 6 are located within one modelled grid cell. The model is unable to fully reproduce the spatial heterogeneity of *in situ* observations. This also applies for subsurface conditions. On Abramov glacier highly variable firn conditions and accumulation rates are found based on firn cores and ground penetrating radar data (Kronenberg et al., 2021a). This study showed that annual accumulation, measured in firn cores, can vary by a factor of 1.5 over a horizontal distance of 250 m. Thus the EBFM satisfyingly reproduces the bulk densities measured at site 2 (Fig. 10), however the lower measured densities at nearby drill sites (c4381 and c4382 in Kronenberg et al. (2021a)) are not reproduced satisfactorily as the model does not simulate the horizontal small scale variability of accumulation and furthermore does not consider processes such as wind redistribution of snow. Another uncertainty related to the model set up is the use of a linearly updated glacier surface elevations and decade-wise changing glacier outlines. These approximations of topographical changes may be responsible for underestimations (overestimations) of melt rates on the glacier tongue if surface elevations are to high (to low). The initial conditions are a further source of uncertainties. It is very likely that the atmospheric conditions

were different from the used data set prior to the modelling period. Nevertheless, modelled subsurface conditions agree well with measurements during early years of the modelling period (Fig. 10a-c).

An important source of uncertainties is related to the model forcing. While station data is available for the first thirty years, data from a gridded climate product (ERA5) has to be used for the remaining modelling period. To homogenize the input, the downscaled ERA5 data is bias corrected to match with monthly averages of observations for the overlapping period. The creation of a cloud cover forcing needed for additional processing steps. The sensitivity of related choices is shown in Figs. S9 and S10. Despite the corrections of the TopoSCALE ERA5 forcing, differences in both data sets affect the model output as evident from the results of the alternative model run which yielded a more negative mass balance for the period for which both data sets are available (alternative forcing: -0.23 m w.e. a^{-1} original forcing -0.05 m w.e. a^{-1}, Figures S11-S15). Uncertainties in the model forcing may thus be a further reason for the misfits between measured and modelled surface mass balances and our study demonstrates that results with higher confidence can be produced for the period for which in situ measurements serve as a model forcing. The differences between both distributed runs further highlight the limitations of gridded products and emphasize the importance of *in situ* data.

The parametrisations used in modelling energy balance and subsurface conditions are based on simplifications that cause further uncertainties. The snow albedo parametrisation serves as an example. Snow albedo is re-set to fresh snow albedo after each snowfall event greater than 3 mm w.e. d^{-1}. Thereby, also the albedo decay scheme starts again with the value for fresh snow. During field visits in summer, we observed the deposition of fresh snow on a longer exposed snow surface with a visibly reduced albedo. The fresh snow then melted away within hours to days again exposing the darker snow. The used parametrisation is not able to reproduce this evolution. This simplification may be compensated by the calibration of $t^*_{wet} = 7$ days, which is more suitable to represent conditions in Central Asia than the higher default value of 15 days used in the Arctic (Bougamont et al., 2005; van Pelt et al., 2019). As previously discussed in van Pelt and Kohler (2015), the model is not able to reproduce the small scale density variability of the subsurface (Fig. 10) as several processes such as wind crust formation, modelling of firn/snow grains or local vertical pooling of melt water on existing high density layers are not included.

Further model uncertainties are related to the choice of parameters. The sensitivity model runs for the modified parameters (Figs. S7 and S8) highlight that parameter perturbations have strong impacts on mass balance and internal accumulation. The deviations between different model runs is highest for the point location in the lower accumulation area (site 1, cf. Fig. 1b). This underlines the sensitivity and critical role of the firn cover in this elevation zone. Whereas, site 3 remains an ablation site for all parameter scenarios, the most extreme parameter scenarios result in almost balanced mass changes at site 2 ($\sim$4400 m a.s.l, Fig. S7a,c). At, site 1 ($\sim$4250 m a.s.l) internal accumulation reduces for almost all parameter scenarios (Fig. S8b). The largest impact on mass balance and internal accumulations is caused by the perturbation of the winter precipitation correction factor ($Prec_{c-w}$), and the fresh snow albedo (α_{snow}), which were both constrained by the exceptional *in situ* data available for Abramov glacier.

The calibration data, however, are only available for point locations. We use spatially and temporally constant parameter values for periods with and without *in situ* measurements. This necessary simplification has implications; for example, we use temporally constant albedo parameters, whereas a darkening of the glacier surface is likely (Sarangi et al., 2019). An

underestimation of recent ablation rates (Fig. 6b) may be related to albedo decreases (Schmale et al., 2017) which are not considered due to a lack of respective calibration data.

Our study shows, that long-term *in situ* measurements are of great value for simulating the long-term evolution of Abramov glacier with a coupled surface energy balance–multilayer subsurface model. The comprehensive model output complements the exceptional observational data set for this glacier. The combination of both data sets provides an opportunity to discuss processes on a high spatial and temporal resolution for a period of more than five decades which is unprecedented for the data sparse HMA.

5 Conclusions

In this study, we apply a distributed coupled surface energy balance and firn model to simulate 52 years of mass balance and firn evolution of Abramov glacier, Pamir Alay. The model is forced with a combination of weather station and downscaled reanalysis data. The modelled surface mass balance and subsurface conditions agree well with *in situ* measurements for the beginning of the modelling period and recent years. We find an overall negative mass balance of -0.27 m w.e. a^{-1} for 1968/1969-2019/2020, which is somewhat less negative than the mass balance determined by previous studies. The first modelled decade 1968/1969-1977/1978 is characterized by the most negative mass balance and is followed by two decades of almost balanced conditions. More recent years are again characterised by clearly negative conditions. Our results indicate that the firn of Abramov glacier is currently losing pore space and that the loss of pore space is more advanced in the lower accumulation area. The warm and also cold infiltration zones of glaciers located at higher locations may not yet be affected. The correlation of annual mass balance with annual precipitation sums (R^2=0.72, p-value < 0.001) is stronger than the correlation with summer air temperature (R^2=0.29, p-value < 0.001). Increasing precipitation rates have thus compensated for increasing air temperatures, preventing an acceleration of mass loss for Abramov glacier during the last five decades. To our knowledge, this is the first application of a model of similar complexity for such a long time period for a glacier in HMA and may thus provide valuable insights into processes of within data scarce region.

Code and data availability. The EBFM code, the model forcing and topographical grid used in this study are available at https://doi.org/10.5281/zenodo.5773796 (Kronenberg et al., 2021b). Due to their large volume, modelled grids are available on request. The majority of in situ mass balance data used for calibration and validation are available from the World Glacier Monitoring Service (doi.org/10.5904/wgms-fog-2021-05) (WGMS, 2021). Additional mass balance data at monthly resolution and for recent years are also available on request. Measurements of the automatic weather station can be downloaded from http://178.217.169.232/sdss/index.php?&page=measure_page (Schöne et al, 2013).

Author contributions. MK performed the analysis and wrote the paper. WvP supplied the EBFM model code and support to use it. MK, HM and MH took place in several field campaigns acquiring *in situ* data. JF applied TopoSCALE to downscale the ERA5 data. FP provided the

historical meteorological and mass balance data as well as extensive clarification on the data set. All authors participated in the discussion of the results.

Competing interests. The authors declare that they have no conflict of interest.

Acknowledgements. We acknowledge all the people who have been involved in the collection of field data on Abramov glacier. Especially we would like to thank to Erlan Azsivov, Ruslan Kenzhebaev Bolot Moldobekov and Ryskul Usubaliev from the Central Asian Institute for Applied Geosciences (CAIAG) and Sultanbek Belekov and Iurii Novomlintsev from KyrgyzHydromet for organizing the mass balance measurements on Abramov glacier during the last years and to Martina Barandun and Tomas Saks for their continuous efforts in coordinating the monitoring activities. We greatly acknowledge the help of Stanislav Kutuzov, Ivan Lavrentiev, Alex Merkushkin, Yuri Tarasov, François Valla and Andrey Yakovlev for providing access to literature and data published in Russian and complementary information. We thank Enrico Mattea for the valuable exchange about the model application and also for sharing his code used for modelling experiments. This study was financed by the Swiss National Science Foundation (SNSF), grant 200021_169453 and the Project CICADA (Cryospheric Climate Services for improved Adaptation, contract no. 81049674 between the Swiss Agency for Development and Cooperation and the University of Fribourg).

References

Aalstad, K., Westermann, S., Schuler, T. V., Boike, J., and Bertino, L.: Ensemble-based assimilation of fractional snow-covered area satellite retrievals to estimate the snow distribution at Arctic sites, The Cryosphere, 12, 247–270, https://doi.org/10.5194/tc-12-247-2018, 2018.

Arthern, R. J., Vaughan, D. G., Rankin, A. M., Mulvaney, R., and Thomas, E. R.: In situ measurements of Antarctic snow compaction compared with predictions of models, Journal of Geophysical Research, 115, 1–12, https://doi.org/10.1029/2009JF001306, 2010.

Azam, M. F., Wagnon, P., Vincent, C., Ramanathan, A. L., Favier, V., Mandal, A., and Pottakkal, J. G.: Processes governing the mass balance of Chhota Shigri Glacier (western Himalaya, India) assessed by point-scale surface energy balance measurements, The Cryosphere, 8, 2195–2217, https://doi.org/10.5194/tc-8-2195-2014, 2014.

Barandun, M., Huss, M., Sold, L., Farinotti, D., Azisov, E., Salzmann, N., Usubaliev, R., Merkushkin, A., Hoelzle, M., A.Merkushkin, and Hoelzle, M.: Re-analysis of seasonal mass balance at Abramov glacier 1968-2014, Journal of Glaciology, 61, 1103–1117, https://doi.org/10.3189/2015JoG14J239, 2015.

Barandun, M., Pohl, E., Naegeli, K., McNabb, R., Huss, M., Berthier, E., Saks, T., and Hoelzle, M.: Hot Spots of Glacier Mass Balance Variability in Central Asia, Geophysical Research Letters, 48, 1–14, https://doi.org/10.1029/2020GL092084, 2021.

Bougamont, M., Bamber, J. L., and Greuell, W.: A surface mass balance model for the Greenland Ice Sheet, Journal of Geophysical Research: Earth Surface, 110, 1–13, https://doi.org/10.1029/2005JF000348, 2005.

Brun, F., Berthier, E., Wagnon, P., Kääb, A., and Treichler, D.: A spatially resolved estimate of High Mountain Asia glacier mass balances from 2000 to 2016, Nature Geoscience, 10, 668–674, https://doi.org/10.1038/ngeo2999, 2017.

Cogley, J. G., Hock, R., Rasmussen, L. A., Arendt, A. A., Bauder, A., Braithwaite, R. J., Jansson, M., Kaser, G., Möller, M., Nicholson, L., and Zemp, M.: Glossary of Glacier Mass Balance, IHP-VII Technical Documents in Hydrology, IACS Contribution No.2, 86, 114, unesdoc.unesco.org/images/0019/001925/192525e.pdf, 2011.

De Kok, R. J., Kraaijenbrink, P. D., Tuinenburg, O. A., Bonekamp, P. N., and Immerzeel, W. W.: Towards understanding the pattern of glacier mass balances in High Mountain Asia using regional climatic modelling, Cryosphere, 14, 3215–3234, https://doi.org/10.5194/tc-14-3215-2020, 2020.

Denzinger, F., Machguth, H., Barandun, M., Berthier, E., Girod, L., Kronenberg, M., Usubaliev, R., and Hoelzle, M.: Geodetic mass balance of Abramov Glacier from 1975 to 2015, Journal of Glaciology, 67, 331–342, https://doi.org/10.1017/jog.2020.108, 2021.

Dyurgerov, M.: Glacier Mass Balance and Regime: Data of Measurements and Analysis, INSTAAR Occasional Paper, p. 268, 2002.

Dyurgerov, M. and Dwyer, J.: The Steepening of Glacier Mass Balance Gradients with Northern Hemisphere Warming, Zeitschrift für Gletscherkunde und Glazialgeologie, 36, 107–118, 2001.

Fiddes, J. and Gruber, S.: TopoSCALE v.1.0: Downscaling gridded climate data in complex terrain, Geoscientific Model Development, 7, 387–405, https://doi.org/10.5194/gmd-7-387-2014, 2014.

Fiddes, J., Endrizzi, S., and Gruber, S.: Large-area land surface simulations in heterogeneous terrain driven by global data sets: Application to mountain permafrost, Cryosphere, 9, 411–426, https://doi.org/10.5194/tc-9-411-2015, 2015.

Fiddes, J., Aalstad, K., and Westermann, S.: Hyper-resolution ensemble-based snow reanalysis in mountain regions using clustering, Hydrology and Earth System Sciences, 23, 4717–4736, https://doi.org/10.5194/hess-23-4717-2019, 2019.

Glazyrin, G. E., Glazyrina, E. L., Kislov, B. V., and Pertziger, F. I.: Water level regime in deep firn pits on Abramov glacier [in Russian], Trudy SARNIGMI, 45, 54–61, 1977.

Glazyrin, G. E., Kamnyansky, G. M., and Pertziger, F. I.: The regime of Abramov glacier [in Russian], Gidrometeoizdat, St. Petersburg, 1993.

Greuell, W. and Konzelmann, T.: Numerical modelling of the energy balance and the englacial temperature of the Greenland ice sheet. Calculations for the ETH-Camp location (West Greenland, 1155 m a.s.l.), Global and Planetary Change, 9, 91–114, https://doi.org/10.1016/0921-8181(94)90010-8, 1994.

Greuell, W., Knap, W. H., and Smeets, P. C.: Elevational changes in meteorological variables along a mid-latitude glacier during summer, Journal of Geophysical Research, 102, 25 941–25 954, https://doi.org/10.1029/97JD02083, 1997.

Hersbach, H., Bell, B., Berrisford, P., Hirahara, S., Horányi, A., Muñoz-Sabater, J., Nicolas, J., Peubey, C., Radu, R., Schepers, D., Simmons, A., Soci, C., Abdalla, S., Abellan, X., Balsamo, G., Bechtold, P., Biavati, G., Bidlot, J., Bonavita, M., De Chiara, G., Dahlgren, P., Dee, D., Diamantakis, M., Dragani, R., Flemming, J., Forbes, R., Fuentes, M., Geer, A., Haimberger, L., Healy, S., Hogan, R. J., Hólm, E., Janisková, M., Keeley, S., Laloyaux, P., Lopez, P., Lupu, C., Radnoti, G., de Rosnay, P., Rozum, I., Vamborg, F., Villaume, S., and Thépaut, J. N.: The ERA5 global reanalysis, Quarterly Journal of the Royal Meteorological Society, 146, 1999–2049, https://doi.org/10.1002/qj.3803, 2020.

Hock, R.: Glacier melt: a review of processes and their modelling, Progress in Physical Geography, 29, 362–391, https://doi.org/10.1191/0309133305pp453ra, 2005.

Hoelzle, M., Azisov, E., Barandun, M., Huss, M., Farinotti, D., Gafurov, A., Hagg, W., Kenzhebaev, R., Kronenberg, M., Machguth, H., Merkushkin, A., Moldobekov, B., Petrov, M., Saks, T., Salzmann, N., Schöne, T., Tarasov, Y., Usubaliev, R., Vorogushyn, S., Yakovlev, A., and Zemp, M.: Re-establishing a monitoring programme for glaciers in Kyrgyzstan and Uzbekistan, Central Asia, Geoscientific Instrumentation, Methods and Data Systems, 6, 397–418, https://doi.org/10.5194/gi-6-397-2017, 2017.

Huintjes, E., Neckel, N., Hochschild, V., and Schneider, C.: Surface energy and mass balance at Purogangri ice cap, central Tibetan Plateau, 2001-2011, Journal of Glaciology, 61, 1048–1060, https://doi.org/10.3189/2015JoG15J056, 2015a.

Huintjes, E., Sauter, T., Schröter, B., Maussion, F., Yang, W., Kropácek, J., Buchroithner, M., Scherer, D., Kang, S., and Schneider, C.: Evaluation of a coupled snow and energy balance model for Zhadang glacier, Tibetan Plateau, using glaciological measurements and time-lapse photography, Arctic, Antarctic, and Alpine Research, 47, 573–590, https://doi.org/10.1657/AAAR0014-073, 2015b.

Huintjes, E., Loibl, D., Lehmkuhl, F., and Schneider, C.: A modelling approach to reconstruct Little Ice Age climate from remote-sensing glacier observations in southeastern Tibet, Annals of Glaciology, 57, 359–370, https://doi.org/10.3189/2016AoG71A025, 2016.

Jakob, L., Gourmelen, N., Ewart, M., and Plummer, S.: Spatially and temporally resolved ice loss in High Mountain Asia and the Gulf of Alaska observed by CryoSat-2 swath altimetry between 2010 and 2019, The Cryosphere, 15, 1845–1862, https://doi.org/10.5194/tc-2020-176, 2021.

Kääb, A., Berthier, E., Nuth, C., Gardelle, J., Arnaud, Y., Kaab, A., Berthier, E., Nuth, C., Gardelle, J., and Arnaud, Y.: Contrasting patterns of early twenty-first-century glacier mass change in the Himalayas, Nature, 488, 495–498, https://doi.org/10.1038/nature11324, 2012.

Kayastha, R. B., T, O., and Ageta, Y.: Application of a mass-balance model to a Himalayan glacier, Journal of Glaciology, 45, 559–567, https://doi.org/10.3189/S002214300000143X, 1999.

Kislov, B. V.: About the question of determining the internal accumulation of temperate glaciers [in Russian], Trudy SARNIGMI, 45, 62–72, 1977.

Kislov, B. V.: Formation and regime of the firn-ice stratum of a mountain glacier [in Russian], Ph.D. thesis, SARNIGMI Tashkent, 1982.

Kislov, B. V., Nozdrukhin, V. K., and Pertziger, F. I.: Temperature regime of the active layer of Abramov Glacier [in Russian], Materialy Glatsiologicheskih Issledovanii (Data of glaciological studies), 30, 199–204, 1977.

Klok, E. J. and Oerlemans, J.: Model study of the spatial distribution of the energy and mass balance of Morteratschgletscher, Switzerland, Journal of Glaciology, 48, 505–518, https://doi.org/10.3189/172756502781831133, 2002.

Konzelmann, T., Van de Wal, R., Gruell, W., Binanja, E., Henneken, C., and Abe-Ouchi, A.: Parameterization of global and longwave incoming radiation for the Greenland Ice Sheet, Global and Planetary Change, 9, 143–164, https://doi.org/10.1016/0921-8181(94)90013-2, 1994.

Kronenberg, M., MacHguth, H., Eichler, A., Schwikowski, M., and Hoelzle, M.: Comparison of historical and recent accumulation rates on Abramov Glacier, Pamir Alay, Journal of Glaciology, 67, 253–268, https://doi.org/10.1017/jog.2020.103, 2021a.

Kronenberg, M., van Pelt, W., Machguth, H., Hoelzle, M., Fiddes, J., Hoelzle, M., and Pertziger, F.: MarleneKro/ebfm_abramov: version 1.0 [code], https://doi.org/10.5281/zenodo.5773796, 2021b.

Lambrecht, A., Mayer, C., Bohleber, P., and Aizen, V.: High altitude accumulation and preserved climate information in the western Pamir, observations from the Fedchenko Glacier accumulation basin, Journal of Glaciology, 66, 219–230, https://doi.org/10.1017/jog.2019.97, 2020.

Ligtenberg, S. R. M., Helsen, M. M., and Van Den Broeke, M. R.: An improved semi-empirical model for the densification of Antarctic firn, Cryosphere, 5, 809–819, https://doi.org/10.5194/tc-5-809-2011, 2011.

Marchenko, S., Pelt, W. V., Claremar, B., Pohjola, V., Pettersson, R., Machguth, H., and Reijmer, C.: Parameterizing deep water percolation improves subsurface temperature simulations by a multilayer firn model, Frontiers in Earth Science, 5, 1–20, https://doi.org/10.3389/feart.2017.00016, 2017.

Mattea, E., Machguth, H., Kronenberg, M., van Pelt, W., Bassi, M., and Hoelzle, M.: Firn changes at Colle Gnifetti revealed with a high-resolution process-based physical model approach, The Cryosphere, 15, 3181–3205, https://doi.org/https://doi.org/10.5194/tc-15-3181-2021, 2021.

Miles, E., McCarthy, M., Dehecq, A., Kneib, M., Fugger, S., and Pellicciotti, F.: Health and sustainability of glaciers in High Mountain Asia, Nature Communications, 12, https://doi.org/10.1038/s41467-021-23073-4, http://dx.doi.org/10.1038/s41467-021-23073-4, 2021.

Mölg, T. and Hardy, D. R.: Ablation and associated energy balance of a horizontal glacier surface on Kilimanjaro, Journal of Geophysical Research D: Atmospheres, 109, 1–13, https://doi.org/10.1029/2003JD004338, 2004.

Mölg, T., Maussion, F., Yang, W., and Scherer, D.: The footprint of Asian monsoon dynamics in the mass and energy balance of a Tibetan glacier, The Cryosphere, 6, 1445–1461, https://doi.org/10.5194/tc-6-1445-2012, 2012.

Obu, J., Westermann, S., Bartsch, A., Berdnikov, N., Christiansen, H. H., Dashtseren, A., Delaloye, R., Elberling, B., Etzelmüller, B., Kholodov, A., Khomutov, A., Kääb, A., Leibman, M. O., Lewkowicz, A. G., Panda, S. K., Romanovsky, V., Way, R. G., Westergaard-Nielsen, A., Wu, T., Yamkhin, J., and Zou, D.: Northern Hemisphere permafrost map based on TTOP modelling for 2000–2016 at 1 km^2 scale, Earth-Science Reviews, 193, 299–316, https://doi.org/10.1016/j.earscirev.2019.04.023, 2019.

Obu, J., Westermann, S., Vieira, G., Abramov, A., Balks, M. R., Bartsch, A., Hrbáček, F., Kääb, A., and Ramos, M.: Pan-Antarctic map of near-surface permafrost temperatures at 1 km^2 scale, The Cryosphere, 14, 497–519, https://doi.org/10.5194/tc-14-497-2020, https://tc.copernicus.org/articles/14/497/2020/, 2020.

Oerlemans, J.: Glaciers and climate change, AA Balkema Publishers, Lisse and Exton (PA), 2001.

Oerlemans, J. and Grisogono, B.: Glacier winds and parameterisation of the related surface heat fluxes, Tellus, Series A: Dynamic Meteorology and Oceanography, 54, 440–452, https://doi.org/10.1034/j.1600-0870.2002.201398.x, 2002.

Pellicciotti, F., Carenzo, M., Helbing, J., Rimkus, S., and Burlando, P.: On the role of subsurface heat conduction in glacier energy-balance modelling, Annals of Glaciology, 50, 16–24, https://doi.org/10.3189/172756409787769555, 2009.

Pertziger, F.: Abramov Glacier Data Reference Book: Climate, Runoff, Mass Balance, Central Asian Hydrometeorlogical Institute, Tashkent, 1996.

Pohl, E., Gloaguen, R., and Seiler, R.: Remote sensing-based assessment of the variability of winter and summer precipitation in the pamirs and their effects on hydrology and hazards using harmonic time series analysis, Remote Sensing, 7, 9727–9752, https://doi.org/10.3390/rs70809727, 2015.

Reijmer, C. H. and Hock, R.: Internal accumulation on Storglaciären, Sweden, in a multi-layer snow model coupled to a distributed energy- and mass-balance model, Journal of Glaciology, 54, 61–72, https://doi.org/10.3189/002214308784409161, 2008.

RGI Consortium: Randolph Glacier Inventory – A Dataset of Global Glacier Outlines: Version 6.0, Global Land Ice Measurements from Space, Colorada, USA. Digital Media, https://doi.org/10.7265/N5-RGI-60, 2017.

Sarangi, C., Qian, Y., Rittger, K., Bormann, K. J., Liu, Y., Wang, H., Wan, H., Lin, G., and Painter, T. H.: Impact of light-absorbing particles on snow albedo darkening and associated radiative forcing over high-mountain Asia: high-resolution WRF-Chem modeling and new satellite observations, Atmospheric Chemistry and Physics, 19, 7105–7128, https://doi.org/10.5194/acp-19-7105-2019, 2019.

Schmale, J., Flanner, M., Kang, S., Sprenger, M., Zhang, Q., Guo, J., Li, Y., Schwikowski, M., and Farinotti, D.: Modulation of snow reflectance and snowmelt from Central Asian glaciers by anthropogenic black carbon, Scientific Reports, 7, 1–10, https://doi.org/10.1038/srep40501, 2017.

Schneider, T. and Jansson, P.: Internal accumulation in firn and its significance for the mass balance of Storglaciären, Sweden, Journal of Glaciology, 50, 25–34, https://doi.org/10.3189/172756504781830277, 2004.

Schöne, T., Zech, C., Unger-Shayesteh, K., Rudenko, V., Thoss, H., Wetzel, H.-U., Gafurov, A., Illigner, J., and Zubovich, A.: A new permanent multi-parameter monitoring network in Central Asian high mountains - from measurements to data bases, Geoscientific Instrumentation, Methods and Data Systems, 2, 97–111, https://doi.org/10.5194/gi-2-97-2013, 2013.

Schuler, T. V. and rn Ims Østby, T.: Sval-Imp: A gridded forcing dataset for climate change impact research on Svalbard, Earth System Science Data, 12, 875–885, https://doi.org/10.5194/essd-12-875-2020, 2020.

Sevruk, B.: Systematischer Niederschlagsmessfehler in der Schweiz, in: Der Niederschlag in der Schweiz, Beiträge zur Geologie der Schweiz - Hydrologie, edited by Sevruk, B., vol. 31, pp. 65–75, 1985.

Shean, D. E., Bhushan, S., Montesano, P., Rounce, D. R., Arendt, A., and Osmanoglu, B.: A Systematic, Regional Assessment of High Mountain Asia Glacier Mass Balance, Frontiers in Earth Science, 7, 1–19, https://doi.org/10.3389/feart.2019.00363, 2020.

Sicart, J. E., Hock, R., Ribstein, P., Litt, M., and Ramirez, E.: Analysis of seasonal variations in mass balance and meltwater discharge of the tropical Zongo Glacier by application of a distributed energy balance model, J. Geophys. Res. Atmos., 116, 1–18, https://doi.org/10.1029/2010JD015105, 2011.

Smith, W. L.: Note on the Relationship Between Total Predictable Water and Surface Dew Point, Journal of Applied Meteorology, 5, 726–727, https://doi.org/10.1175/1520-0450(1966)005<0726:NOTRBT>2.0.CO;2, 1966.

Stainbank, W. D.: Simulation of Abramov glacier energy balance and firn properties, Msc thesis, University of Fribourg, 2018.

Sturm, M., Holmgren, J., König, M., and Morris, K.: The thermal conductivity of seasonal snow, Journal of Glaciology, 43, 26–41, https://doi.org/10.1017/S0022143000002781, 1997.

Suslov, V. F. and Krenke, A. N.: Abaramov Glacier (Alay Range) [in Russian], Gidrometeoizdat, St. Petersburg, 1980.

Thibert, E., Blanc, R., Vincent, C., and Eckert, N.: Glaciological and Volumetric Mass Balance Measurements: Error Analysis over 51 years for the Sarennes glacier, French Alps, Journal of Glaciology, 54, 522–532, 2008.

van Kampenhout, L., Lenaerts, J. T., Lipscomb, W. H., Sacks, W. J., Lawrence, D. M., Slater, A. G., and van den Broeke, M. R.: Improving the Representation of Polar Snow and Firn in the Community Earth System Model, Journal of Advances in Modeling Earth Systems, 9, 2583–2600, https://doi.org/10.1002/2017MS000988, 2017.

van Pelt, W. and Kohler, J.: Modelling the long-term mass balance and firn evolution of glaciers around Kongsfjorden, Svalbard, Journal of Glaciology, 61, 731–744, https://doi.org/10.3189/2015JoG14J223, 2015.

van Pelt, W., Pohjola, V., Pettersson, R., Marchenko, S., Kohler, J., Luks, B., Hagen, J. O., Schuler, T. V., Dunse, T., Noël, B., and Reijmer, C.: A long-term dataset of climatic mass balance , snow conditions , and runoff in Svalbard (1957 – 2018), The Cryosphere, 13, 2259–2280, https://doi.org/10.5194/tc-13-2259-2019, 2019.

van Pelt, W. J., Schuler, T. V., Pohjola, V. A., and Pettersson, R.: Accelerating future mass loss of Svalbard glaciers from a multi-model ensemble, Journal of Glaciology, 67, 485–499, https://doi.org/10.1017/jog.2021.2, 2021.

van Pelt, W. J. J., Oerlemans, J., Reijmer, C. H., Pohjola, V. A., Pettersson, R., and Van Angelen, J. H.: Simulating melt, runoff and refreezing on Nordenskiöldbreen, Svalbard, using a coupled snow and energy balance model, The Cryosphere, 6, 641–659, https://doi.org/10.5194/tc-6-641-2012, 2012.

Vandecrux, B., Mottram, R., L. Langen, P., S. Fausto, R., Olesen, M., Max Stevens, C., Verjans, V., Leeson, A., Ligtenberg, S., Kuipers Munneke, P., Marchenko, S., van Pelt, W., R. Meyer, C., B. Simonsen, S., Heilig, A., Samimi, S., Marshall, S., MacHguth, H., MacFerrin, M., Niwano, M., Miller, O., I. Voss, C., and E. Box, J.: The firn meltwater Retention Model Intercomparison Project (RetMIP): Evaluation of nine firn models at four weather station sites on the Greenland ice sheet, Cryosphere, 14, 3785–3810, https://doi.org/10.5194/tc-14-3785-2020, 2020.

Vionnet, V., Brun, E., Morin, S., Boone, A., Faroux, S., Le Moigne, P., Martin, E., and Willemet, J.-M.: The detailed snowpack scheme Crocus and its implementation in SURFEX v7.2, Geoscientific Model Development, 5, 773–791, https://doi.org/10.5194/gmd-5-773-2012, 2012.

Wang, R., Liu, S., Shangguan, D., Radić, V., and Zhang, Y.: Spatial heterogeneity in glacier mass-balance sensitivity across High Mountain Asia, Water, 11, 776, https://doi.org/10.3390/w11040776, 2019.

Westermann, S., Ostby, T. I., Gisnäs, K., Schuler, T. V., and Etzelmüller, B.: A ground temperature map of the North Atlantic permafrost region based on remote sensing and reanalysis data, The Cryosphere, 9, 1303–1319, https://doi.org/10.5194/tc-9-1303-2015, 2015.

WGMS: Fluctuations of Glaciers Database, https://doi.org/doi.org/10.5904/wgms-fog-2021-05, 2021.

Yao, T., Thompson, L., Yang, W., Yu, W., Gao, Y., Guo, X., Yang, X., Duan, K., Zhao, H., Xu, B., Pu, J., Lu, A., Xiang, Y., Kattel, D. B., and Joswiak, D.: Different glacier status with atmospheric circulations in Tibetan Plateau and surroundings, Nature Climate Change, 2, 663–667, https://doi.org/10.1038/nclimate1580, 2012.

Yen, Y.-C.: Review of thermal properties of snow, ice and sea ice., Tech. rep., CRREL report 81-10, DTIC, Hanover, New Hampshire, USA, 1981.

Zech, C., Schöne, T., Illigner, J., Stolarczuk, N., Queißer, T., Köppl, M., Thoss, H., Zubovich, A., Sharshebaev, A., Zakhidov, K., Toshpulatov, K., Tillayev, Y., Olimov, S., Paiman, Z., Unger-Shayesteh, K., Gafurov, A., and Moldobekov, B.: Hydrometeorological data from a Remotely Operated Multi-Parameter Station network in Central Asia, Earth System Science Data, 13, 1289–1306, https://doi.org/10.5194/essd-13-1289-2021, 2021.

Zhang, G., Kang, S., Fujita, K., Huintjes, E., Xu, J., Yamazaki, T., Haginoya, S., Wei, Y., Scherer, D., Schneider, C., and Yao, T.: Energy and mass balance of Zhadang glacier surface, central Tibetan Plateau, Journal of Glaciology, 59, 137–148, https://doi.org/10.3189/2013JoG12J152, 2013.

Zhu, M., Yao, T., Xie, Y., Xu, B., Yang, W., and Yang, S.: Mass balance of Muji Glacier, northeastern Pamir, and its controlling climate factors, Journal of Hydrology, 590, 1–17, https://doi.org/10.1016/j.jhydrol.2020.125447, 2020.

3. Discussion

The studies on Abramov glacier with a focus on firn go beyond previous mass balance studies for Central Asian glaciers. The length of the study period and the relatively detailed simulation of individual processes are outstanding even for the larger region of High Mountain Asia. As discussed in Paper I and Paper II, different limitations challenged the work and uncertainties remain. In the following, main open questions as well as the relevance of the new insights will be synthesised in the context of glacier changes in Central Asia. For aspects that have so far have received little attention for glaciers in Central Asia, studies from other regions are consulted. The chapter structure follows the main objectives of this thesis: *state of firn*, *firn evolution* and *impact of firn changes on glacier mass balance*.

3.1. State of firn

The state of firn of Abramov glacier could be assessed at two points on the glacier based on the analysis of historical data and own measurements. GPR measurements reveal spatially heterogeneous accumulation patterns, which challenge a comparison of historical and recent measurements.

3.1.1. Challenges

It was the goal to quantify changes in firn properties. To do such a comparison, historical data are essential. The dissertation of Boris Kislov (Kislov, 1982) is of great importance for this work. Its significance was identified through the evaluation of literature previously available at the Department of Geosciences of the University of Fribourg and publications provided by colleagues from Moscow and Tashkent. Thanks to Felix Pertziger and Ivan Lavrentiev, a hard copy of Kislov (1982) was found at the Russian State Library in Moscow and a scan was organized. Possibly a hard copy is also archived in Tashkent. Colleagues from Uzhydromet, however, could only find a summary.

A focus was laid on the site at ~4400 m a.s.l. (s2), for which most historical data was available. It was not possible to drill cores to a larger depth than ~18 m. At depth, many

repeated attempts were necessary to get the firn segments out of the borehole (due to the presence of ice lenses and/or liquid water). One firn core drilled in winter 2018 (c4382) could be shipped to Switzerland for the purpose of dating. As discussed in Paper I, the comparison of historical and recent data was a demanding task as the position of legacy investigations was only reported relative to a local coordinate system and as accumulation on Abramov glacier is spatially heterogeneous.

Although Soviet scientists have studied firn on various glaciers (e.g. Krenke et al., 1970; Golubev et al., 1988; Dyurgerov and Mikhalenko, 1995), only very limited efforts have been undertaken to repeat the historical measurements and to asses firn changes. Thompson et al. (1997) and Kutuzov (2005) compared repeated firn measurements from the summit of Gregoriev ice cap. However, in those studies, the localisation of the historical measurements does not seem to have been a problem.

The study by Lambrecht et al. (2014), who assessed historical ice thickness data for Fedchenko glacier, also report issues regarding the location of the measurements. They could therefore only use the historical data qualitatively. Machguth et al. (2016) have compiled historical mass balance data of Greenland glaciers and ablation data of the Greenland Ice Sheet. For this purpose, data without coordinates were digitised from legacy maps. Such an approach was not possible for the Abramov glacier. The historical maps of Abramov glacier are rather schematic and show numerous symbols in the area of the accumulation studies. The exact locations of measurements cannot be discerned from these visualisations. The digitisation of historical maps of the Abramov glacier therefore does not provide accurate information about the location of the surveys in the accumulation area. Machguth et al. (2016) reports that they were not able to link reported local coordinates to a global system.

As shown in Paper I, connecting local to global coordinates was possible for Abramov coordinates thanks to the combination of various data sources and differential GPS measurements. The used approach may be applicable to other sites as long as benchmarks such as mountain peaks with local coordinates can be clearly identified in the field. Paper I furthermore showed how historical photographs can be used to identify historical investigation sites. However, this approach requires clear topographical features and is only applicable if the glacier surface elevation is relatively stable.

3.1.2. Relevance

The combined data set of historical and recent firn data for Abramov glacier presented in Paper I is the only firn data set available for the Pamir Alay. Furthermore, it represents one of the only reassessments of a historical firn investigation site. The firn data from Abramov

glacier provided insights into processes occurring in the accumulation area. Evidence of frequent melt conditions at ~4250 m a.s.l. and at ~4400 m a.s.l. was found for the 1970s as well as for recent years.

A few firn data were collected in neighbouring regions of Central Asia (Fig. 1.2). Available studies focus on higher locations with cold firn conditions. Gregoriev ice cap (Tien Shan) is the only site for which historical measurements are repeated (Kutuzov, 2005). The firn stratigraphy at 4660 m a.s.l. on this ice cap was already characterised by melt features in the past (e.g. Arkhipov et al., 1997) and a firn warming trend was detected (Thompson et al., 1993). Other Tien Shan *in situ* firn measurements exist for Inilchek glacier (Aizen et al., 1997; Kreutz et al., 2001; Aizen et al., 2004). In the Pamir, a high elevated core was drilled on Muztag Ata (Duan et al., 2015) and firn studies exist for Fedchenko glacier (Aizen et al., 2009; Lambrecht et al., 2020). Except for Gregoriev ice cap, it is difficult to gain a picture of firn evolution in Central Asia based on the available studies. Nevertheless, firn changes due to climate change (e.g. Barzycka et al., 2020; Marshall, 2021) must also be assumed for Central Asian glaciers. Kutuzov (2005) discusses the potential of a firn facies change from the *cold infiltration-recrystallisation (cold firn)* to the *infiltration (firn-ice zone)* for Gregoriev ice cap. The studies for Fedchenko glacier also point out changes in firn conditions. In 2005, no signs of melt water percolation were found at elevations of 5206 and 5365 m a.s.l. (Aizen et al., 2009). According to more recent measurements, Lambrecht et al. (2020) describe evidence of melt events at elevations of up to 5300 m a.s.l. They conclude that elevations above 5200 m a.s.l. are just high enough to guarantee the preservation of annual layers. Whereas Aizen et al. (2009) situated the accumulation area of Fedchenko in the *recrystallisation* zone, Lambrecht et al. (2020) concluded that the conditions are typical for the *cold infiltration* zone.

In order to explore firn changes at other locations in Central Asia and elsewhere, findings from the work on Abramov Glacier can be helpful. An important aspect is the localisation of the drilling site, which may be only approximately known for the historical investigations also elsewhere. Supplementary GPR measurements can provide clarity about the spatial representativeness of the measurement site. Respective data from Abramov shows that accumulation patterns may be highly variable. Paper I furthermore provides a suggestion how to interpret historical firn data. And last but not least, melt influenced firn conditions as found on Abramov glacier are expected to become increasingly abundant.

Paper I furthermore includes evaluation of accumulation rates. The determination of net accumulation rates in a core from 2018 is remarkable in two respects: On the one hand, it is noteworthy from the perspective of firn core dating. Dating of temperate firn is

problematic as many chemical species are relocated within melt affected firn (Eichler et al., 2001; Ginot et al., 2010; Vega et al., 2016). Whereas seasonal signals of water stable isotopes δD, δ^{18}O and Ammonium NH_4^+ were detectable in firn cores from temperate glaciers in the Swiss Alps (Eichler et al., 2001; Sold et al., 2015), the additional analysis of Black Carbon concentration and the observable stratigraphy were of great value for the dating core c4382. In this context it should also be mentioned that the relatively high accumulation rates facilitated the dating. On the other hand, the determination of net accumulation rates provided *in situ* data which is directly related to precipitation rates. This is valuable, as no precipitation measurements exist for the respective period. The net accumulation increase provides *in situ* evidence of a net accumulation increase which is very likely related to increasing precipitation.

3.2. Firn evolution

The long-term firn evolution of Abramov glacier was assessed using a coupled surface energy balance–multilayer subsurface model (EBFM) (van Pelt et al., 2012). The model was forced with weather station measurements and downscaled, bias corrected reanalysis data. At ~4400 m a.s.l., modelled firn characteristics agree well with *in situ* data from the 1970s and 2018. Towards the end of the modelling period, model results for lower elevations near the firn-ice transition zone have larger discrepancies from *in situ* data (site 1 at ~4250 m a.s.l).

3.2.1. Challenges

A major challenge in modelling the long-term firn evolution is the complete lack of *in situ* data for more than one decade after 1998. This data gap concerns the availability of calibration and validation data as well as the availability of a continuous model forcing which had to be completed with bias corrected reanalysis data as described in Paper II. The use of reanalysis data is problematic especially with regards to precipitation data. Several precipitation products have shown large differences to *in situ* data in Central Asia (Pohl et al., 2015). The accuracy of gridded data sets in the region is low due to the limited availability of stations and their bias towards low elevations (Haag et al., 2019). Also other firn and glacier modelling studies discuss the challenges related to the lack of meteorological data. Lambrecht et al. (2020) therefore apply a rather simple firn densification model by Reeh (2008) with relatively low data requirements for Fedchenko glacier. In their study, they used

data from the High Asia Reanalysis (HAR) data set which provides dynamically downscaled ERA-Interim data (Dee et al., 2011; Maussion et al., 2014).

According to Lambrecht et al. (2020) HAR air temperatures correspond well to air temperature measurements, but precipitation rates do not agree with measured accumulation rates. They therefore corrected accumulation rates derived from HAR precipitation. A considerable correction was necessary especially for the lower observation site of their study. Huintjes et al. (2015b), who used bias corrected HAR data in combination with AWS data for modelling mass balance of Zhadang glacier (Tibetan Plateau), report uncertainties related to the precipitation frequency and intensity of the HAR data. According to Pohl et al. (2015), HAR better reproduced the measured precipitation seasonality than other products. The initial HAR dataset does not cover the Pamir Alay and is furthermore only available for 2000 to 2014 (TU Berlin, 2021).

Mean monthly biases between temporally overlapping TopoSCALE ERA5 data and weather station measurements were used in Paper II to bias correct the downscaled reanalysis data. Thereby, not only the overall bias of the reanalysis product could be corrected but also the seasonality was improved. The general sensitivity of the model output regarding the model forcing was discussed in Paper II by comparing the output of the two model runs. Firn conditions in the lower accumulation area were more sensitive to the model forcing than the higher accumulation area (Fig. S13 in the supplement of Paper II in appendix B and Table C.1). Overall, the presented correction approach produced a more than five decades long time series which allowed for an unprecedentedly long firn modelling period. The modelled firn conditions at ~4400 m a.s.l. agree well with recent measurements (Fig. 10d and Fig. 11 in Paper II).

A new version (HAR v2) based on ERA5 data covering larger areas and currently spanning the period of 1991 to 2020 was recently presented by Wang et al. (2021). The authors conclude that precipitation is overestimated in HAR v2 despite a correction based on another reanalysis product. Despite these advances, the quality of available reanalysis data will remain a challenge for modelling firn on Central Asian glaciers. *In situ* data remain fundamental to correct model forcing data. The historical meteorological and glaciological data compiled within this thesis are therefore definitely an asset also if new gridded products such as HAR v2 become available.

3.2.2. Relevance

Paper II puts the Abramov firn observations presented in Paper I into spatial and temporal context. The distributed long term firn evolution was evaluated by applying a coupled

surface energy balance–multilayer subsurface model for 52 years. The modelling results allowed to analyse the firn observations in the context of climatic conditions. It was shown that the years before and during the historical firn observations were characterised by high melt rates and low amounts of solid accumulation. The firn properties observed in the 1970s are thus characteristic for the weather conditions at the time. The similarity of the recently observed firn properties to the historical data is therefore more concerning than assumed in the earlier interpretation in Paper I, which was based on *in situ* data only.

Firn data from Central Asia was related to accumulation conditions by several studies (Aizen et al., 1997, 2004, 2006, 2009; Duan et al., 2015). Only firn core data from the recrystallisation and upper recrystallisation-infiltration zones, where surface melt water refreezes in the same annual layer can be used to quantify accumulation rates. Otherwise firn core data may provide only net accumulation rates, which are a combined signal of accumulation and melt (Schwikowski et al., 2013). Locations that were previously located in the recrystallisation and recrystallisation-infiltration zones might recently have and will in the future likely experience higher melt rates. The cold and also warm infiltration zones will therefore become more abundant under climate change (Barzycka et al., 2020; Marshall, 2021). Under such conditions, it will become increasingly necessary to combine core data with modelling approaches to interpret the firn core records as it was done in van Pelt et al. (2014). Paper II has shown that the EBFM is suitable for modelling the firn evolution over long period under the presence of melt conditions.

There is hardly any study presenting firn modelling of mountain glaciers in Central Asia or High Mountain Asia. None of the previous work have modelled the firn evolution over several decades and with a model of similar complexity as the EBFM applied in this thesis. In the firn densification model applied by Lambrecht et al. (2020) for Fedchenko glacier melt water refreezes within the corresponding annual layer. The model does thus not correctly reproduce firn conditions at lower elevations where melt rates are higher and percolate to lower layers. A few glacier mass balance model application for glaciers in High Mountain Asia include multilayer subsurface models (e.g. Mölg et al., 2012; Huintjes et al., 2015b,a, 2016; Thiel et al., 2020; Arndt et al., 2021), but none of these studies focus on firn and subsurface changes. Firn modelling studies are generally sparse for mountain glaciers. Most firn model applications focus on Arctic glaciers (e.g. van Pelt et al., 2012; Marchenko et al., 2017; van Pelt et al., 2019). A few studies investigate cold firn of Alpine and Andean glaciers, mainly focusing on firn temperatures (e.g. Alean et al., 1983; Suter et al., 2004; Vincent et al., 2007; Gilbert et al., 2010; Hoelzle et al., 2011; Vincent et al., 2020). The EBFM application for Colle Gnifettiy by Mattea et al. (2021) provides continuous and

distributed information of the thermal regime of a cold firn site in the Alps. Overall, firn model applications for mountain glaciers are rare and firn model development mainly focuses on sites on polar ice sheets (e.g. Stevens et al., 2020; Vandecrux et al., 2020).

The current bias towards research of firn on polar ice sheets becomes also evident when looking at the commonly used firn terminology of Benson (1996). This classification is less suitable to describe firn on mountain glaciers than the more differentiated and relatively early published Russian terminology of Shumskii (1964). This reveals that firn on mountain glaciers was well studied in the past by Soviet investigators. Paper I and Paper II showed that the combination of historical firn data with modelling can contribute to understanding aspects of climate change impacts. These aspects have received little attention so far. There are further Soviet and also more recent firn investigation sites to be remeasured and more data to be explored by modelling. In addition to the historical firn investigations on glaciers located in the former Soviet Union, early firn observations were also performed for instance in the European Alps (Haeberli, 1976; Lilboutry et al., 1976) and on Alaskan glaciers (Trabant and Mayo, 1985). A better understanding of the past firn evolution of mountain glaciers is necessary to assess the future glacier development under climate change. Glaciers will respond differently to climatic factors, if conditions in their firn area or even their firn facies changed (e.g. Marshall, 2021).

Simulating the firn evolution of mountain glaciers furthermore contributes to the estimation and evaluation of glacier density estimates (Ochwat et al., 2021). Such estimates of so-called density conversion factors are necessary for the computation of geodetic mass changes from measured elevation changes (e.g. Huss, 2013). A reduction in firn cover extent and an increase of firn densities as modelled for Abramov glacier both lead to an increase of the overall density of a glacier. The EBFM results of changing firn conditions suggest that density conversion factors should be used carefully. Thorough firn assessments may contribute to reduce uncertainties in geodetic mass balances. This may be and become more relevant in the future also for the larger region of High Mountain Asia and especially for areas with positive mass changes. According to Miles et al. (2021), anomalous mass balances are found for glaciers with large accumulation areas. Under changing climate conditions, firn changes will likely affect these accumulation areas.

3.3. Impact of firn changes on glacier mass balance

The effect of firn changes on the glacier mass balance of Abramov glacier was evaluated based on the application of the coupled surface energy balance–multilayer subsurface

model EBFM. This is the first application of a model of comparable complexity for a glacier in Central Asia for such a long time period.

3.3.1. Challenges

In addition to the above (Section 3.2.1) discussed difficulties related to the long-term climate forcing, modelling the long-term evolution of mass balance of Abramov glacier involved further challenges, which shall be examined in the following.

During the 52 modelled years, Abramov glacier experienced important topographical changes. Between 1975 and 2015, the glacier tongue retreated by about 1 km (Barandun et al., 2015) and large parts of the ablation area lowered by more than 30 m (Denzinger et al., 2021). An advance of the glacier tongue was reported for 1972 and 1973 (Mandychev et al., 2017). Initial model attempts for selected grid points, using a reference glacier topography caused unrealistic ablation rates at either the beginning or the end of the modelling period, depending on the parameters/topography chosen. Instead of trying to correct this by time-dependent ablation parameters, changes in glacier topography were approximated. The application of a temporally linear elevation change is a simplification of the real topographical changes, which are not yet fully understood. The 1970s advance is described as a surge by several authors (e.g. Glazyrin et al., 1986; Kotlyakov et al., 2017). Simulating the glacier dynamics and thereby contribute to the debate whether the Abramov glacier advance shall be called a surge was beyond the scope of this thesis. Instead, a linear change with elevation was applied which can be considered to be an efficient alternative to explicitly model the ice dynamics (van Pelt and Kohler, 2015). Because the conventional mass balance was modelled rather than the reference balance, also the glacier area needed to change with time (Elsberg et al., 2001). Therefore, different glacier masks available from previous studies were used to calculate and visualize glacier wide modelling results. These visualisations may also challenge the reader, as illustrations of reference glacier mass balances are much more commonly used as it is also the case for other long-term mass balances in High Mountain Asia (Zhu et al., 2018; Kumar et al., 2020). According to Zhu et al. (2018), the surface of Muztag Ata No. 15, however, has almost not changed over the modelling period of their study (1980-2012).

The modelled subsurface conditions in the lower accumulation area indicate a depletion of the firn cover towards the end of the modelling period (Fig. 8 in Paper II). The *in situ* data could not be used to evaluate whether the firn has changed in this area. It remains unclear, whether the recent observations (core c4225 and snow pit ac1, Fig 1.2) are located at the same position as the historical observations (firn profiles at s1). The coordinates

of the historical measurements at s1 could not be reconstructed as no complementary information was available. Both the historical and the new sites are located in a broad and relatively flat glacier region, relatively far away from the glacier margins. Even if historical images existed (such as used for site s2/core c4395) there are no obvious landmarks nearby suitable to accurately define the location of the historical site. Furthermore, the GPR data from January 2018 indicate that the subsurface is spatially heterogenous around the observation site of core c4225 (Fig. A.2), where firn was still present in 2018 (Fig. A.1a). As discussed in Paper II, the EBFM results are not able to resolve the high spatial variability of observed firn conditions. Walther (2018) previously tested the application of snow distribution grids to account for the observed spatial variability when simulating Abramov glacier with the EBFM. The application of such snow distribution grids did, however, not improve the results compared to field measurements. Therefore a linear precipitation gradient was used in Paper II.

Compared to the observations in firn pit s2 (at 4410 m a.s.l., same location as core c4395), Kislov (1982) observed much more infiltration ice in firn pit s1 (located near ac1 shown in Fig. 1.2). It is likely that Krenke (1982) would have classified that site to be in the *infiltration (firn-ice)* zone already in the 1970s. According to the EBFM results for a grid cell located in this zone (Fig. 8 in Paper II), subsurface temperatures are year-around cold at the end of the modelling period. In the past, such subsurface temperature conditions were only reported for the ablation area of the glacier (Kislov et al., 1977). Indeed, negative mass balances were more frequently modelled for this site in recent years, but positive annual mass balances and refreezing of melt water still occur during the last modelled decade (Table C.2). The percentage of melt water refreezing which takes place within the seasonal snow, has recently increased (Table C.2). The modelling results thus indicate a shift towards conditions which are typical for the *infiltration-congelation* zone, where superimposed ice is built. EBFM applications for other sites have previously been used to simulate superimposed ice (van Pelt and Kohler, 2015) and to identify a reduction of pore space around the long-term ELA (van Pelt et al., 2019). The EBFM is thus able to reasonable reproduce such processes. To validate the modelled changes on Abramov glacier and to better understand the ongoing changes, additional data would be necessary. Such data could consist of further *in situ* measurements such as GPR measurements from the firn-ice transition zone (cf. Pälli et al., 2003) and remote sensing data used to detect firn facies (cf. Barzycka et al., 2020).

3.3.2. Relevance

Modelling the long-term mass balance and firn evolution of Abramov glacier provided insight into processes that are relevant for the data sparse Central Asia. The modelled contribution of internal accumulation to the glacier-wide mass balance of Abramov glacier highlights that refreezing of melt water is a relevant process. Evidence of this process has been observed at several sites in Central Asia as visible from observed ice lenses in firn cores and/or snow pits on Fedchenko glacier (Lambrecht et al., 2020), Gregoriev ice cap (e.g. Thompson et al., 1997) and Inilchek (Aizen et al., 1997). Ice layers were also observed at other high elevated sites in High Mountain Asia (Mayer et al., 2014). The importance of refreezing melt water for cold glaciers in High Mountain Asia was previously emphasized by Fujita and Ageta (2000b). In their modelling experiments, they assumed that temperate glaciers do not retain frozen melt water. Paper II showed that internal accumulation also happens on temperate glaciers in Central Asia thanks to winter cooling. Already, Trabant and Mayo (1985) had demonstrated that internal accumulation is an important mass balance quantity for temperate glaciers in Alaska and Ochwat et al. (2021) recently modelled firn changes related to enhanced refreezing on temperate Kaskawulsh Glacier, Yukon-Alaska. Fujita et al. (1996) furthermore showed that winter cooling is critical to build superimposed ice on a continental glacier on the Tibetan plateau. Nevertheless, numerous mass balance modelling studies for Central Asia and High Mountain Asia exclude refreezing processes (e.g. Azam et al., 2014a; Groos et al., 2017; Kumar et al., 2020). Zhu et al. (2018) modelled the long-term mass balance evolution of Muztag Ata glacier No. 15 and accounted for refreezing following Fujita and Ageta (2000a). This parametrisation does not distinguish for refreezing in the seasonal snow pack and internal accumulation. Moreover, it does not take into account changes of the firn properties. The results for Abramov glacier show, (i) that subsurface properties are critical for refreezing and (ii) that they have a strong variability over time. Mass balance models which completely neglect the refreezing of melt water or use simplified parametrisations (e.g. Barandun et al., 2015; Wang et al., 2019) are not able to (fully) reproduce these processes. Whereas simple parametrisations may be suitable to estimate refreezing for stable firn properties, they are not able to take in account changing firn properties.

Paper II furthermore showed that the mass loss of Abramov glacier was relatively stable over the modelled 52 years, whereas an acceleration of mass loss was identified elsewhere in High Mountain Asia and many other regions of the world (Maurer et al., 2019; Zemp et al., 2015; Chen et al., 2021; Hugonnet et al., 2021). The geodetic mass balance results of

Denzinger et al. (2021), which are in the same range as the modelled mass balance presented in Paper II, confirm a rather constant mass loss of Abramov glacier. *In-situ* data as well as modeling results indicate that increasing precipitation rates may have compensated for raising air temperatures (Paper I; Paper II). High precipitation rates have acted via several processes including high surface accumulation rates and an increase of the albedo. Furthermore, they enfavour conditions for internal accumulation. The model results revealed that at high elevations, increasing precipitation rates allowed the firn to recover after high ablation in the 1970s, which had been reported previously (e.g. Pertziger, 1996). Bhattacharya et al. (2021) found that glaciers in cold and dry regions of High Mountain Asia were strongly influenced by the amounts of solid precipitation. By analyzing geodetic long-term mass balances since the 1960s for several sub-periods, they also identified that recently unfavourable conditions led to mass losses in previously stable regions such as the Eastern Pamir. The recent warming seems to override effects of previously high accumulation rates (Bhattacharya et al., 2021). Also the modelling results for Abramov glacier indicate that relatively high precipitation rates become insufficient to compensate for the consequences of the continuously increasing temperatures. Although Abramov glacier had a continuously negative mass balance, the results of Paper I and Paper II indicate comparable climatic controls of the mass balance as described by Bhattacharya et al. (2021) for previously balanced regions. The findings for Abramov glacier may thus be relevant for understanding processes in zones without *in situ* data characterised by the so-called Karokoram mass balance anomaly.

Beyond these contributions to the process understanding of glaciers in High Mountain Asia, the detected glacier changes may be relevant for the downstream living society. In the generally water-scarce Central Asia, a reduction of refreezing and related acceleration of mass loss will lead to runoff increases (Sorg et al., 2012). On the short term, this additional, but unsustainable meltwater may be seen as relieving in the context of water shortages (Muccione and Cassara, 2019). On the longer term, the decline of glacial runoff after peak water will, however, enhance the water scarcity especially during the dry summer months (Sorg et al., 2014). It is important to assess smaller head-water watersheds of large basins individually, as populations of such sub-catchments might be exposed to water shortages earlier (Huss and Hock, 2018). Moreover, glacier-climate interactions in Central Asia have been found to be strongly variable regionally (Saks et al., 2022). Furthermore, altered flow regimes due to increased glacial runoff, are also expected to raise the potential of natural hazards (e.g. Komatsu and Watanabe, 2014; Kattel et al., 2020; Zheng et al., 2021).

Studying the surface processes of Abramov glacier through historical and recent mea-

surements and modelling further contribute to the understanding of this exceptionally well studied glacier. The new insights may be used for further investigating this particular site such as simulating longer time-periods than the one covered by observations. The modelled fluxes may for example be used as surface conditions for a dynamic model which evaluates the reported glacier advances (Glazyrin et al., 1986; Mandychev et al., 2017).

4. Conclusions and perspectives

4.1. Conclusions

The conclusions are structured following the main research questions (Section 1.3).

State of firn: What are the past and current accumulation rates, firn stratigraphy and density in the accumulation area of Abramov glacier?

Accumulation rates on Abramov glacier as well as firn stratigraphies and densities are spatially heterogenous even for apparently flat parts of the accumulation area. Results for the main investigation site, a point location at ~4400 m.a.s.l. measured in 1973 and 2018, indicate recently higher net accumulation rates. The difference, however, lies within the estimated uncertainties. The firn profiles do furthermore indicate overall similar firn conditions. Continuous ice lenses were more abundant in the 1973 firn profile than in the profile from 2018, when a higher ice content within firn layers was identified. The firn densities have not changed within the bonds of estimated uncertainties.

These firn measurements present a historical and current snap-shot of the state of firn for a point location in the accumulation area of Abramov glacier, which are unique for the region. Capturing these data involved the reconstruction of the position of historical investigations as no coordinate information was reported with the historical firn data.

Firn measurements were also performed at a second point location at ~4250 m.a.s.l. Historical and recent firn profiles for this area appear similar. A comparison is, however, hampered by the unknown exact location of the historical measurements.

Firn evolution: How did the firn of Abramov glacier evolve over the period from 1968 to 2020?

Overall, the comparison of historical (1970s) and recent (2018) firn data of Abramov glacier indicate similar conditions. The evaluation of the firn evolution with a surface energy balance–multilayer subsurface model allow to put these observations into context: The historical measurements were performed during years with unfavourable meteorological

conditions causing low accumulation and high melt rates also in the accumulation area. In the following years, the firn cover at higher elevations recovered, before the subsurface densities started to increase again after 1988/1989 (significant increase of $+1.53\,\mathrm{kg\,m^{-3}\,a^{-1}}$ at ~4400 m a.s.l.). In addition to the firn density increase, the model results suggest an increase of the firn line.

Modelling the firn evolution of Abramov glacier highlights that the firn cover responds to changing climate conditions, which is not evident from solely evaluating the *in situ* observations. Furthermore, the modelling adds a spatial dimension to the analysis which allows to study the entire accumulation zone instead of on or two point sites.

Impact: How are mass exchange processes in the firn and changes therein contributing to the glacier wide mass balance?

A relevant contribution of internal accumulation ($+0.11\,\mathrm{m\,w.e.\,a^{-1}}$) to the glacier wide mass balance ($-0.27\,\mathrm{m\,w.e.\,a^{-1}}$) was found for the period of 1968/1969-2019/2020. Over the 52 years of investigations, no significant trends of change in glacier-wide mass balance or internal accumulation were detected despite increasing air temperatures. A precipitation increase was identified to be the reason.

The coupled surface energy balance–multilayer subsurface model showed that the prevailing meteorological conditions do not only control the climatic mass balance of a certain year but also have consequences for the following years' mass balances through changes in the firn. Whereas unfavourable meteorological conditions lead to higher melt rates in the ablation area during the corresponding years, the effects for the accumulation area last at least for several years. The reduction in the refreezing capacity caused an increased glacier-wide mass loss during subsequent years, even when more favourable meteorological conditions prevailed. Several years of favourable conditions were necessary for the firn to recover from the extreme conditions at the beginning of the investigation period.

As persisting unfavourable meteorological conditions must be expected, there is a major risk that the firn cannot recover and that the firn line will continue to retreat. The combination of the reducing melt water refreezing capacity and the albedo lowering associated with the firn line retreat potentially amplify the future mass loss of Abramov glacier.

4.2. Perspectives

Future research which builds on this work should be carried out in two fields: (i) tackling the challenges, limitations and open questions encountered when assessing the firn changes

and their impact on the glacier mass balance evolution of Abramov glacier and (ii) extend the research to the regional scale by evaluating the effect of firn changes on glacier mass balance for other sites with different firn characteristics. Therefore, it would be desirable to better understand Abramov glacier. Given the exceptional data availability, the glacier is an ideal location to calibrate a mass balance model and to apply it for a larger regional domain. A further engagement with the historical data and a continued exploration of the archives would potentially be valuable. It would be helpful to further deepen the collaboration with different investigators including researchers based in Tashkent and Moscow as well as scientists who were involved in historical investigations. Different types of historical data are definitely an asset for a better understanding of Abramov glacier. To further address the remaining questions and challenges more concretely, the following points are proposed:

- Modelling the accumulation area of Abramov at higher spatial resolution: Such a study could focus on the western branch (orographic right) of the glacier for which already some data is available. Ideally, a complex model which simulates wind fields could be applied (Obleitner and Lehning, 2004; Dadic et al., 2010; Mott and Lehning, 2010; Bavera et al., 2014). For such an application, at least one weather station monitoring the local energy balance would be necessary. Ideally, such a station would include a cosmic ray sensor to measure snow accumulation continuously (Gugerli et al., 2019). Unless Abramov glacier becomes again a site with permanently investigation as it was in the past, operating a station in this environment remains unrealistic. Alternatively, the EBFM could be applied at higher spatial resolution and the use of a precipitation distribution grid replacing the precipitation lapse rate could again be tested (Walther, 2018). The precipitation distribution could be derived from available or complementary *in situ* data such as additional GPR measurements (following point).

- Identifying the spatial distribution pattern of accumulation in the entire accumulation area of Abramov glacier: This could be achieved by performing extensive measurements with a 800 MHz antenna similar do the data presented in Paper I but for wider areas (Machguth et al., 2006; Sold et al., 2015). GPR data could also provide additional insights into firn aquifers (e.g. Christianson et al., 2015). Repeated GPR measurements from different seasons would be interesting to analyze the temporal evolution of liquid water at depth. Complementary common midpoint measurements should be performed at various locations to obtain information about the

wave-speed depth profile (Eisen et al., 2003). The interpretation of the GPR data could be assisted by an application of the EBFM as done by van Pelt et al. (2014).

- Further investigating the modelled retreat of the firn line: Complementary GPR measurements from this zone (cf. Pälli et al., 2003) and remote sensing data (cf. Barzycka et al., 2020) could be used to evaluate the EBFM output. Monthly historical stake data from the firn-ice transition zone could furthermore be used to estimate the position of the ELA along the stake profiles for individual years.

- Incorporating remote sensing data to better constrain EBFM parameters and validate the model output: Albedo information from optical satellite measurements (Naegeli et al., 2017) could be used to constrain albedo parameters and to quantify a possible surface darkening over time (Sarangi et al., 2019; Schmale et al., 2017). Data from such sensors and images from automatic cameras furthermore provide the basis for snowline observations (Barandun et al., 2021), which could be used to validate the modelled snow cover depletion patterns (Barandun et al., 2015; Huintjes et al., 2015b). Moreover, synthetic aperture radar (SAR) back-scatter data from Sentinel-I could be used to analyze the progression of surface melt extents (Small, 2011; Small et al., 2013; Heilig et al., 2019). Such surface melt extents could be used for model validation also under cloudy conditions.

- Modelling the glacier dynamics of Abramov glacier: Applying an ice-flow model (e.g. Peyaud et al., 2020) to simulate Abramov glacier could contribute to a better understanding of the topographical evolution of this glacier, which is supposed to have surged in the 1970s (Glazyrin et al., 1986). The here presented surface mass balance could serve as a boundary condition for such a model application.

Tackling the challenges related to the model forcing is important for the modelling of Abramov glacier, but even more relevant for the application of the EBFM to other sites. In addition, some other suggestions for future work focusing on a more regional context shall be given:

- Evaluating the entire ERA5 data set once it is available: Currently only a preliminary version of the ERA5 data set is available for 1950-1979 (ECMWF, 2021). Once it is ready, the continuous ERA5 data set reaching back to the 1950s should be evaluated for Abramov glacier and other sites with historical data. The downscaled ERA5 which will be provided by the HAR v2 should also be considered once it is available (Wang

et al., 2021). It may make sense to also consider other products, as the precipitation and snow output of ERA5 were found to be problematic (Sun et al., 2021). It has for example been shown that ERA-Interim performed relatively well as it assimilated data from high elevation stations (Orsolini et al., 2019). However, this and also other data sets are not available for such a long period as ERA5.

- Simulating the long-term firn evolution of sites from different firn facies zones: The EBFM is considered suitable for modelling firn sites in Central Asia. By applying the model to several locations for which different firn facies zones are expected, facies transitions and possible tipping points could be identified (Noël et al., 2017). Such simulations could also focus on the evaluation of firn density changes, which are relevant for geodetic mass balance estimates. For such a regional assessment, the EBFM could be run for isolated grid points instead of an application for entire glaciers or applied at a coarser resolution (c.f. van Pelt et al., 2019).

- Applying the EBFM catchment-wide over several decades: A regional model run as performed for Svalbard glaciers (van Pelt et al., 2019) could be used to study the runoff evolution. The effect of firn and mass balance changes on runoff at catchment scale could thereby be investigated. Furthermore, the seasonal snow development in non-glacier terrain could be studied with the same model as presented in van Pelt et al. (2019). Thereby, total runoff estimates could be achieved.

- Analysing firn data from Gregoriev ice cap (Inner Tien Shan) and compare it to historical data: In the context of this thesis, a firn core was drilled and a thermistor chain was installed on Gregoriev ice cap (cf. Appendix F). Comparing these data to previous measurements (Dikikh, 1965; Thompson et al., 1993; Kutuzov, 2005) can potentially provide *in situ* evidence of recent firn changes for another historical firn site in Central Asia. A subsequent application of the EBFM for this well studied site should also be considered.

- *In situ* data remain an asset for glaciological research in Central Asia. Efforts to continue and expand current monitoring networks are necessary. Acquiring complementary field data further contributes to evaluate remote sensing and reanalysis data products used for regional assessments.

Data availability

The data measured and compiled as well as the model code used within this thesis were uploaded to public repositories.

The Abramov glacier data base is available under doi:10.5281/zenodo.7110254. Digitized historical as well as firn measurements from 2018 from Abramov glacier measured and compiled within this thesis can be downloaded from doi:10.5281/zenodo.7112894.

The firn data measured on Gregoriev ice cap are available on a separate repository: doi:10.5281/zenodo.7113282.

The EBFM files as well as the forcing necessary to reproduce the results of paper II are available on the repository github and can be assessed through doi:10.5281/zenodo.5773796 (Model code, forcing and grids for Abramov glacier) and doi:10.5281/zenodo.7110211 (Model code and data used for sensitivity experiments).

Recent mass balance data from Abramov glacier are available through the Department of Geosciences, University of Fribourg and the World Glacier Monitoring Service doi:10.5904/wgms-fog-2021-05 (WGMS, 2021) and the AWS data can be downloaded from here (Schöne et al., 2013).

References

Aizen, V. B., Aizen, E. M., and Melack, J. M. Climate, Snow Cover, Glaciers, and Runoff in the Tien Shan, Central Asia. *Water Ressources Bulletin*, 31(6):1113–1129, 1995. doi:10.1111/j.1752-1688.1995.tb03426.x.

Aizen, V. B., Aizen, E. M., Dozier, J., Melack, J. M., Sexton, D. D., and Nesterov, V. N. Glacial regime of the highest Tien Shan mountain, Pobeda-Khan Tengry massif. *Journal of Glaciology*, 43(145):503–512, 1997. doi:10.3189/S0022143000035115.

Aizen, V. B., Aizen, E. M., Melack, J. M., Kreutz, K. J., and Cecil, L. D. W. Association between atmospheric circulation patterns and firn-ice core records from the Inilchek glacierized area, central Tien Shan, Asia. *Journal of Geophysical Research*, 109(D08304):1–18, 2004. doi:10.1029/2003JD003894.

Aizen, V. B., Aizen, E. M., Joswiak, D. R., Fujita, K., Takeuchi, N., and Nikitin, S. A. Climatic and atmospheric circulation pattern variability from ice-core isotope/geochemistry records (Altai, Tien Shan and Tibet). *Annals of Glaciology*, 43:49–60, 2006. doi:10.3189/172756406781812078.

Aizen, V. B., Mayewski, P. A., Aizen, E. M., Joswiak, D. R., Surazakov, A. B., Kaspari, S., Grigholm, B., Krachler, M., Handley, M., and Finaev, A. Stable-isotope and trace element time series from Fedchenko glacier (Pamirs) snow/firn cores. *Journal of Glaciology*, 55 (190):275–291, 2009. doi:10.3189/002214309788608787.

Alean, J., Haeberli, W., and Schädler, B. Snow accumulation, firn temperature and solar radiation in the area of Colle Gnifetti core. *Zeitschrift für Gletscherkunde und Glazialgeologie*, 19(2):131–147, 1983.

Arkhipov, S. M., Mikhalenko, V. N., and Thompson, L. G. Strucutrual, stratigraphic and geochemical characteristics of the active layer of the Gregoirev Ice Cap, Tien Shan. *Materialy Glatsiologicheskih Issledovanii (Data of glaciological studies)*, 82:24–32, 1997.

Arndt, A., Scherer, D., and Schneider, C. Atmosphere driven mass-balance sensitivity of Halji glacier, Himalayas. *Atmosphere*, 12(426):1–29, 2021. doi:10.3390/atmos12040426.

Arthern, R. J., Vaughan, D. G., Rankin, A. M., Mulvaney, R., and Thomas, E. R. In situ measurements of {A}ntarctic snow compaction compared with predictions of models. *Journal of Geophysical Research*, 115:F03011, 2010. doi:10.1029/2009JF001306.

Azam, M. F., Wagnon, P., Patrick, C., Ramanathan, A., Linda, A., and Singh, V. B. Reconstruction of the annual mass balance of Chhota Shigri glacier, Western Himalaya, India, since 1969. *Annals of Glaciology*, 55(66):69–80, 2014a. doi:10.3189/2014AoG66A104.

Azam, M. F., Wagnon, P., Vincent, C., Ramanathan, A. L., Favier, V., Mandal, A., and Pottakkal, J. G. Processes governing the mass balance of Chhota Shigri Glacier (western Himalaya, India) assessed by point-scale surface energy balance measurements. *The Cryosphere*, 8 (6):2195–2217, 2014b. doi:10.5194/tc-8-2195-2014.

Bader, H. Sorge's law of densification of snow on high polar glaciers. *Journal of Glaciology*, 2(15):319–323, 1954. doi:10.3198/1954JoG2-15-319-323.

Barandun, M., Huss, M., Sold, L., Farinotti, D., Azisov, E., Salzmann, N., Usubaliev, R., Merkushkin, A., Hoelzle, M., A.Merkushkin, and Hoelzle, M. Re-analysis of seasonal mass balance at Abramov glacier 1968-2014. *Journal of Glaciology*, 61(230):1103–1117, 2015. doi:10.3189/2015JoG14J239.

Barandun, M., Fiddes, J., Scherler, M., Mathys, T., Saks, T., Petrakov, D., and Hoelzle, M. The state and future of the cryosphere in Central Asia. *Water Security*, 11(100072):1–14, 2020. doi:10.1016/j.wasec.2020.100072.

Barandun, M., Pohl, E., Naegeli, K., McNabb, R., Huss, M., Berthier, E., Saks, T., and Hoelzle, M. Hot Spots of Glacier Mass Balance Variability in Central Asia. *Geophysical Research Letters*, 48(e2020GL092084):1–14, 2021. doi:10.1029/2020GL092084.

Barzycka, B., Grabiec, M., Błaszczyk, M., Ignatiuk, D., Laska, M., Hagen, J. O., and Jania, J. Changes of glacier facies on Hornsund glaciers (Svalbard) during the decade 2007–2017. *Remote Sensing of Environment*, 251(112060):1–22, 2020. doi:10.1016/j.rse.2020.112060.

Bavera, D., Bavay, M., Jonas, T., Lehning, M., and De Michele, C. A comparison between two statistical and a physically-based model in snow water equivalent mapping. *Advances in Water Resources*, 63:167–178, 2014. doi:10.1016/j.advwatres.2013.11.011.

Benson, C. S. Stratigraphic Studies in the Snow and Firn of the Greenland Ice Sheet. Research Report 70, U.S. Army Snow, Ice and Permafrost Research Establishment, 1996.

Bernauer, T. and Siegfried, T. Climate change and international water conflict in Central Asia. *Journal of Peace Research*, 49(1):227–239, 2012. doi:10.1177/0022343311425843.

Bhattacharya, A., Bolch, T., Mukherjee, K., King, O., Menounos, B., Kapitsa, V., Neckel, N., Yang, W., and Yao, T. High Mountain Asian glacier response to climate revealed by multi-temporal satellite observations since the 1960s. *Nature Communications*, 12(4133): 1–13, 2021. doi:10.1038/s41467-021-24180-y.

Braithwaite, R. J. and Zhang, Y. Modelling Changes in Glacier Mass Balance That May Occur as a Result of Climate Changes. *Geografiska Annaler. Series A, Physical Geography*, 81(4): 489–496, 1999. URL `http://www.jstor.org/stable/521488`.

Braun, L. N. and Aellen, M. Modelling discharge of glacierized basins assisted by direct measurements of glacier mass balance. In Lang, H. and Musy, A., editors, *Hydrology in Mountainous Regions. I- Hydrological Measurements; the Water Cycle (Proceedings of the Lausanne Symposia, 1990)*, pages 99–106, Wallingford, 1990. IAHS Publication No. 193; IAHS Press.

Brun, E., David, P., Sudul, M., and Brunot, G. A numerical model to simulate snow-cover stratigraphy for operational avalanche forecasting. *Journal of Glaciology*, 38(128):13–22, 1992. doi:10.3189/s0022143000009552.

Brun, F., Berthier, E., Wagnon, P., Kääb, A., and Treichler, D. A spatially resolved estimate of High Mountain Asia glacier mass balances from 2000 to 2016. *Nature Geoscience*, 10: 668–674, 2017. doi:10.1038/ngeo2999.

Charalampidis, C., Van As, D., Colgan, W. T., Fausto, R. S., Macferrin, M., and Machguth, H. Thermal tracing of retained meltwater in the lower accumulation area of the Southwestern Greenland ice sheet. *Annals of Glaciology*, 57(72):1–10, 2016. doi:10.1017/aog.2016.2.

Chen, W., Yao, T., Zhang, G., Li, S., and Zheng, G. Accelerated glacier mass loss in the largest river and lake source regions of the Tibetan Plateau and its links with local water balance over 1976-2017. *Journal of Glaciology*, 67(264):577–591, 2021. doi:10.1017/jog.2021.9.

Christianson, K., Kohler, J., Alley, R. B., Nuth, C., and Van Pelt, W. J. Dynamic perennial firn aquifer on an Arctic glacier. *Geophysical Research Letters*, 42:1418–1426, 2015. doi:10.1002/2014GL062806.

Cogley, J. G., Hock, R., Rasmussen, L. A., Arendt, A. A., Bauder, A., Braithwaite, R. J., Jansson, M., Kaser, G., Möller, M., Nicholson, L., and Zemp, M. Glossary of Glacier Mass Balance. *IHP-VII Technical Documents in Hydrology, IACS Contribution No.2*, 86:114, 2011. URL `https://unesdoc.unesco.org/images/0019/001925/192525e.pdf`.

Cuffey, K. M. and Paterson, W. S. B. *The Physics of Glaciers*. Butterworth-Heinemann/Elsevier, 4 edition, 2010.

Cullen, N. J., Mölg, T., Kaser, G., Steffen, K., and Hardy, D. R. Energy-balance model validation on the top of Kilimanjaro, Tanzania, using eddy covariance data. *Annals of Glaciology*, 46:227–233, 2007. doi:10.3189/172756407782871224.

Dadic, R., Mott, R., Lehning, M., and Burlando, P. Wind Influence on Snow Depth Distribution and Accumulation over Glaciers. *Journal of Geophysical Research*, 115(F01012):1–8, 2010. doi:10.1029/2009JF001261.

D'Amboise, C. J., Müller, K., Oxarango, L., Morin, S., and Schuler, T. V. Implementation of a physically based water percolation routine in the crocus/surfex (v7.3) snowpack model. *Geoscientific Model Development*, 10:3547–3566, 9 2017. doi:10.5194/gmd-10-3547-2017.

De Kok, R. J., Kraaijenbrink, P. D., Tuinenburg, O. A., Bonekamp, P. N., and Immerzeel, W. W. Towards understanding the pattern of glacier mass balances in High Mountain Asia using regional climatic modelling. *Cryosphere*, 14(9):3215–3234, 2020. doi:10.5194/tc-14-3215-2020.

Dee, D. P., Uppala, S. M., Simmons, A. J., Berrisford, P., Poli, P., Kobayashi, S., Andrae, U., Balmaseda, M. A., Balsamo, G., Bauer, P., Bechtold, P., Beljaars, A. C. M., Van de Berg, L., Bidlot, J., Bormann, N., Delsol, C., Dragani, R., Fuentes, M., Geer, A. J., Haimberger, L., Healy, S. B., Hersbach, H., Hólm, E. V., Isaksen, L., Kållberg, P., Köhler, M., Matricardi, M., McNally, A. P., Monge-Sanz, B. M., Morcrette, J.-J., Park, B.-K., Peubey, C., de Rosnay, P., Tavolato, C., Thépaut, J. N., and Vitart, F. The ERA-Interim reanalysis: Configuration and performance of the data assimilation system. *Quarterly Journal of the Royal Meteorological Society*, 137:553–597, 2011. doi:10.1002/qj.828.

Denzinger, F., Machguth, H., Barandun, M., Berthier, E., Girod, L., Kronenberg, M., Usubaliev, R., and Hoelzle, M. Geodetic mass balance of Abramov Glacier from 1975 to 2015. *Journal of Glaciology*, 67(262):331–342, 2021. doi:10.1017/jog.2020.108.

Dikikh, A. N. Temperature regime of flat-top glaciers (using Gregoriev as an Example) [in Russian]. *Glyatsiol. Issledovaniya na Tyan-Shane, Frunze*, 11:32–35, 1965.

Duan, K., Xu, B., and Wu, G. Snow accumulation variability at altitude of 7010m a.s.l. in Muztag Ata Mountain in Pamir Plateau during 1958-2002. *Journal of Hydrology*, 531: 912–918, 2015. doi:10.1016/j.jhydrol.2015.10.013.

Dumont, M., Durand, Y., Arnaud, Y., and Six, D. Variational assimilation of albedo in a snowpack model and reconstruction of the spatial mass-balance distribution of an alpine glacier. *Journal of Glaciology*, 58(207):151–164, 2012. doi:10.3189/2012JoG11J163.

Dyurgerov, M. Glacier Mass Balance and Regime: Data of Measurements and Analysis. In Meier, M. and Armstrong, R., editors, *INSTAAR Occasional Paper*, number 55, pages 1–273, Boulder, CO, 2002. Institute of Arctic and Alpine Research, University of Colorado.

Dyurgerov, M. B. and Meier, M. F. Glaciers and the Changing Earth System: A 2004 Snapshot. In *INSTAAR Occasional Paper*, number 58, pages 1–117, Boulder, CO, 2005. Institute of Arctic and Alpine Research, University of Colorado.

Dyurgerov, M. B. and Mikhalenko, V. N., editors. *Glaciation of Tien Shan [in Russian]*. VINITI, Moscow, 1995.

ECMWF. ERA5 dataset, 2021. URL `https://www.ecmwf.int/en/forecasts/datasets/reanalysis-datasets/era5`.

Eichler, A., Schwikowski, M., Gäggeler, H. W., Furrer, V., Synal, H.-A., Beer, J., Saurer, M., and Funk, M. Glaciochemical dating of an ice core from upper Grenzgletscher (4200 m a.s.l.). *Journal of Glaciology*, 46(154):507–515, 2000. doi:10.3189/172756500781833098.

Eichler, A., Schwikowski, M., and Gäggeler, H. W. Meltwater-induced relocation of chemical species in Alpine firn. *Tellus, Series B: Chemical and Physical Meteorology*, 53(2):192–203, 2001. doi:10.1034/j.1600-0889.2001.d01-15.x.

Eisen, O., Nixdorf, U., Keck, L., and Wagenbach, D. Alpine Ice Cores and Ground Penetrating Radar: Combined Investigations for Glaciological and Climatic Interpretations of a Cold Alpine Ice Body. *Tellus*, 55B:1007–1017, 2003. doi:10.3402/tellusb.v55i5.16394.

Elsberg, D. H., Harrison, W. D., Echelmeyer, K. a., and Krimmel, R. M. Quantifying the effects of climate and surface change on glacier mass balance. *Journal of Glaciology*, 47 (159):649–658, 2001. doi:10.3189/172756501781831783.

Farinotti, D., Magnusson, J., Huss, M., and Bauder, A. Snow accumulation distribution inferred from time-lapse photography and simple modelling. *Hydrological Processes*, 24 (15):2087–2097, 2010. doi:10.1002/hyp.7629.

Farinotti, D., Immerzeel, W. W., de Kok, R. J., Quincey, D. J., and Dehecq, A. Manifestations and mechanisms of the Karakoram glacier Anomaly. *Nature Geoscience*, 13:8–16, 2020. doi:10.1038/s41561-019-0513-5.

Fettweis, X. Reconstruction of the 1979-2006 Greenland ice sheet surface mass balance using the regional climate model MAR. *Cryosphere*, 1:21–40, 2007. doi:10.5194/tc-1-21-2007.

Forsythe, N., Fowler, H. J., Li, X. F., Blenkinsop, S., and Pritchard, D. Karakoram temperature and glacial melt driven by regional atmospheric circulation variability. *Nature Climate Change*, 7:664–670, 2017. doi:10.1038/nclimate3361.

Fujita, K. and Ageta, Y. Effect of summer accumulation on glacier mass balance on the Tibetan Plateau revealed by mass-balance model. *Journal of Glaciology*, 46(153):244–252, 2000a. doi:10.3189/172756500781832945.

Fujita, K. and Ageta, Y. Effect of summer accumulation on glacier mass balance on the Tibetan Plateau revealed by mass-balance model. *Journal of Glaciology*, 46(153):244–252, 2000b. doi:10.3189/172756500781832945.

Fujita, K., Seko, K., Ageta, Y., Jianchen, P., and Tandong, Y. Superimposed ice in glacier mass balance on the Tibetan Plateau. *Journal of Glaciology*, 42(142):454–460, 1996. doi:10.3189/S0022143000003440.

Gabbi, J., Carenzo, M., Pellicciotti, F., Bauder, A., and Funk, M. A comparison of empirical and physically based glacier surface melt models for long-term simulations of glacier response. *Journal of Glaciology*, 60(224):1140–1154, 2014. doi:10.3189/2014JoG14J011.

Gardelle, J., Berthier, E., Arnaud, Y., and Kääb, A. Region-wide glacier mass balances over the Pamir-Karakoram-Himalaya during 1999-2011. *The Cryosphere*, 7:1263–1286, 2013. doi:10.5194/tc-7-1263-2013.

Gärtner-Roer, I., Nussbaumer, S. U., Hüsler, F., and Zemp, M. Worldwide assessment of national glacier monitoring and future perspectives. *Mountain Research and Development*, 39(2):A1–A11, 2019. doi:10.1659/MRD-JOURNAL-D-19-00021.1.

Gilbert, A., Wagnon, P., Vincent, C., Ginot, P., and Funk, M. Atmospheric warming at a high-elevation tropical site revealed by englacial temperatures at Illimani, Bolivia (6340 m above sea level, 16°S, 67°W). *Journal of Geophysical Research Atmospheres*, 115(10109): 1–10, 2010. doi:10.1029/2009JD012961.

Ginot, P., Schotterer, U., Stichler, W., Godoi, M. A., Francou, B., and Schwikowski, M. Influence of the Tungurahua eruption on the ice core records of Chimborazo, Ecuador. *Cryosphere*, 4(4):561–568, 2010. doi:10.5194/tc-4-561-2010.

GlaThiDa Consortium. *Glacier Thickness Database 3.1.0.* World Glacier Monitoring Service, Zurich, Zurich, Switzerland, 2020. doi:10.5904/wgms-glathida-2020-10.

Glazyrin, G. E., Kamnyansky, G. M., Maso, A. B., Nozdrukhin, V. K., and Salamatin, A. N. Mechanism of the Abramov glacier surge in 1972-1975 [in Russian]. *Materialy Glatsiologicheskih Issledovanii (Data of glaciological studies)*, 60:84–90, 1986.

Glazyrin, G. E., Kamnyansky, G. M., and Pertziger, F. I. *The regime of Abramov glacier [in Russian]*. Hidrometeoizdat, St. Petersburg, 1993.

Goerlich, F., Bolch, T., Mukherjee, K., and Pieczonka, T. Glacier Mass Loss during the 1960s and 1970s in the Ak-Shirak Range (Kyrgyzstan) from Multiple Stereoscopic Corona and Hexagon Imagery. *Remote Sensing*, 9(3):275, 2017. doi:10.3390/rs9030275.

Golubev, V. N., Mikhalenko, V. N., and Serebrennikov, A. V. Structural studies of the ice core obtained from the Djantugan Firn Plateauin the Central Caucasus. *Materialy Glatsiologicheskih Issledovanii (Data of glaciological studies)*, 64:25–33, 1988.

Greuell, W. and Konzelmann, T. Numerical modelling of the energy balance and the englacial temperature of the Greenland ice sheet. Calculations for the ETH-Camp location (West Greenland, 1155 m a.s.l.). *Global and Planetary Change*, 9:91–114, 1994. doi:10.1016/0921-8181(94)90010-8.

Greuell, W. and Oerlemans, J. Sensitivity studies with a mass balance model including temperature profile calculation sinside the glacier. *Zeitschrift fur Gletscherkunde und Glazialgeologie*, 22(2):101–124, 1986.

Groos, A. R., Mayer, C., Smiraglia, C., Diolaiuti, G., and Lambrecht, A. A first attempt to model region-wide glacier surface mass balances in the Karakoram: Findings and future challenges. *Geografia Fisica e Dinamica Quaternaria*, 40:137–159, 2017. doi:10.4461/GFDQ2017.40.10.

Grosvald'd, M. G. and Kotlyakov, V. M. Present-day Glaciers in the U.S.S.R and some Data on their Mass Balance. *Journal of Glaciology*, 8(52):9–22, 1969. doi:10.3189/S0022143000020748.

Gugerli, R., Salzmann, N., Huss, M., and Desilets, D. Continuous and autonomous snow water equivalent measurements by a cosmic ray sensor on an alpine glacier. *The Cryosphere*, 13:3413–3434, 2019. doi:10.5194/tc-13-3413-2019, 2019.

Gugerli, R., Guidicelli, M., Gabella, M., Huss, M., and Salzmann, N. Multi-sensor analysis of monthly gridded snow precipitation on alpine glaciers. *Advances in Science and Research*, 18:7–20, 2021. doi:10.5194/asr-18-7-2021.

Guidicelli, M., Gugerli, R., Gabella, M., Marty, C., and Salzmann, N. Continuous Spatio-Temporal High-Resolution Estimates of SWE Across the Swiss Alps – A Statistical Two-Step Approach for High-Mountain Topography. *Frontiers in Earth Science*, 9(664648):1–22, 2021. doi:10.3389/feart.2021.664648.

Haag, I., Jones, P. D., and Samimi, C. Central Asia's Changing Climate: How Temperature and Precipitation have changed across Time, Space, and Altitude. *Climate*, 7(123):1–19, 2019. doi:10.3390/cli7100123.

Haeberli, W. Eistemperaturen in den Alpen. *Zeitschrift für Gletscherkunde und Glazialgeologie*, 11(2):203–220, 1976.

Hagg, W., Mayer, C., Lambrecht, a., Kriegel, D., and Azizov, E. Glacier changes in the Big Naryn basin, Central Tian Shan. *Global and Planetary Change*, 110:40–50, 2013. doi:10.1016/j.gloplacha.2012.07.010.

Hammer, C., Clausen, H. B., Dansgaard, W., Gundestrup, N., Johnsen, S. J., and Reeh, N. Dating of Greenland Ice Cores by Flow Models, Isotopes, Volcanic Debris, and Continental Dust. *Journal of Glaciology*, 20(82):3–26, 1978. doi:10.3189/s0022143000021183.

Hawley, R. L., Brandt, O., Morris, E. M., Kohler, J., Shepherd, A. P., and Wingham, D. J. Techniques for measuring high-resolution firn density profiles: Case study from Kongsvegen, Svalbard. *Journal of Glaciology*, 54(186):463–468, 2008. doi:10.3189/002214308785837020.

Heilig, A., Wendleder, A., Schmitt, A., and Mayer, C. Discriminating wet snow and firn for alpine glaciers using sentinel-1 data: A case study at Rofental, Austria. *Geosciences (Switzerland)*, 9(2), 2019. doi:10.3390/geosciences9020069.

Herron, M. M. and Langway, C. C. Firn densification: an empirical model. *Journal of Glaciology*, 25(93):373–385, 1980. doi:10.3189/S0022143000015239.

Hock, R. A distributed temperature-index ice- and snownelt model including potential direct solar radiation. *Journal of Glaciology*, 45(149):101–111, 1999. doi:10.1017/S0022143000003087.

Hock, R. Temperature index melt modelling in mountain areas. *Journal of Hydrology*, 282 (1-4):104–115, 2003. doi:10.1016/S0022-1694(03)00257-9.

Hock, R. Glacier melt: a review of processes and their modelling. *Progress in Physical Geography*, 29(3):362–391, 2005. doi:10.1191/0309133305pp453ra.

Hock, R. and Holmgren, B. A distributed surface energy-balance model for complex topography and its application to Storglaciären, Sweden. *Journal of Glaciology*, 51(172):25–36, 2005. doi:10.3189/172756505781829566.

Hoelzle, M., Darms, G., Lüthi, M. P., and Suter, S. Evidence of accelerated englacial warming in the Monte Rosa area, Switzerland/Italy. *The Cryosphere*, 5:231–243, 2011. doi:10.5194/tc-5-231-2011.

Hoelzle, M., Azisov, E., Barandun, M., Huss, M., Farinotti, D., Gafurov, A., Hagg, W., Kenzhebaev, R., Kronenberg, M., Machguth, H., Merkushkin, A., Moldobekov, B., Petrov, M., Saks, T., Salzmann, N., Schöne, T., Tarasov, Y., Usubaliev, R., Vorogushyn, S., Yakovlev, A., and Zemp, M. Re-establishing a monitoring programme for glaciers in Kyrgyzstan and Uzbekistan, Central Asia. *Geoscientific Instrumentation, Methods and Data Systems*, 6(2): 397–418, 2017. doi:10.5194/gi-6-397-2017.

Hoelzle, M., Barandun, M., Bolch, T., Fiddes, J., Gafurov, A., Muccione, V., Tomas, S., and Shahgedanova, M. The status and role of the alpine cryosphere in Central Asia The status and role of the alpine cryosphere in Central Asia. In Xenarios, S., Schmidt-Vogt, D., Qadir, M., Janusz-Pawletta, B., and Abdullaev, I., editors, *The Aral Sea Basin: Water for Sustainable Development in Central Asia*, chapter 8, pages 100–121. Routledge, London and New York, 2019.

Horlings, A. N., Christianson, K., Holschuh, N., Stevens, C. M., and Waddington, E. D. Effect of horizontal divergence on estimates of firn-air content. *Journal of Glaciology*, 67(262): 287–296, 2021. doi:10.1017/jog.2020.105.

Hugonnet, R., McNabb, R., Berthier, E., Menounos, B., Nuth, C., Girod, L., Farinotti, D., Huss, M., Dussaillant, I., Brun, F., and Kääb, A. Accelerated global glacier mass loss in the early twenty-first century. *Nature*, 592:726–731, 2021. doi:10.1038/s41586-021-03436-z.

Huintjes, E., Neckel, N., Hochschild, V., and Schneider, C. Surface energy and mass balance at Purogangri ice cap, central Tibetan Plateau, 2001-2011. *Journal of Glaciology*, 61(230): 1048–1060, 2015a. doi:10.3189/2015JoG15J056.

Huintjes, E., Sauter, T., Schröter, B., Maussion, F., Yang, W., Kropácek, J., Buchroithner, M., Scherer, D., Kang, S., and Schneider, C. Evaluation of a coupled snow and energy balance model for Zhadang glacier, Tibetan Plateau, using glaciological measurements and time-lapse photography. *Arctic, Antarctic, and Alpine Research*, 47(3):573–590, 2015b. doi:10.1657/AAAR0014-073.

Huintjes, E., Loibl, D., Lehmkuhl, F., and Schneider, C. A modelling approach to reconstruct Little Ice Age climate from remote-sensing glacier observations in southeastern Tibet. *Annals of Glaciology*, 57(71):359–370, 2016. doi:10.3189/2016AoG71A025.

Huss, M. Density assumptions for converting geodetic glacier volume change to mass change. *The Cryosphere*, 7:877–887, 2013. doi:10.5194/tc-7-877-2013.

Huss, M. and Hock, R. Global-scale hydrological response to future glacier mass loss. *Nature Climate Change*, 8(2), 2018. doi:10.1038/s41558-017-0049-x.

Huss, M., Bauder, a., Funk, M., and Hock, R. Determination of the seasonal mass balance of four Alpine glaciers since 1865. *Journal of Geophysical Research*, 113(F01015):1–11, 2008. doi:10.1029/2007JF000803.

Kääb, A., Treichler, D., Nuth, C., and Berthier, E. Brief Communication: Contending estimates of 2003-2008 glacier mass balance over the Pamir-Karakoram-Himalaya. *The Cryosphere*, 9(2):557–564, 2015. doi:10.5194/tc-9-557-2015.

Kapitsa, V., Shahgedanova, M., Severskiy, I., Kasatkin, N., White, K., and Usmanova, Z. Assessment of Changes in Mass Balance of the Tuyuksu Group of Glaciers, Northern Tien Shan, Between 1958 and 2016 Using Ground-Based Observations and Pléiades Satellite Imagery. *Frontiers in Earth Science*, 8(259):1–14, 2020. doi:10.3389/feart.2020.00259.

Kaser, G., Fountain, A., and Jansson, P. A manual for monitoring the mass balance of mountain glaciers, 2003. URL `http://glaciers.pdx.edu/fountain/MyPapers/KaserEtAl2002.pdf`.

Kaser, G., Grosshauser, M., and Marzeion, B. Contribution potential of glaciers to water availability in different climate regimes. *Proceedings of the National Academy of Sciences*, 107(47):20223–20227, 2010. doi:10.1073/pnas.1008162107.

Kattel, D. B., Mohanty, A., Daiyrov, M., Wang, W., Mishra, M., Kulenbekov, Z., and Dawadi, B. Evaluation of glacial lakes and catastrophic floods on the northern slopes of the Kyrgyz range. *Mountain Research and Development*, 40(3):R37–R47, 2020. doi:10.1659/MRD-JOURNAL-D-19-00068.1.

Kenzhebaev, R., Barandun, M., Kronenberg, M., Yaning, C., Usubaliev, R., and Hoelzle, M. Mass balance observations and reconstruction for Batysh Sook Glacier, Tian Shan, from 2004 to 2015. *Cold Regions Science and Technology*, 135:76–89, 2017. doi:10.1016/j.coldregions.2016.12.007.

Khromova, T. E., Osipova, G. B., Tsvetkov, D. G., Dyurgerov, M. B., and Barry, R. G. Changes in glacier extent in the eastern Pamir, Central Asia, determined from historical data and ASTER imagery. *Remote Sensing of Environment*, 102:24–32, 2006. doi:10.1016/j.rse.2006.01.019.

Kislov, B. V. *Formation and regime of the firn-ice stratum of a mountain glacier [in Russian]*. PhD thesis, SARNIGMI Tashkent, 1982.

Kislov, B. V., Nozdrukhin, V. K., and Pertziger, F. I. Temperature regime of the active layer of Abramov Glacier [in Russian]. *Materialy Glatsiologicheskih Issledovanii (Data of glaciological studies)*, 30:199–204, 1977.

Klok, E. J. and Oerlemans, J. Model study of the spatial distribution of the energy and mass balance of Morteratschgletscher, Switzerland. *Journal of Glaciology*, 48(163):505–518, 2002. doi:10.3189/172756502781831133.

Komatsu, T. and Watanabe, T. Glacier-Related Hazards and Their Assessment in the Tajik Pamir: A Short Review. *Geographical Studies*, 88(2):117–131, 2014. doi:10.7886/hgs.88.117.

Kotlyakov, A. V. M., Chernova, L. P., Khromova, T. Y., and Zverkova, N. M. Glacier Surges and Glacial Disasters. *Doklady Earth Sciences*, 472:57–67, 2017. doi:10.1134/S1028334X17010056.

Kotlyakov, V. M., editor. *Glaciological Dictionary [in Russian]*. Gidrometeoizdat, Leningrad, 1984.

Kotlyakov, V. M. and Severskiy, I. V. Glaciers of Central Asia: current situation, changes and possible impact on water resources. In Braun, L. N., Hagg, W., Severskiy, I. V., and Young, G., editors, *Assessment of Snow, Glacier and Water Ressoruces in Asia*, pages 160–177. IHP/HWRP-publications – Book 8, Koblenz, Germany, 2009. URL `https://www.waterandchange.org/en/ihphwrp-publications-book-08-2009/`.

Krenke, A. N. *Mass exchange in glacier systems in the USSR [in Russian]*. Gidrometeoizdat, Leningrad, 1982.

Krenke, A. N., Bashev, A. B., Bascheva, V. Y., Psareva, T., and Surova, T. G. Firn structure, ice formation and water migration of of Marukh glacier [in Russian]. *Materialy Glatsiologicheskih Issledovanii (Data of glaciological studies)*, 17:277–288, 1970.

Kreutz, K. J., Aizen, V. B., Cecil, L. D. W., and Wake, C. P. Oxygen isotopic and soluble ionic composition of a shallow firn core, Inilchek glacier, central Tien Shan. *Journal of Glaciology*, 47(159):548–554, 2001. doi:10.3189/172756501781831819.

Kriegel, D., Mayer, C., Hagg, W., Vorogushyn, S., Duethmann, D., Gafurov, A., and Farinotti, D. Changes in glacierisation, climate and runoff in the second half of the 20th century in the Naryn basin, Central Asia. *Global and Planetary Change*, 110:51–61, 2013. doi:10.1016/j.gloplacha.2013.05.014.

Kronenberg, M., Barandun, M., Hoelzle, M., Huss, M., Farinotti, D., Azisov, E., Usubaliev, R., Gafurov, A., Petrakov, D., and Kääb, A. Mass-balance reconstruction for Glacier No. 354, Tien Shan, from 2003 to 2014. *Annals of Glaciology*, 57(71):92–102, 2016. doi:10.3189/2016AoG71A032.

Kronenberg, M., Machguth, H., Eichler, A., Schwikowski, M., and Hoelzle, M. Comparison of historical and recent accumulation rates on Abramov Glacier, Pamir Alay. *Journal of Glaciology*, 67(262):253–268, 2021. doi:10.1017/jog.2020.103.

Kronenberg, M., van Pelt, W., Machguth, H., Fiddes, J., Hoelzle, M., and Pertziger, F. Long-term firn and mass balance modelling for Abramov glacier in the data-scarce Pamir Alay. *The Cryosphere Discussions (revised and resubmitted manuscript)*, 2021-380:1–33, 2022.

Kumar, A., Negi, H. S., and Kumar, K. Long-term mass balance modelling (1986–2018) and climate sensitivity of Siachen Glacier, East Karakoram. *Environmental Monitoring and Assessment*, 192(368):1–16, 2020. doi:10.1007/s10661-020-08323-0.

Kutuzov, S. *Glacier Changes in the Inner Tien-Shan Mountains since the end of the 19th century [in Russian]*. Msc thesis, Moscow State (Lomonosov) University, 2005.

Kutuzov, S. and Shahgedanova, M. Glacier retreat and climatic variability in the eastern Terskey–Alatoo, inner Tien Shan between the middle of the 19th century and beginning of the 21st century. *Global and Planetary Change*, 69:59–70, 2009. doi:10.1016/j.gloplacha.2009.07.001.

Kuzmichenok, V. A., Vasilenko, B. V., Macheret, Y. Y., and Moskalevskiy, M. Y. Ice thickness and subglacial topography of the Abramov Glacier from radio echo sounding [in Russian]. *Materialy Glatsiologicheskih Issledovanii (Data of glaciological studies)*, 52:63–67, 1992.

Lambrecht, A., Mayer, C., Aizen, V., Floricioiu, D., and Surazakov, A. The evolution of Fedchenko glacier in the Pamir, Tajikistan, during the past eight decades. *Journal of Glaciology*, 60(220):233–244, 2014. doi:10.3189/2014JoG13J110.

Lambrecht, A., Mayer, C., Wendt, A., Floricioiu, D., and Völksen, C. Elevation change of Fedchenko Glacier, Pamir Mountains, from GNSS field measurements and TanDEM-X elevation models, with a focus on the upper glacier. *Journal of Glaciology*, 64(246): 637–648, 2018. doi:10.1017/jog.2018.52.

Lambrecht, A., Mayer, C., Bohleber, P., and Aizen, V. High altitude accumulation and preserved climate information in the western Pamir, observations from the Fedchenko Glacier accumulation basin. *Journal of Glaciology*, 66(256):219–230, 2020. doi:10.1017/jog.2019.97.

Lehning, M., Bartelt, P., Brown, B., and Fierz, C. A physical SNOWPACK model for the Swiss avalanche warning Part III: Meteorological forcing, thin layer formation and evaluation. *Cold Regions Science and Technology*, 35:169–184, 2002. doi:10.1016/S0165-232X(02)00072-1.

Lehning, M., Völksch, I., Gustafsson, D., Nguyen, T. A., Stähli, M., and Zappa, M. ALPINE3D: a detailed model of mountain surface processes and its application to snow hydrology. *Hydrological Processes*, 20:2111–2128, 2006. doi:10.1002/hyp.6204.

Leone, R., Harper, J., Meierbachtol, T., and Humphrey, N. Horizontal ice flow impacts the firn structure of greenland's percolation zone. *The Cryosphere*, 14:1703–1712, 5 2020. doi:10.5194/tc-14-1703-2020.

Licciulli, C., Bohleber, P., Lier, J., Gagliardini, O., Hoelzle, M., and Eisen, O. A full Stokes ice-flow model to assist the interpretation of millennial-scale ice cores at the high-Alpine drilling site Colle Gnifetti, Swiss/Italian Alps. *Journal of Glaciology*, 66(255):35–48, 2019. doi:10.1017/jog.2019.82.

Lilboutry, B. L., Briat, M., Creseveur, M., and Pourchet, M. 15m deep tempeartures in the glaciers of Mont Blanc (French Alps). *Journal of Glaciology*, 16(74):197–203, 1976. doi:10.3189/S0022143000031531.

Liston, G. E. and Sturm, M. A snow-transport model for cotnplex terrain. *Journal of Glaciology*, 44(148):498–516, 1998. doi:10.3189/S0022143000002021.

Luo, Y., Wang, X., Piao, S., Sun, L., Ciais, P., Zhang, Y., Ma, C., Gan, R., and He, C. Contrasting streamflow regimes induced by melting glaciers across the Tien Shan – Pamir – North Karakoram. *Scientific Reports*, 8(16470):1–9, 2018. doi:10.1038/s41598-018-34829-2.

Lüthi, M. and Funk, M. Dating ice cores from a high Alpine glacier with a flow model for cold firn. *Annals of Glaciology*, 31:69–79, 2000. doi:10.3189/172756400781820381.

Machguth, H., Eisen, O., Paul, F., and Hoelzle, M. Strong spatial variability of snow accumulation observed with helicopter-borne GPR on two adjacent Alpine glaciers. *Geophysical Research Letters*, 33(L13503):1–5, 2006. doi:10.1029/2006GL026576.

Machguth, H., Thomsen, H. H., Weidick, A., Ahlstrøm, A. P., Abermann, J., Andersen, M. L., Andersen, S. B., Bjørk, A. A., Box, J. E., Braithwaite, R. J., Bøggild, C. E., Citterio, M., Clement, P., Colgan, W., Fausto, R. S., Gleie, K., Gubler, S., Hasholt, B., Hynek, B., Knudsen, N. T., Larsen, S. H., Mernild, S. H., Oerlemans, J., Oerter, H., Olesen, O. B., Smeets, C. J., Steffen, K., Stober, M., Sugiyama, S., Van As, D., Van Den Broeke, M. R., and Van De Wal, R. S. Greenland surface mass-balance observations from the ice-sheet ablation area and local glaciers. *Journal of Glaciology*, 62(235):861–887, 2016. doi:10.1017/jog.2016.75.

Mandychev, A. N., Usubaliev, R. A., and Azisov, E. A. Changes of the Abramov Glacier (Alay Ridge) from 1850 to 2014 (in Russian). *Led i Sneg*, 57(3):326–333, 2017. doi:10.15356/2076-6734-2017-3-326-333.

Marchenko, S., Pelt, W. V., Claremar, B., Pohjola, V., Pettersson, R., Machguth, H., and Reijmer, C. Parameterizing deep water percolation improves subsurface temperature simulations by a multilayer firn model. *Frontiers in Earth Science*, 5:1–20, 2017. doi:10.3389/feart.2017.00016.

Marshall, S. J. Regime Shifts in Glacier and Ice Sheet Response to Climate Change: Examples From the Northern Hemisphere. *Frontiers in Climate*, 3(702585):1–25, 2021. doi:10.3389/fclim.2021.702585.

Mattea, E. *Measuring and modelling changes in the firn at Colle Gnifetti, 4400 m a.s .l., Swiss Alps.* Msc thesis, University of Fribourg, 2020.

Mattea, E., Machguth, H., Kronenberg, M., van Pelt, W., Bassi, M., and Hoelzle, M. Firn changes at Colle Gnifetti revealed with a high-resolution process-based physical model approach. *The Cryosphere*, 15:3181–3205, 2021. doi:10.5194/tc-15-3181-2021.

Maurer, J. M., Schaefer, J. M., Rupper, S., and Corley, A. Acceleration of ice loss across the Himalayas over the past 40 years. *Science Advances*, 5(6), 2019. doi:10.1126/sciadv.aav7266.

Maussion, F., Scherer, D., Mölg, T., Collier, E., Curio, J., and Finkelburg, R. Precipitation Seasonality and Variability over the Tibetan Plateau as Resolved by the High Asia Reanalysis. *Journal of Climate*, 27:1910–1927, 2014. doi:10.1175/JCLI-D-13-00282.1.

Mayer, C., Lambrecht, A., Oerter, H., Schwikowski, M., Vuillermoz, E., Frank, N., and Diolaiuti, G. Accumulation Studies at a High Elevation Glacier Site in Central Karakoram. *Advances in Meteorology*, (215162):1–12, 2014. doi:10.1155/2014/215162.

Mayo, L., Meier, M., and Tangborn, W. A system to combine stratigraphic and annual mass-balance systems: a contribution to the international hydrological decade. *Journal of Glaciology*, 11(61):3–14, 1972. doi:10.3189/S0022143000022449.

Micklin, P. The Aral Sea disaster. *Annual Review of Earth and Planetary Sciences*, 35:47–72, 2007. doi:10.1146/annurev.earth.35.031306.140120.

Miège, C., Forster, R. R., Box, J. E., Burgess, E. W., Mcconnell, J. R., Pasteris, D. R., and Spikes, V. B. Southeast Greenland high accumulation rates derived from firn cores and ground-penetrating radar. *Journal of Glaciology*, 54(63):322–332, 2013. doi:10.3189/2013AoG63A358.

Miles, E., McCarthy, M., Dehecq, A., Kneib, M., Fugger, S., and Pellicciotti, F. Health and sustainability of glaciers in High Mountain Asia. *Nature Communications*, 12(1), 2021. doi:10.1038/s41467-021-23073-4.

Miller, O., Solomon, D. K., Miège, C., Koenig, L., Forster, R., Schmerr, N., Ligtenberg, S. R., Legchenko, A., Voss, C. I., Montgomery, L., and McConnell, J. R. Hydrology of a Perennial Firn Aquifer in Southeast Greenland: An Overview Driven by Field Data. *Water Resources Research*, 56(8), 2020. doi:10.1029/2019WR026348.

Mölg, T., Maussion, F., Yang, W., and Scherer, D. The footprint of Asian monsoon dynamics in the mass and energy balance of a Tibetan glacier. *The Cryosphere*, 6:1445–1461, 2012. doi:10.5194/tc-6-1445-2012.

Mott, R. and Lehning, M. Meteorological modeling of very high-resolution wind fields and snow deposition for mountains. *Journal of Hydrometeorology*, 11(4):934–949, 2010. doi:10.1175/2010JHM1216.1.

Muccione, V. and Cassara, M. The Climate-Cryosphere-Water Nexus in Central Asia. Technical Report 8, SDC Climate Change and Environment Network, Berne, Switzerland, 2019. URL `https://www.shareweb.ch/site/Climate-Change-and-Environment/Documents/NexusBrief-Cryosphere-ENG-Okt2019.pdf`.

Naegeli, K., Damm, A., Huss, M., Wulf, H., Schaepman, M., and Hoelzle, M. Cross-Comparison of Albedo Products for Glacier Surfaces Derived from Airborne and Satellite (Sentinel-2 and Landsat 8) Optical Data. *Remote Sensing*, 9(2):110, 2017. doi:10.3390/rs9020110.

Narama, C., Kääb, A., Duishonakunov, M., and Abdrakhmatov, K. Spatial variability of recent glacier area changes in the Tien Shan Mountains, Central Asia, using Corona (~1970), Landsat (~2000), and ALOS (~2007) satellite data. *Global and Planetary Change*, 71:42–54, 2010. doi:10.1016/j.gloplacha.2009.08.002.

Navarro, F., Corcuera, M. I., Cuadrado, M. L., and Corrales, J. M. Numerical modelling of dynamics and thermal regime of glaciers by finite element methods. *Materialy Glatsiologicheskih Issledovanii (Data of glaciological studies)*, 87:21–27, 1999.

Nie, Y., Pritchard, H. D., Liu, Q., Hennig, T., Wang, W., Wang, X., Liu, S., Nepal, S., Samyn, D., Hewitt, K., and Chen, X. Glacial change and hydrological implications in the Himalaya and Karakoram. *Nature Reviews Earth and Environment*, 2:91–106, 2021. doi:10.1038/s43017-020-00124-w.

Noël, B., van de Berg, W. J., Lhermitte, S., Wouters, B., Machguth, H., Howat, I., Citterio, M., Moholdt, G., Lenaerts, J. T. M., and van den Broeke, M. R. A tipping point in refreezing accelerates mass loss of Greenland's glaciers and ice caps. *Nature Communications*, 8: 14730, 2017. doi:10.1038/ncomms14730.

Nosenko, G. A., Lavrentiev, I. I., Glazovskii, A. F., Kazatkin, N. E., and Kokarev, A. L. The polythermal structure of Central Tuyuksu glacier. *Earth's Cryosphere*, 20(4):105–115, 2016. doi:10.21782/KZ1560-7496-2016-4(105-115).

Obleitner, F. and Lehning, M. Measurement and simulation of snow and superimposed ice at the Kongsvegen glacier, Svalbard (Spitzbergen). *Journal of Geophysical Research: Atmospheres*, 109(D04106), 2004. doi:10.1029/2003jd003945.

Ochwat, N. E., Marshall, S. J., Moorman, B. J., Criscitiello, A. S., and Copland, L. Evolution of the firn pack of Kaskawulsh Glacier, Yukon: Meltwater effects, densification, and the development of a perennial firn aquifer. *The Cryosphere*, 15:2021–2040, 2021. doi:10.5194/tc-15-2021-2021.

Oerlemans, J. *Glaciers and climate change*. AA Balkema Publishers, Lisse and Exton (PA), 2001.

Oerlemans, J. *The microclimate of valley glaciers*. Igitur, Utrecht Publishing & Archiving Services, University of Utrecht, Utrecht, Netherlands, 2010.

Oerlemans, J. and Klok, E. J. Energy Balance of a Glacier Surface: Analysis of Automatic Weather Station Data rom the Morteratschgletscher, Switzerland. *Arctic, Antarctic and Alpine Research*, 34(4):477–485, 2002. doi:10.1080/15230430.2002.12003519.

Oraschewski, F. and Grinsted, A. Modeling enhanced firn densification due to strain softening. *The Cryosphere Discussions*, 2021_240:1–24, 2021. doi:10.5194/tc-2021-240.

Orsolini, Y., Wegmann, M., Dutra, E., Liu, B., Balsamo, G., Yang, K., De Rosnay, P., Zhu, C., Wang, W., Senan, R., and Arduini, G. Evaluation of snow depth and snow cover over the Tibetan Plateau in global reanalyses using in situ and satellite remote sensing observations. *The Cryosphere*, 13(8):2221–2239, 2019. doi:10.5194/tc-13-2221-2019.

Ostrem, G. and Brugman, M. *Glacier Mass-Balance Measurements: A Manual for Field and Office Work*. Environment Canada, Saskatoon, Canada, 1993.

Pälli, A., Moore, J. C., and Rolstad, C. Firn-ice transition-zone features of four polythermal glaciers in Svalbard seen by ground-penetrating radar. *Annals of Glaciology*, 37:298–304, 2003. doi:10.3189/172756403781816059.

Pellicciotti, F., Brock, B., Strasser, U., Burlando, P., Funk, M., and Corripio, J. An enhanced temperature-index glacier melt model including the shortwave radiation balance: development and testing for Haut Glacier d'Arolla, Switzerland. *Journal of Glaciology*, 51(175): 573–587, 2005. doi:10.3189/172756505781829124.

Pellicciotti, F., Buergi, C., Immerzeel, W. W., Konz, M., and Shrestha, A. B. Challenges and Uncertainties in Hydrological Modeling of Remote Hindu Kush–Karakoram–Himalayan (HKH) Basins: Suggestions for Calibration Strategies. *Mountain Research and Development*, 32(1):39–50, 2012. doi:10.1659/MRD-JOURNAL-D-11-00092.1.

Peña-Ramos, J. A., Bagus, P., and Fursova, D. Water conflicts in Central Asia: Some recommendations on the non-conflictual use of water. *Sustainability*, 13(3479):1–24, 2021. doi:10.3390/su13063479.

Pertziger, F. *Abramov Glacier Data Reference Book: Climate, Runoff, Mass Balance*. Central Asian Hydrometeorlogical Institute, Tashkent, 1996.

Petrakov, D., Shpuntova, A., Aleinikov, A., Kääb, A., Kutuzov, S., Lavrentiev, I., Stoffel, M., Tutubalina, O., and Usubaliev, R. Accelerated glacier shrinkage in the Ak-Shyirak massif, Inner Tien Shan, during 2003-2013. *Science of the Total Environment*, 562:364–378, 2016. doi:10.1016/j.scitotenv.2016.03.162.

Peyaud, V., Bouchayer, C., Gagliardini, O., Vincent, C., Gillet-chaulet, F., Six, D., and Laarman, O. Numerical modeling of the dynamics of the Mer de Glace glacier, French Alps: comparison with past observations and forecasting of near-future evolution. *The Cryosphere*, 14:3979–3994, 2020. doi:10.5194/tc-14-3979-2020.

Pieczonka, T. and Bolch, T. Region-wide glacier mass budgets and area changes for the Central Tien Shan between ˜1975 and 1999 using Hexagon KH-9 imagery. *Global and Planetary Change*, 128:1–13, 2015. doi:10.1016/j.gloplacha.2014.11.014.

Pieczonka, T., Bolch, T., Junfeng, W., and Shiyin, L. Heterogeneous mass loss of glaciers in the Aksu-Tarim Catchment (Central Tien Shan) revealed by 1976 KH-9 Hexagon and 2009 SPOT-5 stereo imagery. *Remote Sensing of Environment*, 130:233–244, 2013. doi:10.1016/j.rse.2012.11.020.

Pohl, E., Knoche, M., Gloaguen, R., Andermann, C., and Krause, P. Sensitivity analysis and implications for surface processes from a hydrological modelling approach in the Gunt catchment, high Pamir Mountains. *Earth Surface Dynamics*, 3:333–362, 2015. doi:10.5194/esurf-3-333-2015.

Purves, R. S., Barton, J. S., Mackaness, W. A., and Sugden, D. E. The development of a rule-based spatial model of wind transport and depostion of snow. *Annals of Glaciology*, 26:197–202, 1998. doi:10.3189/1998AoG26-1-197-202.

Quéno, L., Fierz, C., Van Herwijnen, A., Longridge, D., and Wever, N. Deep ice layer formation in an alpine snowpack: monitoring and modeling. *The Cryosphere*, 14:3449–3464, 2020. doi:10.5194/tc-14-3449-2020.

Ragettli, S. and Pellicciotti, F. Calibration of a physically based, spatially distributed hydrological model in a glacierized basin: On the use of knowledge from glaciometeorological processes to constrain model parameters. *Water Resources Research*, 48(W03509):1–20, 2012. doi:10.1029/2011WR010559.

Reeh, N. A nonsteady-state firn-densification model for the percolation zone of a glacier. *Journal of Geophysical Research*, 113(F03023):1–13, 2008. doi:10.1029/2007JF000746.

Reijmer, C. H. and Hock, R. Internal accumulation on Storglaciären, Sweden, in a multi-layer snow model coupled to a distributed energy- and mass-balance model. *Journal of Glaciology*, 54(184):61–72, 2008. doi:10.3189/002214308784409161.

Réveillet, M., Six, D., Vincent, C., Rabatel, A., Dumont, M., Lafaysse, M., Morin, S., Vionnet, V., and Litt, M. Relative performance of empirical and physical models in assessing the seasonal and annual glacier surface mass balance of Saint-Sorlin Glacier (French Alps). *Cryosphere*, 12(4):1367–1386, 2018. doi:10.5194/tc-12-1367-2018.

RGI Consortium. *Randolph Glacier Inventory – A Dataset of Global Glacier Outlines: Version 6.0*. Global Land Ice Measurements from Space, Colorada, USA. Digital Media, 2017. doi:10.7265/N5-RGI-60.

Rohrer, M. Determination of the transition air temperature from snow to rain and intensity of precipitation. In Sevruk, B., editor, *WMO IAHS ETH, International Workshop on Precipitation Measurement, St. Moritz,1989 Switzerland*, pages 475–482, Zurich, Switzerland, 1989. ETH Zurich. doi:10.13140/RG.2.1.3397.5280.

Saks, T., Pohl, E., Machguth, H., Dehecq, A., Barandun, M., Kenzhebaev, R., Kalashnikova, O., and Hoelzle, M. Glacier Runoff Variation Since 1981 in the Upper Naryn River Catchments, Central Tien Shan. *Frontiers in Environmental Science*, 9:1–16, 2022. doi:10.3389/fenvs.2021.780466.

Sarangi, C., Qian, Y., Rittger, K., Bormann, K. J., Liu, Y., Wang, H., Wan, H., Lin, G., and Painter, T. H. Impact of light-absorbing particles on snow albedo darkening and associated radiative forcing over high-mountain Asia: high-resolution WRF-Chem modeling and new satellite observations. *Atmospheric Chemistry and Physics*, 19(10):7105–7128, 2019. doi:10.5194/acp-19-7105-2019.

Schmale, J., Flanner, M., Kang, S., Sprenger, M., Zhang, Q., Guo, J., Li, Y., Schwikowski, M., and Farinotti, D. Modulation of snow reflectance and snowmelt from Central Asian glaciers by anthropogenic black carbon. *Scientific Reports*, 7(40501):1–10, 2017. doi:10.1038/srep40501.

Schneider, T. and Jansson, P. Internal accumulation in firn and its significance for the mass balance of Storglaciären, Sweden. *Journal of Glaciology*, 50(168):25–34, 2004. doi:10.3189/172756504781830277.

Schöne, T., Zech, C., Unger-Shayesteh, K., Rudenko, V., Thoss, H., Wetzel, H.-U., Gafurov, A., Illigner, J., and Zubovich, A. A new permanent multi-parameter monitoring network in Central Asian high mountains - from measurements to data bases. *Geoscientific Instrumentation, Methods and Data Systems*, 2:97–111, 2013. doi:10.5194/gi-2-97-2013.

Schwikowski, M., Schläppi, M., Santibanez, P., Rivera, A., and Casassa, G. The Cryosphere Net accumulation rates derived from ice core stable isotope records of Pío XI glacier, Southern Patagonia Icefield. *The Cryosphere*, 7:1635–1644, 2013. doi:10.5194/tc-7-1635-2013.

Seligman, G. The structure of a temperate glacier. *The Geographical Journal*, 97:295–315, 1941. URL `https://www.jstor.org/stable/1787399`.

Shean, D. E., Bhushan, S., Montesano, P., Rounce, D. R., Arendt, A., and Osmanoglu, B. A Systematic, Regional Assessment of High Mountain Asia Glacier Mass Balance. *Frontiers in Earth Science*, 7(363):1–19, 2020. doi:10.3389/feart.2019.00363.

Shumskii, P. A. *Principles of structural glaciology*. Dover Publications Inc., New York, 1964.

Shumskiii, P. A. *Principles of structural glaciology [in Russian]*. Izdatel'stvo Akademii Nauk SSSR, Moscow, 1955.

Siegfried, T., Bernauer, T., Guiennet, R., Sellars, S., Robertson, A. W., Mankin, J., Bauer-Gottwein, P., and Yakovlev, A. Will climate change exacerbate water stress in Central Asia? *Climatic Change*, 112(3-4):881–899, 2012. doi:10.1007/s10584-011-0253-z.

Singh, V. P., Singh, P., and Haritashya, U. K., editors. *Encyclopedia of Snow, Ice and Glaciers*. Encyclopedia of Earth Sciences Series. Springer, Dordrecht, Netherlands, 2011. doi:10.1007/978-90-481-2642-2.

Small, D. Flattening Gamma: Radiometric Terrain Correction for SAR Imagery. *IEEE Trans. Geosci. Remote Sens.*, 49(8):3081–3093, 2011. doi:10.1109/TGRS.2011.2120616.

Small, D., Miranda, N., Ewen, T., and Jonas, T. Reliably flattened backscatter for wet snow mapping from wide-swath sensors. *ESA Living Planet Symposium*, 1:1–8, 2013.

Sold, L., Huss, M., Hoelzle, M., Andereggen, H., Joerg, P. C., and Zemp, M. Methodological approaches to infer end-of-winter snow distribution on alpine glaciers. *Journal of Glaciology*, 59(218):1047–1059, 2013. doi:10.3189/2013JoG13J015.

Sold, L., Huss, M., Eichler, A., Schwikowski, M., and Hoelzle, M. Unlocking annual firn layer water equivalents from ground-penetrating radar data on an Alpine glacier. *The Cryosphere*, 9:1075–1087, 2015. doi:10.5194/tc-9-1075-2015.

Sold, L., Huss, M., Machguth, H., C.Joerg, P., Leysinger Vieli, G., Linsbauer, A., Salzmann, N., Zemp, M., and Hoelzle, M. Mass Balance Re-analysis of Findelengletscher, Switzerland; Benefits of Extensive Snow Accumulation Measurements. *Frontiers in Earth Science*, 4 (18), 2016. doi:10.3389/feart.2016.00018.

Sorg, A., Bolch, T., Stoffel, M., Solomina, O., and Beniston, M. Climate change impacts on glaciers and runoff in Tien Shan (Central Asia). *Nature Climate Change*, 2(10):725–731, 2012. doi:10.1038/nclimate1592. URL `http://www.nature.com/doifinder/10.1038/nclimate1592`.

Sorg, A., Huss, M., Rohrer, M., and Stoffel, M. The days of plenty might soon be over in glacierized Central Asian catchments. *Environmental Research Letters*, 9(10):104018, 2014. doi:10.1088/1748-9326/9/10/104018.

Stainbank, W. D. *Simulation of Abramov glacier energy balance and firn properties*. Msc thesis, University of Fribourg, 2018.

Stevens, C. M., Verjans, V., Lundin, J. M., Kahle, E. C., Horlings, A. N., Horlings, B. I., and Waddington, E. D. The Community Firn Model (CFM) v1.0. *Geoscientific Model Development*, 13(9):4355–4377, 2020. doi:10.5194/gmd-13-4355-2020.

Sun, H., Su, F., Yao, T., He, Z., Tang, G., Huang, J., Zheng, B., Meng, F., Ou, T., and Chen, D. General overestimation of ERA5 precipitation in flow simulations for High Mountain Asia basins. *Environmental Research Communications*, 3(12), 2021. doi:10.1088/2515-7620/ac40f0.

Suslov, V. F. and Krenke, A. N. *Abaramov Glacier (Alay Range) [in Russian]*. Gidrometeoizdat, St. Petersburg, 1980.

Suter, S., Hoelzle, M., and Ohmura, A. Energy balance at a cold alpine firn saddle, Seserjoch, Monte Rosa. *International Journal of Climatology*, 24:1423–1442, 2004. doi:10.1002/joc.1079.

Takeuchi, N., Fujita, K., Aizen, V. B., Narama, C., Yokoyama, Y., Okamoto, S., Naoki, K., and Kubota, J. The disappearance of glaciers in the Tien Shan Mountains in

Central Asia at the end of Pleistocene. *Quaternary Science Reviews*, 103:26–33, 2014. doi:10.1016/j.quascirev.2014.09.006.

Thiel, K., Arndt, A., Wang, P., Li, H., Li, Z., and Schneider, C. Modeling of mass balance variability and its impact on water discharge from the urumqi glacier no. 1 catchment, tian shan, china. *Water*, 12:1–30, 2020. doi:10.3390/w12123297.

Thompson, L. G., Mosley-Thompson, E., Davis, M., Lin, P. N., Yao, T., Dyurgerov, M., and Dai, J. "Recent warming": ice core evidence from tropical ice cores with emphasis on Central Asia. *Global and Planetary Change*, 7(1-3):145–156, 1993. doi:10.1016/0921-8181(93)90046-Q.

Thompson, L. G., Mikhalenko, V. N., Mosley-Thompson, E., Dyurgerov, M. B., Lin, P. N., Moskalevsky, M., Davis, M. E., Arkhipov, S., and Dai, J. Ice core records of recent climatic variability: Gregoriev and It-Tish ice caps, in central Tien Shan, Central Asia. *Materialy Glatsiologicheskih Issledovanii (Data of glaciological studies)*, 81:100–109, 1997.

Trabant, D. and Mayo, L. Estimation and effects of internal accumulation on five glaciers in Alaska. *Annals of Glaciology*, 6:114–117, 1985. doi:10.3189/1985AoG6-1-113-117.

TU Berlin. he High Asia Refined analysis (HAR) [Website], 2021. URL `https://www.klima.tu-berlin.de/index.php?show=daten{_}har{&}lan=de`.

Unger-Shayesteh, K., Vorogushyn, S., Farinotti, D., Gafurov, A., Duethmann, D., Mandychev, A., and Merz, B. What do we know about past changes in the water cycle of Central Asian headwaters? A review. *Global and Planetary Change*, 110:4–25, 2013. doi:10.1016/j.gloplacha.2013.02.004.

van Pelt, W. and Kohler, J. Modelling the long-term mass balance and firn evolution of glaciers around Kongsfjorden, Svalbard. *Journal of Glaciology*, 61(228):731–744, 2015. doi:10.3189/2015JoG14J223.

van Pelt, W., Pohjola, V., Pettersson, R., Marchenko, S., Kohler, J., Luks, B., Ove Hagen, J., Schuler, T. V., Dunse, T., Noël, B., and Reijmer, C. A long-term dataset of climatic mass balance, snow conditions, and runoff in Svalbard (1957-2018). *The Cryosphere*, 13(9):2259–2280, 2019. doi:10.5194/tc-13-2259-2019.

van Pelt, W. J. J. *Modelling the dynamics and boundary processes of Svalbard glaciers*. PhD thesis, Utrecht University, 2013.

van Pelt, W. J. J., Oerlemans, J., Reijmer, C. H., Pohjola, V. A., Pettersson, R., and Van Angelen, J. H. Simulating melt, runoff and refreezing on Nordenskiöldbreen, Svalbard,

using a coupled snow and energy balance model. *The Cryosphere*, 6:641–659, 2012. doi:10.5194/tc-6-641-2012.

van Pelt, W. J. J., Pettersson, R., Pohjola, V. A., Marchenko, S., Claremar, B., and Oerlemans, J. Inverse estimation of snow accumulation variability along a snow radar transect on Nordenskioldbreen, Svalbard. *Journal of Geophysical Research: Earth Surface*, 119: 816–835, 2014. doi:10.1002/2013JF003040.

Vandecrux, B., Mottram, R., L. Langen, P., S. Fausto, R., Olesen, M., Max Stevens, C., Verjans, V., Leeson, A., Ligtenberg, S., Kuipers Munneke, P., Marchenko, S., Van Pelt, W., R. Meyer, C., B. Simonsen, S., Heilig, A., Samimi, S., Marshall, S., Machguth, H., MacFerrin, M., Niwano, M., Miller, O., I. Voss, C., and E. Box, J. The firn meltwater Retention Model Intercomparison Project (RetMIP): Evaluation of nine firn models at four weather station sites on the Greenland ice sheet. *Cryosphere*, 14(11):3785–3810, 2020. doi:10.5194/tc-14-3785-2020.

Vega, C. P., Pohjola, V. A., Beaudon, E., Claremar, B., Pelt, W. J. V., Pettersson, R., Isaksson, E., Martma, T., Schwikowski, M., and Bøggild, C. E. A synthetic ice core approach to estimate ion relocation in an ice field site experiencing periodical melt: A case study on lomonosovfonna, svalbard. *The Cryosphere*, 10:961–976, 5 2016. doi:10.5194/tc-10-961-2016.

Vincent, C., Le Meur, E., Six, D., Possenti, P., Lefebvre, E., and Funk, M. Climate warming revealed by englacial temperatures at Col du Dôme (4250 m, Mont Blanc area). *Geophysical Research Letters*, 34(L16502):1–5, 2007. doi:10.1029/2007GL029933.

Vincent, C., Gilbert, A., Jourdain, B., Piard, L., Ginot, P., Mikhalenko, V., Possenti, P., Le Meur, E., Laarman, O., and Six, D. Strong changes in englacial temperatures despite insignificant changes in ice thickness at Dôme du Goûter glacier (Mont Blanc area). *The Cryosphere*, 14:925–934, 2020. doi:10.5194/tc-14-925-2020.

Vionnet, V., Brun, E., Morin, S., Boone, A., Faroux, S., Le Moigne, P., Martin, E., and Willemet, J.-M. The detailed snowpack scheme Crocus and its implementation in SURFEX v7.2. *Geoscientific Model Development*, 5:773–791, 2012. doi:10.5194/gmd-5-773-2012.

Wagnon, P., Ribstein, P., Francou, B., and Pouyaud, B. Annual cycle of energy balance of Zongo Glacier, Cordillera Real, Bolivia. *Journal of Geophysical Research*, 104(D4): 3907–3923, 1999. doi:10.1029/1998JD200011.

Walther, S. *Accumulation distribution on Abramov Glacier from GPR measurements*. Msc thesis, University of Fribourg, 2018.

Wang, Q., Yi, S., and Sun, W. Precipitation-driven glacier changes in the Pamir and Hindu Kush mountains. *Geophysical Research Letters*, 44:2817–2824, 2017. doi:10.1002/2017GL072646.

Wang, R., Liu, S., Shangguan, D., Radić, V., and Zhang, Y. Spatial heterogeneity in glacier mass-balance sensitivity across High Mountain Asia. *Water*, 11(4):776, 2019. doi:10.3390/w11040776.

Wang, X., Tolksdorf, V., Otto, M., and Scherer, D. WRF-based dynamical downscaling of ERA5 reanalysis data for High Mountain Asia: Towards a new version of the High Asia Refined analysis. *International Journal of Climatology*, 41:743–762, 2021. doi:10.1002/joc.6686.

WGMS. *Global Glacier Change Bulletin No. 4 (2018-2019)*. ISC(WDS) / IUGG(IACS) / UNEP / UNESCO / WMO, World Glacier Monitoring Service, Zurich, Switzerland, publication based on database version: doi:10.5904/wgms-fog-2021-05, 2021. URL `https://wgms.ch/ggcb/`.

Winkler, M., Juen, I., Mölg, T., Wagnon, P., Gómez, J., and Kaser, G. Measured and modelled sublimation on the tropical Glaciar Artesonraju , Perú. *The Cryosphere*, 3:21–30, 2009.

Woodward, J. and Burke, M. J. Applications of ground-penetrating radar to glacial and frozen materials. *Journal of Environmental and Engineering Geophysics*, 12(1):69–85, 2007. doi:10.2113/JEEG12.1.69.

Yao, B. T., Thompson, L., Chen, D., Zhang, Y., Wang, N., Zhao, L., Che, T., Xu, B., Wu, G., Zhang, F., Tang, I., Immerzeel, W., Bolch, T., Pellicciotti, F., Xin Li, W. Y., Gao, J., and Wang, W. Third Pole climate warming and cryosphere system changes. *WMO Bulletin*, 69(1):38, 2020. URL `https://public.wmo.int/en/resources/bulletin/third-pole-climate-warming-and-cryosphere-system-changes`.

Yao, T., Thompson, L., Yang, W., Yu, W., Gao, Y., Guo, X., Yang, X., Duan, K., Zhao, H., Xu, B., Pu, J., Lu, A., Xiang, Y., Kattel, D. B., and Joswiak, D. Different glacier status with atmospheric circulations in Tibetan Plateau and surroundings. *Nature Climate Change*, 2(9):663–667, 2012. doi:10.1038/nclimate1580.

Yao, T., Xue, Y., Chen, D., Chen, F., Thompson, L., Cui, P., Koike, T., Lau, W. K., Lettenmaier, D., Mosbrugger, V., Zhang, R., Xu, B., Dozier, J., Gillespie, T., Gu, Y., Kang, S., Piao, S., Sugimoto, S., Ueno, K., Wang, L., Wang, W., Zhang, F., Sheng, Y., Guo, W., Ailikun, Yang, X. X., Ma, Y., Shen, S. S., Su, Z., Chen, F., Liang, S., Liu, Y., Singh, V. P., Yang, K., Yang, D., Zhao, X., Qian, Y., Zhang, Y., and Li, Q. Recent third pole's rapid warming accompanies cryospheric melt and water cycle intensification and interactions between monsoon and

environment: Multidisciplinary approach with observations, modeling, and analysis. *Bulletin of the American Meteorological Society*, 100(3):423–444, 2019. doi:10.1175/BAMS-D-17-0057.1.

Zemp, M., Frey, H., Gärtner-Roer, I., Nussbaumer, U. S., Hoelzle, M., Paul, F., Haeberli, W., Denzinger, F., Ahlstrøm, P. A., Anderson, B., Bajracharya, S., Baroni, C., Braun, N. L., Cáceres, E. B., Casassa, G., Cobos, G., Dávila, R. L., Delgado Granados, H., Demuth, N. M., Espizua, L., Fischer, A., Fujita, K., Gadek, B., Ghazanfar, A., Hagen, J., Holmlund, P., Karimi, N., Li, Z., Pelto, M., Pitte, P., Popovnin, V. V., Portocarrero, A. C., Prinz, R., Sangewar, V. C., Severskiy, I., Sigurðsson, O., Soruco, A., Usubaliev, R., and Vincent, C. Historically unprecedented global glacier decline in the early 21st century. *Journal of Glaciology*, 61(228):745–762, 2015. doi:10.3189/2015JoG15J017.

Zhang, Z., Liu, S., Wei, J., Xu, J., Guo, W., Bao, W., and Jiang, Z. Mass change of glaciers in Muztag Ata-Kongur Tagh, Eastern Pamir, China from 1971/76 to 2013/14 as derived from remote sensing data. *PLoS ONE*, 11(1):e0147327, 2016. doi:10.1371/journal.pone.0147327.

Zheng, G., Allen, S. K., Bao, A., Ballesteros-Cánovas, J. A., Huss, M., Zhang, G., Li, J., Yuan, Y., Jiang, L., Yu, T., Chen, W., and Stoffel, M. Increasing risk of glacial lake outburst floods from future Third Pole deglaciation. *Nature Climate Change*, 11(5):411–417, 2021. doi:10.1038/s41558-021-01028-3.

Zhu, M., Yao, T., Yang, W., Xu, B., Wu, G., Wang, X., and Xie, Y. Reconstruction of the mass balance of Muztag Ata No. 15 glacier, eastern Pamir, and its climatic drivers. *Journal of Glaciology*, 64(244):259–274, 2018. doi:10.1017/jog.2018.16.

Acknowledgements

Throughout my PhD studies I got supported by a lot of people in manifold ways. Without their help, this thesis would not have been possible. I would like to express my sincere gratitude to all of them.

First of all, I would like to thank my supervisors Prof. Horst Machguth and Prof. Martin Hoelzle. I am grateful to have had your complementary support and advice along my PhD studies. At least one of you always had a solution to the problems I encountered. I equally appreciate your willingness to take part in and your efforts during the exhausting fieldwork. I greatly acknowledge the scientific and less scientific but always critical discussions I had with both of you. Horst's attention to detail and Martin's overarching questions have led me to look more thoroughly into the subject matter and thereby improve my scientific understanding again and again. Thanks a lot!

I would also like to thank the other members of the jury of evaluating thesis, namely Dr. Stanislav Kutuzov, Dr. Francesca Pelliciotti and Dr. Ward van Pelt as well as the president of the Jury Prof. Christian Hauck.

I sincerely thank all the people who helped with collecting data on Abramov glacier either by being in the field or by their support with fieldwork logistics. A special thanks goes to all the ones who were participating in the firn measurements and to all my colleagues and friends from the Central Asian Institute for Applied Geosciences (CAIAG) and KyrgyzHydromet who continue to gather data on Abramov glacier.

Accessing the historical data was equally important for this thesis. Especially the dissertation by Boris Kislov organized by Dr. Ivan Lavrentiev was highly relevant for my work. And then there is the incredibly valuable Abramov glacier data base provided by Felix Pertziger. The daily weather station and monthly mass balance measurements provided unforeseen possibilities for this research. I am grateful to have had the opportunity to work with these data and also for having received so many clarifying answers to all my questions. Thanks to both of you and all the others who helped me with access to literature and data published in Russian language.

I would like to express gratitude to all my co-authors, who contributed their time and shared their invaluable knowledge and experience, provided material, methods and data and supported me throughout the analysis. I learned a lot from all of you during (online) discussions. Some of you have accompanied me closely through different stages of my doctorate. I greatly appreciate the manifold support and trust I experienced from Prof. Margit Schwikowski. Thanks also to Dr. Anja Eichler for the introduction to the work in the (cold) lab and the never boring hours we spent freezing despite the summer heat. Thanks a lot to both of you and also to your colleagues for welcoming me and analysing the Central Asian firn cores at the Paul Scherrer Institute. The later work was accompanied by the support of Dr. Ward van Pelt who provided the EBFM and who was always available to answer my questions. I am glad that I could realize the last travel of my PhD studies which took me to Uppsala University, where Ward introduced me step by step to the model and made sure that it is properly set up for Abramov glacier. Back then, nobody expected that travelling will become so challenging. I am thankful for having had the possibility for this short research stay and also thank to all your colleagues for the welcoming atmosphere and the fruitful discussions.

I greatly acknowledge the funding of this thesis by the Swiss National Science Foundation (SNSF) and the complementary financing by the project CICADA (Cryospheric Climate Services for improved Adaptation, Swiss Agency for Development and Cooperation and the University of Fribourg). These donors not only allowed me to continue my work and studies at the University of Fribourg with a focus on Central Asia, but also to set up the program 'Adventure of Science: Women and glaciers in Central Asia.' In this context, I would like to express my gratitude to Dr. Martina Barandun for introducing me to Central Asia. I also would like to thank you and Dr. Tomas Saks for mastering all the smaller and bigger challenges we have repeatedly encountered there.

Even during home office times I had valuable informal exchange with some Fribourg colleagues during our virtual coffee breaks. Of course, I much more appreciate to have a coffee in person at the institute in Fribourg. Thanks to all my current and former colleagues and friends from the Department of Geosciences for the pleasant everyday routine, the practical and technical help and the valuable scientific as well as personal exchange which made it always worth to come to the office. I greatly acknowledge the helpful atmosphere which includes (besides 1000 other things) sharing the the template for writing a PhD thesis. Thanks to Dr. Leo Sold for this.

I got deeply inspired by many women I encountered thanks to Inspiring Girls Expeditions and the related programs. Of course, I greatly enjoyed the time in the mountains. Before the

pandemic, I would never have thought that online exchanges can transmit such inspiration as I experienced several times.

The moments far from science were equally important during the last years. Thanks to the ones who allowed for short breaks by teaching great yoga lessons and to my friends and family with whom I shared longer breaks in the mountains, at concerts, with a beer, a meal or a coffee. Thanks a lot for these breaks and also for your finger crossings, patience and encouragements during my asocial moments and the times I was to busy to share time with you.

And finally thanks to Jonas for everything.

Appendices

A. Additional visualisations of *in situ* measurements performed on Abramov glacier

This appendix contains additional visualisations field measurements performed within this thesis. The data were collected on Abramov glacier in 2018.

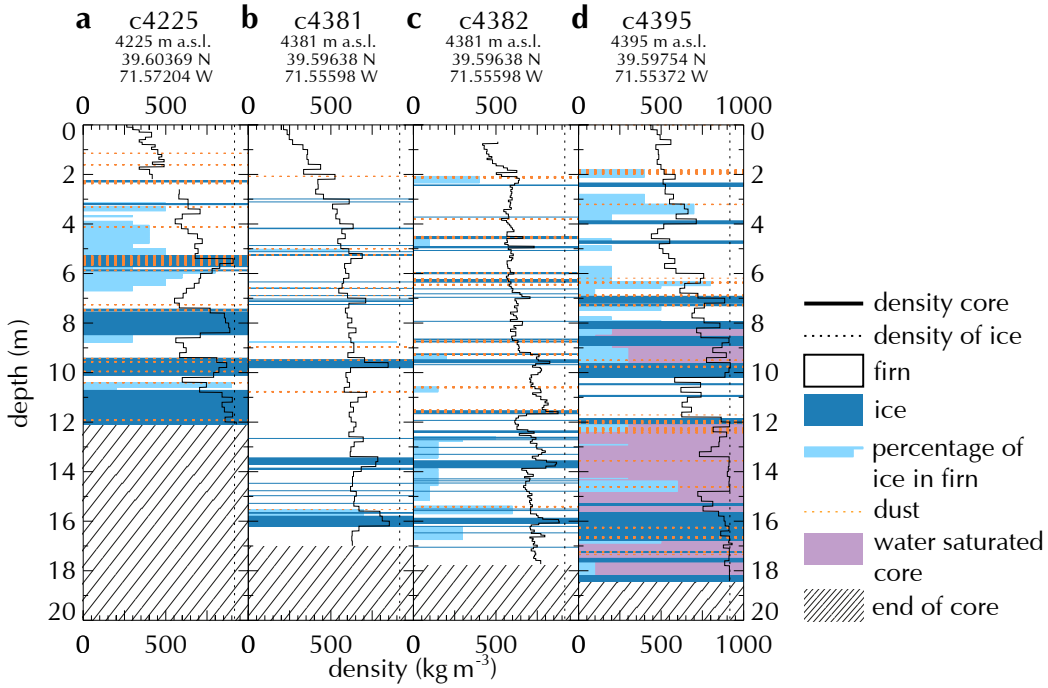

Figure A.1: Firn stratigraphy and density from cores drilled on Abramov glacier in 2018. The visual stratigraphy of all cores was observed in the field. The density of core c4382 (c) was measured at the Paul Scherrer Institute (after shipping to Switzerland), the densities of the other cores (a,b,d) was measured in the field and described in Paper I. The cores shown in a, b and c were drilled in winter 2018, core c4395 was drilled in August 2018. Cores c4382 and c4395 are also shown in Paper I. The drilling locations are shown in Fig. 1.2. Additional information on the visualised cores is given in Table 6 in Paper I.

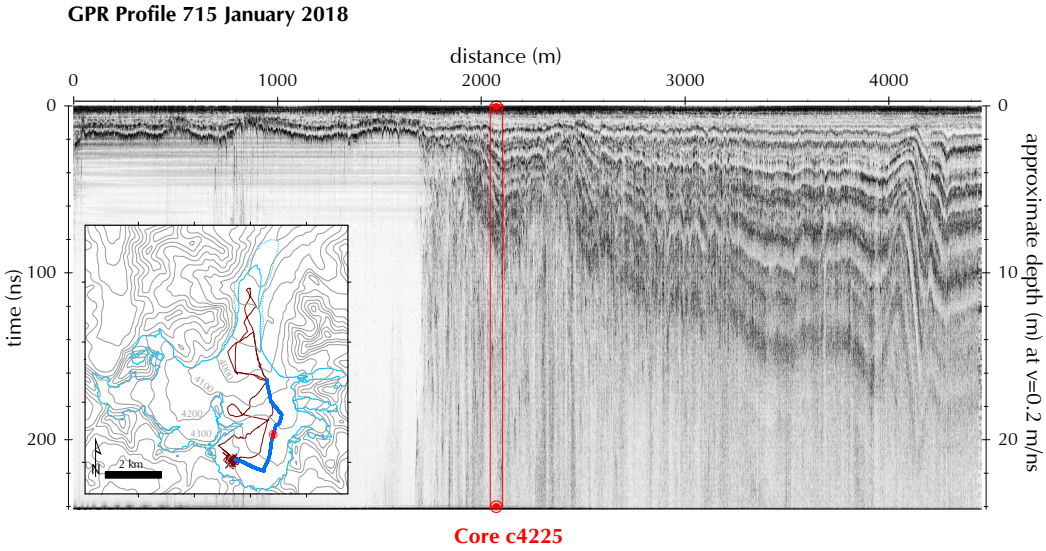

Figure A.2: Processed GPR transect No.0715 (January 2018). The transect goes across the firn ice transition zone. The location of core c4225 is indicated. Distance 0 m refers to the lowermost point of the GPR profile The inset map shows the location of GPR profile No.0715 in blue. The drill site is also indicated (red dot)

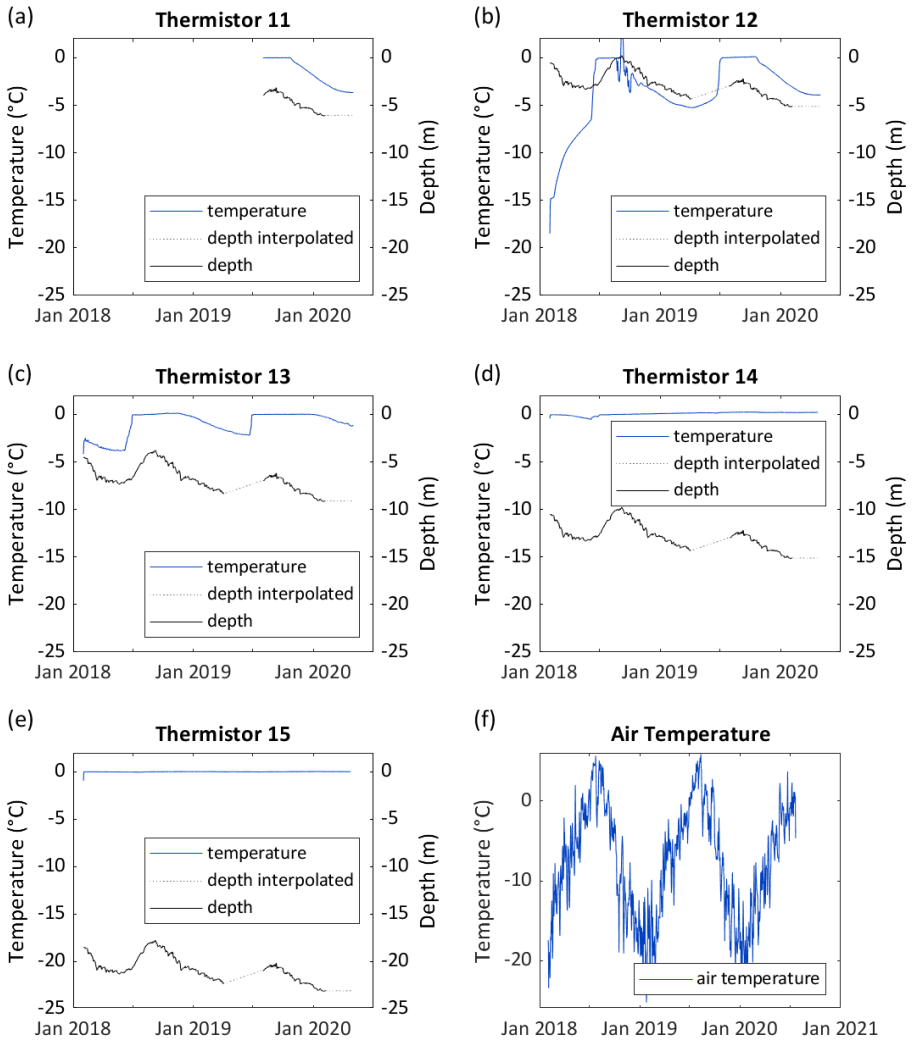

Figure A.3: Subsurface (a-e) and air temperature (f) measurements measured with five thermistors located at depths between 0 and 23 m and one shielded thermometer located about 2-4 m above the glacier surface at ~4380 m a.s.l on Abramov glacier. Data were measured from February 2018 until Summer 2020. Thermistor depths in a-e is estimated from ultrasonic snow height measurements performed at the same station. Data are only shown for the time period when the thermistor became buried.

B. Supplement of Paper II

Supplement of "Long-term firn and mass balance modelling for Abramov glacier, Pamir Alay"

Marlene Kronenberg et al.
Correspondence: Marlene Kronenberg (marlene.kronenberg@unifr.ch)

S1 Supplementary information on data and methods

S1.1 Topographical data

We use digital elevation models (DEM) with an initial resolution of 4 m derived from historical aerial photographs from 1975 (DEM1975) and from three Pléiades stereo pairs from 2015 (DEM2015) provided by Denzinger et al. (2021). Glacier outlines are available for 1975 and 2015 from Denzinger et al. (2021) and for 1986, 1998 and 2005 from Barandun et al. (2015). For the DEM2015, Stainbank (2018) manually removed artefacts and created a gap-filled DEM with 25 m resolution which we use as a reference DEM. Furthermore, we use the 1975 glacier area as the initial glacier surface. We use later glacier extents (one per decade) to estimate the glacier area change (reduction with respect to 1975) over time. Based on these data we calculate an annual height change grid, an elevation grid for 1968 (DEM1968) using the annual height change grid assuming the same linear elevation trend as between 1975 and 2015, and a initial glacier mask (mask1975) with a resolution of 100 m and an extent of 10.7 km $\times$ 10.7 km (107$\times$107 grid points). As we do not account for glacier dynamics, the application of a linearly changing elevation is a straightforward and computationally effective way to include topographical changes.

S1.2 Automatic weather station data

Since August 2012, an automatic weather station (AWS) is operating at 4100 m a.s.l. about 1 km from the glacier tongue (Fig. 1b in the main manuscript) and the site of the historical meteorological observations. Schöne et al. (2013) detail the technical information including sensor specifications. Long data gaps and outliers are abundant during the first operational year and we therefore only use data from January 2014 onwards. In contrast to the original Abramov glacier weather station, only liquid precipitation is measured at the station, which is very rare even in summer. Hence, no precipitation data are available. Here, we use air temperature, air pressure, relative humidity, and incoming short- and longwave radiation. We fix a clock error and apply filtering (as described below) to the raw measurements which are registered 12 times an hour before calculating three-hourly and daily averages of several parameters as described in Stainbank (2018). At least 18 measurements are necessary (50 % of the total measurements) for three-hourly averages, otherwise we set the value to Not a Number (NaN). Daily averages are only calculated if data is available for each three-hourly time step of a day.

For air temperature, air pressure and longwave radiation we first remove extreme outliers by the application of an inter quartile range filter. Second, we calculate three-hourly mean and standard deviation for the entire time series and remove values that are more than three standard deviations from the three-hourly mean. A visual inspection of the time series indicated that for a few short periods, some outliers were not detected by the automatic filters and therefore removed manually before rerunning the second filter. For relative humidity we applied an upper (100 %) and a lower threshold (0 %), setting values below or above to NaN. The four component net radiation sensor delivers incoming short- and longwave radiation which are used here. Furthermore, the measurements may be affected by sensor freezing. We do not specifically correct for these effects, but apply some general filters. Incoming shortwave radiation measurements below 0 W m^{-2} are set to 0 W m^{-2} and measurements above 1500 W m^{-2} are excluded.

S1.3 Monthly point mass balance data 1967-1998

Monthly mass balance was measured on Abramov glacier from the beginning of the hydrological year 1967/1968 until summer 1999. Winter and annual mass balance data are published in Pertziger (1996) who compiled the data in digital formatFo. Observations are reported with local coordinates, which we transferred to WGS84 / UTM Zone 42N as described in Kronenberg et al. (2021). Monthly snow height and density measurements respective to the previous summer horizon are available from up to nine snow pit locations. Eight snow pits are located on the glacier surface and one snow pit is located just below the glacier tongue in the Koksu valley (Fig. 1b in the main manuscript). A total of 165 stakes installed along 13 profiles were used to measure monthly surface height changes since the beginning of the hydrological year (1 October). For stakes in the ablation area, negative height changes are converted to water equivalents (w.e.) using a density of ice 900 kg m^{-3}. For stakes above the firn line, a firn density of 610 kg m^{-3} is used (Kislov, 1977; Pertziger, 1996). Here, we use a constant elevation threshold of 4200 m a.s.l. to select either the firn or ice density for conversion into ablation in w.e. Pertziger (1996) converted positive stake readings to w.e. either using snow densities measured at nearby snow pits or a density of 550 kg m^{-3}. If measured densities were high, they assumed a maximum density of 610 kg m^{-3}. Here, we consistently use a density of 550 kg m^{-3} to convert positive stake readings to w.e. According to Pertziger (1996), the main source of error in mass balance point measurements are errors in density estimates. Another source of uncertainty is related to the time of observation. Exact dates are reported for stake readings. For data from snow pits, we do not know the exact measurement dates as only months are reported. Furthermore, the reference date or exact age of the reference surface in the snow pit are unknown due to the stratigraphic nature of snow pit measurements. We assume these dates to correspond to the beginning of the hydrological year until the end of the investigated month.

S1.4 Cloud cover correction

Monthly precipitation thresholds to set cloud cover to 1 were fixed so that the monthly averages of the final cloud fraction time series correspond to monthly averages prior to this correction. The respective thresholds are 0.14, 0.12 and 0.12 $\times 10^{-4}$ m w.e. s^{-1} for July, August and September.

S1.5 Determination of lapse rates and incoming radiation parameters

We extrapolate the meteorological forcing over the glacier surface by means of linear and temporally constant elevation gradients. For Abramov glacier, Kislov (1982) reported a temperature lapse rate of $dT/dz = -0.005\,\mathrm{K\,m^{-1}}$ which we adopt here. The precipitation lapse rate $dPrec/dz$ is calculated from March snow pit measurements for 1969-98 (243 points). The monthly mass balance measurements available for 1969-98 indicate that no melt occurred before April and therefore, the March snow pit measurements are unaffected by melt. The pressure decay parameter $dPres$ is calculated from average air pressure measurements at 3837 m a.s.l. (January 1968 - December 1998) and 4100 m a.s.l. (October 2014 - September 2020). The gradient of relative humidity dRH/dz= 0.01% $\mathrm{m^{-1}}$ is adopted from Huintjes et al. (2016), who calculated it from High Asia Refined Analysis data (Maussion et al., 2014) for two Tibetan glaciers. The chosen value is corroborated by measured relative humidity on Abramov glacier for June and July (Suslov and Krenke, 1980). The calculation of the vertical lapse rate of potential temperature γ is adopted from Stainbank (2018).

In situ measurements from the AWS for 2014-2020 as well as literature values are used to estimate incoming radiation parameters. The aerosol transmission constant k_{aer} in the SW_{in} formulation is determined using the linear relation between k_{aer} and the elevation proposed by Klok and Oerlemans (2002). We estimate k_{aer} = 0.98 for the median glacier elevation (4300 m a.s.l.). The LW_{in} parameter b = 0.43 is determined based on daily AWS data (T, RH and LW_{in}) for manually identified clear sky conditions. The value is similar to the value found by Klok and Oerlemans (2002) for Morteratsch glacier. The second longwave radiation parameter ϵ_{cl} is set to the default value of 0.96.

S2 Supplementary tables

Table S1. Parameters measured at the original Abramov weather station from October 1967 until summer 1999 (data available until December 1998). The installation height and the sensor types are given for each parameter. Data were either recorded automatically or manually read. The recording frequency as well as the temporal resolution of data available for this study are indicated.

Variable	height	sensor (recording)	frequency	preserved data
Air temperature	2 m	bimetallic strip (recording)	$8 \times \text{day}^{-1}$	daily averages
		mercury thermometer (manual observation)		
Air temperature max	2 m	mercury maximum thermometer	$1 \times \text{day}^{-1}$	daily max
Air temperature min	2 m	alcohol-in-glass minimum thermometer	$1 \times \text{day}^{-1}$	daily min
Air pressure	2 m	aneroid barograph (recording)	$8 \times \text{day}^{-1}$	daily averages
		mercury barometer (manual observation)		
Relative humidity	2 m	hair hygrometer (recording)	$8 \times \text{day}^{-1}$	daily averages
		psychrometer - coupled wet-and-dry-bulb		
		mercury thermometers (manual observation)		
Wind speed	10 m	anemometer	$8 \times \text{day}^{-1}$	daily averages
Wind direction	10 m	anemometer	$8 \times \text{day}^{-1}$	not available
Precipitation	2 m	cylindric zinc bucket ($200\,\text{cm}^2 \times 2\,\text{m}$)	$2 \times \text{day}^{-1}$	daily sums
Cloud cover	-	visual observations	$8 \times \text{day}^{-1}$	daily averages and minimums

Table S2. Mean modelled energy fluxes, mean duration of melt period (p_{melt}) and mean annual precipitation (solid P_s and liquid P_l) per decade for three grid points. The melt period is defined as the amount of days for which the modelled melt amount is >0.002 m w.e. d^{-1}. One point is located in the ablation area at ∼3850 m a.s.l. and two points are located in the accumulation area at site 1 at ∼4250 m a.s.l. and site 2 ∼4400 m a.s.l. The periods are hydrological years (e.g. 1968-1978 refers to 1 October 1968 - 30 September 1978). The locations are indicated in Figure 1b of the main manuscript

point	decade	SW_{in}	SW_{out}	LW_{in}	LW_{out}	R_{net}	Q_{sens}	Q_{lat}	Q_{sub}	Q_{melt}	p_{melt}	P_s	P_l
m a.s.l.		W m^{-2}	W m^{-2}	W m^{-2}	W m^{-2}	W m^{-2}	W m^{-2}	W m^{-2}	W m^{-2}	W m^{-2}	days	m w.e. a^{-1}	m w.e. a^{-1}
3850	1968-1978	217.95	140.57	224.89	274.65	27.62	18.38	-3.61	3.77	46.16	202	1.08	0.19
3850	1978-1988	213.8	143.46	227.61	275.93	22.01	18.04	-1.75	3.62	41.91	191	1.25	0.19
3850	1988-1998	209.84	137.32	231.04	277.47	26.08	17.04	-0.87	3.41	45.65	198	1.22	0.23
3850	1998-2008	201.15	128.05	228.54	276.68	24.96	19.86	-1.18	2.96	46.6	191	1.1	0.27
3850	2008-2018	199.38	127.74	229.27	277.13	23.78	20.01	-1.3	3.07	45.56	196	1.18	0.27
3850	1968-2020	208.29	135.15	228.19	276.39	24.94	18.73	-1.72	3.36	45.3	195	1.16	0.23
4250	1968-1978	215.28	161.23	218.13	268.55	3.63	16.61	-2.7	4.69	22.23	186	1.69	0.15
4250	1978-1988	211.97	160.52	220.48	269.73	2.2	16.24	-1.13	4.31	21.61	181	1.99	0.15
4250	1988-1998	209.09	158.36	223.6	271.11	3.21	15.18	-0.41	4.32	22.29	181	1.97	0.2
4250	1998-2008	202.75	151.74	221.02	270.64	1.4	17.55	-0.6	4.28	22.63	173	1.84	0.25
4250	2008-2018	202.91	149.66	221.56	270.98	3.83	17.58	-0.69	3.98	24.7	180	2	0.24
4250	1968-2020	208.42	156.19	220.86	270.21	2.88	16.68	-1.08	4.29	22.77	180	1.89	0.2
4400	1968-1978	233.22	176.74	215.58	267.99	4.07	15.12	-2.63	4.87	21.44	192	1.93	0.13
4400	1978-1988	230.3	176.06	217.84	269.17	2.91	14.71	-1.22	4.33	20.72	187	2.27	0.13
4400	1988-1998	227.51	173.46	220.88	270.56	4.38	13.65	-0.58	4.3	21.74	184	2.26	0.18
4400	1998-2008	220.36	167.94	218.31	269.68	1.06	16.29	-0.51	4.16	21.01	180	2.12	0.23
4400	2008-2018	220.32	166.94	218.82	270	2.2	16.27	-0.59	4.09	21.97	183	2.31	0.21
4400	1968-2020	226.4	172.21	218.18	269.47	2.9	15.26	-1.08	4.34	21.42	185	2.17	0.17

S3 Supplementary figures

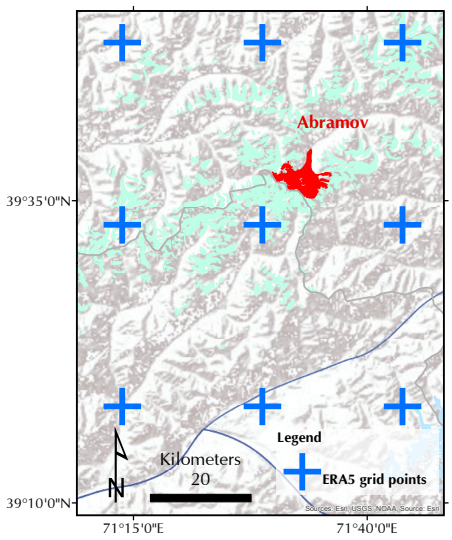

Figure S1. ERA5 grid points of used in the present study. Color tones visualize glaciation of the Pamir Alayn (outlines from RGI 6.0, RGI Consortium, 2017). Background layer sources: Esri, USGS, NOA. (Own map).

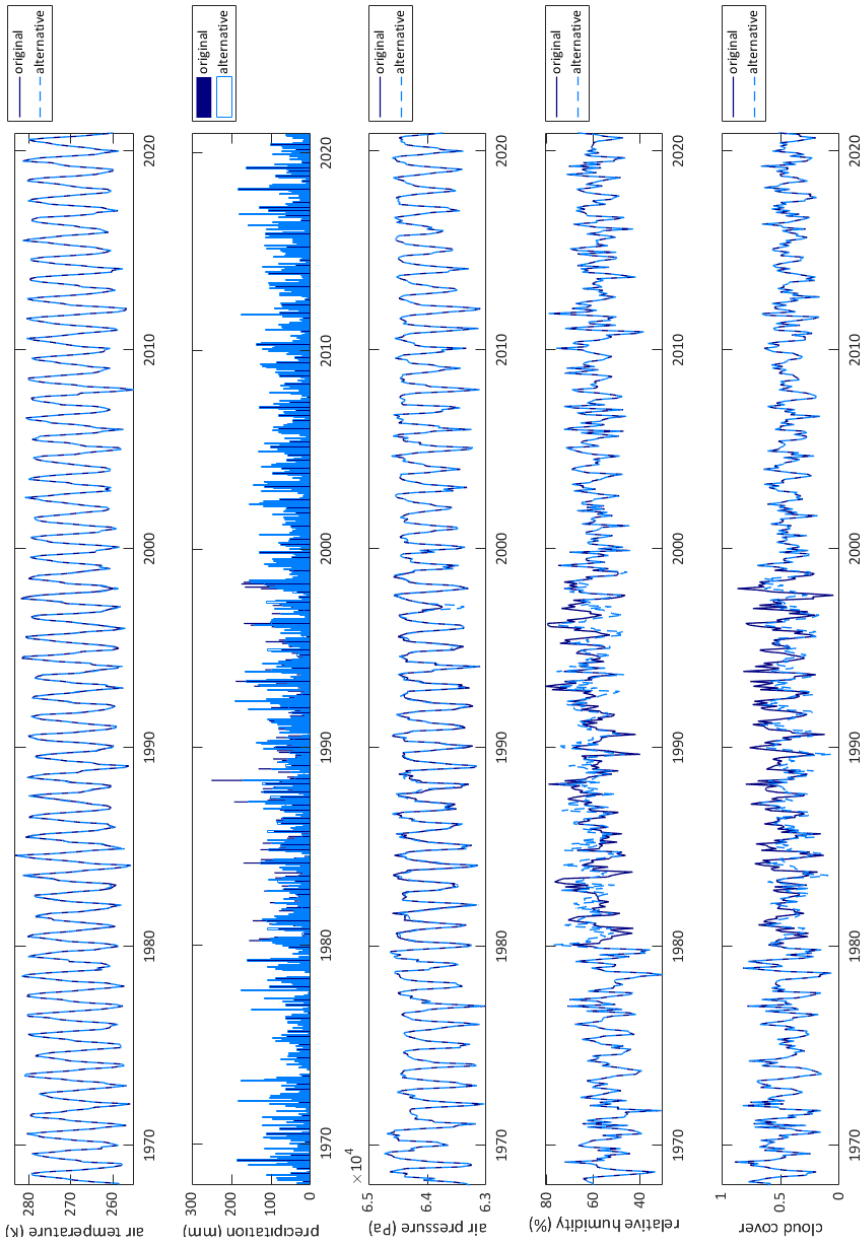

Figure S2. Original and alternative model forcing for entire simulation period at monthly resolution.

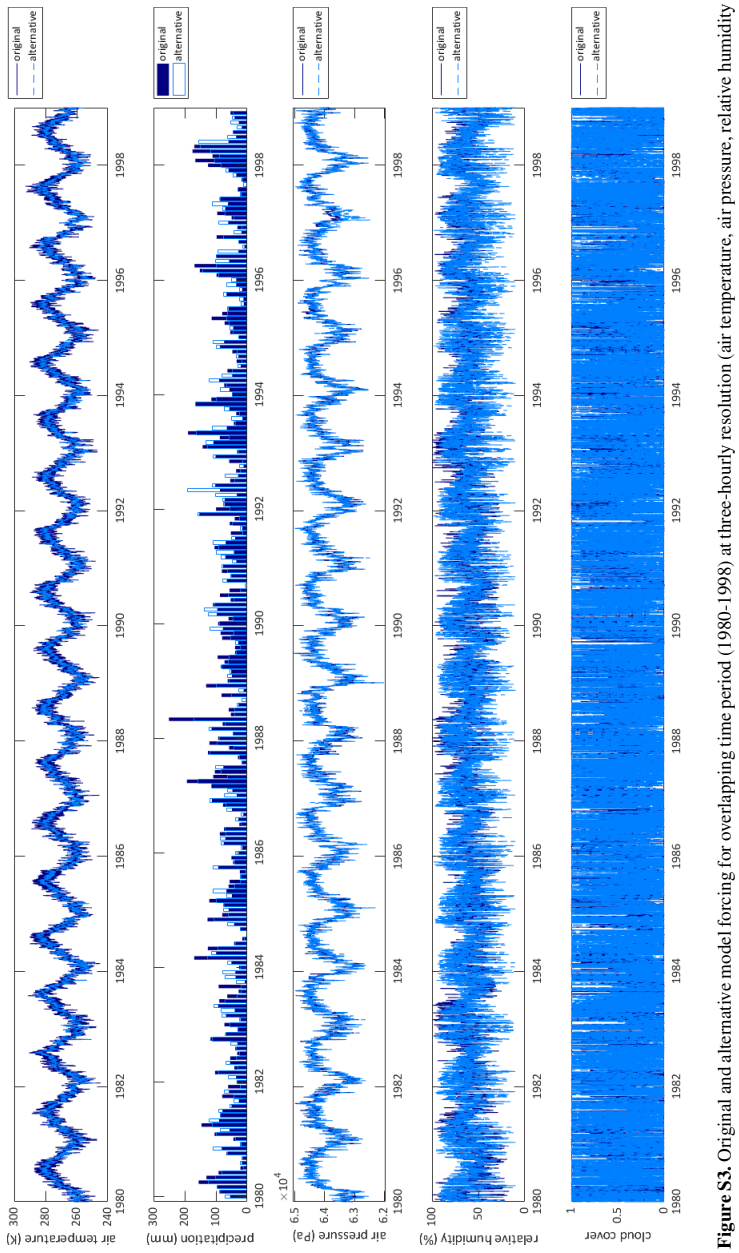

Figure S3. Original and alternative model forcing for overlapping time period (1980-1998) at three-hourly resolution (air temperature, air pressure, relative humidity and cloud cover) and monthly precipitation sums are shown.

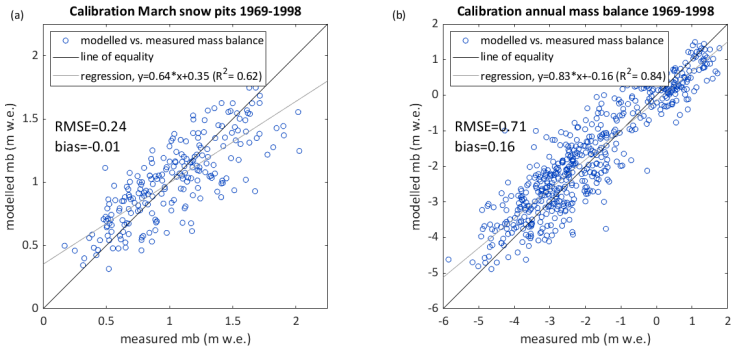

Figure S4. Model parameter calibration: Measured versus modelled surface mass balance for end of March (a) and September (b) for point measurements which are used for model calibration (1968/1969-1997/1998). The final calibration is shown. The bias between modelled and measured w.e. for snow pit measurements at the end of March (a) is minimised by optimising the precipitation correction factor. The bias between modelled and measured September mass balance measurements is optimised by tuning the albedo of ice.

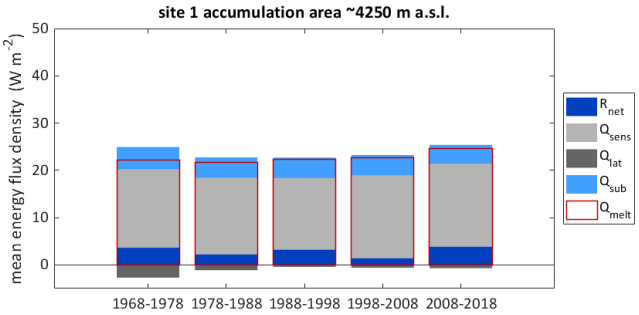

Figure S5. Mean modelled energy fluxes per decade for site 1 located in the accumulation area at ∼4250 m a.s.l. R_{net} is the net radiation, Q_{sens} the sensible and Q_{lat} the latent heat flux, Q_{lat} the heat flux from/into the subsurface and Q_{melt} the total energy available for melt. The periods are hydrological years (e.g. 1968-1978 refers to 1 October 1968 - 30 September 1978). The point location is indicated in Fig. 1b of the main manuscript

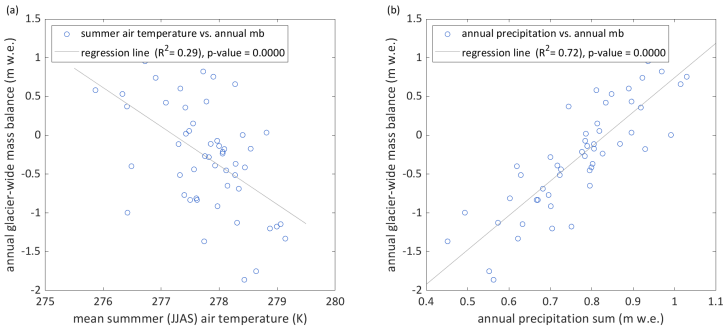

Figure S6. Climate variables at the station location (3837 m a.s.l.) versus modelled mass balance: Mean summer air temperature versus annual mass balance (a) and annual precipitation sums versus mean annual mass balance.

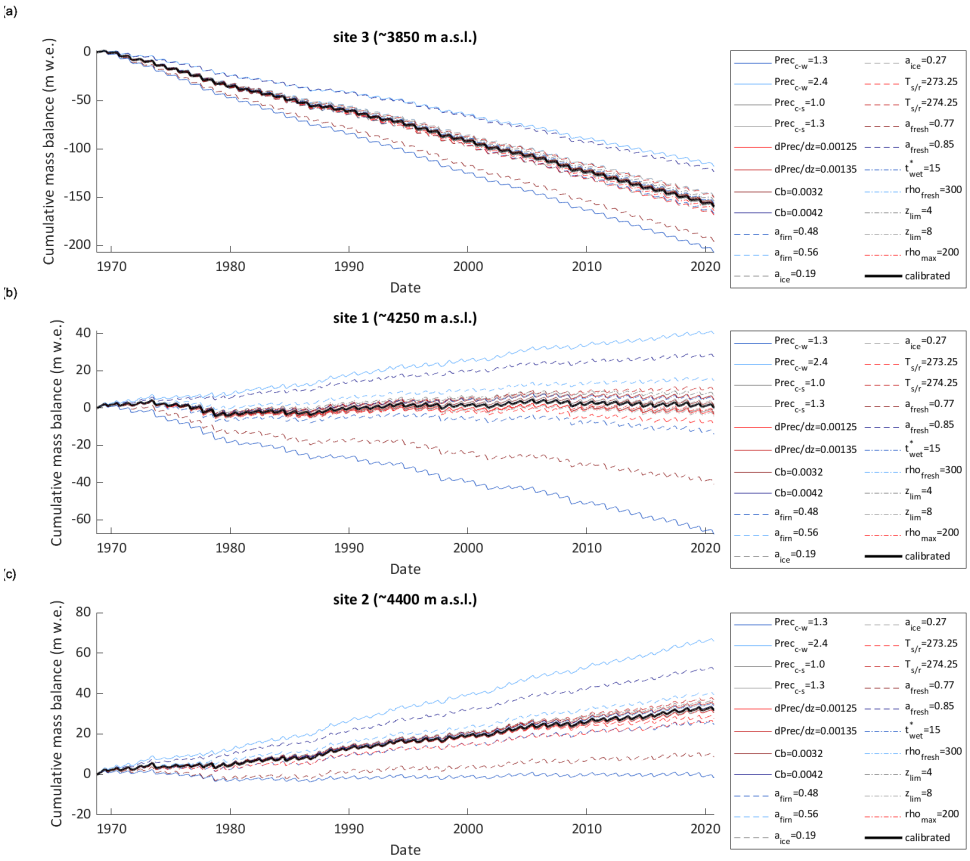

Figure S7. Parameter sensitivity: Cumulative mass balance evolution for disturbed model parameters following Klok and Oerlemans (2002). The cumulative mass balance is shown for three selected points (ablation area (a), lower accumulation area (b) and accumulation area (c)). The point locations are indicated in Figure 1b of the main manuscript.

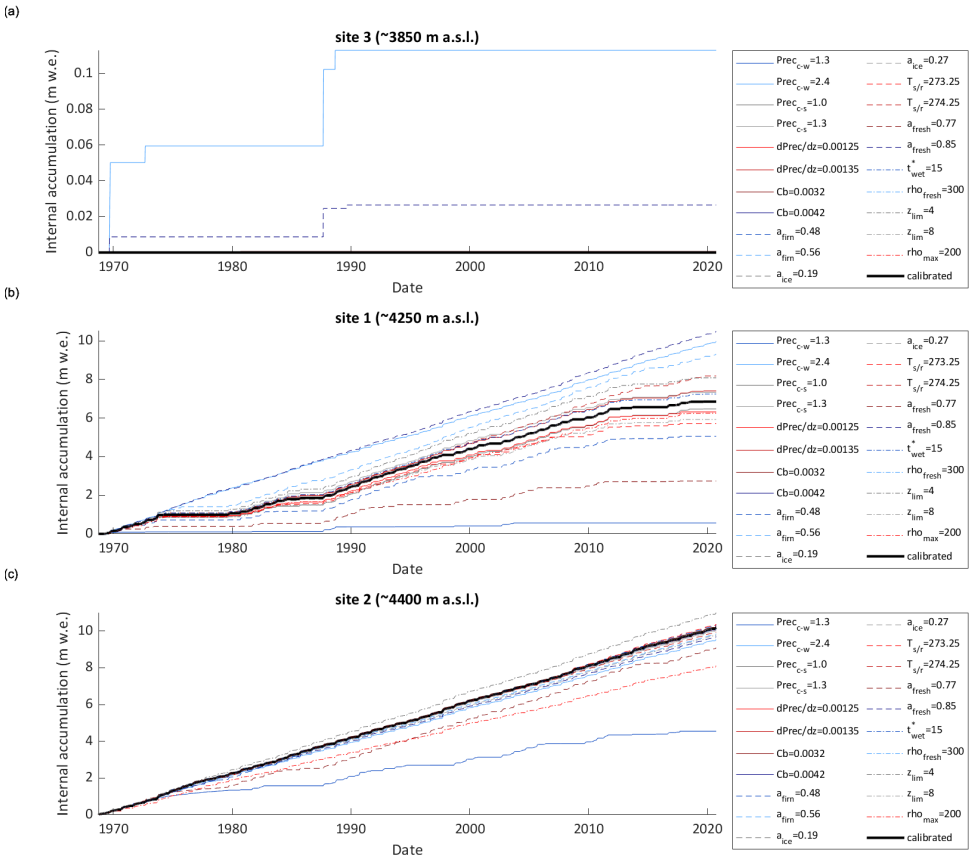

Figure S8. Parameter sensitivity: Cumulative internal accumulation evolution for disturbed model parameters following Klok and Oerlemans (2002). The cumulative internal accumulation is shown for three selected points (ablation area (a), lower accumulation area (b) and accumulation area (c)). The point locations are indicated in Figure 1b of the main manuscript.

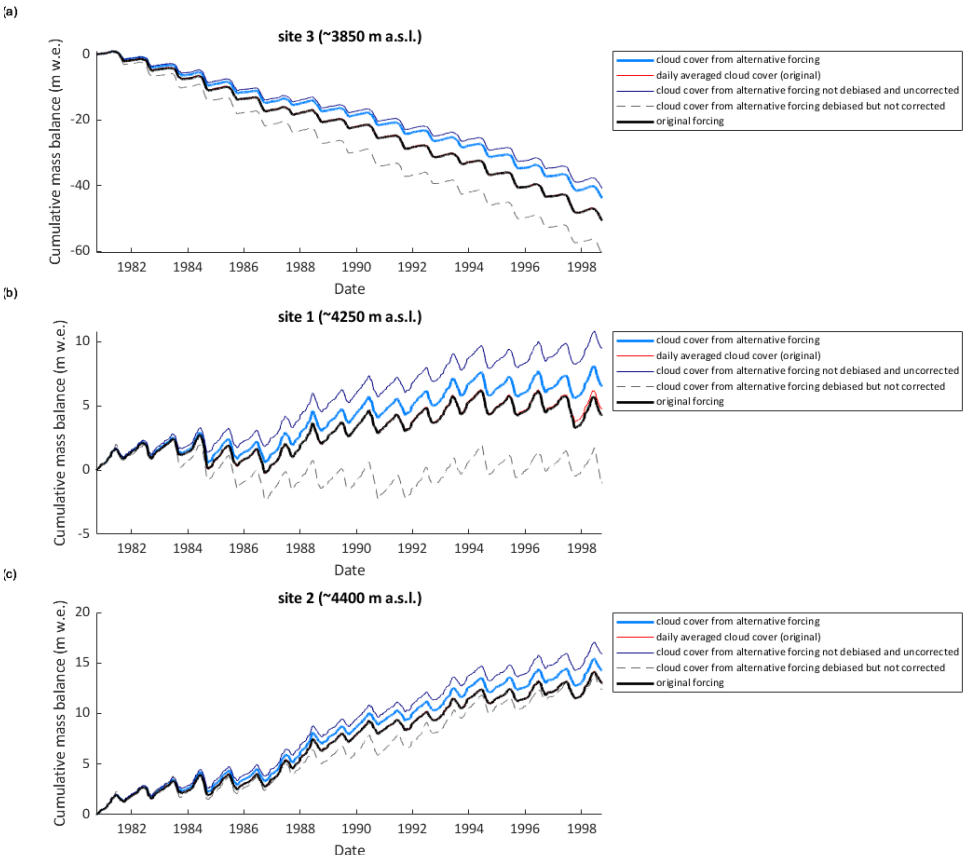

Figure S9. Cloud forcing sensitivity: Cumulative mass balance evolution evolution for altered cloud cover forcing (all other forcing variables are from the original forcing.) 'Daily averaged cloud cover (original)' uses the original data set but daily averaged cloud cover, 'cloud cover from alternative forcing not debiased and uncorrected' is the cloud cover calculated from TopoSCALE ERA5 to any correction,'cloud cover from alternative forcing debiased but not corrected' was debiased using cloud cover observations from the original station but not corrected with summer precipitation (cf. section 2.4.4. of the main manuscript). The cumulative mass balance is shown for three selected points (ablation area (a), lower accumulation area (b) and accumulation area (c)). The point locations are indicated in Figure 1b of the main manuscript.

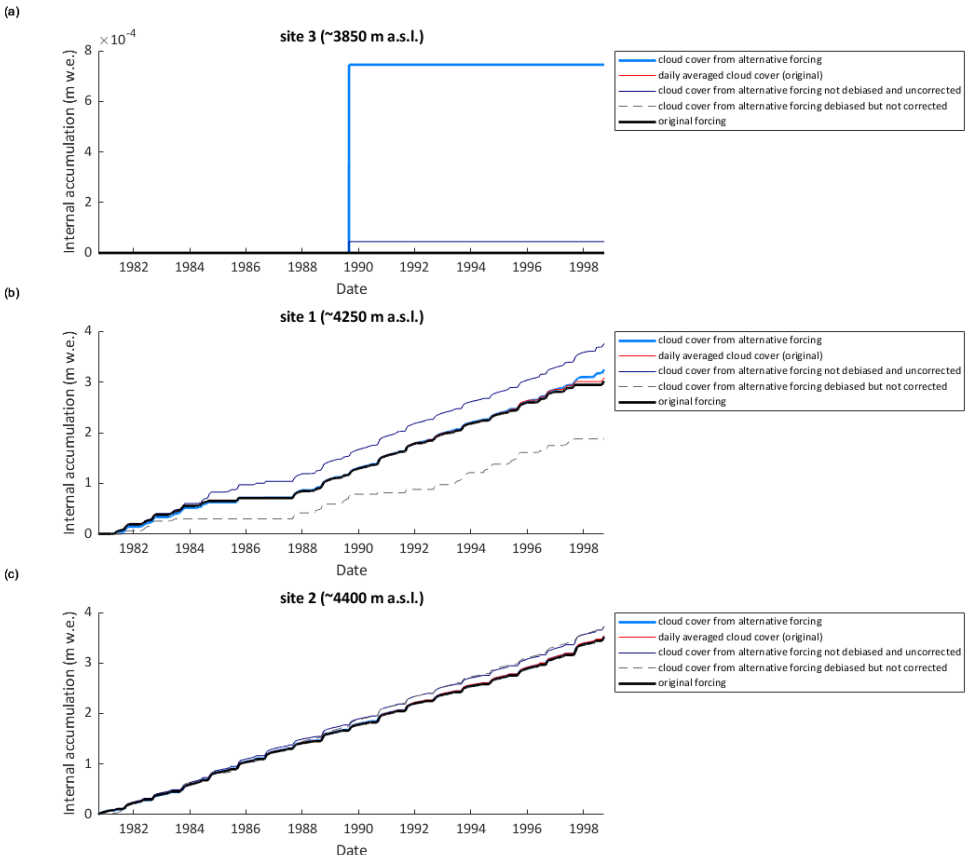

Figure S10. Cloud forcing sensitivity: Cumulative internal accumulation evolution for altered cloud cover forcing (all other forcing variables are from the original forcing.) 'Daily averaged cloud cover (original)' uses the original data set but daily averaged cloud cover, 'cloud cover from alternative forcing not debiased and uncorrected' is the cloud cover calculated from TopoSCALE ERA5 to any correction,'cloud cover from alternative forcing debiased but not corrected' was debiased using cloud cover observations from the original station but not corrected with summer precipitation (cf. section 2.4.4. of the main manuscript). The cumulative internal accumulation is shown for three selected points (ablation area (a), lower accumulation area (b) and accumulation area (c)). The point locations are indicated in Figure 1b of the main manuscript.

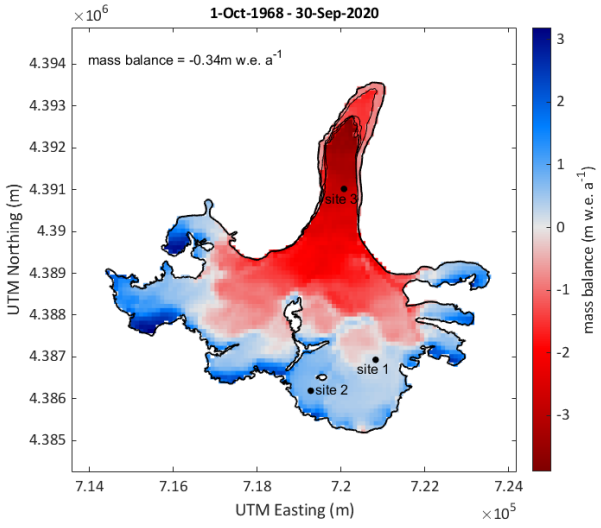

Figure S11. Result of the alternative model run. Modelled mean annual distributed mass balance for updated glacier extents for the period from 1 October 1968 to 30 September 2020. Note, that the mean annual mass balance for the entire period and updated glacier surfaces is shown. Values are thus reduced on the glacier tongue, where the glacier area reduced over time. The different glacier outlines are shown with black lines. Furthermore, the location of three selected points is indicated.

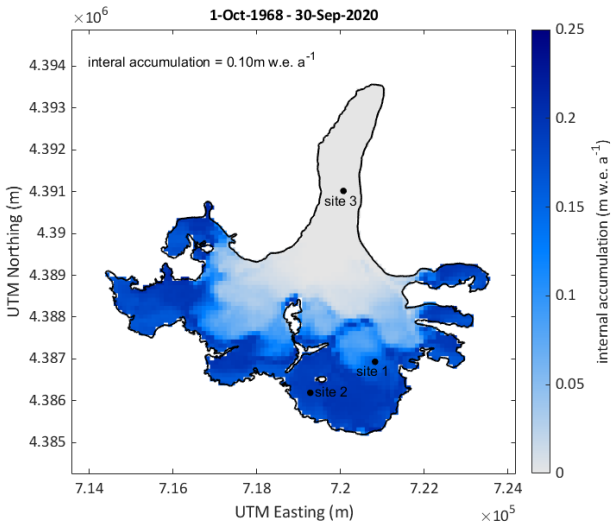

Figure S12. Result of the alternative model run. Map of mean annual internal accumulation for the mass balance years 1968/1969-2019/2020. The location of three selected points is indicated.

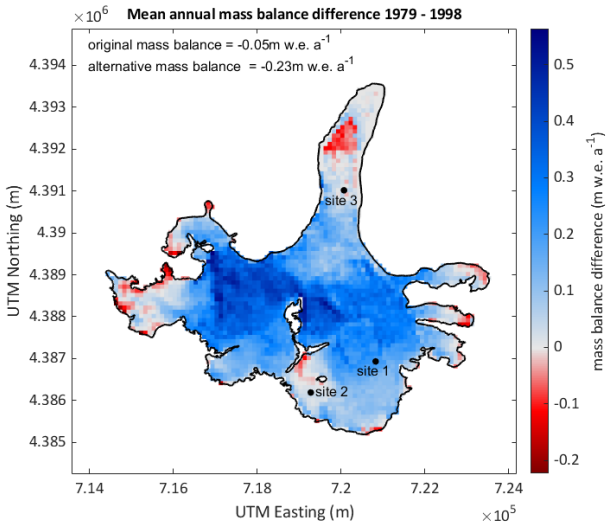

Figure S13. Comparison of original and alternative model run results. Difference of mean annual distributed mass balance for updated glacier extents for the period from 1 October 1968 to 30 September 2020. Note, that the mean annual mass balance for the entire period and updated glacier surfaces is shown. Furthermore, the location of three selected points is indicated.

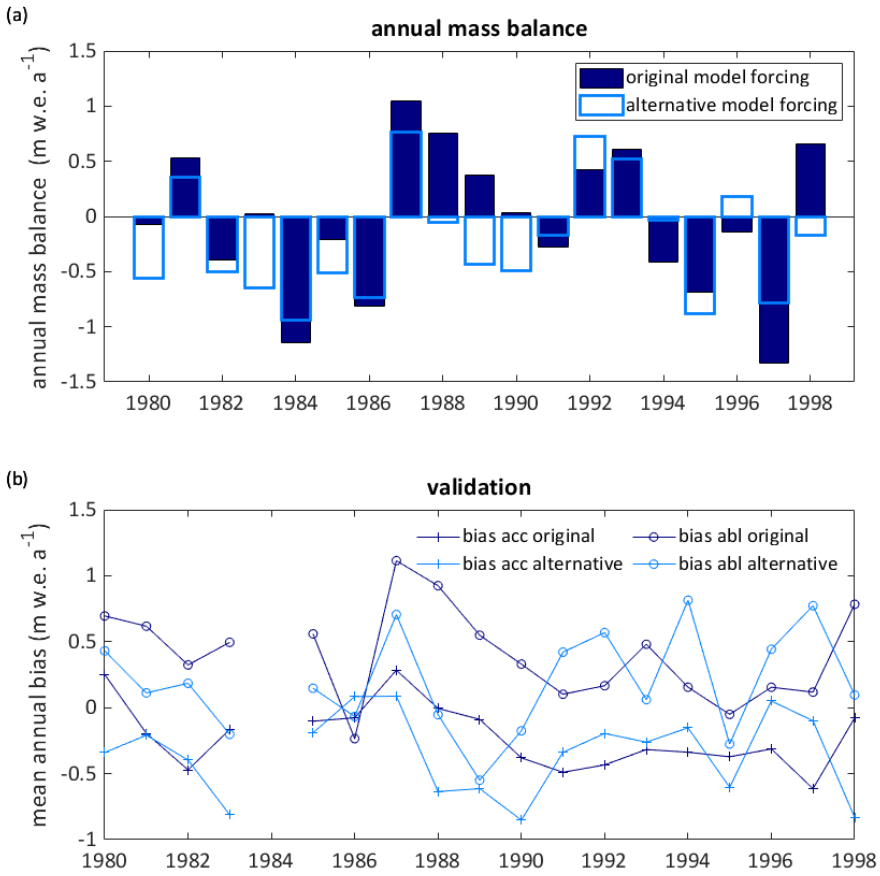

Figure S14. Comparison of mean annual mass balances of the original model run and the alternative model run showing the the annual model forcing sensitivity (a) and mean annual bias between modelled and measured point accumulation for both model runs (b).

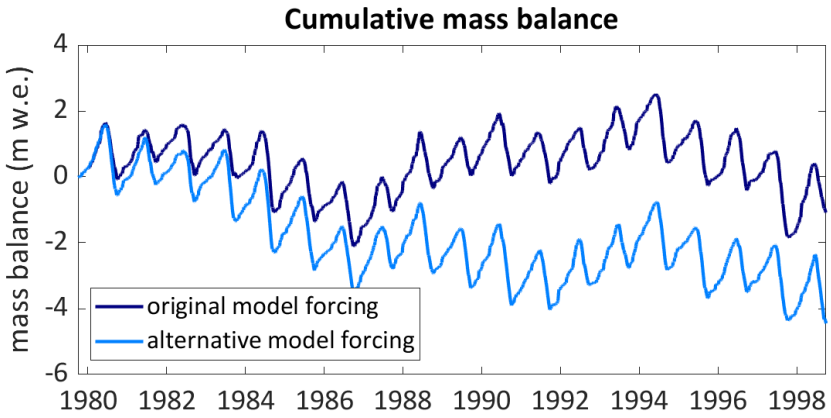

Figure S15. Comparison of cumulative mass balances of the original model run and the alternative model run showing the overall model forcing sensitivity.

S4 Video supplement

The attached animation (Kronenberg_et_al_video.avi) visualizes the annual mass balance evolution together with the spatial extent of internal accumulation. The bar plot of annual mass balance referring to the internal accumulation shown on the map to the right is highlighted in red. The spatial extent of internal accumulation is reduced during years following negative mass balances and is strongly reduced in most recent years.

References

Barandun, M., Huss, M., Sold, L., Farinotti, D., Azisov, E., Salzmann, N., Usubaliev, R., Merkushkin, A., Hoelzle, M., A.Merkushkin, and Hoelzle, M.: Re-analysis of seasonal mass balance at Abramov glacier 1968-2014, Journal of Glaciology, 61, 1103–1117, https://doi.org/10.3189/2015JoG14J239, 2015.

Denzinger, F., Machguth, H., Barandun, M., Berthier, E., Girod, L., Kronenberg, M., Usubaliev, R., and Hoelzle, M.: Geodetic mass balance of Abramov Glacier from 1975 to 2015, Journal of Glaciology, 67, 331–342, https://doi.org/10.1017/jog.2020.108, 2021.

Huintjes, E., Loibl, D., Lehmkuhl, F., and Schneider, C.: A modelling approach to reconstruct Little Ice Age climate from remote-sensing glacier observations in southeastern Tibet, Annals of Glaciology, 57, 359–370, https://doi.org/10.3189/2016AoG71A025, 2016.

Kislov, B. V.: About the question of determining the internal accumulation of temperate glaciers [in Russian], Trudy SARNIGMI, 45, 62–72, 1977.

Kislov, B. V.: Formation and regime of the firn-ice stratum of a mountain glacier [in Russian], Ph.D. thesis, SARNIGMI Tashkent, 1982.

Klok, E. J. and Oerlemans, J.: Model study of the spatial distribution of the energy and mass balance of Morteratschgletscher, Switzerland, Journal of Glaciology, 48, 505–518, https://doi.org/10.3189/172756502781831133, 2002.

Kronenberg, M., MacHguth, H., Eichler, A., Schwikowski, M., and Hoelzle, M.: Comparison of historical and recent accumulation rates on Abramov Glacier, Pamir Alay, Journal of Glaciology, 67, 253–268, https://doi.org/10.1017/jog.2020.103, 2021.

Maussion, F., Scherer, D., Mölg, T., Collier, E., Curio, J., and Finkelburg, R.: Precipitation Seasonality and Variability over the Tibetan Plateau as Resolved by the High Asia Reanalysis, Journal of Climate, 27, 1910–1927, https://doi.org/10.1175/JCLI-D-13-00282.1, 2014.

Pertziger, F.: Abramov Glacier Data Reference Book: Climate, Runoff, Mass Balance, Central Asian Hydrometeorlogical Institute, Tashkent, 1996.

RGI Consortium: Randolph Glacier Inventory – A Dataset of Global Glacier Outlines: Version 6.0, Global Land Ice Measurements from Space, Colorada, USA. Digital Media, https://doi.org/10.7265/N5-RGI-60, 2017.

Schöne, T., Zech, C., Unger-Shayesteh, K., Rudenko, V., Thoss, H., Wetzel, H.-U., Gafurov, A., Illigner, J., and Zubovich, A.: A new permanent multi-parameter monitoring network in Central Asian high mountains - from measurements to data bases, Geoscientific Instrumentation, Methods and Data Systems, 2, 97–111, https://doi.org/10.5194/gi-2-97-2013, 2013.

Stainbank, W. D.: Simulation of Abramov glacier energy balance and firn properties, Msc thesis, University of Fribourg, 2018.

Suslov, V. F. and Krenke, A. N.: Abaramov Glacier (Alay Range) [in Russian], Gidrometeoizdat, St. Petersburg, 1980.

C. Additional visualisations and extracts of EBFM output

This appendix contains additional visualisations and data summaries of the EBFM output presented in Paper II.

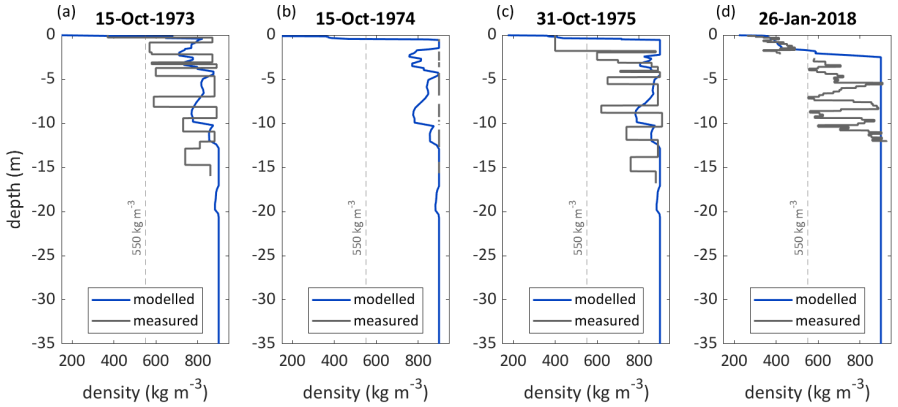

Figure C.1: Modelled and measured subsurface densities for site 1 (~4250 m a.sl.). Measured subsurface densities from the 1970s are digitised from Figs. in Kislov (1982) (a-c) and own measurements are shown for 2018 (d). The location of the site is indicated in Fig. 1b of Paper II

Table C.1: Summary of modelled subsurface densities and temperatures for both model forcings for the hydrological years 1980/1981-1997-1998. Subscript 'or' refers to the original/station data forcing and subscript 'alt' to the alternative/TopoSCALE ERA5 forcing. Data is summarized for two grid cells corresponding to site 1 (~4250 m a.s.l.) and site 2 (~4400 m a.s.l.)

site	$\overline{\rho_{or}}$ ($kg\,m^{-3}$)	$\sigma\rho_{or}$ ($kg\,m^{-3}$)	$\overline{\rho_{alt}}$ ($kg\,m^{-3}$)	$\Delta\rho$ ($kg\,m^{-3}$)	$\overline{T_{or}}$ (K)	σT_{or} (K)	$\overline{T_{alt}}$ (K)	ΔT (K)
1	738	49	778	-40	271.22	0.61	269.89	1.32
2	621	47	637	-16	271.67	0.19	271.42	0.26

Table C.2: Modelled annual mass fluxes for grid cell at site 1 (~4250 m a.s.l.). Annual refers to hydrological years. The year given refers for the end of each hydrological year (e.g. 1969 stands for 1 October 1968 - 30 September 1969). 'mb' is the climatic mass balance, 'melt' is the total melt, $refr_{tot}$ is the total refreezing and $refr_{sn}$ is the refreezing within the annual snowpack

year	mb	melt	$refr_{tot}$	$refr_{sn}$	year	mb	melt	$refr_{tot}$	$refr_{sn}$
-	w.e. a^{-1}	w.e. a^{-1}	w.e. a^{-1}	w.e. a^{-1}	cont	w.e. a^{-1}	w.e. a^{-1}	w.e. a^{-1}	w.e. a^{-1}
1969	1.2	1.79	0.57	0.38	1995	0.03	2.11	0.51	0.3
1970	0.13	1.99	0.52	0.33	1996	0.31	2.32	0.57	0.34
1971	0.2	2.05	0.53	0.37	1997	-0.24	2.32	0.56	0.31
1972	1.01	1.57	0.54	0.32	1998	1.12	2.08	0.58	0.36
1973	-0.62	3.11	0.65	0.36	1999	0.34	1.99	0.53	0.3
1974	0.16	1.51	0.6	0.27	2000	-0.21	2.14	0.53	0.29
1975	0.26	1.81	0.55	0.34	2001	-0.05	1.99	0.47	0.33
1976	-0.55	2.05	0.48	0.3	2002	1.18	1.66	0.45	0.34
1977	-0.42	2.21	0.42	0.31	2003	0.86	1.92	0.53	0.32
1978	-0.72	3.22	0.5	0.41	2004	0.58	1.91	0.52	0.34
1979	0.4	2.23	0.55	0.42	2005	0.15	2.59	0.57	0.37
1980	0.52	2.01	0.56	0.37	2006	-0.08	2.4	0.58	0.34
1981	0.94	1.55	0.46	0.31	2007	0.02	2.43	0.58	0.36
1982	0.09	1.93	0.53	0.31	2008	-0.78	2.68	0.59	0.29
1983	0.35	2.03	0.46	0.33	2009	0.86	2.01	0.48	0.35
1984	-0.39	2.59	0.58	0.33	2010	0.65	2.08	0.52	0.35
1985	0.27	2.27	0.55	0.39	2011	-0.54	2.42	0.57	0.29
1986	-0.29	2.23	0.42	0.31	2012	0.13	2.35	0.5	0.35
1987	1.31	1.7	0.47	0.4	2013	0.19	2.23	0.49	0.34
1988	1.1	2.18	0.54	0.36	2014	-0.68	2.93	0.46	0.45
1989	0.63	1.8	0.53	0.32	2015	0.19	2.24	0.46	0.46
1990	0.34	2.4	0.54	0.34	2016	0.44	2.39	0.56	0.47
1991	0.17	2.04	0.56	0.32	2017	0.34	2.48	0.58	0.42
1992	0.72	1.85	0.51	0.33	2018	-0.07	2.57	0.52	0.39
1993	0.75	2.02	0.54	0.34	2019	0.15	2.32	0.46	0.43
1994	0.02	2.44	0.52	0.36	2020	-0.43	2.41	0.43	0.43

D. Abstracts of co-authored papers

Geodetic mass balance of Abramov Glacier from 1975 to 2015

Reference: Denzinger, F., Machguth, H., Barandun, M., Berthier, E., Girod, L., Kronenberg, M., Usubaliev, R., and Hoelzle, M. Geodetic mass balance of Abramov Glacier from 1975 to 2015. Journal of Glaciology*, 67(262):331–342, 2021. doi:10.1017/jog.2020.108.*

Abstract: Multi-decadal mass loss estimates are available for few glaciers of Central Asia. On Abramov Glacier (Pamir-Alay, Kyrgyzstan), comprehensive long-term glaciological measurements have been carried out from 1968 to 1999 and re-initiated in 2011. A climatological interpretation of this benchmark glacier in Central Asia requires bridging the gap between historical and renewed measurements. This is achieved here by computing the geodetic mass balance from 1975 to 2015 using previously unreleased Soviet aerial imagery and Pléaides stereo-imagery. During 1975– 2015, Abramov Glacier lost 2.2 km^2 (8.2%) of its area. The mean annual thickness change was -0.43 ± 0.14 m a^{-1} for the period 1975–2015, corresponding to a volume change of -0.45 ± 0.15 km^3. The average specific geodetic mass balance amounts to -0.38 ± 0.12 m w.e. a^{-1}. The 1975–2015 glacier mass loss lies within the range of glaciological and geodetic mass-balance estimates that were previously published for disparate and shorter time intervals since 1968. This study covers a much longer time period than earlier geodetic estimates and demonstrates the capacity to geodetically constrain glacier change at high spatial resolution in Central Asia using historic aerial imagery and Structure from Motion techniques. Therefore, it could serve as a benchmark for future studies of regional mass change.

Firn changes at Colle Gnifetti revealed with a high-resolution process-based physical model approach

Reference: Mattea, E., Machguth, H., Kronenberg, M., van Pelt, W., Bassi, M., and Hoelzle, M. Firn changes at Colle Gnifetti revealed with a high-resolution process-based physical model approach. The Cryosphere, *15:3181–3205, 2021. doi:10.5194/tc-15-3181-2021.*

Abstract: Our changing climate is expected to affect ice core records as cold firn progressively transitions to a temperate state. Thus, there is a need to improve our understanding and to further develop quantitative process modeling, to better predict cold firn evolution under a range of climate scenarios. Here we present the application of a distributed, fully coupled energy balance model, to simulate cold firn at the high-alpine glaciated saddle of Colle Gnifetti (Swiss/Italian Alps) over the period 2003–2018. We force the model with high-resolution, long-term and extensively quality-checked meteorological data measured in closest vicinity of the firn site, at the highest automatic weather station in Europe (Capanna Margherita, 4560 m a.s.l.). The model incorporates the spatial variability of snow accumulation rates, and is calibrated using several, partly unpublished high-altitude measurements from the Monte Rosa area. The simulation reveals a very good overall agreement in the comparison with a large archive of firn temperature profiles. Our results show that surface melt over the glaciated saddle is increasing by 3–4 mm w.e. yr^{-2} depending on the location (29%–36% in 16 years), although with large inter-annual variability. Analysis of modeled melt indicates the frequent occurrence of small melt events (< 4 mm w.e.), which collectively represent a significant fraction of the melt totals. Modeled firn warming rates at 20 m depth are relatively uniform above 4450 m a.s.l. (0.4–0.5°C per decade). They become highly variable at lower elevations, with a marked dependence on surface aspect and absolute values up to 2.5 times the local rate of atmospheric warming. Our distributed simulation contributes to the understanding of the thermal regime and evolution of a prominent site for alpine ice cores, and may support the planning of future core drilling efforts. Moreover, thanks to an extensive archive of measurements available for comparison, we also highlight the possibilities of model improvement most relevant to the investigation of future scenarios, such as the fixed-depth parametrized routine of deep preferential percolation.

E. Co-Supervision of Master Theses

Three different MSc theses were co-supervised in the course of the PhD studies. The different works are shortly introduced hereafter.

Simulation of Abramov glacier energy balance and firn properties by Warren Stainbank

This thesis presents the first application of the EBFM for Abramov glacier. AWS data from 2014 to 2017 in combination with reanalysis data served as model forcing. A detailed data filtering and gap-filling routine was set up to prepare the AWS data. Differences between modelling results and *in situ* data were found found for both subsurface conditions and surface mass balance. These differences helped to identify problematic areas. These were amongst others the quality of the model forcing and the subsurface densification routine.

Thesis Reference: Stainbank, W. D. Simulation of Abramov glacier energy balance and firn properties. *Msc thesis, University of Fribourg, 2018.*

Accumulation distribution on Abramov Glacier from GPR measurements by Silas Walther

Several GPR profiles collected in January 2018 were used to derive precipitation distribution grids for Abramov glacier. Furthermore, precipitation distribution grids were created based on legacy measurements and multiple linear regression techniques. These grids were then implemented into the EBFM at 100 m resolution to simulate the mass balance of Abramov glacier. Replacing the precipitation gradient with the precipitation distribution grids did, however, not improve the fit between the EBFM results and measurements.

Thesis Reference: Walther, S. Accumulation distribution on Abramov Glacier from GPR measurements. *Msc thesis, University of Fribourg, 2018.*

Measuring and modelling changes in the firn at Colle Gnifetti, 4400 m a.s.l., Swiss Alps by Enrico Mattea

This thesis applied the EBFM to model the cold firn saddle of Colle Gnifetti in the Swiss-Italian Alps. It is the first deployment of a high-resolution, fully coupled energy balance and firn model for this important ice coring site. Furthermore, previously unused AWS data from the nearby high alpine station Cpanna Margherita was used as a model forcing. The results indicate increasing melt amounts and subsurface temperatures. The paper Mattea et al. (2021) is based on this MSc Thesis.

Thesis Reference: Mattea, E. Measuring and modelling changes in the firn at Colle Gnifetti, 4400 m a.s .l., Swiss Alps. *Msc thesis, University of Fribourg, 2020.*

F. Field data from Gregoriev ice cap

Gregoriev ice cap was visited subsequently after the field trip to Abramov glacier in February 2018. Due to long-lasting bad weather conditions, the field trip on Abramov glacier had to be stopped earlier than planned. The remaining time of the expedition team was invested to drill one 18 m core on Gregoriev ice cap and to install a thermistor chain which was left from Abramov glacier.

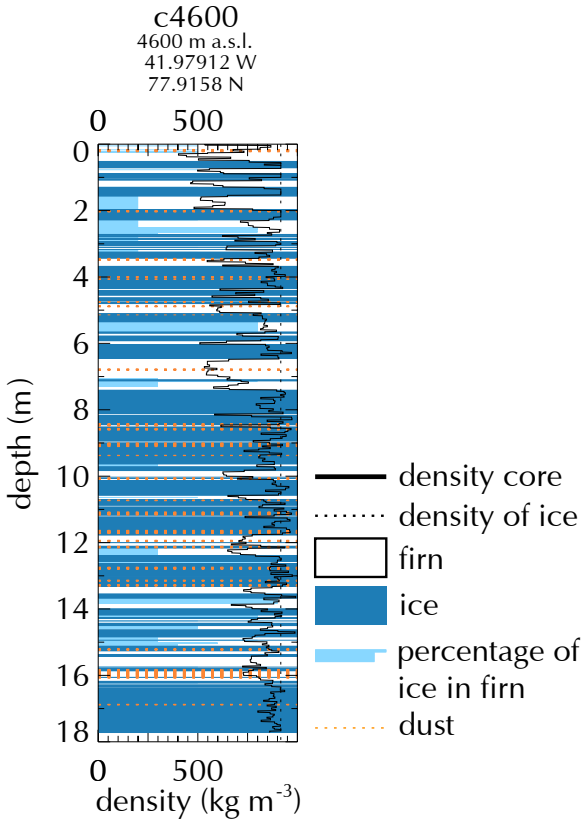

Figure F.1: Firn stratigraphy and density from a core drilled on Gregoriev ice cap on the 7th February 2018. The visual stratigraphy was observed in the field and the density was measured from core samples at the Paul Scherrer Institute (after shipping to Switzerland).

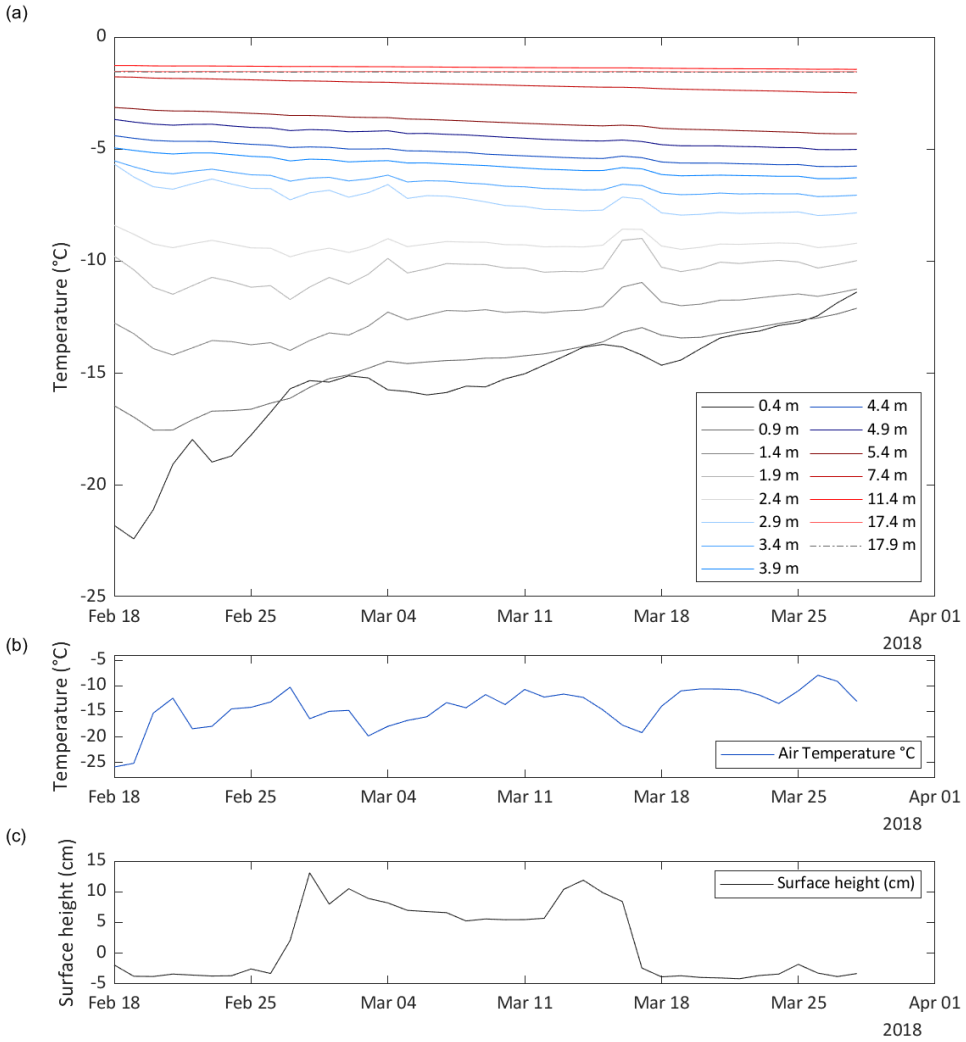

Figure F.2: Subsurface temperature (a) air temperature (b) and surface height (c) data measured at a station installed on the summit of Gregoriev ice cap (4600 m a.s.l.) from 18th February until 28th March 2018. The station was installed on the 8th February 2018, but data could only be recovered from the 18th February 2018 onwards. The temperature sensors failed on the 29th March 2018. Plot a shows data of 15 thermistors. The initial depth of each thermistor is indicated in the legend. The depths varied slightly according to the surface height variations plotted in c.

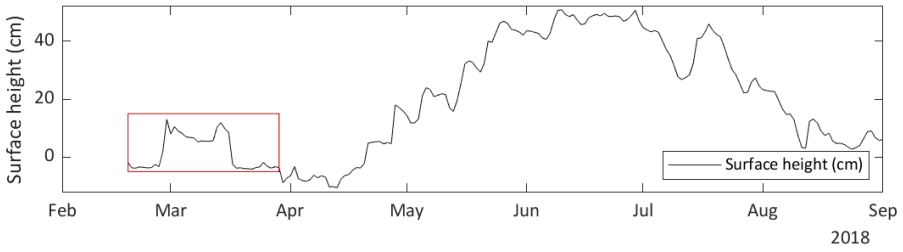

Figure F.3: Surface height data measured with a sonic ranging sensor at a station installed on the summit of Gregoriev ice cap (4600 m a.s.l.) from 18th February until 1st September 2018. The red box highlights the data also plotted in Fig. F.2c

G. Adventure of Science: Women and glaciers in Central Asia

The program 'Adventure of Science: Women and glaciers in Central Asia' organizes female only scientific expeditions for young women from Central Asia. It is embedded into the organization 'Inspiring Girls Expeditions' and adopts the organization's philosophy and teaching concepts (http://inspiringgirls.org/who-we-are). A further aim of 'Adventure of Science: Women and glaciers in Central Asia' is to build a network of young, female scientists across the boarders of the different Central Asian countries.

The idea of organizing a women only expedition and bringing 'Inspiring Girls Expeditions' to Central Asia started several years ago during glaciological fieldwork and capacity building activities, which Martina Barandun and myself organized within the projects 'Capacity building and Twinning for Climate Observing Systems (CATCOS)' and 'Cryospheric Climate Services for improved Adaptation (CICADA)'. Through my own involvement as an instructor and Martina's participation as a volunteer in Girls on Ice Switzerland (the first Inspiring Girls Expeditions in Switzerland), the idea of a Central Asian program took shape and plans turned into actions. From the beginning, Prof. Martin Hoelzle strongly supported our plans. In 2019, the Swiss Agency for Development and Cooperation SDC accepted our additional credit request to contribute financing the 'Adventure of Science: Women and glaciers in Central Asia' program within the CICADA project. Further financial, technical and logistical support was guaranteed from several other companies and institutions including UNESCO Almaty Office. A successful first expedition was organized in September 2019 with participants from Kazakhstan, Kyrgyzstan, Tajikistan and Uzbekistan and an international instructor team including ourselves from Switzerland and women from the four Central Asian countries. Due to the COVID-19 pandemic, the 2020 and 2021 expeditions had to be replaced with online/at home programs.

H. Curriculum vitae

Personal detail	Marlene Kronenberg
Date of Birth	24 June 1988, Sursee LU, Switzerland
Contact	Dahliaweg 14 3004 Berne Switzerland Email: marlene.kronenberg@outlook.com

Education

since April 2017	**PhD student**, University of Fribourg, Switzerland Project: Changing Glacier Firn in Central Asia and its Impact on Glacier Mass Balance. (SNSF project n° 200021_169453).
December 2019	**Guest PhD Student**, Department of Earth Sciences, Uppsala Universitet, Uppsala, Sweden
September 2018	**Summer school** on Ice Sheets and Glaciers in the Climate System, Karthaus, Italy
September 2017	**PhD school**, Ice Core Analysis Techniques, Copenhagen, Denmark
2011–2015	**Master of Science in Geography** Option Dynamics in Glaciology and Geomorphology, Department of Geosciences, University of Fribourg, Switzerland. Thesis: 'Mass balance analysis and reconstruction for Glacier No. 354, Inner Tien Shan, from 2003 to 2014. University of Fribourg.' Thesis supervision Prof. Dr. Martin Hoelzle, Dr. Matthias Huss and Martina Barandun

2008–2011	**Bachelor studies** University of Fribourg, Switzerland, Major in Geography, Minors in Biology and Earth Sciences
2010–2011	**Erasmus** exchange semester, Departemento de Geografía, Universidad Autonoma de Madrid, Spain
Sep-Dec 2007	**Cambridge English C1 Advanced certificate** and preparation course, Atlantic Language School, Galway, Ireland
2001-2007	**Gymnasium and Matura certificate**, Kantonschule Sursee LU, Switzerland, Major in Biology and Chemistry
1995-2001	**Primary school** in Dagmersellen LU, Switzerland

Work experience

since 2019	**Co-founder and instructor** Adventure of Science: Women and Glaciers in Central Asia", Departement of Geosciences, University of Fribourg, Switzerland
2017–2019	**Program coordinator/instructor** Paul Scherrer Insitute, Villigen AG, Switzerland, project 'Girls on Ice Switzerland'
2015–2016	**Scientific collaborator** Meteodat GmbH, Zurich, Switzerland, project "Glaciares+"
2013–2015	**Under assistant**, Department of Geosciences, University of Fribourg, Switzerland, project "Capacity Building and Twinning for Climate Observing Systems (CATCOS)"
Apr-May 2014	**Scientific Internship**, Central Asian Institute for Applied Geosciences, Bishkek, Kyrgyzstan (Department II Climate, Water and Natural Resources)
2011-2013	**Sociocultural animator**, Centre Fries, University of Fribourg, Switzerland
Jan-Jul 2008	**Au-pair** in Cheseaux-sur-Lausanne, Switzerland

Teaching

Bachelor Level	**Geomorphology** (University of Fribourg) Exercises **Introduction to Atmospheric Science** (University of Fribourg) Exercises **Introduction to Human Geography** (University of Fribourg) Exercises
Various	**Adventure of Science: Women and glaciers in Central Asia** (Glacier expeditions and online courses for young women from Central Asia), Co-Initiator, coordinator and instructor, http://inspiringgirls.org/central-asia-en **Girls on Ice Switzerland** (Glacier expeditions and school workshops), Program coordinator, course instructor and lectures/exercises in high school classes, http://inspiringgirls.org/switzerland **Mammut glacier excursion** (Mammut Alpine School), scientific inputs for guests of a glacier trekking **Capacity Building Glaciares+** (Glaciology training for professionals from different institutions: INAIGEM, UGRH and UNASAM in Huaraz, Perú) Lectures and exercices **WGMS Course Mass Balance Measurements and Analysis 2016** (La Paz, Bolivia) Lectures and exercises **WGMS Course on Mass Balance Measurements and Analysis 2015** (Bishkek, Kyrgyzstan) Course organisation

Personal Bibliography

As Part of the Thesis

Kronenberg, M., van Pelt, W., Machguth, H., Fiddes, J., Hoelzle, M., and Pertziger, F. Long-term mass balance and firn modelling for Abramov glacier, Pamir Alay. *The Cryosphere Discussions* 2021-380. 2022. doi:10.5194/tc-2021-380

Kronenberg, M., Machguth, H., Eichler, A., Schwikowski, M., and Hoelzle, M. Comparison of historical and recent accumulation rates on Abramov Glacier, Pamir Alay. *Journal of Glaciology*, 67(262):253–268, 2021. doi:10.1017/jog.2020.103

Others and Co-Authored

Denzinger, F., Machguth, H., Barandun, M., Berthier, E., Girod, L., Kronenberg, M., Usubaliev, R., and Hoelzle, M. Geodetic mass balance of Abramov Glacier from 1975 to 2015. *Journal of Glaciology*, 67(262):331–342, 2021. doi:10.1017/jog.2020.108

Hoelzle, M., Azisov, E., Barandun, M., Huss, M., Farinotti, D., Gafurov, A., Hagg, W., Kenzhebaev, R., Kronenberg, M., Machguth, H., Merkushkin, A., Moldobekov, B., Petrov, M., Saks, T., Salzmann, N., Schöne, T., Tarasov, Y., Usubaliev, R., Vorogushyn, S., Yakovlev, A., and Zemp, M. Re-establishing a monitoring programme for glaciers in Kyrgyzstan and Uzbekistan, Central Asia. *Geoscientific Instrumentation, Methods and Data Systems*, 6(2): 397–418, 2017. doi:10.5194/gi-6-397-2017

Kenzhebaev, R., M. Barandun, M. Kronenberg, C. Yaning, R. Usubaliev, and M. Hoelzle. Mass Balance Observations and Reconstruction for Batysh Sook Glacier, Tian Shan, from 2004 to 2015. *Cold Regions Science and Technology* 135:76–89.2017. doi:10.1016/j.coldregions.2016.12.007

Kronenberg,M., Barandun, M., Hoelzle, M., Huss,M., Farinotti, D., Azisov, E., Usubaliev, R., Gafurov, A., Petrakov, D., and Kääb, A. Mass-balance reconstruction for Glacier No. 354, Tien Shan, from 2003 to 2014. Annals of Glaciology, 57(71):92–102, 2016. doi:10.3189/2016AoG71A032.

Kronenberg, M., Schauwecker, S., Huggel, C., Salzmann, N., Drenkhan, F., Frey, H., Giráldez, C., Gurgiser, W., Kaser, G., Juen, I., Suarez, W., García Hernández, J., Fluixá Sanmartín, J., Ayros, E., Perry, B., and Rohrer, M. The Projected Precipitation Reduction over the

Central Andes may Severely Affect Peruvian Glaciers and Hydropower Production. Energy Procedia, 97:270–277, 2016b. doi:10.1016/j.egypro.2016.10.072.

Mattea, E., Machguth, H., Kronenberg, M., van Pelt, W., Bassi, M., and Hoelzle, M. Firn changes at Colle Gnifetti revealed with a high-resolution process-based physical model approach. *The Cryosphere*, 15:3181–3205, 2021. doi:10.5194/tc-15-3181-2021

Conference Contributions

Kronenberg, M. et al. Long-term mass balance and firn modelling for Abramov glacier, Pamir Alay (Online presentation). EGU General Assembly 2021, online (EGU21-10205), 2021.

Kronenberg, M. et al. Modelling the long-term mass balance and firn evolution of Abramov glacier, Pamir Alay (Online). 18h Swiss Geoscience Meeting. Zurich, Switzerland, 2020.

Kronenberg, M. et al. Empowering young women from Central Asia on glaciers: A new scientific communications program (Poster). 17th Swiss Geoscience Meeting. Fribourg, Switzerland, 2019.

Kronenberg, M. et al. No firn changes in Central Asia? (Poster). 17th Swiss Geoscience Meeting. Fribourg, Switzerland, 2019.

Kronenberg, M. et al. Girls on Ice Switzerland – field-based science short courses (Poster). Geophysical Research Abstracts (Vol. 21, EGU2019-9336). Vienna, Austria, 2019.

Kronenberg, M. et al. Spatially heterogenous firn on a remotely located mountain glacier in Central Asia (Pico presentation). Geophysical Research Abstracts (Vol. 21, EGU2019-4875). Vienna, Austria, 2019.

Kronenberg, M. et al. Changing firn properties on glaciers in Central Asia (Talk). 16th Swiss Geoscience Meeting, Berne, Switzerland, 2018.

Kronenberg, M. et al. Historical and recent firn investigations on Abramov glacier, Kyrgyzstan (Talk). Alpine Glaciology Meeting. Chamonix, France, 2018.

Kronenberg, M. et al. Mass balance monitoring and capacity building in Central Asia (Poster). IGU Thematic Conference dedicated to the centennial of the Institute of Geography of Russian Academy of Science. Moscow, Russia, 2018.

Kronenberg, M. et al. Changing firn properties on Glaciers in Central Asia (Talk). IGU Thematic Conference dedicated to the centennial of the Institute of Geography of Russian Academy of Science. Moscow, Russia, 2018.

Kronenberg, M. et al. Are Accumulation Regimes of Central Asian Glaciers Changing? (Talk). POLAR 2018 Abstract Proceedings, Davos, Switzerland, 2018.

Kronenberg, M. et al. Investigating firn changes of Abramov glacier, Pamir Alay (Poster). 15th Swiss Geoscience Meeting. Davos, Switzerland, 2017.

Kronenberg, M. et al. Simulating firn changes on Abramov Glacier, Pamir Alay, Central Asia (Poster). RETAIN Workshop. Copenhagen, Denmark, 2017.

Kronenberg, M. et al. ¿Cuál es el futuro del caudal den las cuencas glaciadas de los Andes Centrales? (Talk). Congreso Latinoamericano de Hidráulica XXVII. Lima, Perú, 2016.

Kronenberg, M. et al. Future runoff from glacierized catchments in the Central Andes could substantially decrease (Poster). Geophysical Research Abstracts (Vol. 18, pp. EGU2016-4553), Vienna, Austria, 2016.

Kronenberg, M. et al. Mass balance reconstruction for Glacier No. 354, Tien Shan, from 2003 to 2014 (Poster). 13th Swiss Geoscience Meeting. Basel, Switzerland, 2015.

Kronenberg, M. et al. Mass balance reconstruction for Glacier No. 354, Tien Shan, from 2003 to 2014 (Talk). 26th General Assembly of the International Union of Geodesy and Geophysics (IUGG). Prague, Czech Republic, 2015.

Kronenberg, M. et al. Mass-balance reconstruction for Glacier No. 354, Akshiirak, inner Tien Shan, from 2003 to 2014 (Talk). Proceedings of the IGS Kathmandu Symposium. Kathmandu Nepal, 2015.

Other presentations

Panel member: “A fragile future: can mountain communities adapt to climate change?“, COP26 Geneva Cryosphere HUB. Geneva, Switzerland, November 2021.

Panel member: ’Generationentalk Ewiges Eis’, UND das Generationentandem. Berne, Switzerland, March 2021.

Public talk: ’Girls on Ice Switzerland’, Mammut Gletscher-Abend, Seon, Switzerland, May 2018.

Public talk: 'Glaciares y clima', Foro Académico, Autoridad Nacional del Agua, Huaraz, Perú, November 2016.

Public lecture: "CATCOS: Re-establishing Long-term Glacier Monitoring in Kyrgyzstan, Central Asia", University of Central Asia, Bishkek, May 2014.

Code and data sets as part of this thesis

Kronenberg, M. MarleneKro/ebfm_abramov_sensitivity: (1.0) [code]. Zenodo. 2022. doi:10.5281/ZENODO.7110211

Kronenberg, M., Cheremnykh, A., Eichler, A., Esenaman Uluu, M., Gilbert, A., Hoelzle, M., Kenzhebaev, R., Kummert, M., Lavrentiev, I., Machguth, H., Schwikowski, M., Schuppli, P., Walther, S., and Wicky, J. Abramov glacier firn data [data set]. Zenodo. 2022. doi:10.5281/ZENODO.7112894

Kronenberg, M., Lavrentiev, I., Machguth, H., Schuppli, P., and Wicky, J. Gregoriev firn data [data set]. Zenodo. 2022. doi:10.5281/zenodo.7113282.

Kronenberg, M., van Pelt, W., Machguth, H., Hoelzle, M., Fiddes, J., Hoelzle, M., and Pertziger, F. MarleneKro/ebfm_abramov: (1.0) [code]. Zenodo. 2022. doi:10.5281/zenodo.5773796

Pertziger F., and Kronenberg M. Abramov glacier data base [data set]. Zenodo. 2022. doi:10.5281/ZENODO.7110254